

Institute of Fundamental Technological Research
Polish Academy of Sciences



Doctoral thesis

**Nanostructured soft platforms based on the
combination of nanofibers and hydrogels for
biomedical applications**

Yasamin Ziai, M.Sc. Eng.

Discipline of science: Biomedical Engineering

Supervisor: dr hab. Filippo Pierini

Co-supervisor: dr Chiara Rinoldi

Warsaw 2024

This research was supported by the First TEAM grant number POIR.04.04.00-00-5ED7/18-00, Which is carried out within the framework of the First TEAM program of the Foundation for Polish Science (FNP).

I acknowledge the POWER Och! Doc scholarship supported by ESF, number POWR.03.02.00-00-I028/17-00.

First and foremost, I would like to express my gratitude to my supervisor, dr hab. Filippo Pierini, for his support, guidance, and patience throughout my research. I extend my heartfelt thanks to my co-supervisor, dr Chiara Rinoldi, for her constant support, motivation, and insightful advice. A sincere thanks to all our lab members for their support along the way. Finally, I am deeply grateful to my wonderful friends and family, both near and far, for always being by my side.

برای هنگامه، رضا و نازنین

To Hengameh, Reza, and Nazanin, my incredible family, whose unwavering love and support have turned my dreams into reality.

To all 61 students on Flight PS-752 who never got the chance to defend their theses. Not a day goes by without thinking of you.

Table of Contents

Abstract	9
1. Biomaterials in Biomedical Engineering	11
2. Biomaterials Design and Fabrication techniques	15
2.1. Electrospun fibers	15
2.2. Hydrogels	19
2.3. Layered nanostructures	22
3. Biomedical applications	26
3.1. Biosensing	26
3.1.1. Optical biosensing based on plasmonics	28
3.2. Brain-machine interfaces	30
4. Aims and thesis	32
5. Materials and methods	33
5.1. Materials	33
5.1.1. Hydrogel precursor solution	33
5.1.2. Electrospun nanofibers	34
5.2. Characterization Methods	36
6. Articles included in the publication cycle of the dissertation	37
7. Summary of the articles included in the publication cycle of the dissertation	42
7.1. Smart plasmonic hydrogels based on gold and silver nanoparticles for biosensing application ..	42
7.2. Chameleon-inspired multifunctional plasmonic nanoplatfoms for biosensing applications	45
7.3. Lysozyme-sensitive plasmonic hydrogel nanocomposite for colorimetric dry-eye inflammation biosensing	48
7.4. Developing strategies to optimize the anchorage between electrospun nanofibers and hydrogel for multi-layered plasmonic biomaterials	51
7.5. Conducting polymer-based nanostructured materials for brain-machine interfaces	55
8. Conclusions	60
9. Summary and Future Prospects	61
10. References	63
11. Original Articles	71

Abstract

In this thesis, extensive research on hydrogel-based materials integrated with nanofibers and plasmonic nanoparticles has been conducted, focusing on their potential applications in biomedical fields such as biosensing and brain-machine interfaces. Hydrogels and nanofibers are significant materials in biomedical applications due to their unique properties. Hydrogels provide a highly hydrated, three-dimensional network ideal for biomolecule diffusion and cell growth, which is crucial for biosensing and BMIs. Nanofibers, with their high surface area-to-volume ratio, offer excellent mechanical support and tunable properties. Combining these two materials alongside plasmonic nanoparticles into multi-layered structures enhances the resulting composites' mechanical properties and functional versatility, making them great candidates for further applications. After extensive research on the literature regarding the application of hydrogel-based materials for biosensing and BMIs, the investigations in my thesis started with developing NIPAAm-based hydrogels with VPTT close to body temperature, suitable for physiological integrations. I continued with formulating nanofibrous mats from PCL, PLCL, and PCL/PEO through electrospinning to achieve defect-free nanofibers. Significant efforts were devoted to embedding plasmonic nanoparticles like silver nanocubes and gold nanorods into these hydrogel and nanofiber matrices. This inclusion aimed to take advantage of their unique optical properties to enhance the functionality of the resultant biomedical platforms. These nanoparticles' uniform distribution and stability were critical and confirmed through various characterization techniques to ensure optimal performance in final applications. The fabrication of multi-layered structures combining these materials was studied. Chemical, Morphological, optical, mechanical, and biological investigations focused on exploring the impact of properties such as fiber dimension and alignment, surface treatment, and hydrogel crosslinking density on the enhancement of interlayer adhesion were performed. This was crucial for ensuring the mechanical stability of the composite materials under physiological conditions, assessed through innovative fiber-pullout experiments designed to measure adhesion strength accurately and biocompatibility tests, investigating cell-material interactions. Ultimately, two biosensing applications were tested on separate composited platforms: a chameleon skin-inspired biosensor for non-invasive glucose monitoring and a lysozyme detection platform for diagnosing eye inflammation. The glucose biosensor incorporated silver nanocubes within a hydrogel matrix, showing exceptional antibacterial properties and rapid photothermal responsiveness when tested with real human urine, demonstrating its potential for diabetes monitoring. Meanwhile, the lysozyme biosensor utilized silver nanoplates embedded in PLCL nanofibers covered by a hydrogel layer, successfully indicating eye health through

visible color changes and confirmed by LSPR biosensing techniques using standard solutions and real human tears.

1. Biomaterials in Biomedical Engineering

The rapid evolution of materials science, coupled with the increasing importance of medical advancements, has led to a significant merge of these two fields [1]. Biomedical engineering is a field that harnesses the advancements in materials science to address the growing health and safety challenges that the world faces on a daily basis. The synergy between these disciplines is not only crucial in advancing medical technology but also essential in developing innovative solutions that can adapt to the dynamic nature of healthcare needs. This integration is particularly evident in the development of new materials and technologies that can be employed in medical applications, ranging from diagnostic tools to therapeutic interventions [2]. In the primary definitions of biomaterials, they were described as synthetic materials designed to replace parts of a living system or to function in intimate contact with living tissues. However, as the field evolved, the definition was broadened to a more diverse range of applications and materials as a material, natural or man-made, that comprises the whole or part of a living structure or biomedical device that performs, augments, or replaces a natural function. This evolution highlights a shift from a narrow focus on synthetic replacements for biological components to a more universal approach that covers a wide array of materials and technologies [3].

Biomaterials include a diverse range of materials, each class offering unique properties suitable for specific medical applications [4][5]. The primary classes of biomaterials include polymers, ceramics, and metals, each with distinct characteristics and functionalities, as shown in Figure 1 [6][7]. Polymers, in particular, are widely used due to their versatility and ability to be tailored to meet specific requirements. They can be broadly categorized into synthetic and natural polymers, each with its own set of advantages and applications [8].

Natural polymers, derived from biological sources, are reportedly the first biodegradable biomaterials used for biomedical applications [9]. Extracted from biological systems such as plants, microorganisms, and animals, natural-based polymers are particularly appealing due to their inherent biocompatibility and bioactivity. The most common natural polymers include polysaccharides (chitosan and alginate) [10] and proteins such as silk, collagen, and gelatin [10]. The main advantage of natural polymers lies in their ability to facilitate cell attachment, proliferation, and differentiation, which is crucial for tissue regeneration [11]. However, due to the lack of adequate mechanical properties, the fabrication process of these materials can face complications. Certain actions, such as using the derivatives and blending with other biomaterials, have been investigated through the years [12].

Synthetic polymers offer the advantage of tailor-made properties to suit specific biomedical applications. They can be engineered to have a wide range of mechanical, physical, and chemical properties, degradation rates, and surface characteristics [13]. The versatility of synthetic polymers allows for the design of biomaterials with controlled porosity, degradation, and mechanical properties, making them highly suitable for a variety of biomedical applications [14]. The most commonly used synthetic polymers include polycaprolactone (PCL), poly(L-lactic acid) (PLLA), and poly(glycolic acid) (PGA) and their blends [15].

Metals and ceramics, while less versatile than polymers, are much needed in certain biomedical applications. Metals have been used as biomedical implants for a long time, although shortcomings such as corrosion have limited their conventional use [16]. Metals such as titanium, stainless steel, and cobalt-chromium alloys are widely used in orthopedic and dental implants due to their high strength and durability, and noble metals such as gold and silver and their alloys are used as particles and layers for biosensing and photothermal therapy [17]. Ceramics, including bioactive glass and hydroxyapatite, are used in bone grafts and coatings for metal implants due to their excellent biocompatibility and similarity to bone minerals [18], [19].

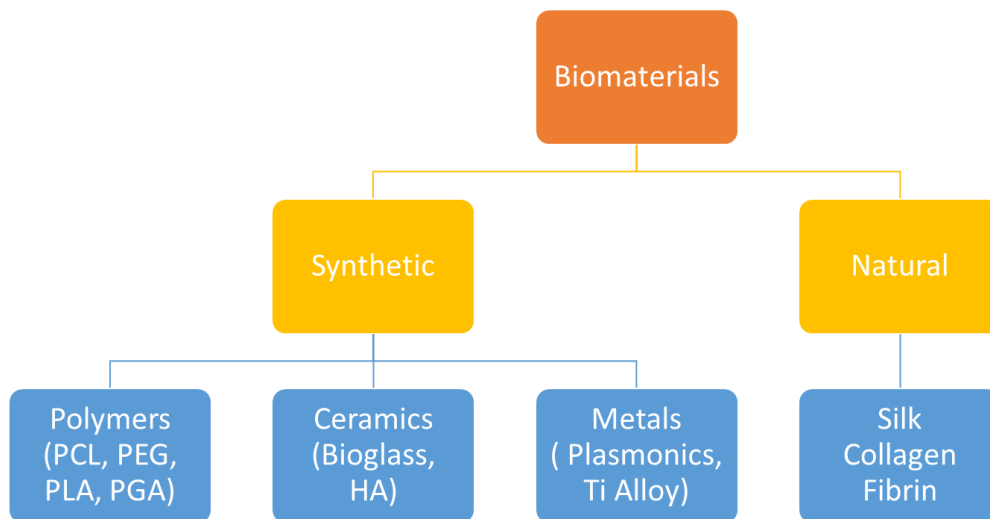


Figure 1. General classification of biomaterials into natural and synthetic groups.

The design and selection of biomaterials for medical applications are dependent on a set of properties, including biocompatibility, non-toxicity, absence of foreign body reactions, and appropriate mechanical characteristics (Figure 2). These properties are not only crucial for the immediate functionality of the biomaterial but also for its long-term success and integration within the biological system [2]. A fundamental requirement for any biomaterial is biocompatibility, which refers to the ability of a material to perform with an appropriate host response in a specific application. This property not only includes the absence of cytotoxicity, genotoxicity, and immunogenicity but also the ability to support appropriate cellular activity, including adhesion, proliferation, and differentiation [20]. The biocompatibility of a material is not an intrinsic property but is highly dependent on the biological context, involving complex interactions between the material, the body's tissues, and biological fluids [21].

Another essential property of biomaterials is their non-toxicity. This characteristic ensures that the material does not release substances in quantities that can cause harm to the body. The evaluation of toxicity involves a series of tests, ranging from in vitro cell culture studies to in vivo animal models, to assess the material's impact on cellular viability, metabolism, and overall tissue health. The absence of toxic residues and degradation products is particularly crucial for materials intended for long-term implantation. Moreover, the degradation products of biodegradable biomaterials should be non-toxic and easily metabolized or excreted by the body, ensuring safety throughout the material's lifecycle [22].

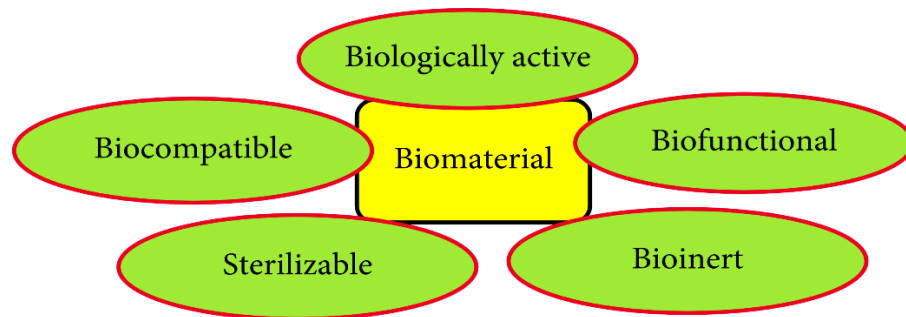


Figure 2. Properties of biomaterials required for biomedical applications: the diagram illustrates the essential properties that define a biomaterial, including biocompatibility, biofunctionality, biological activity, bio-inertness, sterilizability, and biocompatibility [23].

The absence of foreign body reactions is another critical attribute of biomaterials, especially those intended for implantation. A foreign body reaction is an immune response triggered by the body's recognition of the biomaterial as a foreign object. This reaction can lead to chronic inflammation and, ultimately, the failure of the implant. To minimize such reactions, biomaterials are often designed to mimic natural tissues' physical and chemical properties, thereby reducing their recognition as foreign entities by the immune system. Surface modifications, such as coating with biologically active molecules or patterning at the nanoscale, have been explored to improve the integration of biomaterials with the surrounding tissue and to modulate the host response [24]. Furthermore, the mechanical properties of biomaterials are of significant importance, which involves matching the biomaterial's strength, elasticity, and modulus with the native tissue to ensure proper functioning and durability of the implant. Inadequate mechanical properties can lead to implant failure due to fracture, wear, or deformation [25]. Additionally, the mechanical environment can influence cellular responses, making the mechanical design of biomaterials a key factor in their success [26].

2. Biomaterials Design and Fabrication techniques

Biomaterials' design and fabrication techniques circle back directly to the application requirements and the properties expected from the platform. Biomaterials need to be tailored to mimic the physical, chemical, and biological properties of native tissues for their integration and functionality within the human body [27]. Advanced fabrication techniques such as 3D printing, electrospinning, and nanotechnology have revolutionized the development of biomaterials, allowing for the creation of structures with precise geometries, porosities, and surface characteristics. These techniques enable the production of biomaterials that can closely replicate the extracellular matrix's complex architecture, providing the necessary cues for cell attachment, proliferation, and differentiation. Furthermore, the design of biomaterials with specific degradation rates, mechanical properties, and surface functionalities can significantly affect their biocompatibility, bioactivity, and overall therapeutic efficacy, underscoring the importance of thoughtful biomaterial design in biomedical applications [28]. Moreover, the evolution of biomaterials design and fabrication techniques has opened new avenues for personalized medicine, where biomaterials can be custom-designed to meet the specific needs of individual patients. For instance, the electrospinning technique offers significant advantages for designing custom structures in biomedical applications. Firstly, electrospinning allows for precise control over the fiber diameter and pore size, enabling scaffold fabrication that support cell attachment and proliferation, enhancing tissue regeneration [29]. Also, electrospun nanofibers can be functionalized with various biomolecules, drugs, or growth factors, making them ideal for controlled drug delivery systems. The high surface area-to-volume ratio of these fibers increases their efficiency in drug loading and release kinetics, which can be finely tuned by adjusting the electrospinning parameter [30]. Additionally, the incorporation of stimuli-responsive materials into the design of biomaterials has led to the development of smart therapeutic systems capable of responding to physiological signals for targeted drug delivery or tissue regeneration. These advancements highlight the critical interplay between biomaterials design and fabrication techniques in addressing the complex challenges of biomedical applications, ultimately leading to more effective and personalized healthcare solutions.

2.1. Electrospun fibers

Electrospinning, dating back to the early 20th century, is one of the most used fabrication techniques for many biomedical applications. This technique was first conceptualized for textile

manufacturing, but it gained importance for its ability to fabricate ultrafine fibers resembling the extracellular matrix, which is ideal for tissue engineering and regenerative medicine [31][32]. Growing research exploring the use of various biocompatible and biodegradable polymers has led to innovations in scaffold-like designs for diverse biomedical applications. The versatility of electrospinning in manipulating polymer solutions into fibers with controlled morphology and properties increased the application to wound healing, biosensing, and drug delivery systems [33]. Up to now, electrospinning techniques have become more sophisticated, integrating advancements in nanotechnology and materials science by the development of composite and core-shell fibers, enabling the incorporation of bioactive agents and drugs [34]. The development of the electrospinning technique throughout the years can be seen in Figure 3 [35].

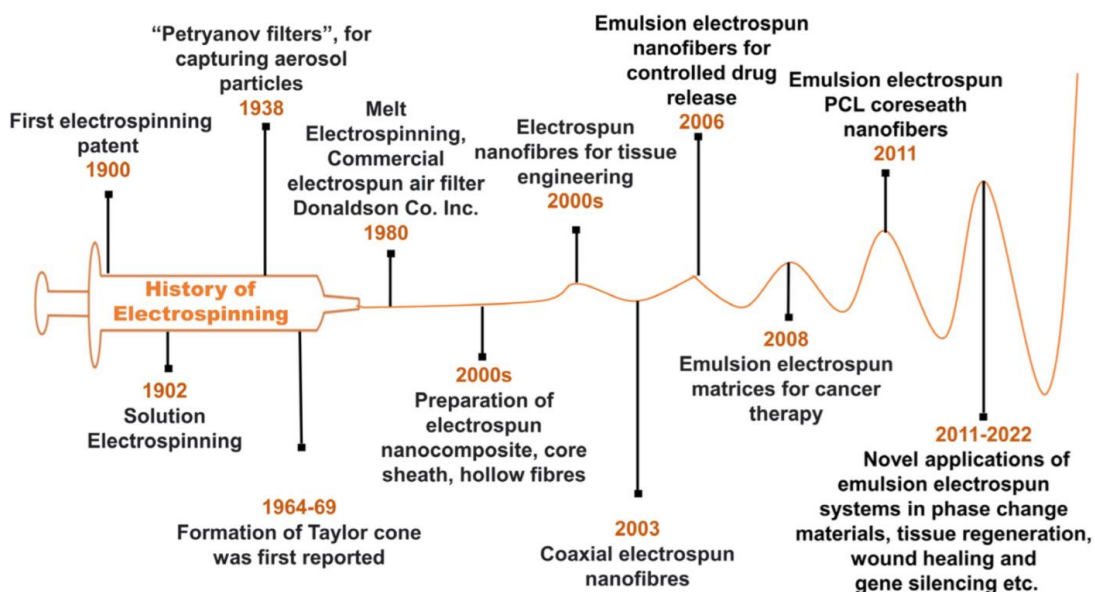


Figure 3. Evolution of electrospinning technique throughout the years. The first electrospinning patents started from solutions to melt spinning, followed by discovering diverse fibers and applications for tissue engineering, drug delivery, and evolution for various biomedical applications [35].

Electrospinning is a versatile and efficient technique for producing ultrafine fibers with diameters ranging from micrometers to nanometers [36]. At its core, electrospinning utilizes electrostatic forces to draw a viscoelastic polymer solution or melt into fine fibers. This process begins with the preparation of a polymer solution, where a polymer is dissolved in an appropriate solvent to create a solution with specific viscosity, conductivity, and surface tension properties (Figure 4). The solution is then loaded into a syringe equipped with a metallic needle or nozzle, which acts as the spinneret. When a high voltage is

applied to the needle, the polymer solution becomes charged. As the voltage reaches a critical value, electrostatic repulsion counteracts the surface tension of the polymer droplet formed at the tip of the needle, leading to the formation of what is known as a Taylor cone. With a further increase in the electric field, the repulsive electrostatic forces overcome the surface tension completely, and a charged jet of the polymer solution is ejected from the tip of the Taylor cone. As the solvent evaporates or the melt solidifies, solid fibers are formed and collected on a grounded or oppositely charged collector, typically positioned a few centimeters away from the needle. The collector can be a static plate, a rotating drum, or a mandrel, depending on the desired fiber alignment and structure [36]–[38]. It is worth mentioning that there are several key parameters that play a crucial role in determining the properties of the resulting fibers and optimizing these parameters is essential for tailoring the fibers to specific applications. The most influential parameters can be categorized into three classes: 1. Instrument parameters (flow rate of the polymer solution, applied voltage, the distance between the needle and collector, and the needle gauge size), 2. Solution parameters (viscosity, conductivity, and surface tension) and 3. Ambient conditions (temperature, humidity) [36].

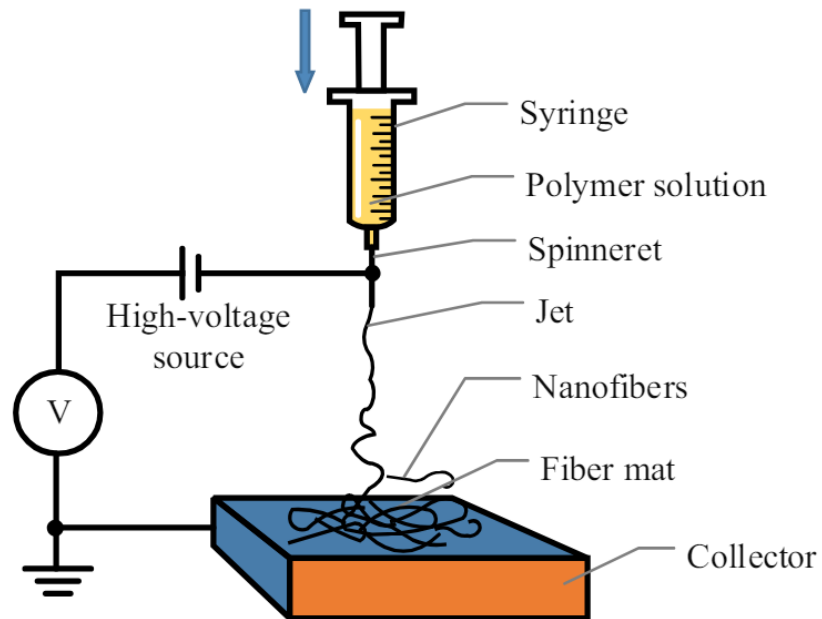


Figure 4. Schematic of the electrospinning setup. The polymer solution is loaded in the syringe and placed at a working distance from the collector. The whole setup is connected to a high-voltage source; as a result, the solution jet is formed, and nanofibers are collected [39].

The resulting nonwoven mat of nano and microfibers is characterized by its outstanding properties and features, making it an excellent candidate for many applications and novelties. One of the most notable properties of electrospun fibers is their high surface area-to-volume ratio [40]. This characteristic is particularly advantageous where a high surface area can enhance encounters with nanoparticles, functionalization, cell adhesion, proliferation, and differentiation. The increased surface area also facilitates a higher loading capacity for therapeutic agents, making these fibers ideal for targeted drug delivery applications. Additionally, the porosity of the electrospun mats can be precisely controlled, allowing for the adjustment of properties like permeability to gases and fluids [41]. Another significant aspect of electrospun nano and microfibers is their ability to mimic natural tissues' extracellular matrix (ECM). The ECM is a complex network of proteins and polysaccharides that provides structural and biochemical support to cells. Electrospun fibers can replicate the nanofibrous structure of the ECM, providing a more biomimetic environment for cell growth compared to traditional flat substrates. This biomimicry is essential for tissue engineering applications, where the scaffold must provide an appropriate microenvironment for cells to form new tissue. Furthermore, the mechanical properties of these fibers, such as elasticity and tensile strength, can be tuned to match those of the native tissue, ensuring that the scaffold can withstand physiological stresses while supporting tissue regeneration [42].

The versatility of electrospinning also allows for the incorporation of various functional materials into the fibers. Bioactive molecules such as growth factors, enzymes, and antibiotics can be embedded within the fibers or coated on their surface [43]. This incorporation can provide additional functionalities like enhanced cell signaling, sensing biomolecules, antimicrobial properties, or controlled release of drugs, further expanding the potential applications of these materials in biomedicine.

Moreover, the electrospinning process is compatible with a wide range of materials, including natural polymers, synthetic polymers, and composites, allowing for the creation of fibers with tailored properties for specific applications. In addition to these properties, electrospun fibers offer advantages in terms of scalability and cost-effectiveness, making them viable for commercial production [44].

To summarize, the unique properties of nano and microfibers produced by electrospinning, such as high surface area-to-volume ratio, biomimetic structure, mechanical tunability, and functional versatility, make them significant in the biomedical field. Their application in brain-machine interfaces [45], wound healing [46], drug delivery [47], biosensing [48], and other medical areas highlights their potential to address a wide range of healthcare challenges, paving the way for advanced therapeutic strategies and improved patient outcomes.

2.2. Hydrogels

Hydrogels, as a form of three-dimensional polymeric networks, were first conceptualized in the early 1960s. The initial development was driven by the need for materials that could mimic the natural living tissue environment. As shown in Figure 5, the first hydrogels demonstrated the potential of these materials to interface with biological tissues, owing to their biocompatibility and similar mechanical properties to natural tissues. Over the following decades, the application of hydrogels expanded from ophthalmology into more diverse biomedical fields. The 1980s and 1990s witnessed significant advancements in hydrogel technology, with the development of stimuli-responsive hydrogels that could change their properties in response to environmental factors like temperature, pH, or ionic strength. This innovation opened new avenues for drug delivery systems, where hydrogels could release therapeutic agents in a controlled manner. The turn of the century saw further evolution, with the integration of nanotechnology leading to the development of nanocomposite hydrogels. Their offered properties made them suitable for more demanding applications such as tissue engineering scaffolds, biosensors, and wound dressings [49]–[51].

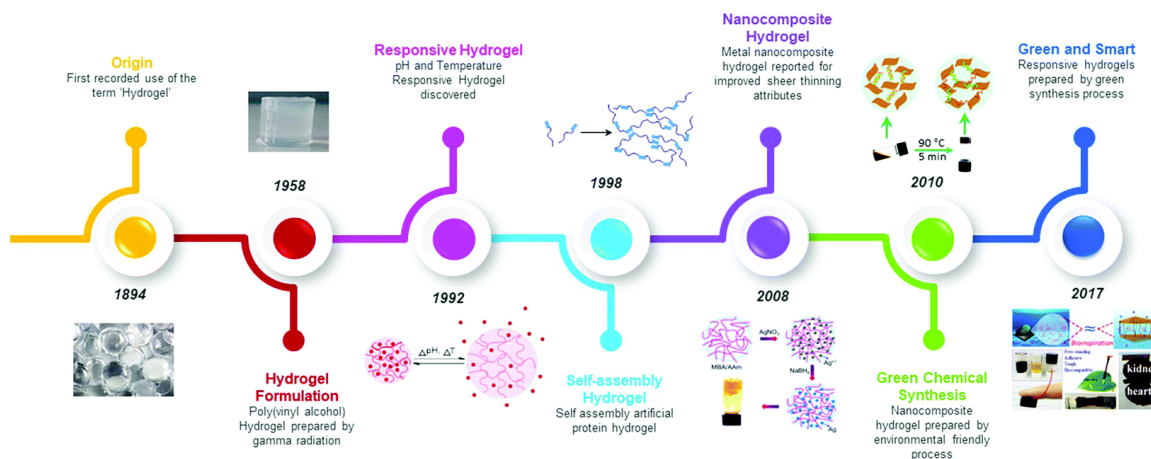


Figure 5. Timeline of the advancement of hydrogels [50].

Hydrogels are a unique class of polymeric materials distinguished by their ability to retain a significant amount of water within their structures. Fundamentally, they are three-dimensional, hydrophilic networks of polymer chains capable of swelling in water to hold a large volume of fluid relative to their dry weight [52]. The defining characteristic of hydrogels is their high water content, which typically ranges from 10% to over 90% of their total weight. This property is primarily due to the presence of

hydrophilic groups within the polymer network, such as hydroxyl, amine, and carboxyl groups. Hydrogels can be formed from a wide range of natural or synthetic polymers, and their physical properties can vary significantly depending on the nature of the polymer and the crosslinking method used to create the network[53], [54].

In the biomedical field, hydrogels' physical and chemical properties are pivotal in determining their suitability and effectiveness for various applications. Physically, the most critical property of hydrogels is their high water content, which imparts a degree of softness and flexibility similar to natural tissues. This characteristic is essential for applications that require contact with biological tissues and biomolecules, such as wound dressings or biosensing [55]. The porosity of hydrogels is another vital physical property, influencing not only their ability to allow the diffusion of nutrients and oxygen but also their capacity to facilitate cell migration and proliferation. This is particularly important in tissue engineering, where the scaffold's porosity must be optimized to support cell infiltration and tissue formation [56]. Furthermore, the mechanical properties of hydrogels, such as elasticity, stiffness, and tensile strength, can be finely tuned to match those of the native tissue, which is essential for applications in brain-machine interfaces and tissue engineering. [57].

From the chemical point of view, biocompatibility plays the most significant role in biomedical applications. Since they closely mimic the natural tissue environment in terms of their high water content and soft, rubbery consistency, they are less likely to elicit an adverse immune response when used in the body [58]. Additionally, hydrogels can be engineered to be biodegradable, allowing them to break down into non-toxic components easily eliminated or absorbed by the body [59].

Another significant property of a class of hydrogels is their ability to respond to environmental stimuli, such as changes in temperature, pH, or ionic strength. These so-called "smart" or "responsive" hydrogels (Figure 6) can undergo abrupt changes in their swelling behavior or mechanical properties in response to external stimuli, making them ideal for controlled drug release applications [60]. For instance, a thermo-responsive hydrogel might swell and release its drug payload when exposed to environment temperature more than its lower critical solution temperature (LSCT), providing targeted drug delivery [61]. Poly(N-isopropylacrylamide), known as PNIPAAm as one of the most important and well-known smart polymers, has been used in the shape of hydrogel for biomedical applications. This polymer, with LSCT close to body temperature, has been explored for biomedical applications [23][62].

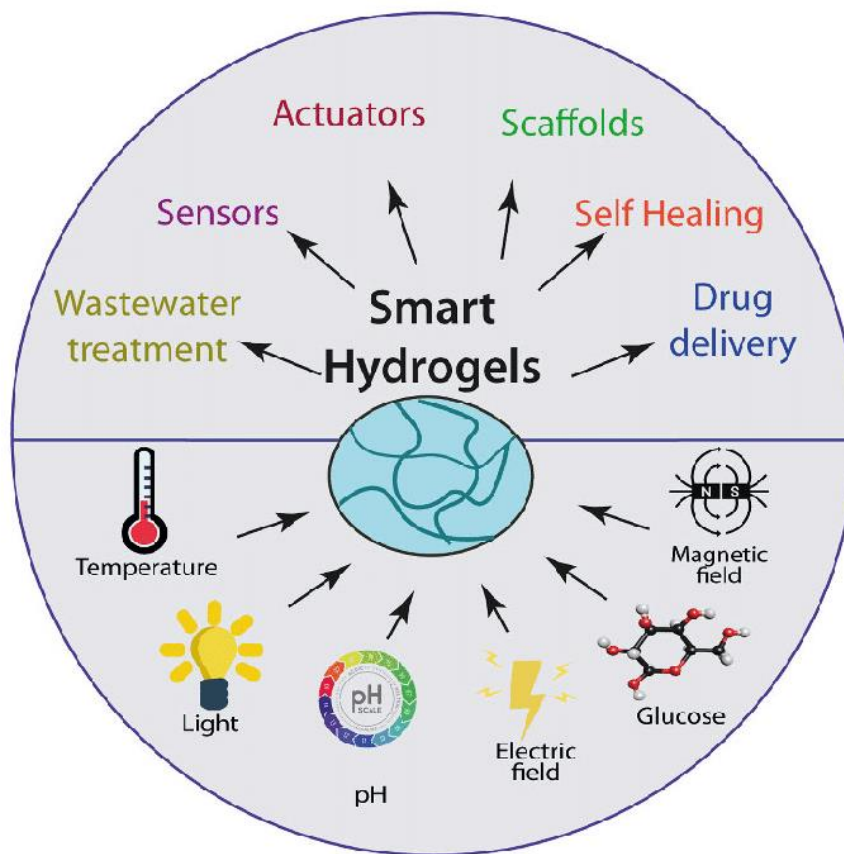


Figure 6. Smart stimuli-responsive hydrogels and their application in different biomedical fields [63].

While promising, the application of hydrogels in the biomedical field is not without challenges, particularly due to their inherently soft nature and weak mechanical properties [64]. One of the primary concerns is their lack of sufficient mechanical strength, especially in load-bearing applications. Hydrogels, by their very nature, are designed to be highly hydrophilic and absorbent, which imparts a degree of softness and flexibility akin to natural tissues. However, this also means they often lack the necessary tensile strength and structural integrity to withstand physiological stresses. This limitation can lead to premature degradation or deformation of the hydrogel when in use, potentially compromising its functionality and the overall success of the treatment. Additionally, the soft and often fragile nature of hydrogels makes them challenging to handle and manipulate during surgical procedures, posing practical difficulties in their clinical application [58].

To address these challenges, significant research efforts are being directed toward enhancing the mechanical properties of hydrogels without compromising their biocompatibility and other beneficial characteristics [65]. Strategies include the development of composite hydrogels, which incorporate

reinforcing materials such as nanoparticles [66], fibers [67], or mesh structures to improve mechanical strength. Another approach is the design of interpenetrating polymer networks within hydrogels, which can provide a balance between flexibility and robustness [68]. However, these modifications must be carefully optimized to ensure that the hydrogel remains biocompatible and retains its essential properties, such as porosity and water content. Furthermore, the challenge extends to maintaining the hydrogel's responsiveness and degradation rate, which are crucial for applications like drug delivery and tissue regeneration. Overcoming these challenges is key to unlocking the full potential of hydrogels in biomedical applications, particularly in scenarios where mechanical resilience is as crucial as biological functionality [65].

Incorporating fibers as a layer in a multi-layered structure with hydrogels presents an innovative solution to enhance the mechanical properties of hydrogels while retaining their inherent biocompatibility and biofunctionality [67]. Fibers, especially those fabricated through techniques like electrospinning, can provide the necessary tensile strength and structural support that hydrogels inherently lack. When integrated into a layered structure, these fibers act as a reinforcing scaffold, imparting durability and resistance to mechanical stresses. This combination harnesses the flexibility and high water content of hydrogels with the robustness of fibrous materials, creating a strong and biologically effective composite. Such a synergistic approach is particularly beneficial in applications requiring both mechanical integrity and a soft, tissue-like environment, such as in load-bearing tissue engineering or in creating durable yet comfortable biomedical devices. The fiber-reinforced hydrogel structures thus offer a promising pathway to overcome one of the significant limitations of hydrogels in biomedical applications [69].

2.3. Layered nanostructures

Layered nanostructures that combine hydrogels and fibers represent an innovative class of biomaterials ingeniously designed to leverage the advantages of both components while minimizing their respective limitations. At its core, this hybrid structure typically involves a nano-fibrous scaffold layered with hydrogel matrices, creating a composite material exhibiting each constituent's unique properties. The fibers, often fabricated through techniques like electrospinning, provide mechanical strength and structural integrity, addressing one of the primary shortcomings of hydrogels – their relatively weak mechanical properties. These fibrous layers can be precisely engineered at the nanoscale to achieve desired characteristics such as porosity, alignment, and tensile strength. On the other hand, the hydrogel component, known for its high water content and excellent biocompatibility, contributes to the composite's overall bioactivity and soft, tissue-like consistency. This layered arrangement allows for a

synergistic interaction where the hydrogel enhances the biocompatibility and cell-friendly nature of the scaffold, while the fibers confer the necessary mechanical support [70].

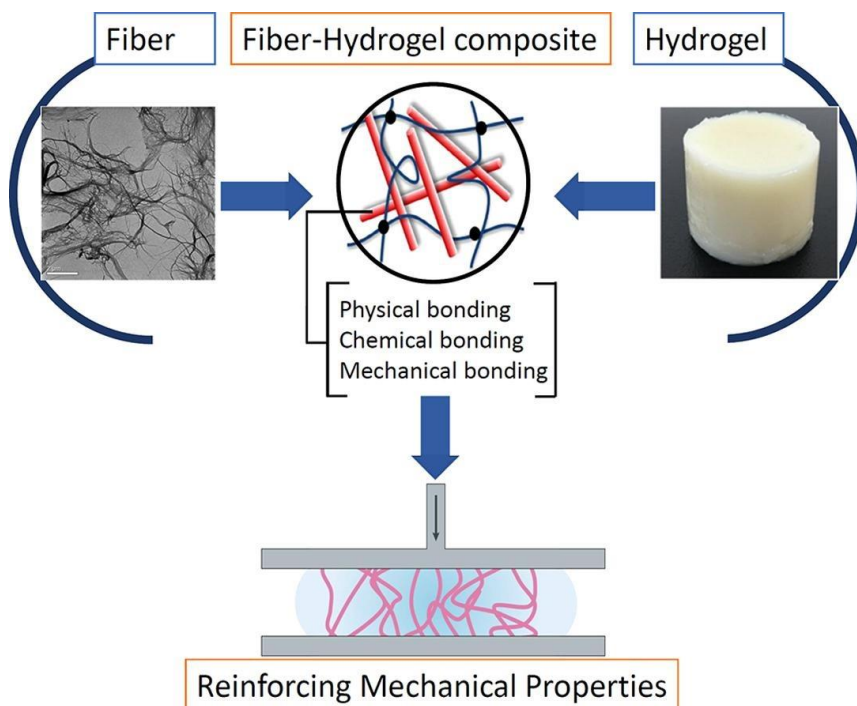


Figure 7. Fiber-hydrogel layered composite structure, showing the combination of hydrogel matrix and nanofibers, can strengthen the stability of the platform via physical, chemical, and mechanical bonding [71].

The integration of hydrogels and fibers into a layered nanostructure as shown in Figure 7, is not just a mere combination of two materials; it's a strategic coalescence that results in a material with enhanced functionalities. The hydrogel layers can be tailored to provide a conducive cell growth and proliferation environment. They can also be functionalized to release bioactive molecules, such as biomarkers or drugs, in a controlled manner, thereby adding the functionality of controlled release systems. Apart from imparting strength, the fibrous layers also add to the scaffold's overall surface area, facilitating better cell attachment and nutrient transport. This multi-layered approach effectively addresses the challenge of creating mechanically robust and biologically active biomaterials, a critical requirement for many biomedical applications. By benefiting from hydrogels and fibers, these layered nanostructures open up new possibilities in designing advanced scaffolds for tissue regeneration, wound healing, and drug delivery systems, overcoming some of the critical limitations faced by traditional materials in these fields [23].

Many biomedical applications have used the idea of multi-layered structures consisting of hydrogel and fibrous layers. One field that has benefited from these nanocomposite structures is biosensing. These multi-layered composites offer a unique platform for the development of sensitive, flexible, and biocompatible sensors. The hydrogel component provides a hydrophilic environment conducive to biological interactions and analyte diffusion, which is essential for biosensing applications. At the same time, the fibrous layer, in touch with both hydrogel and sensing agents such as nanoparticles, can act as a steady substrate for the platform. This combination enhances the sensitivity and selectivity of biosensors, making them suitable for detecting a wide range of biological markers, from glucose levels to pathogenic bacteria. The flexibility and mechanical stability the fibrous layer provides also enable the fabrication of wearable biosensors that can conform to the body, offering continuous, real-time monitoring of physiological parameters [72].

In BMI systems and neural tissue engineering, layered nanostructures of hydrogels and fibers are particularly advantageous because they provide a supportive and conducive environment for nerve regeneration. The hydrogel layer can be engineered to mimic the soft and hydrated nature of neural tissues, offering a biocompatible matrix for neuronal cell growth and differentiation. The fibrous layer, on the other hand, provides the necessary mechanical support and can be aligned to guide the directional growth of neural cells, which is crucial for the regeneration of neural pathways. Additionally, the incorporation of conductive materials into the fibrous layer or the hydrogel porous structure can enhance neuronal signaling and interaction, further promoting neural tissue repair and regeneration [73], [74].

Layered nanostructures combining hydrogels and fibers have also emerged as a versatile platform for controlled drug delivery systems and wound dressings. The hydrogel layer, known for its high water content and biocompatibility, can be loaded with therapeutic agents and designed to release them in a controlled manner. This is particularly useful for localized and sustained drug release, reducing systemic side effects and improving therapeutic efficacy. The fibrous layer, often made from biodegradable materials, adds structural integrity to the system and can be engineered to degrade at a predetermined rate, further controlling the release of the drug. There are various design setups for drug release, as both components can be loaded with drugs, and based on the target delivery method, singular or dual delivery can be performed. Additionally, incorporating stimuli-responsive materials into these layers can enable targeted drug delivery, where specific physiological conditions, such as pH changes or enzymatic activity, trigger the drug's release. This multi-layered approach allows for the precise control of drug release kinetics, making it highly suitable for a wide range of therapeutic applications [75]. In wound dressing applications, layered nanostructures of hydrogels and fibers offer an optimal combination of moisture

management, mechanical protection, and bioactivity. The hydrogel layer provides a moist environment that promotes wound healing, facilitates gas exchange, and absorbs wound exudate. Its high water content also helps to maintain a cool temperature at the wound site, providing comfort to the patient. The fibrous layer, typically made from materials like chitosan or collagen, adds mechanical strength to the dressing, protecting the wound from external stresses while still allowing for flexibility and conformability to the body. The fibrous layer can also be functionalized with antimicrobial agents or growth factors to further promote wound healing and prevent infection. This layered approach to wound dressing design addresses the key requirements of an ideal wound dressing: maintaining a moist healing environment, providing mechanical protection, and supporting the natural wound healing process [76], [77].

3. Biomedical applications

3.1. Biosensing

Healthcare is vital at the meeting point of science and technology, constantly evolving to address new challenges. The availability of simple, accessible diagnostic tools capable of identifying a wide array of biologically relevant analytes is indispensable for enhancing disease prevention and therapeutic measures [78]. Improvements in healthcare are vital across various domains, including hygiene, pharmaceutical development, food safety, environmental science, forensics, and both medical and clinical diagnostics [79]. Given the increasing proliferation of toxic substances in these areas, the early detection of such materials is paramount. Timely identification allows for immediate and effective response measures, underscoring the need for sophisticated detection technologies [80].

Biosensors, first pioneered by Clark and Lyons in the 1960s with the development of enzyme electrodes for glucose measurement, have significantly evolved to address these detection challenges [81]. A biosensor is an apparatus combining a biological component, such as an enzyme or antibody, with an electronic element to produce a quantifiable signal. This electronic component is responsible for detecting, recording, and transmitting information about physiological changes or the presence of various chemical or biological substances in the environment. Biosensors vary in size and shape and can detect and quantify low concentrations of specific pathogens, toxic chemicals, and pH levels. The typical structure of a biosensor includes several key components: (a) an analyte, (b) a bioreceptor, (c) a transducer, (d) electronic processing units, and (e) a display interface. Each part plays a vital role in the detection and measurement process, from identifying the target substance to presenting the results in a user-friendly format [82], [83].

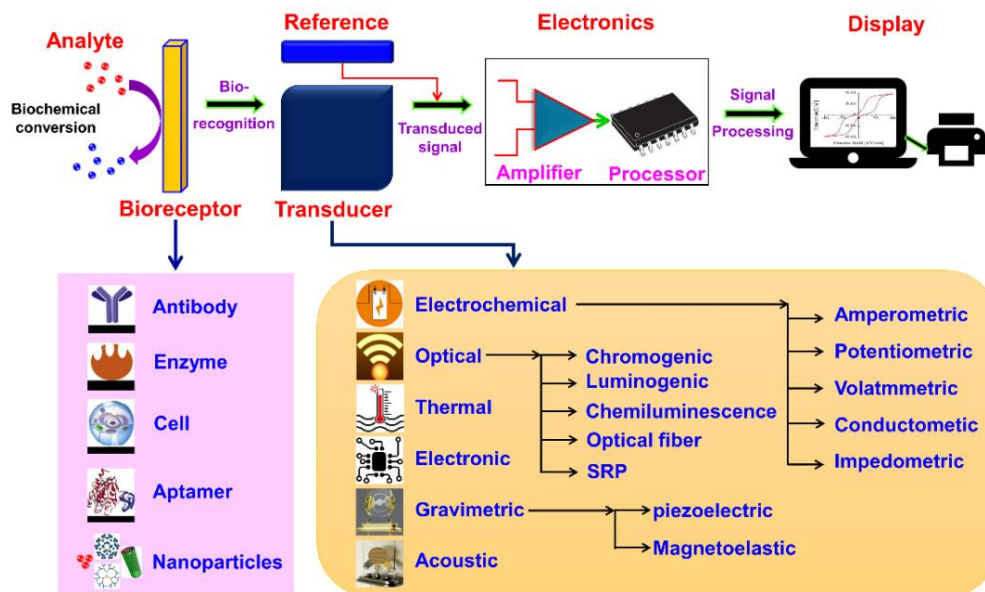


Figure 8. Diagram of typical biosensors, showing each part of the system, specifying types of bioreceptors and transducers [84].

Biosensors can be categorized based on the type of bioreceptor or transducer they utilize, as demonstrated in detail in Figure 8. Bioreceptors, which are biological elements that recognize and bind to specific analytes, dictate the specificity and selectivity of the biosensor. Common bio-receptors include enzymes, antibodies, nucleic acids, and cellular structures, each tailored to target specific molecules or biochemical processes. This variety allows biosensors to be finely tuned for applications ranging from medical diagnostics to environmental monitoring [80].

Transducers in biosensors convert the biological reaction into a measurable signal, classified based on the nature of this signal conversion. The main types include electrochemical, optical, thermal, piezoelectric, and electronic transducers. Electrochemical transducers, for example, measure changes in current or voltage that occur due to chemical reactions at the electrode surface. Optical transducers detect changes in light properties, while thermal transducers measure heat changes caused by biochemical reactions [85].

3.1.1. Optical biosensing based on plasmonics

Optical biosensing is a versatile approach within the broader field of biosensor technologies, utilizing light-based interactions to detect and quantify biological phenomena[86]. These biosensors work by measuring alterations in light properties such as intensity, phase, wavelength, or polarization, which occur as a result of specific biochemical interactions on a sensor surface. This method is highly valued for its non-contact, non-destructive nature and ability to provide real-time, label-free monitoring of a wide range of biological and chemical processes. The technology behind optical biosensing is rich and varied, encompassing several techniques each suited to different applications [87]. Techniques such as fluorescence, luminescence, and absorbance offer dynamic range and sensitivity solutions, pivotal for detecting low-abundance biomarkers. Another widely used method involves interferometry, which can effectively measure minute changes in the optical path length caused by biological reactions, offering ultra-sensitive detection capabilities ideal for clinical diagnostics and environmental monitoring [88]. Given its significant advantages in terms of sensitivity and specificity, optical biosensing has critical applications in medical diagnostics [48], environmental monitoring [89], and food safety [90]. It allows for detecting enzymes like lysozyme, monitoring of glucose levels, or detection of contaminants in real-time, with minimal sample preparation. This technology enhances traditional diagnostic methods' capabilities and opens new avenues for advanced therapeutic monitoring and personalized medicine.

Plasmonic biosensors, a subset of optical biosensors, have garnered attention for their ability to manipulate light properties at the nanoscale [91]. These sensors utilize the resonant coupling of electromagnetic waves, driven by the oscillations of free electrons in metals, a process known as plasmonic activity. This phenomenon enables light confinement to wavelengths much smaller than the incoming light [85]. Plasmonic biosensors are mainly categorized into two classes of detecting platforms. Surface Plasmon Resonance (SPR) has been a significant part of optical biosensing, known for its ability to detect changes in refractive index near a plasmonic sensor surface, typically a thin metal film. SPR biosensors are highly sensitive and have been widely used for real-time, label-free detection of biomolecular interactions [92]. However, moving towards Localized Surface Plasmon Resonance (LSPR) offers several advantages. LSPR, associated with nanostructured materials like gold and silver nanoparticles, provides enhanced sensitivity and miniaturization possibilities. The light-matter interaction resulting from nanoparticles leads to the collective oscillation of conduction band electrons, resulting in strong absorption and scattering of light at specific wavelengths [93]. The LSPR wavelength is highly sensitive to the size, shape, and material of the nanoparticles and the surrounding environment. This

sensitivity makes LSPR an excellent tool for biosensing applications, as changes in the local refractive index near the nanoparticle surface (due to biomolecular binding events) result in measurable shifts in the LSPR spectrum [94]. Unlike SPR, which requires a planar metal surface, LSPR can occur in nanoparticles, allowing for more versatile sensor designs and the possibility of integrating these sensors into a variety of platforms, including hydrogels (Figure 9). This shift to LSPR opens up new avenues for creating more compact, sensitive, and versatile biosensing devices [95]. Furthermore, LSPR-based sensors can be designed to target specific biomolecules by functionalizing the nanoparticle surface with selective recognition elements. The ability to tune the optical properties of nanoparticles through their physical parameters provides a customizable platform for a wide range of biosensing applications, from disease diagnostics to healthcare monitoring [96], [97].

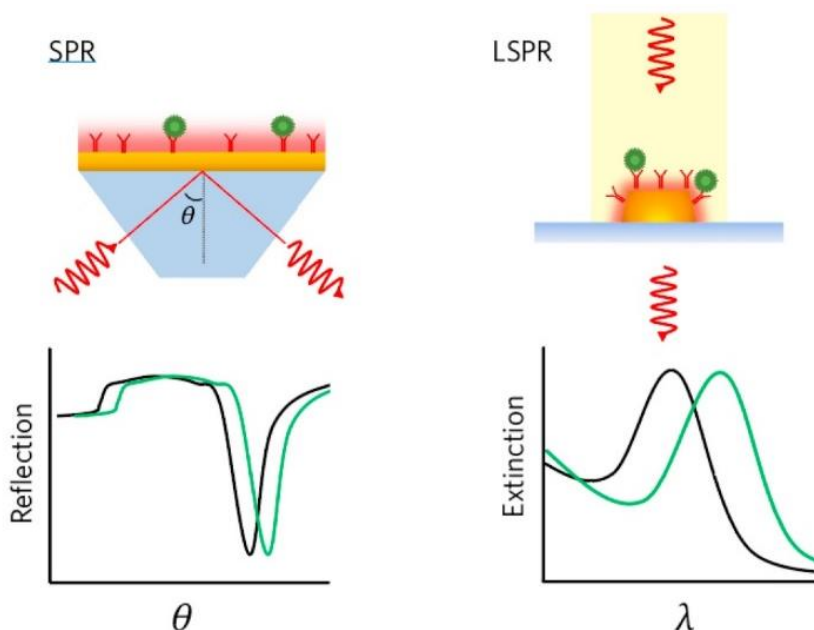


Figure 9. Comparison of SPR and LSPR techniques: The left side illustrates the SPR method, which measures changes in the reflection angle (θ) at a metal-dielectric interface, with a graph showing the corresponding reflection dip. The right side depicts the LSPR method, which measures changes in extinction (absorption/scattering) of light by plasmonic nanoparticles, with a graph showing the shift in the extinction peak (λ). Both techniques are used for sensitive detection of molecular interactions, with SPR monitoring large planar surfaces and LSPR focusing on nanoscale interactions at the surface of nanoparticles [93].

3.2. Brain-machine interfaces

Neurological disorders and injuries pose significant challenges in healthcare, impacting millions worldwide, ranging from traumatic brain injuries to chronic neurodegenerative diseases like Alzheimer's and Parkinson's disease. These conditions can severely disrupt the normal functioning of the nervous system, leading to a wide range of symptoms, including motor dysfunction, memory loss, and altered mental states, which significantly decrease the quality of life [98]. The central nervous system (CNS), comprising the brain and spinal cord, is particularly vulnerable as it has a limited capacity for self-repair, making neuroregeneration a complex and often insurmountable challenge. Consequently, neurological disorders remain some of the most difficult conditions to treat effectively in modern medicine. The peripheral nervous system (PNS) does show some regenerative abilities; however, these are typically limited and slow, often failing to return full function to the affected areas. This disparity in healing capacities highlights the necessity for ongoing research and development in medical technologies and therapies that can bridge the gap in neuro regenerative needs [99].

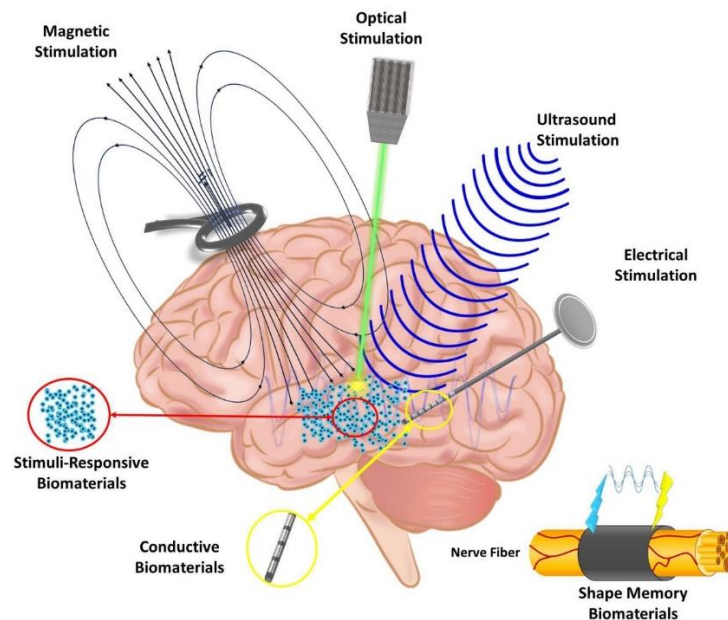


Figure 10. Overview of neural stimulation techniques and biomaterials: The image depicts various brain stimulation methods, including magnetic, optical, ultrasound, and electrical stimulation. It highlights the integration of different biomaterials, such as stimuli-responsive biomaterials, conductive biomaterials, and shape memory biomaterials, to enhance neural interface technologies [99].

One of the promising approaches in advancing neural electrodes involves integrating advanced biomaterials, neuroprotective strategies, and potentially natural compounds with neuroregenerative properties, nicely shown in Figure 10 [100]. These biomaterials significantly enhance neural interfaces' functionality, compatibility, and longevity, facilitating more effective brain-device communication [101]. A less invasive interaction with neural circuits is achieved by applying novel biomaterials at the neural device interface, maintaining long-lasting functionality. For instance, biocompatible coatings, such as nanostructured hydrogels, reduce tissue inflammation and prevent scar tissue formation around the implant, thereby improving the safety and stability of neural interfaces over time. Such biomaterials provide a physical buffer and actively participate in biofunctionalization, enhancing the interface's integration with neural tissue. This is crucial for developing reliable and durable neural communication pathways for applications like brain-machine interfaces (BMIs), neuroprosthetics, and deep brain stimulation [45][102].

Biomaterials have revolutionized the field of neural electrodes, providing critical advancements in the interface between electronic devices and neural tissue. Neural electrodes require materials that can reliably record and stimulate neural activity while minimizing tissue damage and immune responses [103]. Traditional conductive materials like metals and silicon often face challenges related to mechanical mismatch with the soft, delicate brain tissue, leading to inflammation, scarring, and implant failure. Biomaterials, particularly those that are soft, flexible, and biocompatible, offer significant improvements by closely mimicking the mechanical properties of neural tissue, thereby reducing adverse biological responses and enhancing the longevity and functionality of neural implants. Among the various biomaterials, hydrogels, conducting polymers, and composite materials have shown great promise. Hydrogels, with their high water content and tissue-like consistency, provide a hydrated environment that supports cell viability and integration [104]. Conducting polymers, such as polypyrrole and poly(3,4-ethylenedioxythiophene) (PEDOT), combine electrical conductivity with flexibility, making them ideal for neural interfaces. These materials can be engineered to possess specific electrical and mechanical properties that enhance their performance in recording and stimulating neural signals. Additionally, composite materials that incorporate nanoparticles, carbon nanotubes, or graphene within hydrogel matrices or conducting polymers further enhance neural electrodes' electrical, mechanical, and biological properties. This combination of materials science and biomedical engineering is paving the way for next-generation neural electrodes that are more efficient, durable, and capable of providing higher-fidelity neural interfaces for advanced therapeutic and diagnostic applications [105].

4. Aims and thesis

The aim of my study was to design, fabricate and optimize:

- Hydrogel 3D structures based on thermoresponsive PNIPAAm.
- Electrospun nanofibers based on biopolymers with desirable properties.

And

- Fabricate multi-layer combinations of these materials.

With

- Incorporation of plasmonic nanoparticles such as gold and silver.

For

- Biosensing of molecules such as glucose and lysozyme from body fluids (e.g., urine, tears).
- Brain-machine interfaces.

These aims were achieved through

- Extensive revision of available literature.
- Chemical, structural, morphological, optical, photothermal, and mechanical characterization of each component and step.
- Optimizing polymerization steps for hydrogel preparation.
- Optimizing the electrospinning formulations, polymer selection, and conditions for nanofibers.
- Optimizing the plasmonic particles needed for each application.
- Multi-layer composite optimization and introduce a new custom-made approach for measuring the interlayer adhesion strength.
- Antibacterial assessment of bio-inspired platform.
- Biocompatibility assessment of multi-layered platforms.
- Glucose sensing from real human urine samples.
- Colorimetric naked-eye detection of Lysozyme using saline solution
- Lysozyme sensing from real human tear samples.

5. Materials and methods

5.1. Materials

5.1.1. Hydrogel precursor solution

Poly(N-isopropylacrylamide) known as PNIPAAm is the main component of the hydrogel used in the studies. The chemical structure of this polymer can be seen in Figure 11, where this polymer is synthesized via radical polymerization of the monomer N-isopropylacrylamide.

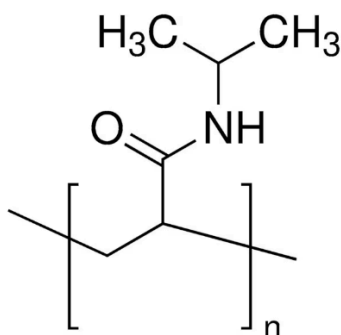


Figure 11. Chemical structure of PNIPAAm

PNIPAAm is non-biodegradable and undergoes a distinct phase transition near human body temperature, specifically around 32°C in pure water. Below this volume phase transition temperature (VPTT), the polymer maintains an extended coil conformation, displaying stable structural properties. Notably, the VPTT can be adjusted to suit different applications, enhancing the polymer's versatility. To successfully reach body temperature for bio-applications, we have used NIPMAAm monomer alongside to reach a VPTT of ~37°C.

To prepare the hydrogel precursor at a concentration of 4.8 wt%, 578.13 mg of NIPAAm, 15.63 mg of NIPMAAm, and 31.25 mg of BIS-Aam (crosslinker) were added to 12.5 mg of Irgacure 2959 (photoinitiator). This mixture was dissolved in 10 ml of deionized water to reach a 95.2 wt% solution. The mixture was wrapped in aluminum foil for protection from light and stirred overnight until complete dissolution. In the case of the addition of chemical initiators, 0.1 wt% APS solution and 0.04% v/v of TEMED were added to the precursor solution. Polymerization was done according to the specifics of each research via UV-irradiation, while the solution was kept in an ice bath to control the temperature rise during polymerization. The general idea of the preparation methods and polymerization steps is shown as schematics in each research paper.

5.1.2. Electrospun nanofibers

Poly(ϵ -caprolactone) (PCL) is one of the most important and most used polymers in biomedical applications. PCL is a biodegradable polyester with a low melting point of around 60°C, which facilitates easy processing and a slow degradation rate, making it ideal for long-term biomedical use. PCL's mechanical properties include high flexibility and good impact resistance, which can be adjusted through copolymerization or blending with other polymers. Its ability to be tailored for specific applications, coupled with its biocompatibility, makes PCL a preferred material in bio-based applications. The chemical structure of PCL can be seen in Figure 12.

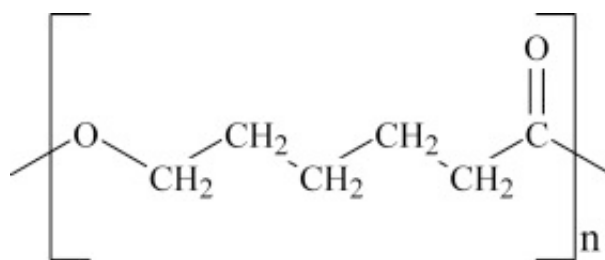


Figure 12. Chemical structure of PCL

To prepare nanofibers via electrospinning, solutions containing PCL at concentrations of 10% and 14% w/v were prepared in a solvent mixture comprising chloroform and DMF (9 : 1) for the electrospinning process. Through a series of optimizations, nanofibers were successfully generated, with key electrospinning parameters set as follows: a flow rate of 0.5 mL h⁻¹, employment of a 26 G needle featuring an outer diameter of 0.45 mm, and an applied voltage of 12.5 kV. In order to collect the resulting nanofibers in either a random or aligned configuration, a flat collector and a drum collector with a rotating speed of 2000 rpm were employed, positioned at a working distance of 15 cm from the electrospinning needle, respectively. Temperature of 20 °C and 40% relative humidity were used during the process.

In order to improve the the hydrophilicity of PCL nanofibers, in one of the research, we have added polyethylene oxide (PEO) to the mixture. PEO is a polymer known for its high solubility in water and excellent biocompatibility, making it a popular choice in pharmaceutical and medical applications. Its properties include a high degree of flexibility and low toxicity, and its role in creating hydrogels that can deliver cells or drugs effectively is particularly valued. Chemical structure of this blend can be seen in Figure 13.

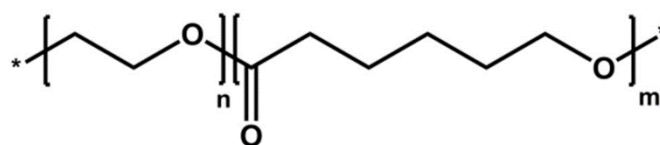


Figure 13. Chemical structure of PCL/PEO

To prepare nanofibers, a solution of 12% (w/v) PCL/PEO in a 75:25 weight ratio was dissolved in an 80:20 volume ratio of dichloromethane to dimethylformamide (DCM:DMF). The solution was stirred overnight at room temperature using a magnetic stirrer before electrospinning. The electrospinning was carried out at a flow rate of 300 $\mu\text{L}/\text{h}$ and a voltage of 15 kV. Fibers were collected on a drum positioned 13 cm from the 21G needle, rotating at 500 rpm, in conditions maintained at approximately 21–22°C with 50% humidity.

Another approach was to use Poly(L-lactide-co- ϵ -caprolactone) (PLCL) copolymer to achieve nanofibers. PLCL (Figure 14) is a copolymer that combines the beneficial properties of polylactic acid (PLA) and PCL, offering a versatile balance between mechanical strength and flexibility. It is known for its good biodegradability and biocompatibility, making it highly suitable for medical applications. PLCL degrades slower than PLA, providing a longer structural support in biomedical implants. Its mechanical properties and degradation rate can be tailored by adjusting the ratio of lactide to caprolactone, allowing for specific applications that require precise control over these parameters.

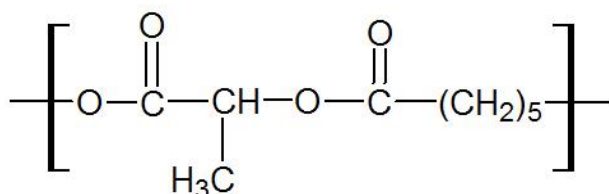


Figure 14. Chemical structure of PLCL.

For the electrospinning process, A 10% (w/w) PLCL solution was prepared in a 90:10 chloroform/DMF mixture and stirred overnight using a magnetic stirrer before electrospinning. The electrospinning parameters were set to a 15 kV positive voltage, 800 $\mu\text{L}/\text{h}$ flow rate, and a 26G needle positioned 15 cm from a rotating drum at 500 rpm to form desirable fibers. The fibers, forming a mat, were collected after utilizing 2 mL of solution to achieve the required thickness under conditions of 25°C and 40% relative humidity.

5.2. Characterization Methods

The list of characterization methods and equipment used in my research are as follows:

- Scanning electron microscopy (SEM)
- Field emission scanning electron microscopy (FE-SEM)
- Transmission electron microscopy (TEM)
- Energy-dispersive X-ray spectroscopy (EDX)
- Atomic force microscope (AFM)
- Dynamic light scattering (DLS)
- Fourier-transform infrared spectroscopy (FT-IR)
- X-ray scattering (XRD)
- Gel permeation chromatography (GPC)
- UV-Vis spectrophotometer
- Fluorometer plate reader
- Ultrasonic Liquid Processor
- Oxygen plasma generator
- Ultra-violet (UV) lamp
- lyophilizer Freeze-dryer
- Contact angle measurement goniometer
- Near-infrared light source (NIR)
- High-resolution thermal camera
- Laser cutting system
- Mini sputter coater
- Texture Analyzer (Tensile and compression mode)
- Macrotensile measurements
- Antibacterial tests
- *In vitro* biological tests (Cell viability by PrestoBlue assay, Live/Dead assay and cell morphology using Actin/Dapi staining)
- Confocal microscope

6. Articles included in the publication cycle of the dissertation

This Ph.D. thesis is presented as a series of research publications. It includes the following cycle of published research articles:

1. Smart plasmonic hydrogels based on gold and silver nanoparticles for biosensing application.

Yasamin Ziai, Chiara Rinoldi, Paweł Nakielski, Luciano De Sio and Filippo Pierini, F.

Current Opinion in Biomedical Engineering, p.100413.

Impact factor: 4.16

2. Chameleon-inspired multifunctional plasmonic nanoplatforms for biosensing applications.

Yasamin Ziai, Francesca Petronella, Chiara Rinoldi, Paweł Nakielski, Anna Zakrzewska, Tomasz A. Kowalewski, Weronika Augustyniak, Xiaoran Li, Antonella Calogero, Izabela Sabała, Bin Ding, Luciano De sio, and Filippo Pierini.

NPG Asia Materials, 14(1), p.18., 2022

Impact factor: 10.76

3. Developing strategies to optimize the anchorage between electrospun nanofibers and hydrogel for multi-layered plasmonic biomaterials.

Yasamin Ziai, Massimiliano Lanzi, Chiara Rinoldi, Seyed Shahrooz Zargarian, Anna Zakrzewska, Alicja Kosik-Kozioł, Paweł Nakielski, and Filippo Pierini*

Nanoscale Advances 6, no. 4 (2024): 1246-1258.

Impact factor: 4.7

4. Lysozyme-sensitive plasmonic hydrogel nanocomposite for colorimetric dry-eye inflammation biosensing.

Yasamin Ziai, Chiara Rinoldi, Francesca Petronella, Anna Zakrzewska, Luciano De Sio, Filippo Pierini.

RSC nanoscale, 2024 (Revision submitted)

Impact factor: 8.3

- 5. Conducting polymer-based nanostructured materials for brain–machine interfaces.**
Yasamin Ziai, Seyed Shahrooz Zargarian, Chiara Rinoldi, Paweł Nakielski, Antonella Sola, Massimiliano Lanzi, Yen Bach Truong, and Filippo Pierini.

Wiley Interdisciplinary Reviews: Nanomedicine and Nanobiotechnology, p.e1895, 2023

Impact factor: 9.42

Additional studies as supporting role in the research:

- 6. *In vivo* chronic brain cortex signal recording based on a soft conductive hydrogel biointerface.**

Chiara Rinoldi, Yasamin Ziai, Seyed Shahrooz Zargarian, Paweł Nakielski, Krzysztof Zembrzycki, Mohammad Ali Haghghat Bayan, Anna Beata Zakrzewska, Roberto Fiorelli, Massimiliano Lanzi, Agnieszka Kostrzewska-Ksiezyk, Rafał Czajkowski, Ewa Kublik, Leszek Kaczmarek, Filippo Pierini
ACS Applied Materials & Interfaces, 15(5), pp.6283-6296, 2022.

Impact factor: 10.38

- 7. Chronic Probing of Deep Brain Neuronal Activity Using Nanofibrous Smart Conducting Hydrogel-Based Brain-Machine Interface Probes**

Seyed Shahrooz Zargarian, Chiara Rinoldi, Yasamin Ziai, Anna Beata Zakrzewska, Roberto Fiorelli, Małgorzata Gazińska, Martina Marinelli, Magdalena Majkowska, Bartosz Mindur, Paweł Hottowy, Rafał Czajkowski, Ewa Kublik, Paweł Nakielski, Massimiliano Lanzi, Leszek Kaczmarek and Filippo Pierini
ACS Nano, 2024 (Submitted)

Impact factor : 16.6

- 8. Multifunctional platform based on electrospun nanofibers and plasmonic hydrogel: A smart nanostructured pillow for near-infrared light-driven biomedical applications.**

Paweł Nakielski, Sylwia Pawłowska, Chiara Rinoldi, Yasamin Ziai, Luciano De Sio, Olga Urbanek, Krzysztof Zembrzycki, Michał Pruchniewski, Massimiliano Lanzi, Elisabetta Salatelli, Antonella Calogero, Tomasz A Kowalewski, Alexander L Yarin, Filippo Pierini
ACS Applied Materials & Interfaces, 12(49), pp.54328-54342, 2020.

Impact factor: 10.38

9. Ultraviolet Light-Assisted Electrospinning of Core-Shell Fully Cross-Linked P (NIPAAm-co-NIPMAAm) Hydrogel-Based Nanofibers for Thermally Induced Drug Delivery Self-Regulation.

Sylvia Pawłowska, Chiara Rinoldi, Paweł Nakielski, Yasamin Ziai, Olga Urbanek, Xiaoran Li, Tomasz Aleksander Kowalewski, Bin Ding, Filippo Pierini.

Advanced Materials Interfaces, 7(12), p.2000247, 2020.

Impact factor: 6.38

10. Advances in Biomaterials and Strategies for Enhancing Bone Tissue Regeneration: A Comprehensive Review

Syed Ahmed Shah, Muhammad Sohail, Paweł Nakielski, Chiara Rinoldi, Shahrooz Zargarian, Alicja Kosik-Kozioł, Yasamin Ziai, Mohammad Ali Haghighat Bayan, Daniel Rybak, Magdalena Bartolewska, Filippo Pierini

Nanotechnology (Under revision)

Impact factor: 3.5

Other publications conducted during PhD studies:

11. Utilization of compressible hydrogels as electrolyte materials for supercapacitor applications.

Amrita Jain*, Yasamin Ziai*, Kamil Bochenek, Sai Rashmi Manippady, Filippo Pierini, Monika Michalska.

RSC advances, 13(17), pp.11503-11512, 2023.

Impact factor: 4.036

12. Laser-assisted fabrication of Injectable Nanofibrous Cell Carriers.

Paweł Nakielski, Chiara Rinoldi, Michał Pruchniewski, Sylvia Pawłowska, Małgorzata Gazińska, Barbara Strojny, Daniel Rybak, Katarzyna Jezierska-Woźniak, Olga Urbanek, Piotr Denis, Emilia Sinderewicz, Wioleta Czelejewska, Joanna Staszkiwicz-Chodor, Marta Grodzik, Yasamin Ziai, Monika Barczewska, Wojciech Maksymowicz, Filippo Pierini

Small, 18(2), p.2104971, 2022.

Impact factor: 13.3

13. Influence of the active layer structure on the photovoltaic performance of water-soluble polythiophene-based solar cells.

Massimiliano Lanzi, Debora Quadretti, Martina Marinelli, Yasamin Ziai, Elisabetta Salatelli, Filippo Pierini.

Polymers, 13(10), p.1640, 2021.

Impact factor: 5.0

14. Ionic Push–Pull Polythiophenes: A Further Step towards Eco-Friendly BHJ Organic Solar Cells

Marinelli, Martina, Massimiliano Lanzi, Filippo Pierini, Yasamin Ziai, Alberto Zanelli, Debora Quadretti, Francesca Di Maria, and Elisabetta Salatelli.

Polymers, 14(19), p.3965, 2022.

Impact factor: 5.0

15. A new alcohol-soluble dye-tetraphenyl porphyrin functionalized copolymer: inside the role as a third component/cathode interlayer in halogen-free OSCs

Marinelli, Martina, Massimiliano Lanzi, Debora Quadretti, Yasamin Ziai, Filippo Pierini, Alberto Zanelli, Riccardo Medri, and Elisabetta Salatelli.

Reactive and Functional Polymers, 2024.

Impact factor: 3.97

16. Influence of conductive carbon content in hydrogel-based composite on morphological and electrical properties for electrochemical energy conversion.

Pawłowska, Sylwia, Karolina Cysewska, Yasamin Ziai, Jakub Karczewski, Piotr Jasiński, and Sebastian Molin.

Beilstein Archives, 2023(1), p.30, 2023.

Impact factor: 3.64

Publication number	IF	Publication Date	Scores MniSW 2023	Citations May 2024
1	4.16	12.2022	20	30
2	10.76	03.2022	140	56
3	4.7	01.2024	20	2
4	8.3	Under revision	140	-
5	9.42	09.2023	140	7

7. Summary of the articles included in the publication cycle of the dissertation

7.1. Smart plasmonic hydrogels based on gold and silver nanoparticles for biosensing application

Before the experimental part of my research, I reviewed the literature and led a review article fused on foundational research in the hydrogel-based materials integrated with plasmonic nanoparticles, specifically for applications in biosensing. This study allows us to understand the development, explore the possibilities, identify the shortcomings, forecast the future prospects of this field for performing experimental parts, and provide guidelines for fellow contributors to the field. Recognizing the critical need for fast, accurate, and reusable biosensors in healthcare, I focused on the integration of these hydrogels as matrices due to their hydrophilic nature and efficient biorecognition capabilities. In this work, I have focused on the application of localized surface plasmon resonance (LSPR) enabled by plasmonic nanoparticles, which enhances biosensor sensitivity and detection limits.

The study was initiated by explaining the optical biosensing principles within the SPR-LSPR method. Gold and silver are the most prominent plasmonic nanoparticles used in biosensing due to their exceptional ability to enhance and localize electromagnetic fields at their surface. This unique property significantly improves the sensitivity and specificity of biosensors by facilitating the detection of low-concentration biomolecules. Hydrogels are highly valued in biosensing for their biocompatibility and high water content, which closely mimic the natural environment of biological markers and particles. These characteristics enable hydrogels to effectively integrate with biological components, enhancing the stability and responsiveness of biosensors to target analytes. By combining these two materials, we can benefit from their combined properties to create a platform that exhibits enhanced sensitivity and responsiveness (Figure 15).

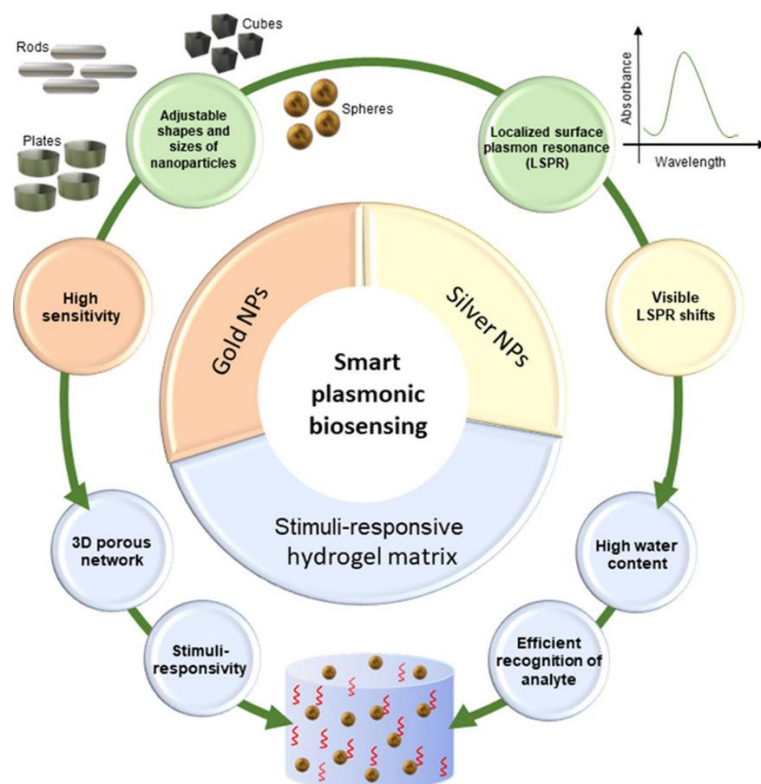


Figure 15. Schematic illustration of the general idea of the review paper, investigating smart plasmonic biosensors using plasmonic particles like gold and silver, introducing the benefits of each component [97].

Gold nanoparticles (AuNPs) are extensively utilized in sensing due to their noticeable shift in absorption peak and elevated sensitivity. Additionally, AuNPs boast chemical stability and have undergone extensive research over the years, leading to advancements in their surface chemistry and biocompatibility. While AuNPs are thoroughly researched for their localized surface plasmon resonances, silver nanoparticles (AgNPs) are notably more effective for sensing applications. Several researches indicate that AgNPs exhibit shifts in their LSPR band that are significantly more pronounced—up to five times greater—when interacting with specific molecules compared to AuNPs. Excellent research papers were investigated in this review to investigate the important aspects of both particles in different systems and various biosensing applications.

Research into plasmonic hydrogels is opening new possibilities in biosensing, modifying the way for advancements in clinical diagnostics and therapeutic monitoring. These materials enhance sensor functionality by bringing in the unique properties of plasmonic nanoparticles, such as their ability to undergo changes in Localized Surface Plasmon Resonance frequencies upon interacting with target

analytes. This tunability, dependent on the nanoparticles' size and shape, allows for the precise tailoring of biosensors to various applications. The integration of such technologies into fabricated materials, such as hydrogel systems, could further enhance the detection processes, making them faster and more efficient.

Looking forward, the potential for innovation in plasmonic hydrogel biosensors is extensive. Enhancements in hydrogel structures could improve the accessibility of target molecules to sensing receptors, optimizing the detection environment. Additionally, incorporating stimuli-responsive materials could expand the capabilities of these biosensors, allowing for more versatile, label-free detection of biomolecules and potentially creating reusable, dual-responsive systems. As research progresses, the synthesis of nanoparticles in diverse shapes and the development of core-shell structures combining different metals may significantly boost the sensitivity and range of these biosensing platforms.

7.2. Chameleon-inspired multifunctional plasmonic nanoplatforms for biosensing applications

In this study, I explore the utilization of chameleon-inspired multifunctional plasmonic nanoplatforms for biosensing applications. The fascination with bioinspired and biomimetic materials stems from their unique ability to interact with light and their potential for sensitive biosensing applications. Specifically, this research develops a nanostructured material platform that mimics the structure of chameleon skin. The aim was to create a device capable of sensing glucose in body fluids without requiring external energy inputs, using the natural responsiveness of the plasmonic materials to environmental changes. This innovative approach holds promise for enhancing non-invasive medical diagnostics and offers a sustainable alternative to traditional power-dependent devices.

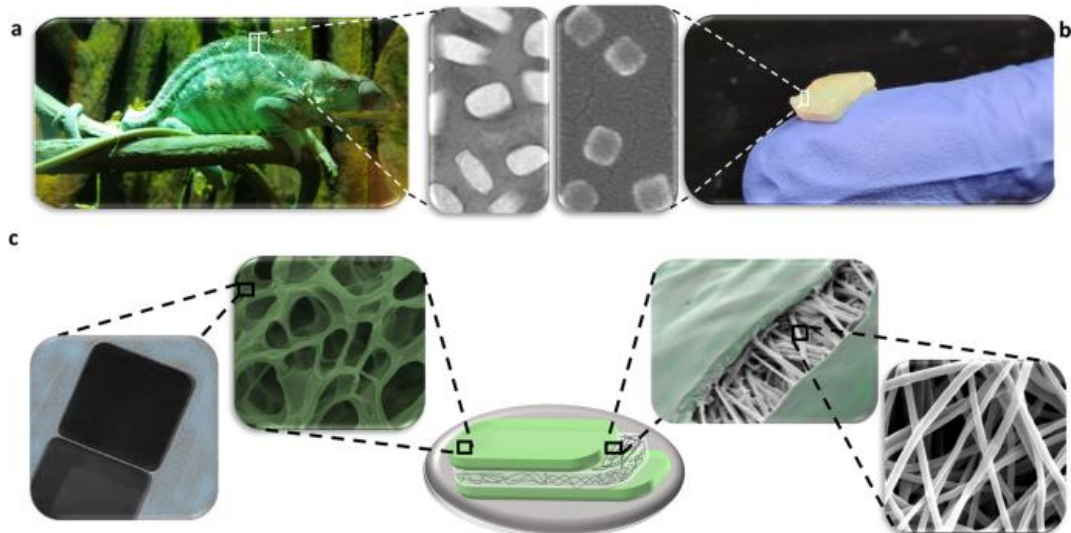


Figure 16. Bioinspired multi-layered platform inspired by particles in chameleon skin. a) nanoparticles in the shape of cubes and rectangles found in the skin of chameleon vs. b) silver nanocubes used in our system, c) multi-layered structure of our platform, showing the porous hydrogel and AgNCs, covering the layer of PCL/PEO nanofiberous mat [48].

The nanoplatfrom as shown in Figure 16 comprises a three-layer structure with two outer layers of a nanocomposite plasmonic hydrogel and an inner layer of an electrospun mat. Silver nanocubes embedded in a poly(*N*-isopropyl acrylamide)-based hydrogel network and layered with an electrospun mat not only to facilitate homogeneous hydrogel coating but also to significantly improve the mechanical and structural properties of the system.

Extensive chemical, morphological, and optical characterizations were done on each component and the whole structure to confirm the multifunctional capabilities of the platform. The synergistic effects of the nanostructured system's components contribute to its photothermal responsivity and antibacterial activity. The optical properties of the silver nanocubes are essential in enabling the platform's use in glucose-sensing applications, as demonstrated through sensitive detection linked to changes in the LSPR properties of the nanocubes.

The practical application of this nanoplatform in glucose sensing was a significant focus of this research, as shown in Figure 17. The platform's ability to detect glucose from urine at concentrations relevant to medical diagnostics without the need for blood samples is a critical advancement. The device's optical response, based on changes in the LSPR absorption peaks induced by varying glucose levels, allows for easy and rapid readings, potentially simplifying diabetes management.

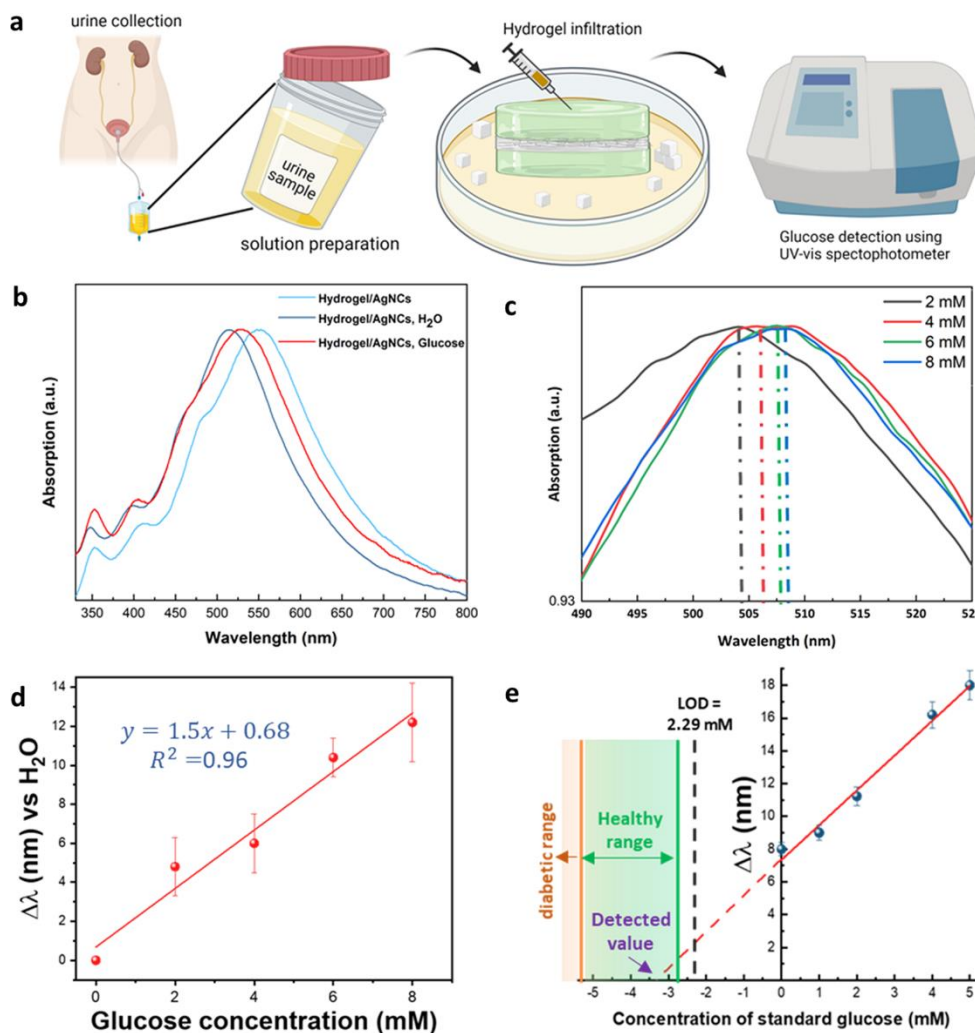


Figure 17. Biosensing application of the platform. a) schematic representation of the glucose monitoring using bodily fluid (e.g., urine). b,c)The absorption spectra of the platform in different environments and the shift in the absorption peaks. d,e) The limit of detection of the system (LOD) was measured, showing the platform's ability to detect both glucose levels in the healthy and diabetic ranges.

In this study, we developed a multifunctional, antibacterial, photothermal-responsive glucose-sensing platform, inspired by chameleon skin. The design features a central layer of PEO/PCL electrospun fibers sandwiched between two layers of P(NIPAAm-co-NIPMAAm)-based hydrogels embedded with silver nanoclusters (AgNCs) for enhanced sensing. These AgNCs confer the hydrogel layers with antibacterial and photothermal properties while enabling glucose detection. Tests with a laser beam and thermal camera confirmed the platform's photothermal response, and its structural integrity was supported by the nanofibrous mat, ensuring durability and consistent performance even under physical stress. The platform efficiently detected glucose in human urine, showcasing its potential for non-invasive glucose monitoring with a lower detection limit compared to typical glucose levels in healthy and diabetic individuals. This system's integration of antibacterial, photothermal, and sensing capabilities marks it as a promising tool for biomedical applications.

7.3. Lysozyme-sensitive plasmonic hydrogel nanocomposite for colorimetric dry-eye inflammation biosensing

In this study, I have focused on non-invasive biosensing of Lysozyme, a key biomarker for various health problems such as dry-eye disease. For this reason, I have fabricated a plasmonic hydrogel nanocomposite tailored for the colorimetric detection of inflammation in dry-eye conditions (Figure 18). The motivation for this research was the critical need for rapid, user-friendly biosensors capable of monitoring lysozyme levels in ocular fluids. The innovative aspect of my research lies in the integration of hydrogel, electrospun nanofibers, and plasmonic nanoparticles to create a highly sensitive, easy-to-use biosensor that operates based on localized surface plasmon resonance (LSPR) which can also detect the changes using a colorimetric approach. This sensor aims to provide non-invasive, fast, visualistic, and accurate monitoring capabilities, making it a promising tool for early diagnosing and managing eye-related health issues.

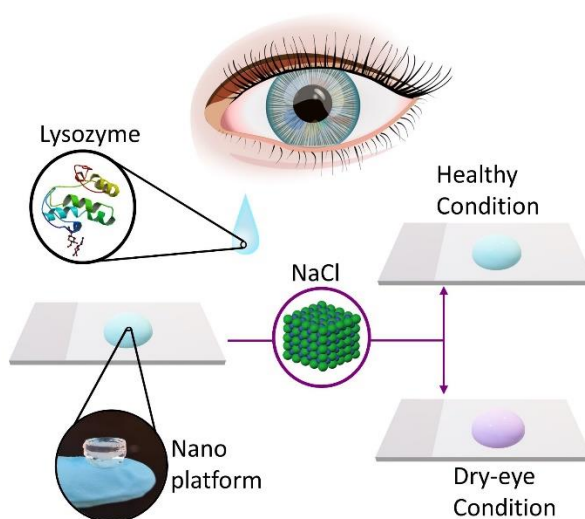


Figure 18. Schematic illustration of the research idea, showing the colorimetric changes in the platform by varying the concentration of lysozyme in the tear.

The fabrication involved a process of integrating poly(L-lactide-co-caprolactone) (PLCL) nanofibers with silver nanoplates (AgNPIs) followed by embedding within a poly(N-isopropylacrylamide)-based hydrogel. This multi-component system brings out the unique properties of each material, providing a stable plasmonic platform that enhances the mobility and integration of biomolecules. I performed comprehensive chemical, structural, thermal, and optical characterization of the entire platform. FE-SEM images of the particles inside the solution and in the structure show their good distribution and stability

without aggregation. Contact angle measurements showed the enhanced hydrophilicity of the fibers after deposition of the nanoparticles, making them better candidates to form a platform with hydrogel materials. After applying the hydrogel layer, the FE-SEM of the cross-section confirms the well-structured platform with a stable and robust penetration of the fibers into the hydrogel matrix. Photothermal imaging of the platform shows the fast responsiveness of the system upon turning on and off the laser, which allows the system to be reusable.

One of the standout features of the biosensor is its ability to provide results that are easily visible to the naked eye, bypassing the need for sophisticated instrumentation. This is particularly advantageous for point-of-care diagnostics. Additionally, incorporating stimuli-responsive hydrogels allows for reversible physical changes in the biosensor's structure in response to environmental stimuli, which can be used to fine-tune the sensing mechanism.

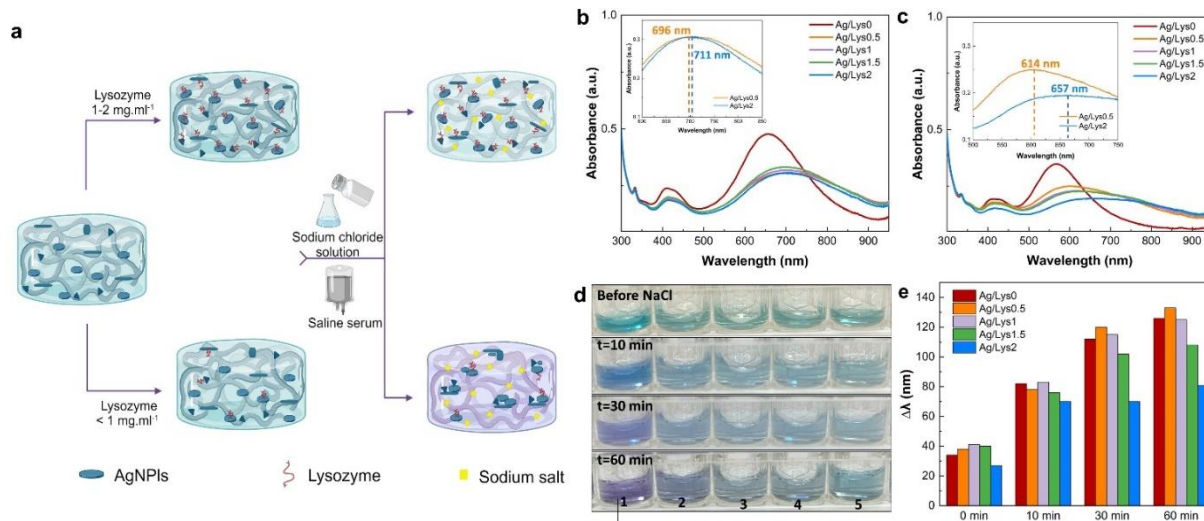


Figure 19. a) Scheme of the procedure explaining the chemistry of colorimetry detection mechanism upon the addition of NaCl salt present in the saline serum. b-c) Absorbance vs. wavelength of the samples with different amounts of lysozyme before and after adding salt. d) Photographs of the aqueous solutions containing silver nanoplates show the color change of the solutions upon the addition of salt over time. e) $\Delta\lambda$ is presented with respect to the measured time points.

The colorimetric assay of the system was done using NaCl as an aggregating agent, which changes the color of the system from blue shades into purple shades when the amount of the lysozyme is insufficient (Figure 19). This colorimetric assay shows its capability to detect lysozyme at concentrations relevant to clinical settings, specifically those found in patients with dry eye syndrome. The sensitivity and timely response of the biosensor were highlighted in the graphs and absorption spectra.

From the LSPR sensing point of view, the absorption spectrum of Ag nanoplates-based platforms shows a peak in absorption intensity at 540nm with notable features attributed to the plasmonic properties of AgNPs. Notably, the derivative analysis highlights distinct shifts in the plasmon band dependent on nanoparticle shape and the surrounding medium's refractive index, which is useful for biosensing applications such as lysozyme detection. Experimental setups using these platforms demonstrate their capability to respond to changes in lysozyme concentration in real human tears, suggesting potential for non-invasive monitoring of biomarkers in body fluids like tears, indicating possible medical applications for monitoring physiological changes.

In this research, I successfully integrated several advanced materials to construct a novel biosensor that significantly improves the ease and accuracy of monitoring dry-eye inflammation. The lysozyme-sensitive plasmonic hydrogel nanocomposite represents a significant approach in the field of biosensing, particularly for ocular health monitoring. Its development addresses a vital clinical need and showcases the potential of hybrid biomaterial systems in improving diagnostic methodologies. The findings from this study could pave the way for further innovations in biosensor technology, potentially expanding its applications beyond eye health to other biomarker detections in medical diagnostics.

7.4. Developing strategies to optimize the anchorage between electrospun nanofibers and hydrogel for multi-layered plasmonic biomaterials

In recent years, biomedical materials have significantly progressed, particularly in developing structures and platforms tailored explicitly for unique applications. These advancements have aimed to use the capabilities of various materials at the same time while addressing their inherent limitations. A particularly promising approach involves using composite materials, which combine the strengths of multiple materials within a single platform. Among these composites, the combination of hydrogels and fibers has garnered substantial attention due to the potential synergistic benefits they offer while mitigating the respective shortcomings of each material. To address all the aspects of my research, I conducted a study focusing on multi-layered biomaterial structures as part of my PhD work. As I have utilized hydrogels and nanofibrous mats to create composite layers, providing a stable platform is critical from a fabrication perspective. Ensuring a robust and stable interconnection among these layers is essential, mainly since the applications may involve physical deformations.

The primary aim of this study was to explore the strategic optimization of the anchorage between electrospun nanofibers and hydrogels in multi-layered plasmonic biomaterials. This research focused on the influence of fiber dimensions, orientation, and surface modifications on the nanofibrous layer and the hydrogel layer's crosslinking density on their inter-layer interface. The ultimate goal as illustrated in Figure 20 was to determine the optimal conditions for these interfaces to enhance the functional integrity and structural stability of the resultant multi-layered biomaterials in their intended biomedical applications.

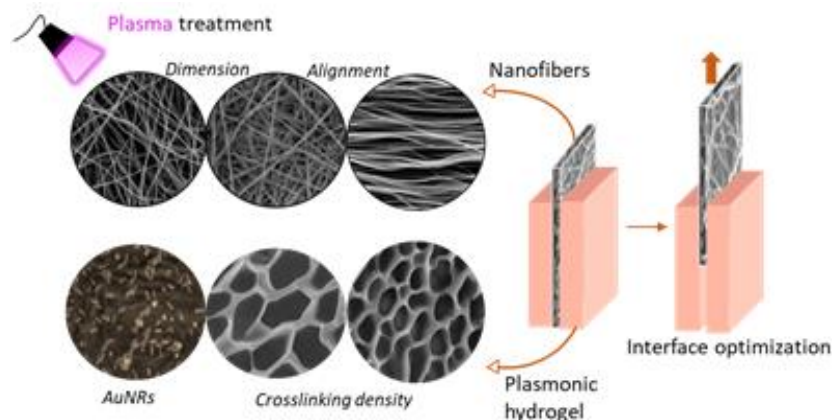


Figure 20. Overview of the tested parameters and the pull-out mechanical test done on the nanoplateforms [23].

Different samples were prepared with 10% and 14% solutions, each providing fiber dimensions less and more than $1\mu\text{m}$, respectively. In the electrospinning process, each nanofibrous mat was collected on both flat and drum collectors. The surface of the nanofibers was treated with plasma before the hydrogel layer was applied. The hydrogel precursor solution was prepared with either a photo-initiator (Ph-P) or a photoinitiator and chemical initiator (Ph-P+C-P).

Thorough structural, chemical, and mechanical investigations were done on the platforms and each component to check their impact on the final structure. In order to determine the adhesion strength between the hydrogel and fibrous layer, a novel pull-out test was designed for the material. This test is a crucial method for assessing the bonding strength between layers in composite materials. It involves embedding a filament or fibers into a hydrogel matrix and then measuring the force required to pull the fiber out. This fiber pull-out test provides essential insights into the durability and integrity of the fiber-matrix interface, influencing the composite's overall structural performance. The adhesion level between the components serves as a reliable measure of the composite's capacity to handle loads and resist deformation. A custom-made setup was designed to facilitate this test and handle the hydrogel, as seen in Figure 21a. Overcoming one of the primary challenges of this test, such as securing the hydrogel within the tensile machine, required an innovative approach. A 3D-printed holder was designed to distribute the pressure exerted by the tensile grips without imposing stress on the hydrogel.

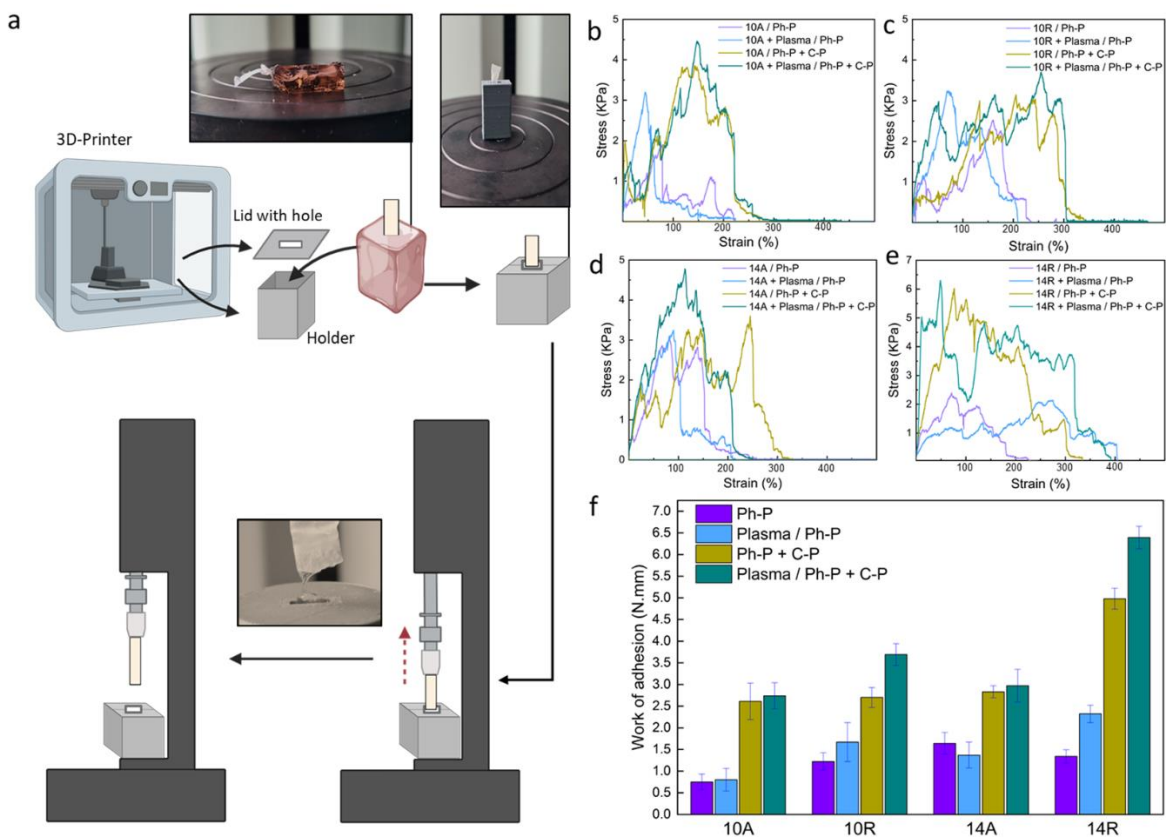


Figure 21. Fiber pull-out test. a) schematic of the custom-made test. b-e) Stress-strain curves for all conditions and f) Nanoplatfom's toughness as an indicative of interlayer adhesion [23].

The study revealed several key findings regarding the interaction between the electrospun nanofibers and hydrogels. Plasma treatment of the hydrophobic nanofibers significantly enhanced the mechanical effort required for fiber extraction from the hydrogels, indicating improved anchorage. This enhancement in anchorage was further corroborated by comprehensive mechanical pull-out tests, which provided insights into the interfacial adhesion and mechanical integrity between the layers. The crosslinking density of the hydrogel layer was a critical factor that influenced the overall properties of the composite materials. Higher crosslinking density led to a more robust interface, which is pivotal for the performance of layered nanostructures under physical stress. The study's findings suggest that the fibers and hydrogels' physical and chemical properties can be finely tuned to create optimized biomaterials that meet the specific needs of various biomedical applications.

Biocompatibility assessments confirmed the potential biomedical applications of the proposed nanoplatfoms. These platfoms demonstrated enhanced structural and mechanical properties and high biocompatibility, which is critical for any biomedical application. The integration of plasmonic

nanoparticles within the hydrogel contributed to the structural integrity and endowed the hydrogels with responsive properties that are beneficial for applications such as biosensing and photothermal therapy. In conclusion, the research provides valuable insights into the design and fabrication of advanced nanocomposite hybrid platforms that leverage the benefits of both hydrogels and nanofibers. The findings from this study highlight the importance of carefully considering the interfacial interactions and mechanical integration in the development of next-generation biomaterials, setting a foundation and approach for examining the stability of multi-layered structures.

7.5. Conducting polymer-based nanostructured materials for brain-machine interfaces

As a part of my research during my PhD, I have also participated in studies regarding the application of hydrogel-based materials for brain-machine interfaces (BMIs) [45]. In order to have a guideline for conducting research, I have done an extensive review of the literature available in this field. In this study, I investigated the potential of conducting polymer-based nanostructured materials for application in BMIs. Integrating these materials into BMIs is crucial due to their inherent properties that align well with the needs of neural interfaces: biocompatibility, suitable electrical conductivity, and mechanical properties comparable to soft brain tissue. My objective was to study the potential properties of these materials to ensure high signal fidelity for both recording and stimulation tasks and address the shortcomings in the field, such as mechanical mismatch that often hampers the efficacy and safety of neural implants. This research is significant as it supports the broader goal of enhancing neuroprosthetic devices, potentially revolutionizing therapeutic approaches for various neurological conditions (Figure 22).

As also mentioned in the introduction, bioelectronic signals are crucial to our body's regular functions, including electrophysiological and biochemical activities, and play a vital role in regulating simple and complex nervous system functions like muscle movements and cognitive processes. However, neurological disorders, injuries, and degenerative conditions can impair these functions, reducing the nervous system's ability to self-repair and leading to long-term impairments. These injuries often result from accidents such as car crashes or falls, affecting millions globally and imposing significant healthcare costs annually. Accurate detection of neural signals is critical for understanding cognitive processes and diagnosing neurological diseases such as schizophrenia and Alzheimer's. Recent advancements have focused on developing electrically conductive devices for bioelectronics, such as brain-machine interfaces (BMIs). These devices function as implantable electrodes that record and digitize brain signals in real-time, facilitating their transfer to computers for analysis and visualization.

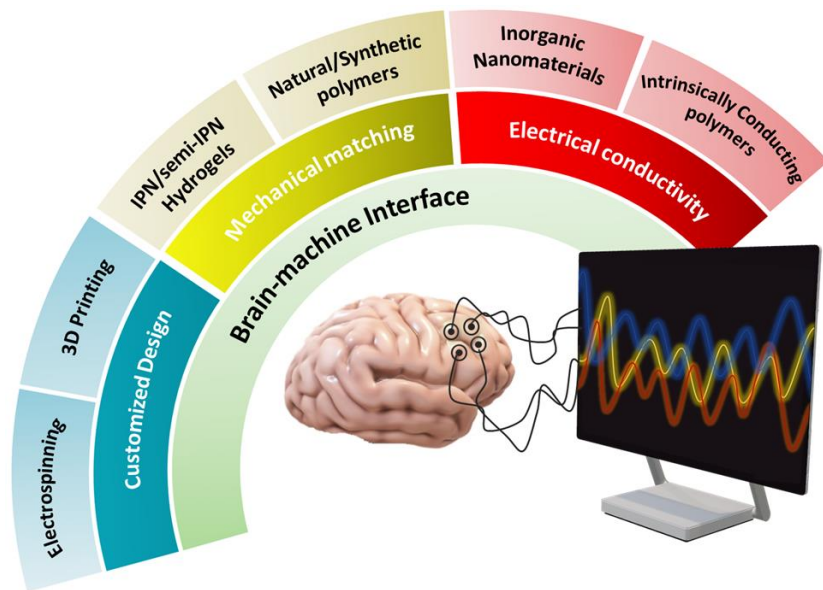


Figure 22. Overview of the designs and characteristics of each biomaterial used for BMIs [45].

Designing optimal electronic devices for brain implantation requires minimal trauma during surgery and flexibility to match brain tissue movements to prevent micromotions. Many current devices, such as those made from metals and silicon, fail to match the mechanical properties of soft brain tissue, leading to poor integration and potential injury at the implant site. This often results in chronic inflammation and decreased signal detection and stimulation efficiency. Ideal materials for brain-machine interfaces (BMIs) should be biocompatible, mechanically similar to brain tissue, and highly conductive to optimize signal acquisition. Researchers focus on developing soft, biocompatible devices using conducting polymers (CPs), which are ideal for brain-machine interfaces due to their tunable physical, electrical, and optical properties. CPs can be engineered to match the mechanical softness of brain tissue, enhancing electrode integration and signal transmission while minimizing mechanical mismatches and interfacial impedance. These properties make CPs excellent for creating and coating biomedical devices, improving their functionality and application specificity in a cost-effective manner.

In this study, I have first focused on intrinsic CPs and blends, where unsaturated bonds are present in their main chain, allowing them to delocalize their electron, making them conduct. These materials from different categories, such as Polyaniline, polypyrrole, and Polythiophene, have been used widely for BMI applications. Another critical category is conductive interpenetrating hydrogels, which are widely used in biomedical fields, as hydrogels can significantly decrease the mechanical mismatch of the system

with the brain tissue. Moreover, hydrogels as 3D polymeric networks can meet the needs of the field, as the water- and ion-rich hydrogels can improve stimulation/recording performance. Also, they can incorporate other conductive materials into their porous structure, which allows bringing even more properties to the mix. Interpenetrating polymer networks (IPNs) are networks formed from two polymers polymerized together without forming chemical bonds between them. These are divided into subclasses like block copolymers, semi-IPNs, and full IPNs based on the crosslinking of the polymeric chains. The advantage of IPNs includes enhanced mechanical stability without phase separation under stress. Combining natural and synthetic polymers allows for customizable chemical properties, achieving synergistic benefits significant in brain-machine interface applications, where conductive polymers (CPs) integrate while maintaining conductivity and hydrogel properties (Figure 23). For electrode materials, inorganic materials, such as noble metallic particles, have been extensively researched for their exceptional electrical conductivity, chemical stability, and biocompatibility. Gold nanoparticles are particularly valued for their ability to easily bind with various biomolecules, facilitating the creation of biomimetic structures. Carbon nanotubes, graphene, and metal particles are a big category of materials used in this application, especially with hydrogels, to improve the applicability of neural electrodes.

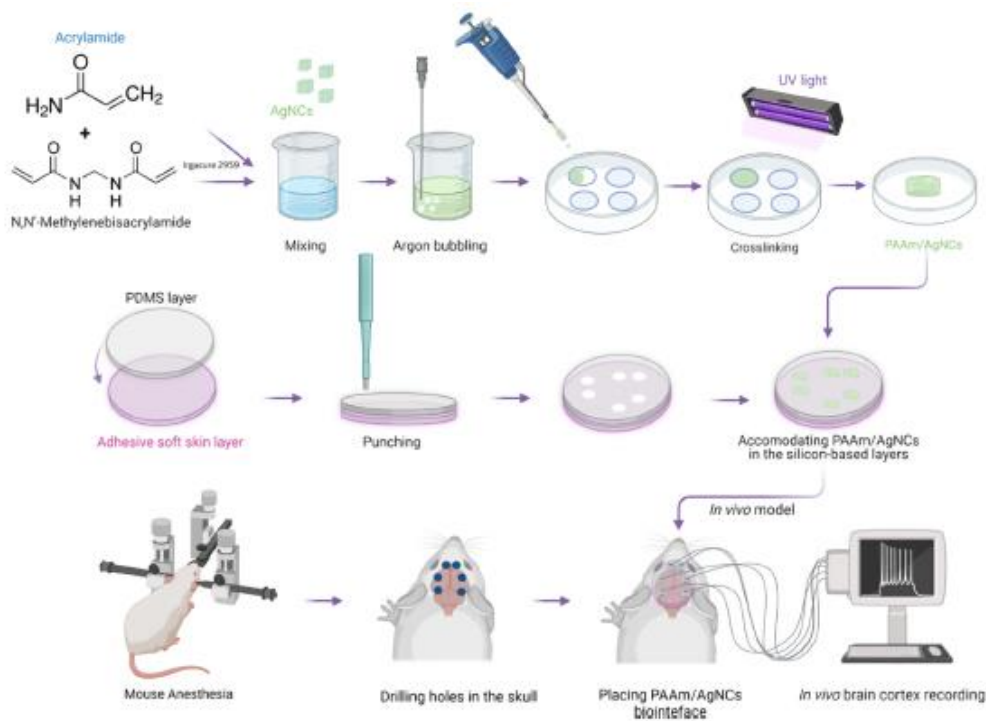


Figure 23. Fabrication and application of the semi-IPN hydrogel-based structure embedded with silver nanocubes. The final platform was placed on the mouse skull to reach the brain cortex via holes to perform EcoG signal acquisition [45].

Apart from the materials that are used in preparing BMIs, the technique to fabricate these structures is also of great significance. Fabrication techniques directly influence the devices' functionality, reliability, and integration with biological tissues. Advanced methods like electrospinning and additive manufacturing are instrumental in creating nanostructured materials that are essential for enhancing signal accuracy and device longevity. The two primary techniques in the field are electrospinning and additive manufacturing.

Electrospinning allows for producing ultra-fine fibers with diameters in the nanometer range, providing a high surface area-to-volume ratio. This high surface area is advantageous for increasing biosensors' electrical conductivity and sensitivity, crucial for capturing minute neuroelectrical activities. Furthermore, the porous structure of electrospun fibers facilitates better integration with neural tissues, promoting cell adhesion and growth. Additive manufacturing, or 3D printing, offers bespoke fabrication capabilities, enabling the creation of tailored devices that fit the unique anatomical features of individual patients. This customization ensures a better fit and reduces discomfort for BMIs users, enhancing the overall effectiveness of neural signal transmission and reception. Additionally, 3D printing can integrate

multiple materials into a single structure, creating complex, multi-functional devices that can perform several tasks simultaneously. These advanced fabrication techniques pave the way for more sophisticated, efficient, and patient-friendly neuroprosthetic devices.

The new trends in the field highlight the pivotal role of innovative fabrication methods like electrospinning and additive manufacturing. These methods enhance the functional properties of BMIs by enabling precise control over material structures at the nanoscale. Electrospinning is notable for producing nano-fibers that improve the interface with neural tissues, thereby increasing neural recordings' sensitivity and signal clarity. Additive manufacturing supports the customization of implants to match patient-specific anatomical structures, improving comfort and integration. These techniques are crucial for advancing next-generation neural interfaces' practical application and effectiveness. Advancements in neuroscience and neurotechnology have significantly driven the development of BMIs using CPs, which are ideal due to their tunability and excellent biocompatibility. These materials enable the fabrication of devices that integrate closely with brain tissue, reducing inflammatory responses and enhancing the quality of neural signal recordings. Emerging trends include the use of CPs for creating advanced, non-invasive devices with improved electrical and mechanical properties, and the potential for these materials in high-resolution and multifunctional BMIs is particularly promising.

8. Conclusions

In this thesis, I have made an extensive literature study of hydrogel-based materials and investigated nanoplatforms based on the combination of hydrogels and nanofibers incorporated with plasmonic nanoparticles for use in biomedical applications such as biosensing and brain-machine interfaces. The following conclusions can be drawn from conducted studies:

- NIPAAm-based hydrogels were formulated to achieve the VPTT close to the body's temperature to adjust to the bio-based applications. The polymerization steps were optimized, and the final hydrogel was characterized.

- Nanofibrous mats based on PCL, PLCL, and PCL/PEO were formulated, electrospun, and optimized to achieve uniform, defect-less nanofibers for further application.

- Plasmonic nanoparticles such as silver nanocubes, silver nanoplates, and gold nanorods were incorporated into the hydrogel matrix or the surface of nanofibers. The uniform distribution and stability of the nanoparticles were confirmed through investigations to ensure their maximum efficiency for the final application.

- Multi-layered structures based on the combination of materials mentioned above were fabricated, and the impact of the size of the nanofibers, their alignment and surface treatment, and the crosslinking density of hydrogels on the interlayer adhesion strength was examined. This examination was done using a custom-made fiber-pullout experiment to assess the interlayer adhesion and measure the stability of these platforms for any use. Further biocompatibility tests were performed to guarantee the possible biomedical application of such a platform.

- Inspired by the particles in the chameleon skin, silver nanocubes were embedded into the NIPAAm-based hydrogel matrix and layered with a modified PCL/PEO nanofibrous layer, resulting in a stable platform. The platform was used as a non-invasive glucose biosensor with remarkable antibacterial properties and fast photo-thermal responsiveness. Tested with real-human urine samples, the platform showed a limit of detection, which could detect both healthy and diabetic amount levels of glucose.

- PLCL nanofibers were decorated with silver nanoplates and layered with a NIPAAm-based hydrogel layer. This platform was used as a non-invasive biosensor of lysozyme to detect eye inflammation. NaCl was used as an aggregating agent into the matrix to visualize the detection by the naked eye through color change into a purple shade in the case of a healthy amount of lysozyme. The platform's capability for LSPR biosensing was successfully tested and confirmed using the standard solution method and real human tears.

9. Summary and Future Prospects

The purpose of this thesis was to design biomaterials based on hydrogels and nanofibers and to develop composite structures that integrate these materials. Additionally, plasmonic particles were incorporated to enhance the functionality of these composites for biomedical applications. This innovative work bridges materials science and biomedical engineering and indicates the potential of hydrogel-based materials combined with plasmonic nanoparticles for use in biosensing and brain-machine interfaces (BMIs).

The research began with a comprehensive review of the current state of hydrogel-based materials, focusing on their integration with plasmonic nanoparticles to create advanced biosensing platforms. Hydrogels, known for their biocompatibility and high water content, were combined with nanofibers to form composite materials with improved mechanical properties and functional versatility. Incorporating plasmonic nanoparticles such as gold and silver, which exhibit unique optical properties through localized surface plasmon resonance (LSPR), significantly enhanced the sensitivity and detection limits of these biosensors, making them invaluable in biomedical diagnostics. A key achievement in this thesis was the development of NIPAAm-based hydrogels with a VPTT close to body temperature, ensuring their suitability for physiological applications. Defect-free nanofibrous mats were created from polymers using electrospinning techniques. The integration of plasmonic nanoparticles into these matrices was precisely optimized to ensure uniform distribution and stability, which are critical for the performance of the final biomedical platforms. Two significant applications of the developed nanoplatforms were explored in detail. The first application was a non-invasive glucose biosensor inspired by chameleon skin. This platform utilized silver nanocubes embedded in a NIPAAm-based hydrogel matrix layered with a modified PCL/PEO nanofibrous mat. The resulting biosensor demonstrated exceptional antibacterial properties and rapid photo-thermal responsiveness, effectively detecting glucose levels in human urine. This innovative approach shows great promise for diabetes monitoring, providing a non-invasive and reliable diagnostic tool. The second application focused on lysozyme detection for diagnosing eye inflammation. This platform employed PLCL nanofibers decorated with silver nanoplates, layered with a NIPAAm-based hydrogel. It enabled the detection of lysozyme in human tears through a visible color change, offering a non-invasive diagnostic tool for conditions like dry-eye syndrome. This research highlights the potential of these nanocomposites in providing rapid, user-friendly biosensing solutions for various medical conditions.

As a next step, extensive research was conducted on the optimization of anchorage between electrospun nanofibers and hydrogels for multi-layered plasmonic biomaterials aimed at enhancing their functional integrity and structural stability for biomedical applications. The research explores the strategic optimization of the interface between electrospun nanofibers and hydrogels, investigating variables such as fiber dimensions, orientation, and surface modifications alongside the hydrogel's crosslinking density. The study demonstrates that plasma treatment of nanofibers and optimized hydrogel crosslinking significantly improve interlayer adhesion through detailed chemical, structural, and mechanical characterizations, including a novel fiber pull-out test. Biocompatibility of these platforms was also tested to ensure further possible applications amid modifications. These findings are crucial for developing robust, multi-layered plasmonic biomaterials with enhanced functional integrity, suitable for applications like biosensing and brain-machine interfaces, ultimately contributing to more effective and reliable biomedical devices.

Moreover, the thesis explored using polymer-based nanostructured materials in BMIs. Integrating these materials into neural interfaces is crucial due to their biocompatibility, suitable electrical conductivity, and mechanical properties comparable to brain tissue. This research addressed the challenges of mechanical mismatch that often hampers the efficacy and safety of neural implants, paving the way for more reliable and effective neuroprosthetic devices.

The future prospects of this research are vast and promising. Advancements in the design of these biomaterials could lead to the development of more sophisticated biosensing platforms capable of detecting a broader range of biomarkers. This would expand their application beyond glucose and lysozyme to include the detection of cancer markers, infectious agents, and other critical biomolecules. Additionally, integrating stimuli-responsive materials into these nanocomposites could revolutionize drug delivery systems, enabling targeted and sustained release of therapeutic agents with minimal side effects. The development of soft, biocompatible conducting polymers for BMIs holds the potential to significantly enhance neural interfaces, improving their performance in neuroprosthetics and brain signal monitoring.

In conclusion, this thesis not only provides a comprehensive foundation for the development of innovative multi-layered plasmonic biomaterials and their applications in biosensing and BMIs but also sets the stage for future advancements in the field, with significant implications for biomedical diagnostics, therapeutic applications, and beyond.

10. References

- [1] W. He and R. B.-A. plastics engineering Handbook, "Polymeric biomaterials," *Elsevier*, 2017.
- [2] G. Raghavendra and V. K, "Biomaterials: design, development and biomedical applications," *Elsevier*, 2015.
- [3] J. Hollinger, *An introduction to biomaterials*. 2011.
- [4] S. Prete, M. Dattilo, F. Patitucci, G. Pezzi, O. I. Parisi, and F. Puoci, "Natural and Synthetic Polymeric Biomaterials for Application in Wound Management," *J. Funct. Biomater.* 2023, Vol. 14, Page 455, vol. 14, no. 9, p. 455, Sep. 2023.
- [5] J. K. Kim, H. J. Kim, J. Y. Chung, J. H. Lee, S. B. Young, and Y. H. Kim, "Natural and synthetic biomaterials for controlled drug delivery," *Arch. Pharm. Res.*, vol. 37, no. 1, pp. 60–68, Jan. 2014.
- [6] P. Parida, A. Behera, and S. C. Mishra, "Classification of Biomaterials used in Medicine," *Int. J. Adv. Appl. Sci.*, vol. 1, no. 3, pp. 31–35, 2012.
- [7] S. H. R. Ali, M. M. Almaatoq, and A. S. A. Mohamed, "Classifications, Surface Characterization and Standardization of Nanobiomaterials," *Int. J. Eng. Technol.*, vol. 2, no. 3, pp. 187–199, Jun. 2013.
- [8] E. T. J. Chong, J. W. Ng, and P. C. Lee, "Classification and Medical Applications of Biomaterials—A Mini Review," *BIO Integr.*, vol. 4, no. 2, pp. 54–61, 2023.
- [9] L. Nair and C. L.-P. in polymer Science, "Biodegradable polymers as biomaterials," *Elsevier*, 2007.
- [10] K. Rai, Y. Sun, A. Shaliutina-Kolesova, R. Nian, and M. Xian, "Proteins: Natural Polymers for Tissue Engineering," *J. Biomater. Tissue Eng.*, vol. 8, no. 3, pp. 295–308, Sep. 2018.
- [11] M. Puertas-Bartolomé, A. Mora-Boza, and L. García-Fernández, "Emerging Biofabrication Techniques: A Review on Natural Polymers for Biomedical Applications," *Polym.* 2021, Vol. 13, Page 1209, vol. 13, no. 8, p. 1209, Apr. 2021.
- [12] A. Aldana, F. Valente, R. Dilley, and B. D. Bioprinting, "Development of 3D bioprinted GelMA-alginate hydrogels with tunable mechanical properties," *Elsevier*, 2021.
- [13] M. F. Maitz, "Applications of synthetic polymers in clinical medicine," *Biosurface and Biotribology*, vol. 1, no. 3, pp. 161–176, Sep. 2015.
- [14] H. Tian, Z. Tang, X. Zhuang, X. Chen, and X. Jing, "Biodegradable synthetic polymers: Preparation, functionalization and biomedical application," *Prog. Polym. Sci.*, vol. 37, no. 2, pp. 237–280, Feb. 2012.

- [15] S. Bhatia, "Natural Polymers vs Synthetic Polymer," *Nat. Polym. Drug Deliv. Syst.*, pp. 95–118, 2016.
- [16] R. Fazel-Rezai, "BIOMEDICAL ENGINEERING – FROM THEORY TO APPLICATIONS Edited by Reza Fazel-Rezai," p. 498, 2011.
- [17] "Biomedical Applications of Metals."
- [18] T. Kokubo, H. Kim, ... M. K.-... the A. C., and U. 2000, "Novel ceramics for biomedical applications," *inis.iaea.org*.
- [19] Y. Zhang and ... B. L. B. M. R. P. B., "Long-term strength of ceramics for biomedical applications," *Wiley Online Libr.*, vol. 69, no. 2, pp. 166–172, May 2004.
- [20] L. Ghasemi-Mobarakeh, D. Kolahreez, S. Ramakrishna, and D. Williams, "Key terminology in biomaterials and biocompatibility," *Curr. Opin. Biomed. Eng.*, vol. 10, pp. 45–50, Jun. 2019.
- [21] D. F. Williams, "There is no such thing as a biocompatible material," *Biomaterials*, vol. 35, no. 38, pp. 10009–10014, Dec. 2014.
- [22] D. F. Williams, "On the nature of biomaterials," *Biomaterials*, vol. 30, no. 30, pp. 5897–5909, Oct. 2009.
- [23] Y. Ziai *et al.*, "Developing strategies to optimize the anchorage between electrospun nanofibers and hydrogels for multi-layered plasmonic biomaterials," *Nanoscale Adv.*, vol. 6, no. 4, pp. 1246–1258, Feb. 2024.
- [24] M. Saini, Y. Singh, P. Arora, V. Arora, and K. Jain, "Implant biomaterials: A comprehensive review," *World J. Clin. Cases WJCC*, vol. 3, no. 1, p. 52, Jan. 2015.
- [25] M. Capurro and F. Barberis, "Evaluating the mechanical properties of biomaterials," *Biomater. Bone Regen. Nov. Tech. Appl.*, pp. 270–323, Jan. 2014.
- [26] L. Wang, C. Wang, S. Wu, Y. Fan, and X. Li, "Influence of the mechanical properties of biomaterials on degradability, cell behaviors and signaling pathways: current progress and challenges," *Biomater. Sci.*, vol. 8, no. 10, pp. 2714–2733, May 2020.
- [27] J. Kohn, "New approaches to biomaterials design," *Nat. Mater. 2004 311*, vol. 3, no. 11, pp. 745–747, 2004.
- [28] S. Preethi Soundarya, A. Haritha Menon, S. Viji Chandran, and N. Selvamurugan, "Bone tissue engineering: Scaffold preparation using chitosan and other biomaterials with different design and fabrication techniques," *Int. J. Biol. Macromol.*, vol. 119, pp. 1228–1239, Nov. 2018.
- [29] N. G. Rim, C. S. Shin, and H. Shin, "Current approaches to electrospun nanofibers for tissue engineering," *Biomed. Mater.*, vol. 8, no. 1, p. 014102, Jan. 2013.
- [30] M. Doostmohammadi, H. Forootanfar, and S. Ramakrishna, "Regenerative medicine and drug

- delivery: Progress via electrospun biomaterials,” *Mater. Sci. Eng. C*, vol. 109, p. 110521, Apr. 2020.
- [31] S. Agarwal, J. Wendorff, and A. G.- Polymer, “Use of electrospinning technique for biomedical applications,” *Elsevier*, 2008.
- [32] N. Bhardwaj and S. K.-B. Advances, “Electrospinning: A fascinating fiber fabrication technique,” *Elsevier*, 2010.
- [33] B. Dhandayuthapani, Y. Yoshida, and ... T. M.-, “Polymeric scaffolds in tissue engineering application: a review,” *Int. J. Polym. Sci.*, 2011.
- [34] H. P. S. Abdul Khalil, A. H. Bhat, and A. F. Ireana Yusra, “Green composites from sustainable cellulose nanofibrils: A review,” *Carbohydr. Polym.*, vol. 87, no. 2, pp. 963–979, Jan. 2012.
- [35] J. Bullon *et al.*, “Unique Fiber Morphologies from Emulsion Electrospinning—A Case Study of Poly(ϵ -caprolactone) and Its Applications,” *Colloids Interfaces 2023, Vol. 7, Page 19*, vol. 7, no. 1, p. 19, Feb. 2023.
- [36] A. T. Odularu, “Basic Principles of Electrospinning, Mechanisms, Nanofibre Production, and Anticancer Drug Delivery,” *J. Chem.*, vol. 2022, 2022.
- [37] J. Xue, T. Wu, Y. Dai, and Y. Xia, “Electrospinning and electrospun nanofibers: Methods, materials, and applications,” *Chem. Rev.*, vol. 119, no. 8, pp. 5298–5415, Apr. 2019.
- [38] L. Sultan Lipol and M. M. Rahman, “Electrospinning and Electrospun Nanofibers,” *World J. Nano Sci. Eng.*, vol. 06, no. 02, pp. 45–50, 2016.
- [39] D. Gospodinova and ... N. T.-, “Design Modifications in Electrospinning Setup for Medical Patches,” *12th Electr. Eng. Fac. Conf.*, 2020.
- [40] T. Lin, “Nano fibers - Production, properties and functional,” p. 468, 2011.
- [41] U. Stachewicz, T. Qiao, S. Rawlinson, F. A.-A. Biomaterialia, and undefined 2015, “3D imaging of cell interactions with electrospun PLGA nanofiber membranes for bone regeneration,” *Elsevier*.
- [42] U. Stachewicz, T. Qiao, and S. Rawlinson, “3D imaging of cell interactions with electrospun PLGA nanofiber membranes for bone regeneration,” *Elsevier acta Biomater.*, 2015.
- [43] H. Nazari *et al.*, “Incorporation of two-dimensional nanomaterials into silk fibroin nanofibers for cardiac tissue engineering,” *Polym. Adv. Technol.*, vol. 31, no. 2, pp. 248–259, Feb. 2020.
- [44] S. Agarwal, J. H. Wendorff, and A. Greiner, “Use of electrospinning technique for biomedical applications,” *Polymer (Guildf.)*, vol. 49, no. 26, pp. 5603–5621, Dec. 2008.
- [45] Y. Ziai *et al.*, “Conducting polymer-based nanostructured materials for brain–machine interfaces,” *Wiley Interdiscip. Rev. Nanomedicine Nanobiotechnology*, vol. 15, no. 5, p. e1895, Sep. 2023.
- [46] Y. Liu *et al.*, “Highly Adhesive, Stretchable and Breathable Gelatin Methacryloyl-based Nanofibrous

- Hydrogels for Wound Dressings,” *ACS Appl. Bio Mater.*, vol. 5, no. 3, pp. 1047–1056, Mar. 2022.
- [47] P. Nakielski *et al.*, “Multifunctional Platform Based on Electrospun Nanofibers and Plasmonic Hydrogel: A Smart Nanostructured Pillow for Near-Infrared Light-Driven Biomedical Applications,” *ACS Appl. Mater. Interfaces*, vol. 12, no. 49, pp. 54328–54342, Dec. 2020.
- [48] Y. Ziai *et al.*, “Chameleon-inspired multifunctional plasmonic nanoplatforms for biosensing applications,” *NPG Asia Mater. 2022 141*, vol. 14, no. 1, pp. 1–17, Mar. 2022.
- [49] S. J. Buwalda, K. W. M. Boere, P. J. Dijkstra, J. Feijen, T. Vermonden, and W. E. Hennink, “Hydrogels in a historical perspective: From simple networks to smart materials,” *J. Control. Release*, vol. 190, pp. 254–273, Sep. 2014.
- [50] S. Das, T. Parandhaman, M. D.-G. Chemistry, and U. 2021, “Biomolecule-assisted synthesis of biomimetic nanocomposite hydrogel for hemostatic and wound healing applications,” *RSC*, 2021.
- [51] N. Chirani, H. Yahia, L. Gritsch, F. L. Motta, S. Chirani, and S. Faré, “History and Applications of Hydrogels,” *J. Biomed. Sci.*, vol. 04, no. 02, pp. 1–23, 2021.
- [52] N. A. Peppas and A. S. Hoffman, “Hydrogels,” *Biomater. Sci. An Introd. to Mater. Med.*, pp. 153–166, Jan. 2020.
- [53] O. Okay, “General Properties of Hydrogels,” pp. 1–14, 2009.
- [54] B. Kaczmarek, K. Nadolna, and A. Owczarek, “The physical and chemical properties of hydrogels based on natural polymers,” *Hydrogels Based Nat. Polym.*, pp. 151–172, Jan. 2020.
- [55] T. C. Ho *et al.*, “Hydrogels: Properties and Applications in Biomedicine,” *Mol. 2022, Vol. 27, Page 2902*, vol. 27, no. 9, p. 2902, May 2022.
- [56] A. Jazayeri, K. H., M. Fahmy, and M. Razavi, “Biomaterials for Tissue Engineering - Google Books,” 2017. .
- [57] A. Vedadghavami *et al.*, “Manufacturing of hydrogel biomaterials with controlled mechanical properties for tissue engineering applications,” *Acta Biomater.*, vol. 62, pp. 42–63, Oct. 2017.
- [58] H. Kamata, X. Li, U. Il Chung, and T. Sakai, “Design of Hydrogels for Biomedical Applications,” *Adv. Healthc. Mater.*, vol. 4, no. 16, pp. 2360–2374, Nov. 2015.
- [59] Q. Chai, Y. Jiao, and X. Yu, “Hydrogels for Biomedical Applications: Their Characteristics and the Mechanisms behind Them,” *Gels 2017, Vol. 3, Page 6*, vol. 3, no. 1, p. 6, Jan. 2017.
- [60] Z. Li, Y. Zhou, T. Li, J. Zhang, and H. Tian, “Stimuli-responsive hydrogels: Fabrication and biomedical applications,” *View*, vol. 3, no. 2, p. 20200112, Mar. 2022.
- [61] S. Chatterjee and P. C. L. Hui, “Review of Applications and Future Prospects of Stimuli-Responsive Hydrogel Based on Thermo-Responsive Biopolymers in Drug Delivery Systems,” *Polym. 2021, Vol.*

- 13, Page 2086, vol. 13, no. 13, p. 2086, Jun. 2021.
- [62] X. D. Xu, H. Wei, X. Z. Zhang, S. X. Cheng, and R. X. Zhuo, "Fabrication and characterization of a novel composite PNIPAAm hydrogel for controlled drug release," *J. Biomed. Mater. Res. Part A*, vol. 81A, no. 2, pp. 418–426, May 2007.
- [63] M. Bustamante-Torres, D. Romero-Fierro, B. Arcenales-Vera, K. Palomino, H. Magaña, and E. Bucio, "Hydrogels classification according to the physical or chemical interactions and as stimuli-sensitive materials," *Gels*, vol. 7, no. 4, Dec. 2021.
- [64] D. G. Pedley, P. J. Skelly, and B. J. Tighe, "Hydrogels in Biomedical Applications," *Br. Polym. J.*, vol. 12, no. 3, pp. 99–110, Sep. 1980.
- [65] P. Sánchez-Cid, M. Jiménez-Rosado, A. Romero, and V. Pérez-Puyana, "Novel Trends in Hydrogel Development for Biomedical Applications: A Review," *Polym. 2022, Vol. 14, Page 3023*, vol. 14, no. 15, p. 3023, Jul. 2022.
- [66] J. Zaragoza, S. Fukuoka, M. Kraus, J. Thomin, and P. Asuri, "Exploring the Role of Nanoparticles in Enhancing Mechanical Properties of Hydrogel Nanocomposites," *Nanomater. 2018, Vol. 8, Page 882*, vol. 8, no. 11, p. 882, Oct. 2018.
- [67] L. E. Beckett, J. T. Lewis, T. K. Tonge, and L. S. T. J. Korley, "Enhancement of the Mechanical Properties of Hydrogels with Continuous Fibrous Reinforcement," *ACS Biomater. Sci. Eng.*, vol. 6, no. 10, pp. 5453–5473, Oct. 2020.
- [68] Y. Qiu and K. Park, "Superporous IPN hydrogels having enhanced mechanical properties," *AAPS PharmSciTech*, vol. 4, no. 4, pp. 406–412, 2003.
- [69] W. R. K. Illeperuma, J. Y. Sun, Z. Suo, and J. J. Vlassak, "Fiber-reinforced tough hydrogels," *Extrem. Mech. Lett.*, vol. 1, pp. 90–96, Dec. 2014.
- [70] S. Xu, L. Deng, J. Zhang, L. Yin, and A. Dong, "Composites of electrospun-fibers and hydrogels: A potential solution to current challenges in biological and biomedical field," *J. Biomed. Mater. Res. Part B Appl. Biomater.*, vol. 104, no. 3, pp. 640–656, Apr. 2016.
- [71] H. Khalesi, W. Lu, K. Nishinari, and Y. Fang, "Fundamentals of composites containing fibrous materials and hydrogels: A review on design and development for food applications," *Food Chem.*, vol. 364, p. 130329, Dec. 2021.
- [72] Y. Ziai *et al.*, "Chameleon-inspired multifunctional plasmonic nanoplatfoms for biosensing applications," *NPG Asia Mater. 2022 141*, vol. 14, no. 1, pp. 1–17, Mar. 2022.
- [73] R. J. Miller *et al.*, "Combining electrospun nanofibers with cell-encapsulating hydrogel fibers for neural tissue engineering," *J. Biomater. Sci. Polym. Ed.*, vol. 29, no. 13, pp. 1625–1642, Sep. 2018.

- [74] B. Niemczyk-Soczynska *et al.*, "Hydrogel, Electrospun and Composite Materials for Bone/Cartilage and Neural Tissue Engineering," *Mater. 2021, Vol. 14, Page 6899*, vol. 14, no. 22, p. 6899, Nov. 2021.
- [75] P. Nakielski *et al.*, "Multifunctional Platform Based on Electrospun Nanofibers and Plasmonic Hydrogel: A Smart Nanostructured Pillow for Near-Infrared Light-Driven Biomedical Applications," *ACS Appl. Mater. Interfaces*, vol. 12, no. 49, pp. 54328–54342, Dec. 2020.
- [76] M. O. Teixeira, J. C. Antunes, and H. P. Felgueiras, "Recent Advances in Fiber–Hydrogel Composites for Wound Healing and Drug Delivery Systems," *Antibiot. 2021, Vol. 10, Page 248*, vol. 10, no. 3, p. 248, Mar. 2021.
- [77] F. Ahmad, B. Mushtaq, F. A. Butt, A. Rasheed, and S. Ahmad, "Preparation and characterization of wool fiber reinforced nonwoven alginate hydrogel for wound dressing," *Cellulose*, vol. 28, no. 12, pp. 7941–7951, Aug. 2021.
- [78] A. P. F. Turner, "Biosensors: sense and sensibility," *Chem. Soc. Rev.*, vol. 42, no. 8, pp. 3184–3196, Mar. 2013.
- [79] R. Monošík, M. Stred'anský, and E. Šturdík, "Biosensors - classification, characterization and new trends," *Acta Chim. Slovaca*, vol. 5, no. 1, pp. 109–120, May 2012.
- [80] H. A. Alhadrami, "Biosensors: Classifications, medical applications, and future prospective," *Biotechnol. Appl. Biochem.*, vol. 65, no. 3, pp. 497–508, May 2018.
- [81] F. W. Scheller *et al.*, "Second generation biosensors," *Biosens. Bioelectron.*, vol. 6, no. 3, pp. 245–253, Jan. 1991.
- [82] P. Mehrotra, "Biosensors and their applications – A review," *J. Oral Biol. Craniofacial Res.*, vol. 6, no. 2, pp. 153–159, May 2016.
- [83] U. Chadha *et al.*, "Recent progress and growth in biosensors technology: A critical review," *J. Ind. Eng. Chem.*, vol. 109, pp. 21–51, May 2022.
- [84] V. Naresh and N. Lee, "A Review on Biosensors and Recent Development of Nanostructured Materials-Enabled Biosensors," *Sensors 2021, Vol. 21, Page 1109*, vol. 21, no. 4, p. 1109, Feb. 2021.
- [85] H. Kaur and A. Bhosale, "Biosensors: Classification, Fundamental Characterization and New Trends: A Review," 2018.
- [86] S. M. Borisov and O. S. Wolfbeis, "Optical biosensors," *Chem. Rev.*, vol. 108, no. 2, pp. 423–461, Feb. 2008.
- [87] C. Chen and J. Wang, "Optical biosensors: an exhaustive and comprehensive review," *Analyst*, vol. 145, no. 5, pp. 1605–1628, Mar. 2020.

- [88] A. K. Singh, S. Mittal, M. Das, A. Saharia, and M. Tiwari, "Optical biosensors: a decade in review," *Alexandria Eng. J.*, vol. 67, pp. 673–691, Mar. 2023.
- [89] K. Sharma and M. Sharma, "Optical biosensors for environmental monitoring: Recent advances and future perspectives in bacterial detection," *Environ. Res.*, vol. 236, p. 116826, Nov. 2023.
- [90] N. Khansili, G. Rattu, and P. M. Krishna, "Label-free optical biosensors for food and biological sensor applications," *Sensors Actuators B Chem.*, vol. 265, pp. 35–49, Jul. 2018.
- [91] R. Hill, "Plasmonic biosensors," *Interdiscip. Rev. Nanomedicine Nanobiotechnology*, vol. 7, no. 2, pp. 152–168, Mar. 2015.
- [92] J. Homola, "Present and future of surface plasmon resonance biosensors," *Anal. Bioanal. Chem.*, vol. 377, no. 3, pp. 528–539, Oct. 2003.
- [93] H. Kurt *et al.*, "Nanoplasmonic biosensors: Theory, structure, design, and review of recent applications," *Anal. Chim. Acta*, vol. 1185, p. 338842, Nov. 2021.
- [94] T. Xu and Z. Geng, "Strategies to improve performances of LSPR biosensing: Structure, materials, and interface modification," *Biosens. Bioelectron.*, vol. 174, p. 112850, Feb. 2021.
- [95] F. C. Chien and S. J. Chen, "A sensitivity comparison of optical biosensors based on four different surface plasmon resonance modes," *Biosens. Bioelectron.*, vol. 20, no. 3, pp. 633–642, Oct. 2004.
- [96] S. R. Beeram and F. P. Zamborini, "Selective attachment of antibodies to the edges of gold nanostructures for enhanced localized surface plasmon resonance biosensing," *J. Am. Chem. Soc.*, vol. 131, no. 33, pp. 11689–11691, Aug. 2009.
- [97] Y. Ziai, C. Rinoldi, P. Nakielski, L. De Sio, and F. Pierini, "Smart plasmonic hydrogels based on gold and silver nanoparticles for biosensing application," *Curr. Opin. Biomed. Eng.*, vol. 24, Dec. 2022.
- [98] P. Zarrintaj, M. R. Saeb, S. Ramakrishna, and M. Mozafari, "Biomaterials selection for neuroprosthetics," *Curr. Opin. Biomed. Eng.*, vol. 6, pp. 99–109, Jun. 2018.
- [99] A. Sadeghi, E. Afshari, M. Hashemi, D. Kaplan, and M. Mozafari, "Brainy biomaterials: Latest advances in smart biomaterials to develop the next generation of neural interfaces," *Curr. Opin. Biomed. Eng.*, vol. 25, p. 100420, Mar. 2023.
- [100] B. Ramesh *et al.*, "A Review on Biomaterials for Neural Interfaces: Enhancing Brain-Machine Interfaces," *E3S Web Conf.*, vol. 505, p. 01005, Mar. 2024.
- [101] C. H. Thompson, M. J. Zoratti, N. B. Langhals, and E. K. Purcell, "Regenerative Electrode Interfaces for Neural Prostheses," *Tissue Eng. - Part B Rev.*, vol. 22, no. 2, pp. 125–135, Apr. 2016.
- [102] P. Fattahi *et al.*, "A Review of Organic and Inorganic Biomaterials for Neural Interfaces," *Adv. Mater.*, vol. 26, no. 12, pp. 1846–1885, Mar. 2014.

- [103] R. A. Green, N. H. Lovell, G. G. Wallace, and L. A. Poole-Warren, "Conducting polymers for neural interfaces: Challenges in developing an effective long-term implant," *Biomaterials*, vol. 29, no. 24–25, pp. 3393–3399, Aug. 2008.
- [104] M. Rahmati *et al.*, "Electrospinning for tissue engineering applications," *Prog. Mater. Sci.*, vol. 117, p. 100721, Apr. 2021.
- [105] A. Vázquez-Guardado, Y. Yang, A. J. Bandodkar, and J. A. Rogers, "Recent advances in neurotechnologies with broad potential for neuroscience research," *Nat. Neurosci. 2020 2312*, vol. 23, no. 12, pp. 1522–1536, Nov. 2020.

11. Original Articles

Smart plasmonic hydrogels based on gold and silver nanoparticles for biosensing application

Yasamin Ziai¹, Chiara Rinoldi¹, Paweł Nakielski¹,
Luciano De Sio^{2,3} and Filippo Pierini¹

Abstract

The importance of having a fast, accurate, and reusable track for detection has led to an increase investigation in the field of biosensing. Optical biosensing using plasmonic nanoparticles, such as gold and silver, introduces localized surface plasmon resonance (LSPR) sensors. LSPR biosensors are progressive in their sensing precision and detection limit. Also, the possibility to tune the sensing range by varying the size and shape of the particles has made them extremely useful. Hydrogels being hydrophilic 3D networks can be beneficial when used as matrices, because of a more efficient biorecognition. Stimuli-responsive hydrogels can be great candidates, as their response to a stimulus can increase recognition and detection. This article highlights recent advances in combining hydrogels as a matrix and plasmonic nanoparticles as sensing elements. The end capability and diversity of these novel biosensors in different applications in the near future are discussed.

Addresses

¹ Department of Biosystems and Soft Matter, Institute of Fundamental Technological Research, Polish Academy of Sciences, Warsaw 02-106, Poland

² Department of Medico-Surgical Sciences and Biotechnologies - Research Center for Biophotonics, Sapienza University of Rome Corso Della Repubblica 79, 04100 Latina, Italy

³ CNR-Lab. Licryl, Institute NANOTEC, Arcavacata di Rende, 87036, Italy

Corresponding author: Pierini, Filippo (fpierini@ippt.pan.pl)

Current Opinion in Biomedical Engineering 2022, 24:100413

This review comes from a themed issue on **Intelligent Biomaterials 2023**

Edited by **Seeram Ramakrishn, Ravin Narai, Himansu Sekhar Nanda, Masoud Mozafari and Gulden Camci-Unal**

For complete overview of the section, please refer the article collection - **Intelligent Biomaterials 2023**

Received 30 May 2022, revised 27 July 2022, accepted 24 August 2022

<https://doi.org/10.1016/j.cobme.2022.100413>

2468-4511/© 2022 The Author(s). Published by Elsevier Inc. This is an open access article under the CC BY-NC-ND license (<http://creativecommons.org/licenses/by-nc-nd/4.0/>).

Keywords

Smart materials, Plasmonic hydrogel, Biosensing.

Introduction

Healthcare is considered one of the most crucial issues challenging science and technology [1]. Having simple,

easy-to-use diagnostic devices for the wide range of biologically significant analytes is essential for any further disease prevention and treatment [2,3]. Improving healthcare is essential in various fields, such as hygiene, drug development, food, environment, forensic, medicine, and clinical diagnoses [4]. Considering the growing release of toxic materials generated and released each year, an early detection of these materials used in all the aforementioned fields is of absolute importance, in order to prompt action to be guaranteed [5]. Biosensors were introduced in the 1960s by Clark and Lyons to meet these requirements. These devices have been developed for glucose determination and named enzyme electrodes [6].

Biosensors are defined as platforms that use specific reactions to detect the effect of electrical, thermal, or optical signals on a medium's chemical, physical, or biological characteristics [5]. Biosensors are usually based on receptors and transducers. Bio-components interact with the target analyte through the receptor; the transducer transfers the result of the reaction into a measurable signal. Bio-components, also known as bio-receptors, may include enzymes, antibodies, nucleic acids, and cells. Depending on the different types of transducers, biosensors can be electrochemical, electrical, optical (absorbance, fluorescence, and chemiluminescence), piezoelectric (also known as mass-sensitive), and thermometric [5,7].

Plasmonic biosensors, as a subgroup of optical biosensors, have been recently exploited due to the possibility of controlling light properties at a nanometric scale [8]. The plasmonic activity of these biosensors is commonly described as the resonant coupling of electromagnetic waves, resulting from the oscillations of free electrons in metals. This physical phenomenon makes it possible to constrain the light within significantly smaller wavelengths than the incident light [9]. Plasmonic biosensors are mainly categorized into two classes of detecting platforms. The first class uses thin metallic films, while the second is based on individual inorganic plasmon resonant nanostructures. In surface plasmon resonance (SPR) biosensors, the incident light is coupled with a thin metallic layer where specific conditions, such as polarization, angle, and wavelength should be met [10]. Following the advancements in nanotechnology, metal nanoparticles (NPs) have been widely explored. In the case of biosensors, these

transducers confine the light within a localized surface, creating what are known as localized surface plasmon resonance (LSPR) biosensors, which allow for a more miniaturized sensing procedure [11]. LSPR-based biosensors differ in NP size, shape, and composition. The versatility of these systems makes them suitable for biological sensor devices since the wavelength can be tuned to not overlap the absorbing spectral features of the biological chromophores, thus resulting in more precise sensing and offering the possibility of multiplex detection [11]. The typical wavelength of LSPR for most noble metals lies in the range of visible to near-infrared regions. This range can vary from shorter to longer wavelengths with low (spherical) and high (rods and prisms) aspect ratios [8]. Nowadays, due to the high efficiency of the LSPR approach, the sensitivity scale of biosensing has been reduced to nano-scales, resulting in more accurate and precise biosensors [12].

Over the years, various types of LSPR biosensors based on polymer substrates have been developed for different applications. Within this framework, gold nanodots have been introduced into polymer films and used to detect biomolecules such as biotin [13]. On the other hand, a plasmonic bioink based on an organosiloxane polymer was also prepared for point-of-care (POC) biosensing [14]. Hydrogels, being a class hydrophilic of 3D-structured biomaterials, have also been used as substrates for plasmonic particles. The unique properties of hydrogels are primarily due to their high water content, which results in their soft and rubbery consistency. Their ability to swell with considerable water uptake makes their structure more similar to living tissues and mimics the extracellular matrix (ECM), which plays a vital role in tissue and organs morphogenesis, as well as cell differentiation and proliferation [15,16]. For these reasons, hydrogel has been considered beneficial in many industrial, environmental, and biomedical fields [17], including electronics [18], tissue engineering [19], drug delivery [20], and biosensing [21].

This report focuses on reviewing the recent developments in smart plasmonic biosensors in the form of hydrogel platforms. Challenges, development, and approaches for assisting in the development of these types of biosensors are the main topics of this article.

Challenges

Currently, array-based LSPR biosensors are the most commonly used in the case of detection of low amounts of molecules, where there is a need to push through the limit of detection of the system and push high throughput capabilities to the limit [22,23]. Even though LSPR-based biosensors have the advantage of detecting several molecules (i.e., number of interactions), their resulting analytical performance is very similar compared to other high-resolution SPR setups

[24]. In detection systems based on conventional 2D methods, low concentration targets were difficult to detect because the exposure to continuous flow results in a limited interaction time with the sensing surface. The drawbacks of these methods can be overcome by using hydrogels, thus exploiting their ability to accommodate a large amount of water without their structure dissolving and their similarity to body tissues. From the sensing standpoint, the biorecognition of the analyte may take place more efficiently and easily when the matrix is in a hydrogel form. In addition, the sensing precision of LSPR-based sensors might be improved as the thin hydrogel can also act as a dielectric optical waveguide [25,26]. Overall, soft materials such as hydrogels can modify sensing properties when used as substrates. Due to their mechanical and structural properties, they offer more sensitive, selective, efficient, and fast sensing capabilities.

Smart biosensors based on plasmonic hydrogels

Two main transduction mechanisms have been introduced in LSPR-based biosensing platforms, including NP aggregation and the change in the refractive index of the system [27]. The first strategy provides the functionalization of plasmonic particles with binding molecules, resulting in a colorimetric variation. The indicator of this variation can be visualized in the LSPR red-shift in the absorbance spectrum, which can be detected by the naked eye. However, some limitations related to the non-specific aggregation have been reported, restricting the application of these platforms to laboratory analysis [28]. The second mechanism provides the immobilization of plasmonic particles on the surface of the substrate, making them refractive index optical sensors [27].

In order to develop LSPR-based optical enzyme biosensors, researchers have focused their attention on stimuli-responsive hydrogels [29]. The physical changes in stimuli-responsive hydrogels in response to marked variations in environmental conditions have been reported previously [30,31]. Stimuli-responsive hydrogels are water-swollen, cross-linked networks that show a reversible change in their physical characteristics in response to specific stimuli. Based on these features, the constituent hydrogels of the stimuli-responsive network can incorporate molecular recognition elements (i.e., enzymes). When the recognition elements react with specific chemical substances, the monomer units bearing the recognition elements undergo a change in either solubility or charge state. A solubility alteration can cause the swelling or shrinking of the hydrogel network. Alternatively, changes in the charge state may result in altered interactions between the charged groups and a variation in the electrolyte concentration in the hydrogel. In both cases, the

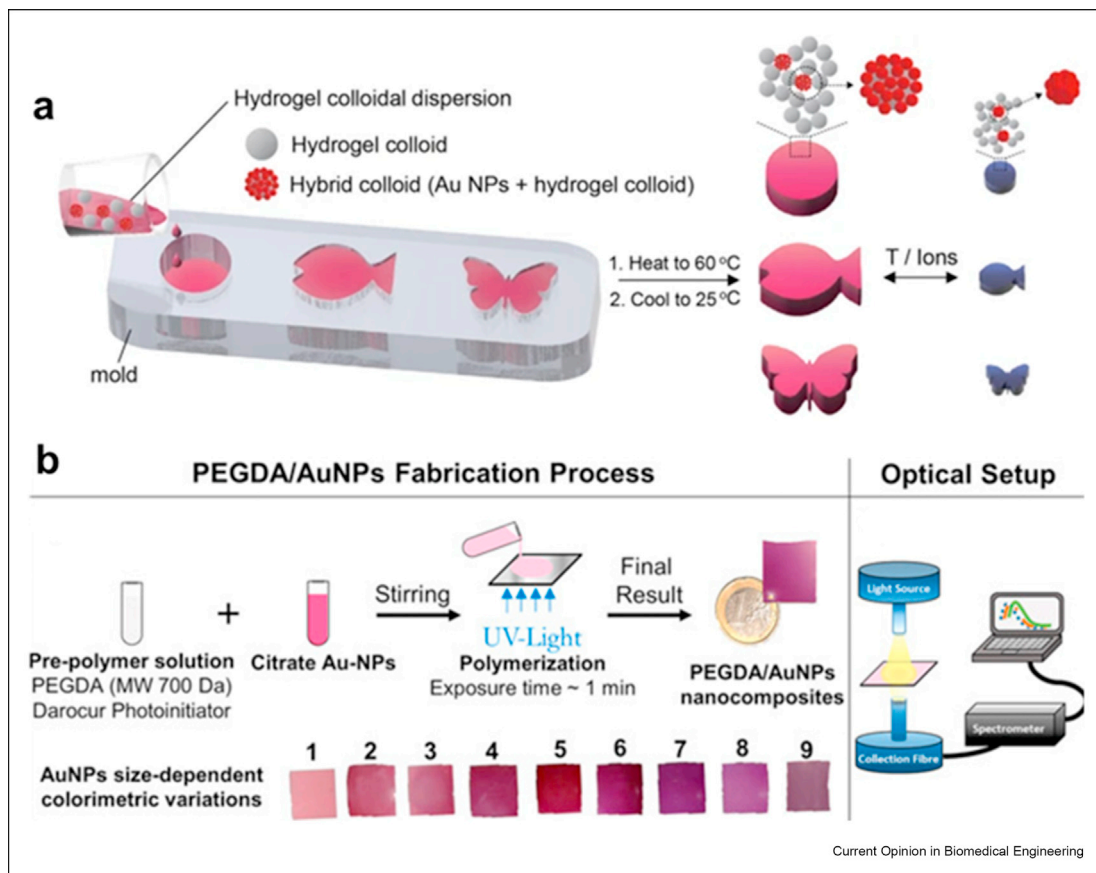
described processes result in changes in the hydrogel volume. Considering these outstanding advantages, several research groups have used stimuli-responsive hydrogels to fabricate biosensors and chemical sensors for medical and environmental applications [32]. Within this framework, scientists have recognized the suitability of these materials for the production of enzyme biosensors and their further exploitation in LSPR-based biosensor development.

Gold nanoparticle-based sensors

LSPR-based biosensors, which function using noble metal nanomaterials, such as gold and silver, have been expected to achieve the highly sensitive detection of target molecules in medical applications. Gold nanoparticles (AuNPs) are widely used in sensing applications due to the visible shift in their absorption peak and high sensitivity. Moreover, AuNPs are chemically stable and have been investigated more through the years and have thus been improved in terms of surface chemistry and biocompatibility [33]. A sensor concept was demonstrated in the work of Muri et al. where they

embedded AuNPs in the 3D hydrogel network of hydrogel fibers. This immobilization of the AuNPs makes the LSPR signal stronger while reducing the analyte binding to plasmonic surfaces [34]. Inspired by animals such as squid, butterflies, and chameleons, biomimetic hydrogel systems have been recently devised to alter their internal nanostructure, undergoing an optical transformation based on changes in their environment. A dual-responsive three-dimensional plasmonic hydrogel platform has been fabricated to indicate volume and color change in an aqueous surrounding. AuNPs embedded in the hydrogel colloid are responsible for the color changes caused by temperature and ion variation in the system. The fabrication process can be seen in Figure 1a, where hydrogel changes according to the temperature are also shown. The volume change as a result of temperature stimuli was best shown here [35]. A polyol-based hydrogel has been fabricated by Randriantsilefisoa et al. while AuNPs are entrapped in the system to offer a stable material to sense the influenza A virus (IAV) and indicate a color change in this medium. Bindings between the IAV and AuNPs

Figure 1



The fabrication process of hydrogel-based biosensors with AuNPs. (a) A schematic showing the process and its responses to temperature and ionic changes [35]. (b) Platform polymerization under UV light and the colorimetric variation in the platform depending on the growth step are also shown [37].

result in an aggregation of the particles, which produce an SPR-induced shift in the absorption spectra, producing a visible color change from red to blue. The reversibility of this phenomenon makes it a good detector for biomolecule quantification [36].

Moreover, an optical 3D biosensor based on poly(ethylene glycol) diacrylate (PEGDA) hydrogel with AuNPs has been fabricated and optimized. These hydrogel patches, having spherical AuNPs, are physically retained in the network and show great stability as well as sensing capability. By optimizing the NPs size and shape, the order of detection indicates that it is a perfect candidate for small molecule (e.g., biotin) detection and can be used in wearable sensors. [Figure 1b](#) shows the polymerization process of the system in between coverslips. UV light has been used here to perform the crosslinking, and NPs with different sizes varying from 20 nm to 70 nm were used [37]. Label-free detection of biomolecules can also benefit from plasmonic hydrogels. The use of the hydrogel matrix provides an environment that resembles the perfect matrix for biomolecular interactions. The porous network with high water content improves the performance of biosensors by capturing more analyte molecules. Recently, a stimuli-responsive hydrogel based on oligo (ethylene glycol) grafted with thermo-responsive polyisocyanates was developed. The gold-coated surface of the sensor is linked to the glycol group to demonstrate the LSPR and has been used as an affinity binding system for the biosensing of biotin [38]. Proteins can also be detected using the same platforms with an LSPR-sensing method. Culver et al. have developed a biosensor to detect proteins, using poly(N-isopropylacrylamide-co-methacrylic acid) (PNM) hydrogels embedded with gold nanoshells. Hydrogels are synthesized on the surface of gold nanoshells, as they can detect changes in the concentration of lysozyme and lactoferrin – the protein biomarkers of chronic dry eye. PNM/gold nanoshells are a suitable material in this case, as the system shows a largely increased refractive index, and a strong red-shift when in contact with human tears [39]. Glucose monitoring apparatus has also been prepared using hydrogel fibers based on acrylamide-based materials, where gold AuNPs are immobilized. Volume expansion which happens as a result of the presence of glucose molecules can modulate the LSPR effect of the hydrogel fibers, allowing quantitative measurements [40].

Sensing environmental molecules, such as arsenic – crucial in the geochemical and anthropogenic fields – can be achieved by using this technique. Poly(N-isopropylacrylamide) (PNIPAAm)-based hydrogel coated on an AuNP surface can provide an LSPR sensing platform for the real-time detection of arsenic. However, this platform offers a wide range of detection potential

with a simple change in the size and shape of plasmonic particles and the concentration of the monomer [41].

Silver nanoparticle-based biosensors

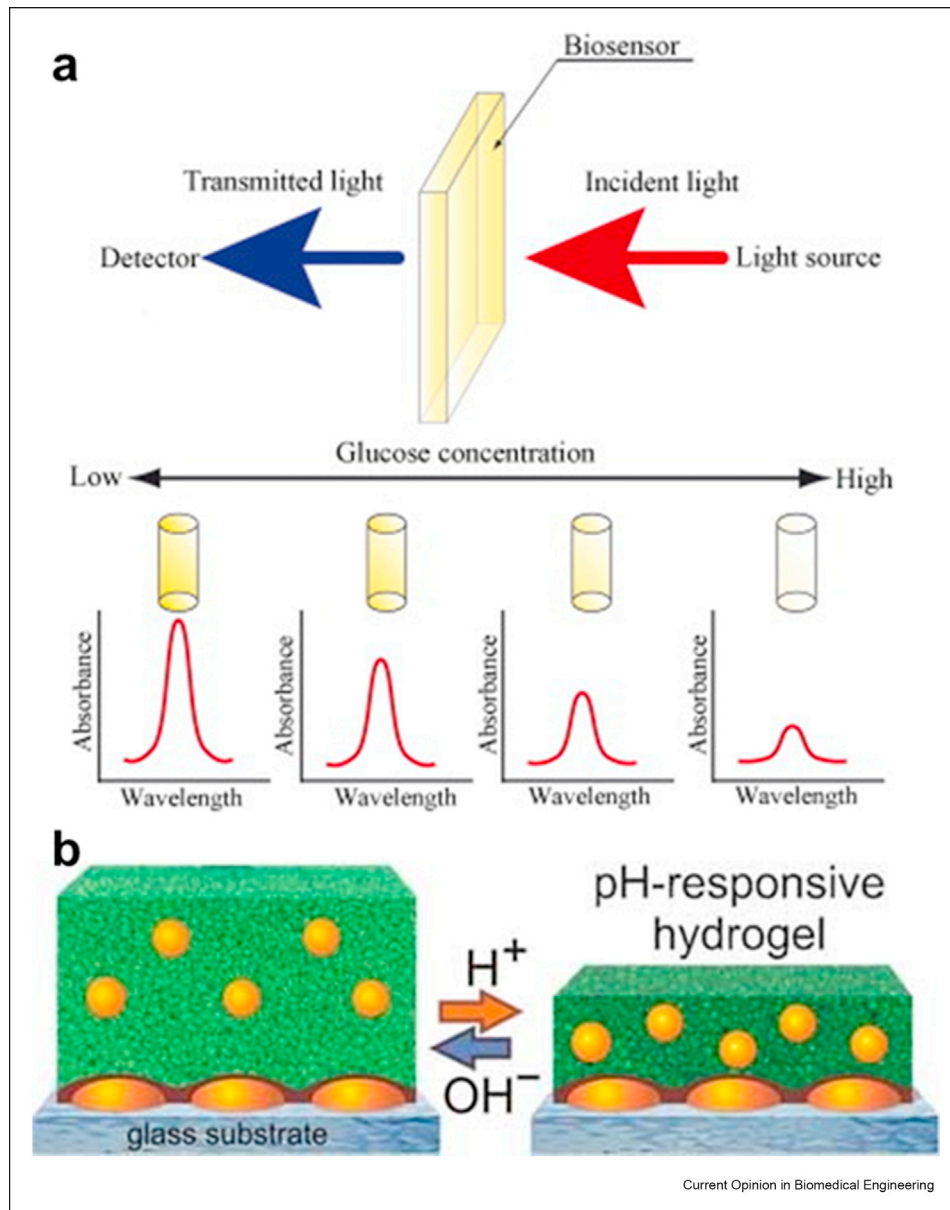
Among metallic NPs exhibiting LSPRs, although AuNPs have been studied in depth, silver NPs (AgNPs) are particularly efficient for sensing purposes [42]. Studies have shown that AgNPs demonstrate shifts in the LSPR band that are five times stronger when they are in contact with specific molecules, compared to AuNPs [43].

Hydrogen peroxide detection is of vital importance because the presence of the substance can be considered an environmental, industrial, or even clinical hazard. Filippo et al. have developed a biosensor that determines the presence of hydrogen peroxide in rainwater, which has a simplified, low-cost fabrication process, and, most importantly, is reusable [44]. This sensor is made of PVA due to its wide range of potential applications in the optical, pharmaceutical, medical, and membrane fields, as well as benefits from AgNPs for LSPR-sensing method. The strong shift in the absorption spectra and the color changing of the platform prove the LSPR sensing of the hydrogel.

Glucose is one of the most important biomolecules that requires precise detection to prevent and treat the complications associated with diabetes. Silver NPs have been widely used in this specific molecule detection. Endo et al. worked on a stimuli-responsive acrylamide-based hydrogel with polyvinylpyrrolidone (PVP) covered with silver NPs to entrap glucose molecules [45]. Stimuli-responsive hydrogels contain molecular recognition elements – such as enzymes – that specifically react with the analyte. This recognition event causes the stimuli-responsive hydrogels to swell due to an increased osmotic pressure. The swelling of stimuli-responsive hydrogels increases the average internal distance between one noble metal particle and another, thus reducing the LSPR absorbance strength [45]. [Figure 2a](#) shows the principles of the sensing platform with the use of different glucose solution concentrations. Changes in the absorption peak define the effect of surroundings on the sensing precision. Images taken of differences in the color strengths shows that the variations in AgNPs concentrations could be observed with the naked eye. Hence, AgNPs concentrations were found to affect the optical characteristics of the LSPR-based optical enzyme biosensor.

A novel glucose sensor was fabricated by Tokarev et al. as a combination of a pH-responsive hydrogel incorporated with AgNPs for two critical applications: the analysis of biomolecules (biosensing) and the probing (monitoring) of the local properties of biomaterials. [Figure 2b](#) shows the schematic of this construct under pH variation, and changes in the volume of the hydrogel can be observed. LSPR effects in noble metal NPs are observed through

Figure 2

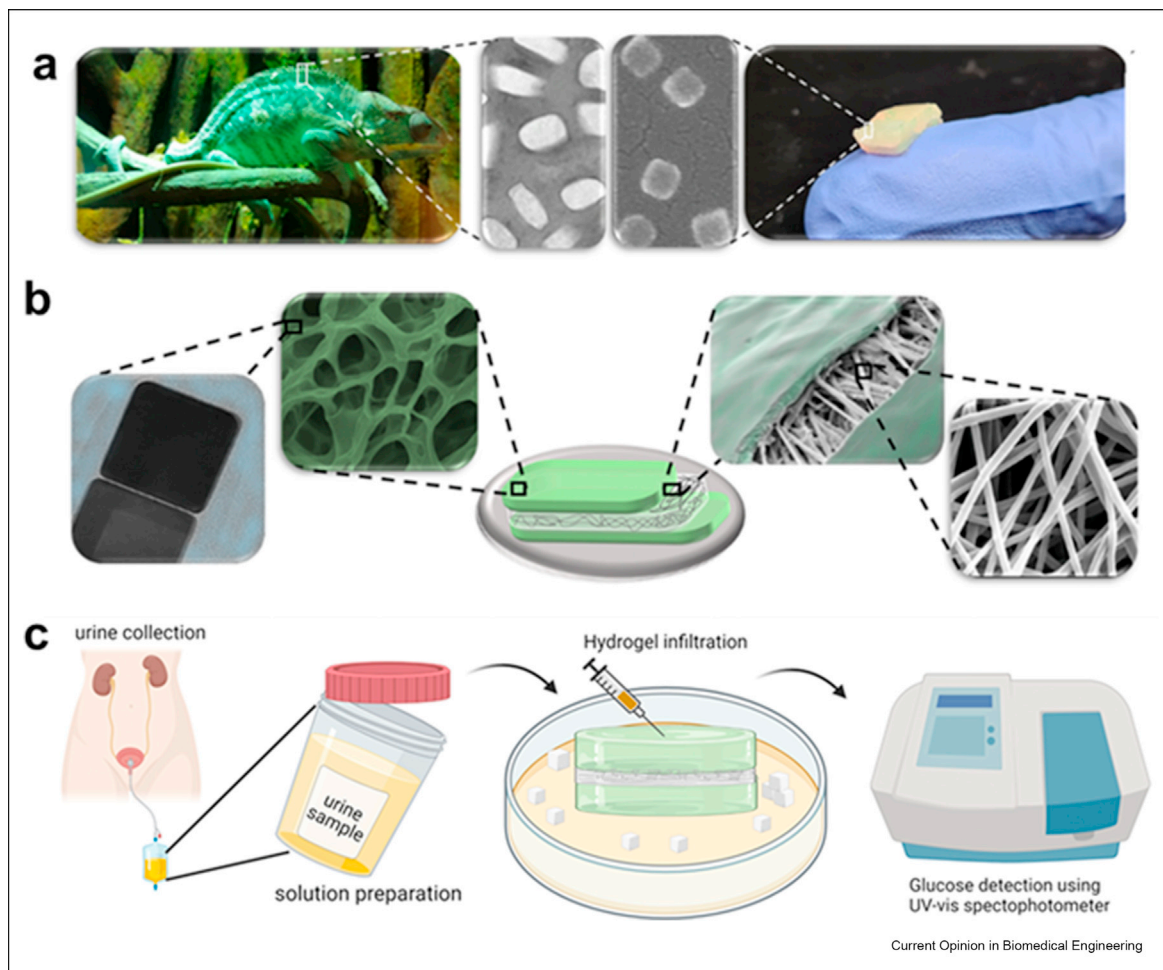


Stimuli-responsive hydrogel embedded with AgNPs. (a) Schematic illustration of detection principle of LSPR-based optical enzyme biosensor [45]. (b) Schematic of volume change in the construct under pH variation [46].

color variations by the naked eye or in a visible light spectrum that reveals characteristic absorbance bands. LSPR spectra are also sensitive to variations in the immediate particle environment. In particular, changes in the refractive index of the environment in the close vicinity to particle surface or in the interparticle plasmon coupling result in an alteration of the spectrum [46]. Recently, a photo-thermal responsive polymer combined with AgNPs has been investigated as a multifunctional platform to detect glucose level in urine. Ziai *et al.* used a poly(*N*-isopropylacrylamide) (PNIPAAm)-based hydrogel matrix embedded with Ag

nanocubes, inspired by the unique features of chameleon skin that changes its color as a result of the light–matter interactions in the skin layers. The inspiration and the similarities between the structure of NPs can be seen in Figure 3a. Hydrogel layers were made with a layer of electrospun nanofibers. The image of the construct can be seen in Figure 3b, where each layer is shown separately, with an image from the intersection, verifying the layer-by-layer construction. Fast photo-thermal responsiveness and significant red-shift in the LSPR absorbance peak in the presence of different glucose concentrations are indicators of efficient sensing

Figure 3



Chameleon-inspired platform, based on AgNPs. (a) Inspiration from the layers of chameleon skin to choose the silver nanocubes as the plasmonic particle. (b) Construction based on a layer-by-layer composite, with two layers of plasmonic hydrogel and one layer of electrospun nanofibers in between them. (c) Application of the biosensor as a glucose detector, using urine as the body fluid [21].

features of the platform [21]. This platform was used as a biosensor to detect glucose in the urine of healthy and diabetic people, where sample solutions were infiltrated into the platform, and the absorbance peak was determined via UV–Vis (Figure 3c).

Future perspectives and conclusion

Studies on plasmonic hydrogels have upgraded the biosensing field. As a result, clinical and therapeutic detection and medication are expected to be achieved quickly, easily, and efficiently within a short time. Plasmonic particles are responsible for changes in relevant SPR frequencies when in contact with the target analyte. These changes are significantly dependent on the size and shape of NPs, thus making it possible to tune the properties to meet the requirements for different applications. The greater interest in LSPR-based biosensors compared to regular SPR sensors is mainly due to their unique features, which allow for

label-free and real-time biomolecular analysis with possible detection of biomolecular interactions (antigen–antibody interaction, DNA hybridization, etc.) at low concentrations.

In addition, the simple detection mechanism of optical-based biosensors makes it possible to be integrated with different sensing platforms for lab-on-a-chip applications.

On the other hand, as 3D nanostructured materials with a considerable amount of water within their structure, hydrogels are powerful platforms for biosensor fabrication. The sensor's performance is determined mainly by the contact between the sensing receptor and the analyte. The structure of hydrogel provides an accessible environment for target molecules to be in contact with the sensing receptor. These 3D matrixes indicate high permeability for small molecules, metabolites, oxygen, and water-soluble components, making them essential

for body fluid biosensors. Considering the benefits of both materials, plasmonic hydrogels are among the best candidates for biosensing applications.

Alongside the many advantages of hydrogel materials, there are aspects of the hydrogel platform which can be further improved. The use of hydrogels as 3D networks affords a greater affinity with the analyte, hence, more label-free detection possibilities. The use of stimuli-responsive materials can help us even more to have more opportunities to detect label-free biomolecules. In this way, both fabrication and detection are more accessible, while the applicability of the biosensor can be improved. Also, the use of stimuli-responsive materials will enhance the efficiency and precision of the sensor in the case of dual-responsivity, in which — in this case — there is a possibility to detect more than one target. Additionally, having a re-useable system can enhance its applicability and usability in real life. As the LSPR shift in the absorption of the plasmonic material varies with the shape and size of NPs, there is always room for improvement in terms of sensing range. Nowadays, NPs are synthesized into various shapes, such as cubes, rods, stars, wires, prisms, etc. These shapes or even different sizes of identical particles can be used in the same platform to obtain multiple sensing windows for the same material, making it more applicable for sensing molecules. Furthermore, different NPs are being prepared using both silver and gold, combined in a core-shell structure. These NPs can improve the limit of detection and the efficiency of the sensing platform compared to using single particles.

Declaration of competing interest

The authors declare that they have no known competing financial interests or personal relationships that could have appeared to influence the work reported in this paper.

Acknowledgments

This study was supported by the First TEAM grant number POIR.04.04.00-00-5ED7/18-00, which is carried out within the framework of the First TEAM program of the Foundation for Polish Science (FNP), co-financed by the European Union under the European Regional Development Fund. The authors are also grateful for the support of this work by the National Agency for Academic Exchange (NAWA) grant no. PPI/APM/2018/1/00045/U/001. Chiara Rinoldi, Paweł Nakielski, and Filippo Pierini acknowledge the financial support from the Polish Ministry of Science and Higher Education through scholarships for outstanding young scientists. Chiara Rinoldi was partially supported by the Foundation for Polish Science (FNP).

References

Papers of particular interest, published within the period of review, have been highlighted as:

- * of special interest
- ** of outstanding interest

1. Turner Anthony PF: **Biosensors: sense and sensibility.** *Chem Soc Rev* 2013, **42**:3184–3196.
 2. Eggins Brian R: **Biosensors: an introduction.** Springer-Verlag; 2013.
 3. Kissinger Peter T: **Biosensors—a perspective.** *Biosens Bioelectron* 2005, **20**:2512–2516.
 4. Rastislav Monosik, Stredansky Miroslav, Sturdik Ernest: **Biosensors—classification, characterization and new trends.** *Acta Chim Slov* 2012, **5**:109–120.
 5. Alhadrami Hani A: **Biosensors: classifications, medical applications, and future prospective.** *Biotechnol Appl Biochem* 2018, **65**:497–508.
 6. Scheller Frieder W, *et al.*: **Second generation biosensors.** *Biosens Bioelectron* 1991, **6**:245–253.
 7. Mejía-Salazar JR, Oliveira Jr Osvaldo N: **Plasmonic biosensing: focus review.** *Chem Rev* 2018, **118**:10617–10625.
 8. Hill Ryan T: **Plasmonic biosensors.** *Wiley Interdiscip Rev: Nanomed Nanobiotechnol* 2015, **7**:152–168.
 9. Hardeep Kaur, Bhosale Aakash, Shrivastav Suraj: **Biosensors: classification, fundamental characterization and new trends: a review.** *Int J Health Sci Res* 2018, **8**:315–333.
 10. Špačková Barbora, *et al.*: **Optical biosensors based on plasmonic nanostructures: a review.** *Proc IEEE* 2016, **104**:2380–2408.
 11. Soler, María, Huertas Cesar S, Lechuga Laura M: **Label-free plasmonic biosensors for point-of-care diagnostics: a review.** *Exp Rev Mol Diagnos* 2019, **19**:71–81.
 12. Sannomiya Takumi, Janos Vörös: **Single plasmonic nanoparticles for biosensing.** *Trends Biotechnol* 2011, **29**:343–351.
 13. Vazquez-Mena Oscar, *et al.*: **High-resolution resistless nanopatterning on polymer and flexible substrates for plasmonic biosensing using stencil masks.** *ACS nano* 2012, **6**:5474–5481.
 14. Yin, Ze, *et al.*: **Ultrastable plasmonic bioink for printable point-of-care biosensors.** *ACS Appl Mater Interfaces* 2020, **12**:35977–35985.
- In this paper a point-of-care, printable biosensor platform using Gold nanorods and organosiloxane polymer was synthesized and antibodies were encapsulated in the platform. This biosensor shows excellent thermal and biological properties, while the biosensing can take place in harsh conditions such as high temperature and ultrasonic agitation. The importance of this study in the present paper is the use of gold nanoparticles as a plasmonic material for biosensing applications and different platforms which can embed the particles.
15. Rinoldi, Chiara, *et al.*: **Three-dimensional printable conductive semi-interpenetrating polymer network hydrogel for neural tissue applications.** *Biomacromolecules* 2021, **22**:3084–3098.
- This research was based on synthesizing the semi-IPN hydrogel network based on poly(N-isopropylacrylamide), incorporated with intrinsically conducting polymers. This electrically conductive platform can be used as a UV-curable ink for printing applications. Our paper noted hydrogels as a candidate platform for biosensing, and acrylamide-based hydrogels are one of the most commonly-used platforms for biosensing.
16. Yang Canhui, Suo Zhigang: **Hydrogel iontronics.** *Nat Rev Mater* 2018, **3**:125–142.
 17. Pawłowska Sylwia, *et al.*: **Ultraviolet light-assisted electrospinning of core-shell fully cross-linked P (NIPAAm-co-NIPMAAm) hydrogel-based nanofibers for thermally induced drug delivery self-regulation.** *Advanced Materials Interfaces* 2020, **7**:2000247.
 18. Pardo-Yissar Vered, *et al.*: **Gold nanoparticle/hydrogel composites with solvent-switchable electronic properties.** *Adv Mater* 2001, **13**:1320–1323.
 19. Nezhad-Mokhtari, Parinaz, Akrami-Hasan-Kohal Mohammad, Ghorbani Marjan: **An injectable chitosan-based hydrogel scaffold containing gold nanoparticles for tissue engineering applications.** *Int J Biol Macromol* 2020, **154**:198–205.
- The focus of this research was to synthesize and characterize an injectable hydrogel that contains gold nanoparticles. The hydrogel is based on aldehyde-cellulose and collagen for tissue engineering purposes. The study of this paper helped us to understand more about the hydrogels embedded with plasmonic particles, their synthesis, and

morphological characterization. Also, biodegradability and cell viability tests show us the potential of using this medium for bio-applications.

20. Nakielski, Paweł, *et al.*: **Multifunctional platform based on electrospun nanofibers and plasmonic hydrogel: a smart nanostructured pillow for near-infrared light-driven biomedical applications.** *ACS Appl Mater Interfaces* 2020, **12**: 54328–54342.

A bioinspired drug delivery system was fabricated in this research, based on a composite of hydrogels embedded with gold nanoparticles and electrospun fibers. Using an acrylamide-based hydrogel with plasmonic nanoparticles shows fast photo-thermal responsivity. This nanostructure accelerates the drug release with the effect of localized temperature rise. This article helps us to understand the hydrogel performance with the presence of plasmonic nanoparticles.

21. Ziai, Yasamin, *et al.*: **Chameleon-inspired multifunctional plasmonic nanoplatfoms for biosensing applications.** *NPG Asia Mater* 2022, **14**:1–17.

Inspired by the features of the chameleon skin, a biosensor was designed in this research article using silver nanocubes. Acrylamide-based hydrogels were used here with the support of a layer of nanofibrous mat. The glucose present in the urine can be detected using this platform with antibacterial properties. This paper is the main source to study the biosensors with plasmonic hydrogels.

22. Yu Ting, Xianyu Yunlei: **Array-Based Biosensors for bacteria detection: from the perspective of recognition.** *Small* 2021, **17**: 2006230.
23. Mesch Martin, *et al.*: **Functionalized hydrogel on plasmonic nanoantennas for noninvasive glucose sensing.** *ACS Photonics* 2015, **2**:475–480.
24. Estevez, M-Carmen, *et al.*: **Trends and challenges of refractometric nanoplasmonic biosensors: a review.** *Anal Chim Acta* 2014, **806**:55–73.
25. Toma, Mana, *et al.*: **Active control of SPR by thermoresponsive hydrogels for biosensor applications.** *J Phys Chem C* 2013, **117**:11705–11712.
26. Andersson, Olof, *et al.*: **Gradient hydrogel matrix for microarray and biosensor applications: an imaging SPR study.** *Biomacromolecules* 2009, **10**:142–148.
27. Zhang, Zhiyang, *et al.*: **Plasmonic colorimetric sensors based on etching and growth of noble metal nanoparticles: strategies and applications.** *Biosens Bioelectron* 2018, **114**:52–65.
28. Sun, Jingwei, *et al.*: **Colorimetric sensor array based on gold nanoparticles: design principles and recent advances.** *TrAC, Trends Anal Chem* 2020, **122**:115754.
29. Diehl Fiona, *et al.*: **Plasmonic nanomaterials with responsive polymer hydrogels for sensing and actuation.** *Chem Soc Rev* 2022.
30. Koetting, Michael C, *et al.*: **Stimulus-responsive hydrogels: theory, modern advances, and applications.** *Mater Sci Eng R Rep* 2015, **93**:1–49.
31. Ryssy Joonas, *et al.*: **DNA-Engineered hydrogels with light-adaptive plasmonic responses.** *Adv Funct Mater* 2022: 2201249.
32. Sood, Nikhil, *et al.*: **Stimuli-responsive hydrogels in drug delivery and tissue engineering.** *Drug Deliv* 2016, **23**:748–770.
33. Lee, Jin-Ho, *et al.*: **Application of gold nanoparticle to plasmonic biosensors.** *Int J Mol Sci* 2018, **19**:2021.
34. Muri, Harald Ian, Andon Bano, Dag Roar Hjelme: **A single-point, multiparameter, fiber optic sensor based on a combination of**

interferometry and LSPR. *J Lightwave Technol* 2018, **36**: 1159–1167.

35. Song, Eun Ji, Chul Cho Eun: **Dual-responsive and multifunctional plasmonic hydrogel valves and biomimetic architectures formed with hydrogel and gold nanocolloids.** *Sci Rep* 2016, **6**:1–10.
36. Randriantsilefisoa, Rotsiniaina, *et al.*: **Double trouble for viruses: a hydrogel nanocomposite catches the influenza virus while shrinking and changing color.** *Chem Commun* 2020, **56**: 3547–3550.
37. Miranda B, *et al.*: **A PEGDA hydrogel nanocomposite to improve gold nanoparticles stability for novel plasmonic sensing platforms.** *J Appl Phys* 2021, **129**:33101.

A hydrogel-based biosensor was presented in this paper, using gold nanoparticles. This sensor has a reversible double response, a color change, and also a change of volume. This sensor detects the influenza virus by changing the color from pink to blue by increasing the virus concentration. This research also is a very good example of the plasmonic hydrogels used for biosensing applications.

- Using PEGDA and gold nanoparticles, a biosensor was fabricated and investigated. Biotin as a small molecule was used to be detected optically by this wearable biosensor. The importance of this paper, lies in the information on the effect of the size of the plasmonic particles on the sensing application, with the hydrogel medium.
38. Kotlarek, Daria, *et al.*: **Thin-film polyisocyanide-based hydrogels for affinity biosensors.** *J Phys Chem C* 2021, **125**: 12960–12967.
39. Culver, Heidi R, Marissa E, Wechsler, Nicholas A Peppas: **Label-free detection of tear biomarkers using hydrogel-coated gold nanoshells in a localized surface plasmon resonance-based biosensor.** *ACS Nano* 2018, **12**:9342–9354.
40. Guo, Jingjing, *et al.*: **Soft and plasmonic hydrogel optical probe for glucose monitoring.** *Nanophotonics* 2021, **10**: 3549–3558.
41. Liu, Chang, *et al.*: **A 3D localized surface plasmon resonance biosensor for the study of trivalent arsenic binding to the ArsA ATPase.** *Biosens Bioelectron* 2012, **38**:19–26.
42. Loiseau, Alexis, *et al.*: **Silver-based plasmonic nanoparticles for and their use in biosensing.** *Biosensors* 2019, **9**:78.
43. Lismont, Marjorie, Laurent Dreesen: **Comparative study of Ag and Au nanoparticles biosensors based on surface plasmon resonance phenomenon.** *Mater Sci Eng C* 2012, **32**: 1437–1442.
44. Filippo E, Serra A, Manno D: **Poly (vinyl alcohol) capped silver nanoparticles as localized surface plasmon resonance-based hydrogen peroxide sensor.** *Sensor Actuator B Chem* 2009, **138**: 625–630.
45. Endo, Tatsuro, *et al.*: **Stimuli-responsive hydrogel–silver nanoparticles composite for development of localized surface plasmon resonance-based optical biosensor.** *Anal Chim Acta* 2008, **611**:205–211.
46. Tokarev, Ihor, *et al.*: **Specific biochemical-to-optical signal transduction by responsive thin hydrogel films loaded with noble metal nanoparticles.** *Adv Mater* 2010, **22**:1412–1416.

ARTICLE

Open Access

Chameleon-inspired multifunctional plasmonic nanoplatforms for biosensing applications

Yasamin Ziai¹, Francesca Petronella², Chiara Rinoldi¹, Paweł Nakielski¹, Anna Zakrzewska¹, Tomasz A. Kowalewski¹, Weronika Augustyniak³, Xiaoran Li⁴, Antonella Calogero⁵, Izabela Sabała³, Bin Ding⁴, Luciano De Sio^{5,6} and Filippo Pierini¹

Abstract

One of the most fascinating areas in the field of smart biopolymers is biomolecule sensing. Accordingly, multifunctional biomimetic, biocompatible, and stimuli-responsive materials based on hydrogels have attracted much interest. Within this framework, the design of nanostructured materials that do not require any external energy source is beneficial for developing a platform for sensing glucose in body fluids. In this article, we report the realization and application of an innovative platform consisting of two outer layers of a nanocomposite plasmonic hydrogel plus one inner layer of electrospun mat fabricated by electrospinning, where the outer layers exploit photoinitiated free radical polymerization, obtaining a compact and stable device. Inspired by the exceptional features of chameleon skin, plasmonic silver nanocubes are embedded into a poly(N-isopropylacrylamide)-based hydrogel network to obtain enhanced thermoresponsive and antibacterial properties. The introduction of an electrospun mat creates a compatible environment for the homogeneous hydrogel coating while imparting excellent mechanical and structural properties to the final system. Chemical, morphological, and optical characterizations were performed to investigate the structure of the layers and the multifunctional platform. The synergetic effect of the nanostructured system's photothermal responsivity and antibacterial properties was evaluated. The sensing features associated with the optical properties of silver nanocubes revealed that the proposed multifunctional system is a promising candidate for glucose-sensing applications.

Introduction

Currently, bioinspired and biomimetic materials, methods, and algorithms are widely used, as nature is an excellent source of inspiration for a wide range of procedures and designs. There has been a comprehensive classification of inspiration and mimetics from nature, including processes, designs, and materials¹. One of the critical aspects of bioinspired materials lies in their ability to modify, recover and rebuild their structure under environmental changes over time². Bioinspiration is useful

in various applications such as architecture³, robotics⁴, textiles⁵, and, more specifically, biomaterials used for energy storage⁶, sensors⁷, water filtration⁸, wearable electronics⁹, and biomedical applications¹⁰.

Many living organisms have developed the ability to change their properties via physical interaction of external visible light with their nanostructured natural structures. Coloration is an excellent example of these changes, which can be described as “structural.” Indeed, this phenomenon is generated by periodic arrays of nano- and microstructures, known as photonic crystals (PCs), which create colors through optical interference effects¹¹. Animals such as chameleons are capable of locomotion for consumption and escape, using coloration for attraction, warning, and disguise¹². In addition, chameleons cannot generate any body heat, but the color of their skin can be

Correspondence: Luciano De Sio (luciano.desio@uniroma1.it) or Filippo Pierini (fpierini@ippt.pan.pl)

¹Department of Biosystems and Soft Matter, Institute of Fundamental Technological Research, Polish Academy of Sciences, Warsaw 02-106, Poland

²Institute of Crystallography CNR-IC, National Research Council of Italy, Via Salaria Km 29,300, 00015 Monterotondo - Rome, Italy

Full list of author information is available at the end of the article

© The Author(s) 2022



Open Access This article is licensed under a Creative Commons Attribution 4.0 International License, which permits use, sharing, adaptation, distribution and reproduction in any medium or format, as long as you give appropriate credit to the original author(s) and the source, provide a link to the Creative Commons license, and indicate if changes were made. The images or other third party material in this article are included in the article's Creative Commons license, unless indicated otherwise in a credit line to the material. If material is not included in the article's Creative Commons license and your intended use is not permitted by statutory regulation or exceeds the permitted use, you will need to obtain permission directly from the copyright holder. To view a copy of this license, visit <http://creativecommons.org/licenses/by/4.0/>.

used as feedback to regulate their body temperature^{13,14}. In particular, the skin of the chameleon is characterized by two superimposed layers of iridophores, namely, cells responsible for skin coloration. The lower layer provides thermoregulation, while the upper layer controls the color changes. Iridophores of the upper layer contain guanine nanocrystals in a regular packed lattice. These guanine nanocrystals are interposed to the cytoplasm, resulting in an arrangement where a higher refractive index material (guanine) is assembled with a lower refractive index material (cytoplasm), thus generating a lattice-like structure similar to that of photonic crystals¹⁵. This light-matter mechanism can inspire the design of biosensors to produce photo/photothermal-driven devices that can monitor changes without requiring any external energy input.

Biosensors are defined as devices that involve specific biochemical and physical reactions mediated by immune systems, tissues, organelles, or biomimetic components to detect chemical compounds, usually by electrical, thermal, or optical signals¹⁶. In recent years, the development of nanomaterials for the ultrasensitive detection of biological species has received significant attention because of their unique optical, electronic, chemical, and mechanical properties. Different nanomaterials have been investigated to determine their properties and possible biosensing applications¹⁷. Considering the increasing prevalence of diabetes and hypoglycemia, glucose sensing has received much interest in recent years^{18,19}. Recently, there have been outstanding investigations into electrochemical^{20,21} and spectroscopic²² methods for glucose monitoring. The main challenge, which concerns fast, personalized tracking, consists of sensing the glucose rate without blood-letting, thus making it as user-friendly as possible. Glucose levels can be measured using urine²³, perspiration²⁴, saliva²⁵, ocular fluid²⁶, and even breath analysis²⁷. Within this framework, over the past several decades, soft elastic materials have become of great interest due to their body compliance and are being used for wearable electronics and wearable biosensors. Compared to physical sensors, these devices require the integration of specific bioreceptors into sensing elements that are capable of recognizing target analytes in complex samples at physiologically significant concentrations. To enable ultrafast glucose monitoring, it is generally necessary to entrap the enzyme glucose oxidase within a flexible device. Elsherif et al. fabricated wearable contact lens optical sensors based on hydrogel networks for continuous glucose measurement under physiological conditions²⁸. Organic biosensors can be processed inexpensively on flexible substrates by using printing techniques; the organic material can also be tailored to adjust the properties¹⁷. In addition, other properties such as wearability, flexibility, and the possibility of fabricating these platforms using

low-cost processes ensure favorable prospects for these materials^{29,30}.

Among materials, hydrogels are considered one of the best alternatives for the fabrication of organic biosensors. Hydrogels are defined as crosslinked polymeric networks with an extensive water swelling capacity and can be synthesized by a simple reaction of one or more monomers. The essential property of these polymeric materials is their ability to swell and retain a significant fraction of water within their structure without dissolving in water³¹. The ability of hydrogels to absorb water arises from the hydrophilic functional groups attached to the polymeric backbone, while their intrinsic resistance to dissolution comes from crosslinks between network chains. Usually, synthetic polymers have well-defined structures that can be modified to yield on-demand degradability and functionality³². Hydrogels are engineered to exhibit a significant volume variation in response to small changes in their environmental factors, such as pH, ionic strength, temperature, solvent, and applied electric/magnetic field, which can be used for sensing applications. Recent advancements in polymer science have led to the development of biopolymers suitable for synthesizing various hydrogels. Hydrogels can be responsive to external stimuli such as temperature, pH, or the ionic strength of the surrounding medium³³. These systems are called smart hydrogels, as they respond immediately to environmental changes. They can be categorized into two classes based on the chemical or physical nature of the crosslinked interactions. Crosslinking due to chemical interactions leads to a permanent junction in the polymer network, while physical interactions are due to either polymer chain entanglements or physical interactions such as ionic interactions, hydrogen bonding, or hydrophobic interactions^{34,35}.

Most of the thermoresponsive polymers used in biomedical applications form colloidal systems when the temperature increases, a property known as lower critical solution temperature (LCST) behavior. This process is reversible: polymers return to a sol form when the temperature is lowered below the LCST²⁷. When the macromolecular chains of these thermoresponsive polymers are crosslinked to form hydrogels, the behavior of the final materials is significantly influenced by the volume phase transition temperature (VPTT). Indeed, when the temperature exceeds the typical VPTT, the polymer network shrinks, and the water contained in the hydrogel is expelled from the structure³⁶. Thus, crosslinked thermoresponsive hydrogels reversibly switch from a hydrophilic, swollen state to a hydrophobic, shrunken state when heated above the volume phase transition temperature³⁷.

Several types of hydrogels based on natural polymers have been investigated in the field of thermoresponsivity³⁸; in particular, poly(*N*-isopropylacrylamide)

(PNIPAAm) has attracted high interest in recent years. Indeed, PNIPAAm is nonbiodegradable and has a sharp phase transition, with a VPTT close to the human body temperature (at $\sim 32^\circ\text{C}$ in pure water)³⁹. According to its thermoresponsive behavior, the polymer shape is an extended coil conformation below the VPTT (32°C), showing a well-defined structure and properties⁴⁰. Interestingly, the VPTT can be finely tuned according to the specific application⁴¹.

Plasmonic nanoparticles (NPs) are metallic subunits with a dimensional range smaller than the wavelength of visible light; they possess unique physical and optical properties such as localized surface plasmon resonance (LSPR), which is a coherent and dipolar oscillation of the bulk-free electrons localized at the metallic/dielectric interface. Moreover, the confinement effect confers reactivity and mechanical, electromagnetic, chemical, and optical properties that differ from those of bulk metals^{42,43}. The SPR band is much stronger for plasmonic NPs than for other metals, as their SPR band appears in the visible region of the electromagnetic spectrum. In contrast, other metals have weak bands in the ultraviolet (UV) region. Among all metallic NPs, gold (Au) and silver (Ag) NPs have the most attractive physical properties for biosensing-related applications. Because of their excellent chemical stability and biocompatibility, gold nanoparticles (AuNPs) are the most investigated in this research area, most frequently for drug delivery systems and cancer therapy applications⁴⁴. Due to their excellent chemical stability and biocompatibility⁴⁵, AuNPs are widely used in drug delivery systems and cancer therapy. On the other hand, silver nanoparticles (AgNPs) offer better results in terms of sensitivity⁴⁶, and thus, they are mainly used for sensing applications. AgNPs with different shapes, including cubes, wires, spheres, triangles, and rods, have distinct crystal faces. In particular, the contact area in silver nanocubes (AgNCs) is more significant than that in nanospheres or other morphologies, resulting in more grain boundaries. The higher the percentage of contact area on a specific NP shape, the more active the NP will be^{47,48}. Accordingly, a few studies have recently reported the combination of thermoresponsive polymer composites and metal NPs to enhance their specific properties.

He et al. used NIPAAm and sodium acrylate as functional monomers to form a hydrogel layer, and AgNPs were loaded inside them for antibacterial purposes. It was possible to effectively kill the contacting and surrounding bacteria. The attached dead bacteria were then detached as a result of the increased surface hydrophilicity and degree of surface swelling by reducing the temperature below the VPTT⁴⁹. AgNPs are frequently used as antibacterial agents to effectively reduce bacterial viability. Bactericidal surfaces can prevent the formation of biofilms for a certain period until AgNPs are completely

consumed. This behavior shows that the antibacterial property can be maintained only for a limited time, motivating researchers to design and construct environment-responsive antibacterial surfaces, including thermoresponsive, pH-responsive, enzyme-responsive, and photoresponsive surfaces⁴⁹.

Ultrathin fibers fabricated by electrospinning have attracted much attention for various biomedical applications, such as tissue engineering⁵⁰, drug delivery⁵¹, wound dressing, bioscaffolds⁵², and biosensors^{53,54}. The nanofibers obtained using this technique can have a size range close to 100 nm, extremely high surface-to-volume ratio, tunable porosity, and controllable properties and functionalities^{55,56}.

In this article, taking inspiration from light-matter interactions and the functionalities of chameleon skin, we report the development of a fast, sensitive, smart, antibacterial glucose-sensing system. The proposed innovative system consists of hydrogels as three-dimensional networks responding to stimuli and electrospun fibers with their unique structure and properties. To fabricate such smart platforms, a PNIPAAm-derivative plasmonic hydrogel containing AgNCs was synthesized. Using the electrospinning technique, a mat consisting of polycaprolactone (PCL) and polyethylene oxide (PEO) was also prepared, providing ultrathin fibers with a high surface area in a facile and inexpensive way. The composites consisted of two outer layers of hydrogel and an inner layer of electrospun mat. Their resulting unique hierarchical structure was deeply characterized, while structural and optical properties were thoroughly investigated to embrace the full potential of the platform. In addition, the antibacterial and photothermal responses of the samples were evaluated. Finally, the application of the developed nanostructured platform as an LSPR biosensor was evaluated by quantifying the glucose level in the human body. The change in glucose concentration in human urine produced a shift in the LSPR bands of AgNCs. By applying the proposed organic-based inexpensive, smart, nanostructured platform, glucose levels in urine can be rapidly and easily monitored without any external energy input requirement, equipment, or bloodletting.

Materials and methods

Materials

N,N-isopropylacrylamide (NIPAAm, 97%, Sigma Aldrich, Poland), N-isopropylmethacrylamide (NIPMAAm, 97%, Sigma Aldrich, Poland), N,N'-methylene bisacrylamide (BIS-AAm, 99.5%, Sigma Aldrich, Poland), 2-hydroxy-4'-(2-hydroxyethoxy)-2-methylpropiophenone (Irgacure 2959, 98%, Sigma Aldrich, Poland), silver nanocubes (AgNCs, 75 nm, PVP, Nanocomposix, USA), polycaprolactone (PCL, Mn 80 kDa), polyethylene oxide

(PEO, Mn 100 kDa), dichloromethane (DCM, POCh, Poland), and N,N-dimethylformamide (DMF, POCh, Poland) were purchased and used as received.

Hydrogel precursor sol including silver nanocubes

To prepare the hydrogel precursor solution at a concentration of 4.8 wt%, 578.13 mg of NIPAAm, 15.63 mg of NIPMAAm, and 31.25 mg of BIS-AAm were added to 12.5 mg of Irgacure 2959. This mixture was dissolved in 10 ml of deionized water to reach a 95.2 wt% solution. The mixture was wrapped in aluminum foil for protection from light and stirred overnight until complete dissolution.

To optimize the final embedding of AgNCs into the solution, a suspension of AgNCs with three different proportions—2%, 5%, and 20% wt/wt_{monomer}—was added to the hydrogel precursor solution.

Preparation of electrospun fibers

First, 12% (w/v) PCL/PEO, which was prepared at the ratio of 75:25 (w/w) PCL/PEO, was dissolved into 80:20 (v/v) dichloromethane:dimethylformamide (DCM:DMF) solution and stirred overnight at room temperature by using a magnetic stirrer prior to electrospinning. The desired structure was achieved by performing the procedure with a flow rate of 300 $\mu\text{L h}^{-1}$ and a positive voltage of 15 kV. The rotating drum used to collect fibers was placed 13 cm away from the 21 G needle tip and rotated at 500 rpm. The electrospinning process was performed at a temperature of $\sim 21\text{--}22\text{ }^{\circ}\text{C}$ with 50% humidity. Electrospun fibers were placed on glass slides, and small circular holes were cut into the fibrous mat with a laser cutting system (Optec) on a high-precision motorized X-Y-Z linear stage (Newport, Irvine, CA) controlled by a PC. A picosecond laser with a wavelength of 355 nm, a 200 kHz repetition rate of the laser pulse, and a minimum laser spot size of 3 mm was used. The laser power was $\sim 0.5\text{ W}$ (7%), the translation speed of the laser head was set at 2000 mm s^{-1} , and the laser head moved eleven times along the same line to cut the microstructures correctly. A $\times 5$ objective (Mitutoyo, Japan) was used to focus laser pulses. The hole is necessary to enable the laser beam to pass through just the hydrogel layer and, in return, to avoid any possible interference generated by the electrospun membrane during glucose quantification.

Fabrication of the nanostructured platform

To fabricate the final platform structure, a tailor-designed metal mold was used as a template. A 2.5 ml hydrogel precursor solution was poured into the mold; then, an electrospun fiber mat was cut into strips ($6 \times 1\text{ cm}$) and placed gently on the solution. Next, 2.5 ml of hydrogel was poured over the fibrous strips to obtain the final platform. The obtained system was placed in a petri

dish inside an ice bath and irradiated with a UV lamp for 2 min. Samples were dried in a hood overnight and rinsed with deionized water for one week to remove all the unpolymerized material and the residual photoinitiator.

Structural characterization

To ensure the presence of AgNCs and their distribution in the hydrogel matrix, each separate layer and the whole final construct were characterized morphologically.

Field emission scanning electron microscopy (FE-SEM) and scanning electron microscopy (SEM) were performed with FEI Nova NanoSEM 450 and JEOL JSM-6390LV microscopes, respectively. Hydrogel disks and the final construct were frozen in liquid nitrogen before cross-sectional cutting, and then, freeze-dried samples were obtained. Before imaging, samples were sputtered with gold layers of approximately 8 nm in thickness using a SC7620 Polaron mini sputter coater (Quorum Technologies Ltd., Ashford, UK). The samples were freeze-dried, and then, the lyophilized materials were cut into small pieces, immersed in ethanol, and placed on a copper mesh with an amorphous carbon membrane. For transmission electron microscopy (TEM), samples were analyzed on an FEI Talos F200X TEM (acceleration voltage of 200 kV) after four hours of drying in a vacuum drier.

Energy-dispersive X-ray spectroscopy (EDX) was performed in STEM mode. For this purpose, a high-angle annular dark-field detector and a Super-X EDX system with four silicon drift detectors (SDDs) were used. The sample surface topography was evaluated by atomic force microscopy (AFM, Ntegra, NT-MDT) equipped with a silicon cantilever (NSG01, NT-MDT, tip radius 10 nm). Measurements were performed in semicontact mode, with a resonance frequency of 150 kHz and 500×500 points per image. The hydrodynamic diameter of AgNCs was analyzed by dynamic light scattering (DLS) with a Zetasizer Nano ZS system (Malvern, UK). Dispersions of 0.1 wt% AgNCs in water were prepared, and samples were loaded into quartz microcuvettes and measured in triplicate, with the mean value recorded.

Chemical characterization

A Multiskan GO spectrophotometer (Thermo Scientific, USA) was used to collect data for ultraviolet–visible (UV–Vis) spectra. The UV–Vis spectrophotometer scanned from 400 nm to 1000 nm at 5 nm intervals. X-ray scattering (XRD) analyses were performed to confirm the presence of AgNCs in the hydrogel matrix and to detect any potential changes in the hydrogel structure caused by the inclusion of AgNCs. Measurements were carried out on a Bruker D8 Discover diffractometer in reflection mode using Bragg–Brentano geometry. The analysis was conducted in the angular range (2θ) of $5\text{--}50^{\circ}$. Data were collected with a step of 0.02° per 1.0 s at each point.

Fourier transform infrared (FT-IR) spectroscopy was used to characterize the functional groups in each layer. FT-IR analyses were conducted in attenuated total reflectance (ATR) mode with a Bruker Vertex70 FT-IR spectrometer and carried out in the wavenumber range of 400–4000 cm^{-1} with a resolution of 2 cm^{-1} and 12 scans for each sample.

Mechanical testing

Macrotensile measurements were performed using a tensile tester (Model EZ 50, Lloyd Instruments strength machine, Germany). Specimens were obtained by cutting the final construct into strips of a size of $6.0 \times 1.0 \text{ cm}^2$. All samples were mounted between holders at a distance of 1 cm (Pneumatic Action grips, Elancourt, France). Tensile testing was conducted at a rate of 5 mm min^{-1} at room temperature (21 °C). Specimens were kept wet by immersing them in water at the test temperature. A 50 N load was set on the instrument.

Antibacterial characterization

The antibacterial activity of the hydrogel disks was tested on the *Staphylococcus aureus* 8325-4 strain. One milliliter of overnight inoculum was added to 50 ml of liquid tryptic soy broth (TSB) and incubated at 37 °C with shaking (80 rpm) until the cultures reached an OD_{600} of 0.6. The bacterial cells were harvested by centrifugation, and the palette was resuspended in phosphate-buffered saline (PBS) until reaching an OD_{600} of 1.0 corresponding to 10^8 CFU ml^{-1} , followed by further dilution to obtain the desired number of bacteria in 50 μL , namely, 1000, 10,000, 100,000, and 1,000,000.

Fifty microliters of bacteria were placed on hydrogel disks and spread gently and uniformly over the whole surface. Control samples were made by pipetting 50 μL of bacterial suspensions into Eppendorf tubes. These samples were then incubated at room temperature (~ 20 °C) for 4 h. Afterward, solutions were taken from the hydrogel disks and subjected to serial dilutions to perform a droplet test: 5 μL of each dilution of every sample was placed on TSB agar plates and incubated at 37 °C overnight, and then, the colonies were counted to estimate the number of bacteria in each sample.

Photothermal responsivity characterization

The thermo-optical setup used a TEM00 mode CW diode-pumped solid-state laser (Laser Quantum) operating at 532 nm in the high absorption range of AgNCs (longitudinal plasmon band). A high-resolution thermal camera (FLIR, A655sc) was used to map and identify both the spatial heating distribution and the temperature profile under laser illumination. The camera produced thermal images of 640×480 pixels with an accuracy of ± 0.2 °C; it worked seamlessly with a proprietary software

program (FLIR ResearchIR Max) to record and process the thermal data acquired by the camera.

Glucose sensing tests

The absorption spectra of the P(NIPAAm-co-NIP-MAAm) hydrogel samples embedded with AgNCs were collected by using a UV-Vis spectrometer (USB 2000, Ocean Optics). The sensitivity of the AgNCs was tested by preparing four standard solutions of D-glucose in water at the same concentrations used to build the calibration curve for the hydrogel samples. A volume of AgNCs (from a colloidal dispersion of 1 mg/mL) was added to each glucose solution suitable to achieve the desired AgNC: water mass ratio. The resulting dispersions were kept under magnetic stirring for 5 min, and then, the corresponding absorption spectra were collected.

Hydrogel samples were placed on a glass substrate, with 50 μm glass microspheres added as spacers, and then covered with a glass slide (100 μm thick). The resulting gap was infiltrated via capillary flow, with 50 μL of the solution being studied. Samples were allowed to rest for 10 min to promote a uniform and complete distribution of the solution within the samples before evaluating the optical response as a function of local refractive index changes. Each measurement was performed by examining five different areas of the hydrogel samples. The spectral shifts ($\Delta\lambda$) were reported as the mean value \pm standard deviation of five different measurements.

To construct the D-glucose calibration curve, hydrogel samples embedded with AgNCs were infiltrated with 50 μL of standard water solutions of D-glucose at concentrations from 2 mM to 8 mM, and the respective absorption spectra were collected to measure the wavelength of the respective plasmonic peak (λ_{glu}). To quantify the $\Delta\lambda$ value associated with the respective D-glucose standard solution, the wavelength of the plasmonic peak from the absorption spectrum of a P(NIPAAm-co-NIP-MAAm)/AgNC sample was infiltrated with Milli-Q water (λ_{water}) and used as a reference. $\Delta\lambda$ was then calculated as the difference between λ_{water} and λ_{glu} , and the calibration curve was obtained by plotting $\Delta\lambda$ as a function of the concentration of standard solutions of D-glucose.

The limit of detection (LOD) was calculated as 3 times the standard deviation of the intercept, calculated from the linear interpolation resulting from plotting the $\Delta\lambda$ values as a function of the concentration of standard solutions⁵⁷.

The D-glucose concentration in human urine samples was calculated by following the standard addition method. A defined volume (0 mL, 0.2 mL, 0.4 mL, 0.8 mL, and 1 mL) of a 10 mM D-glucose standard solution was introduced into 2 mL volumetric flasks previously filled with 1 mL of a human urine sample. The resulting solutions were suitably diluted with Milli-Q water and mixed.

Subsequently the solutions were used to infiltrate P (NIPAAm-*co*-NIPMAAm)/AgNC samples to acquire the corresponding absorption spectra. The resulting $\Delta\lambda$ values were plotted as a function of the concentration of standard solutions, thus obtaining the standard addition plot. To obtain statistically reliable data, five different solutions were prepared, infiltrated into the hydrogel, and analyzed for each condition studied.

Results and discussion

Bioinspired nanostructured platform

Chameleon skin, shown in Fig. 1a, offered inspiration for the multilayer structure described in this article. The rapid active tuning of skin hue has been described in only a handful of species and generally involves structural rather than pigmentary components. Multilayer nanoreflectors cause these structural changes by alternating high and low refractive indices that generate the interference of light waves. In a similar way, the unique characteristics of the structure of chameleon skin are primarily due to the nano- and microstructured arrangements of chameleon skin tissue, giving rise to photonic crystals (PCs). The layer underneath revealed the presence of fibroblast cells, collagenous fibrils, nerve axons, melanosomes, and mast cells in the connective tissue core. This layer has a general

structure similar to that of the electrospun fibrous mat. The structure of the particles in chameleon skin and their similarity to plasmonic nanocubes (Fig. 1b), resulting in the light-matter interaction of the skin and the resemblance between the particle fibrous tissue layers, were the most significant features imitated in the fabrication of this multilayer structure.

The scheme illustrated in Fig. 1c shows the structure of the final construct. An electrospun fiber mat obtained from a blend of poly(ϵ -caprolactone)/polyethylene glycol (PCL/PEO) was placed between two layers of nanostructured hydrogel based on N-isopropylacrylamide-*co*-N-isopropylmethacrylamide P(NIPAAm-*co*-NIPMAAm) with embedded AgNCs. The structure of the guanine particles existing in the chameleon skin (Fig. 1a, right panel) was replicated in the proposed plasmonic nanoplatform by introducing silver nanocubes (Fig. 1b). Therefore, the development of a structure evoking guanine nanocrystals in the cytoplasm of chameleon iridophores and the resemblance between the particle fibrous tissue layer were the most important features when fabricating this multilayer structure. This system is designed to show photothermal responsivity due to the nanostructure of the particles and the nature of the P(NIPAAm-*co*-NIPMAAm) hydrogel. The electrospun mat between

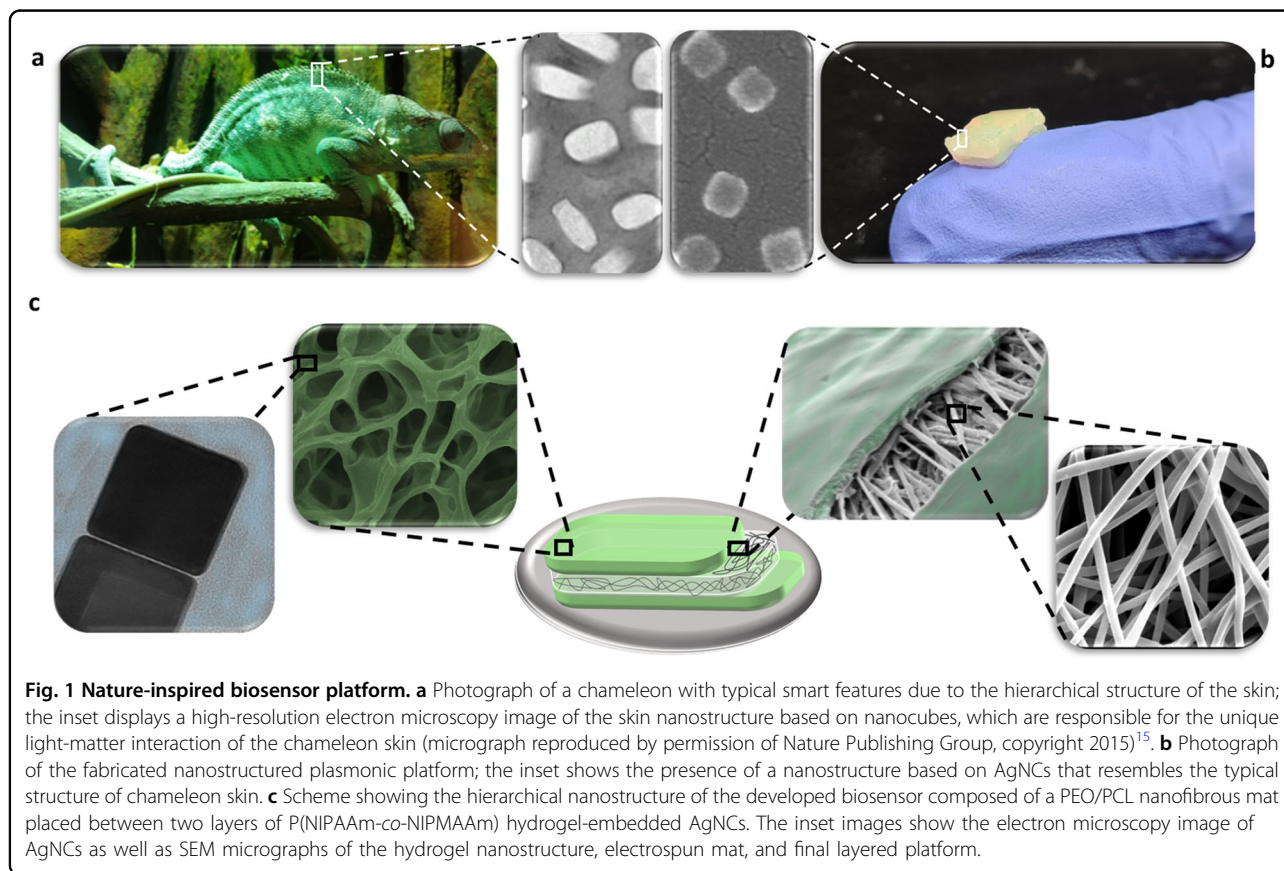
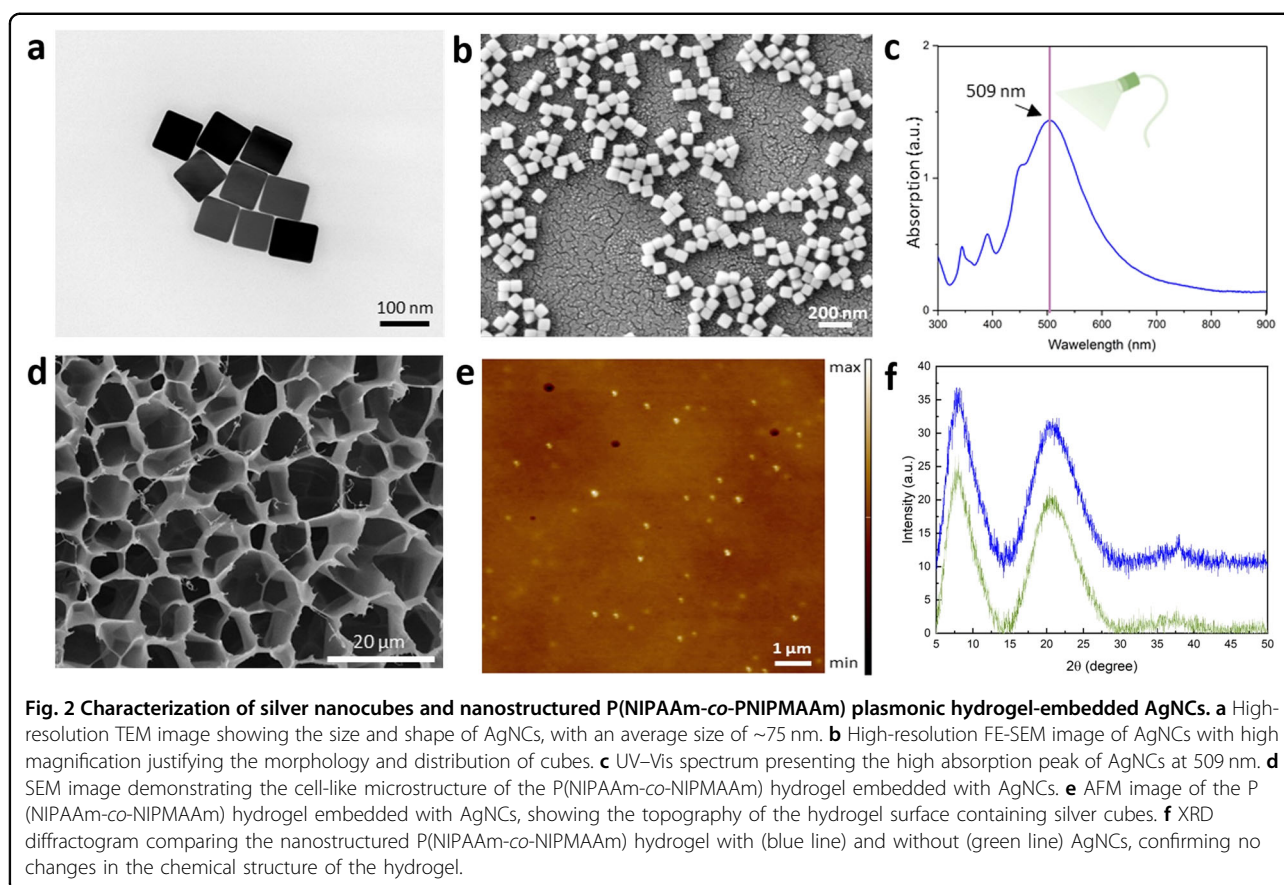


Fig. 1 Nature-inspired biosensor platform. **a** Photograph of a chameleon with typical smart features due to the hierarchical structure of the skin; the inset displays a high-resolution electron microscopy image of the skin nanostructure based on nanocubes, which are responsible for the unique light-matter interaction of the chameleon skin (micrograph reproduced by permission of Nature Publishing Group, copyright 2015)¹⁵. **b** Photograph of the fabricated nanostructured plasmonic platform; the inset shows the presence of a nanostructure based on AgNCs that resembles the typical structure of chameleon skin. **c** Scheme showing the hierarchical nanostructure of the developed biosensor composed of a PEO/PCL nanofibrous mat placed between two layers of P(NIPAAm-*co*-NIPMAAm) hydrogel-embedded AgNCs. The inset images show the electron microscopy image of AgNCs as well as SEM micrographs of the hydrogel nanostructure, electrospun mat, and final layered platform.



hydrogel layers provides mechanical support and makes it easier to handle as a biomedical device⁵⁸.

Silver nanocubes embedded in the thermoresponsive P(NIPAAm-co-NIPMAAm) hydrogel

AgNCs introduced into the proposed platform have an average dimension of 75 ± 3 nm, as shown by both FE-SEM and TEM images. TEM and EDS elemental mapping images are shown in Fig. 2a and Fig. S1, indicating the size, shape, and distribution of the AgNCs. Field-emission SEM images of the cubes are also presented in Fig. S2 and Fig. 2b, with two different levels of magnification. AgNCs have a perfect cubic shape: the edges and corners are perfectly visible, revealing that the synthesis and the utilized protocol produced the desired shape. This observation is good evidence of the homogeneity and regularity of the cubes that we used in this study. It is worth pointing out that even during the sample preparation for imaging, where the medium of the sols was completely removed, there was no sign of visible aggregations in the microscopic images, and the AgNCs were well distributed. Thus, the stability and homogeneity of the precursor solution used to prepare the hydrogel were proved. The DLS results (Fig. S3) showed a single peak: an average hydrodynamic diameter of AgNCs of approximately

109 nm. The data appear consistent since one single population is present; thus, one single peak in the DLS graph is expected. The visible difference between the DLS results and the reported morphological determination of the size of the cubes obtained by electron microscopy is because DLS is a technique developed to analyze nanoobjects and, as a result, determines the equivalent hydrodynamic size of the particles. It is worth noting that the hydrodynamic radius of a particle is generally more prominent than its physical radius. Moreover, DLS detects the radius of an equivalent spherical particle, having the same rheological behavior like that of our single nanocubes dispersed in the analyzed colloidal sol. Therefore, it is not possible to directly compare the diameter obtained by electron microscopy with DLS results. In any case, the DLS outcomes are consistent with the previous quantitative data obtained by FE-SEM and TEM in terms of sol stability and absence of any aggregates under the utilized experimental conditions. As shown in Fig. 2c, the UV-Vis spectra of AgNCs show a strong light absorbance peak centered at $\lambda = 509$ nm, which is the expected wavelength for AgNCs with the described shape and size to absorb light due to their LSPRe.

In recent years, PNIPAAm has been extensively studied, as it is a thermoresponsive hydrogel that undergoes

reversible phase transitions at specific temperatures. The coil-to-globule transition of the polymer consists of at least two different thermal processes. First, water molecules around the hydrophobic isopropyl group and hydrophilic amide groups can rearrange in bulk water. Second, intra- and interchain hydrogen bonds are created between amide groups, and this phenomenon is accompanied by a loss in polymer chain-water hydrogen bonds. This transition depends on several factors, e.g., polymer concentration, crosslinking agent concentration, and copolymerization with other monomers. To increase the VPTT, two monomers, NIPAAm and NIPMAAm, were copolymerized. The VPTT of PNIPAAm in water is approximately 32 °C, while that of PNIPMAAm is higher, ~42 °C. According to the literature, the VPTT of the resulting copolymer with a smaller quantity of NIPMAAm (as in our case) should increase to ~33–34 °C when macromolecule chains are not crosslinked⁵⁹. In our case, the use of *N,N'*-methylene bisacrylamide (BIS-AAm) shifted the VPTT. This shift led to the formation of a broad peak due to the faster reaction of BIS-AAm than that of NIPAAm and NIPMAAm during polymerization.

The SEM micrograph of the hydrogel reported in Fig. 2d was taken from the cross-section of the samples, which were dried before use. The image shows the cell-like network structure of the hydrogel with a pore size ranging from 8 μm to 10 μm. The cell-like structure with interconnected pores is highly significant, as it makes it possible for the network to absorb a great amount of water and gain the desired hydrogel properties⁶⁰. An SEM image of the neat hydrogel network not filled with AgNCs is shown in Fig. S4. The cell-like structure shows that there are no visible differences in the structure and pore sizes with and without the introduction of AgNCs. It can be clearly seen, however, that the presence of AgNCs in the hydrogel network can impart the hydrogel with new optical properties due to the optical properties of well-dispersed AgNCs (Fig. S5a, b). As shown in the AFM topography of the hydrogel with embedded AgNCs (Fig. 2e), there were few signs of AgNCs on the hydrogel surface. Therefore, it may be concluded that AgNCs (20 wt%) are trapped within the porous network of the hydrogel, which also appears on the surface. This process gives rise to both the photothermal responsivity and antibacterial properties of the material and affects the platform's sensing features for the ultimate application of the system. Two more different concentrations of AgNCs in the hydrogel (i.e., 2 and 5 wt%) were tested, and the AFM images in Fig. S6a, b show the distribution of AgNCs on the surface of the hydrogel. However, 20 wt% AgNCs was selected due to a sufficient number of AgNCs, providing effective antibacterial and photothermal responsiveness, thus allowing a more sensitive sensing capability. The effect of AgNCs on the chemical structure of the

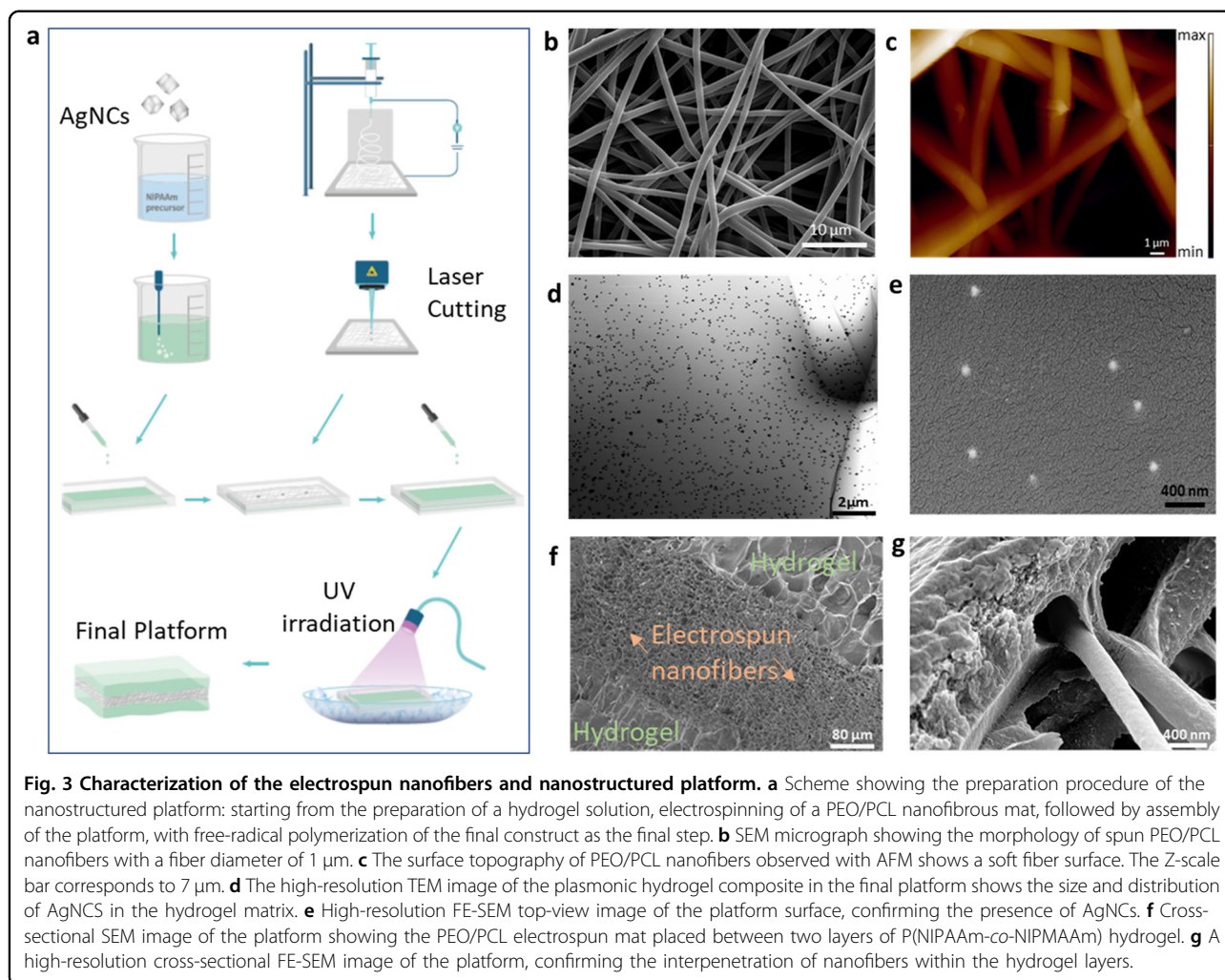
hydrogels can also be proven through the comparison between XRD measurements of the pure hydrogel and the hydrogel embedded with AgNCs. Typical broad peaks at ~8.0 and 20.7° are shown in the XRD diffractogram (Fig. 2f), which is attributed to the polymer's amorphous state. The presence of AgNCs is proved by the small additional peak at 38.0°, but otherwise, there is no other visible change in the XRD diffractogram, which demonstrates that the addition of AgNCs does not change the chemical structure of the hydrogel. Thus, adding nanocubes does not affect the crystallinity of the polymer; hence, no changes in the XRD diffractogram are observed.

Electrospun nanofibers and nanostructural platform fabrication

A schematic of the final composite fabrication is shown in Fig. 3a. First, the nanofibrous mat was electrospun from the prepared solution and collected on a planar collector. As previously described, the electrospun mat was then subjected to laser cutting, and 3 mm-diameter holes were cut into it to ensure the passage of light through the entire layered platform for biosensing tests. Meanwhile, after argon bubbling to remove oxygen molecules, the hydrogel precursor solution was added to a prepared rectangular mold. The electrospun fiber mat was then added on top of the hydrogel precursor solution, and a layer of the hydrogel precursor solution was poured gently over it. UV-irradiated polymerization was performed while the platform was in an ice bath to control the heat generated during the polymerization process. The crosslinked hydrogel was removed from the mold and cut into strips for further investigations.

Polycaprolactone (PCL) is a biodegradable polyester commonly used in the biomedical field for drug delivery systems and three-dimensional (3D) scaffolds for tissue engineering⁶¹. This polymer is biocompatible and biodegradable, and owing to its semicrystalline and hydrophobic nature, PCL has a very slow degradation rate and mechanical properties suitable for several applications. The transformation of this polymer to nanofibers to achieve a desirable structure by electrospinning is quite easy, thus revealing its excellent value in terms of final applicability/applications. PCL is compatible with a wide range of other polymers and is thus a great choice when multifunctional mats are needed. PEO is also a biocompatible and biodegradable polymer with a hydrophilic structure and water-soluble, nonionic, and nontoxic properties; it is introduced here as a component to modify the hydrophilic properties of the PCL mat. The combination of these two polymers increases the hydrophilicity of PCL/PEO nanofibers compared to pure PCL⁶² and improves the mechanical properties compared to pure PEO⁶³.

As shown in the SEM image of the electrospun fibers in Fig. 3b, PCL/PEO nanofibers with fiber dimensions of

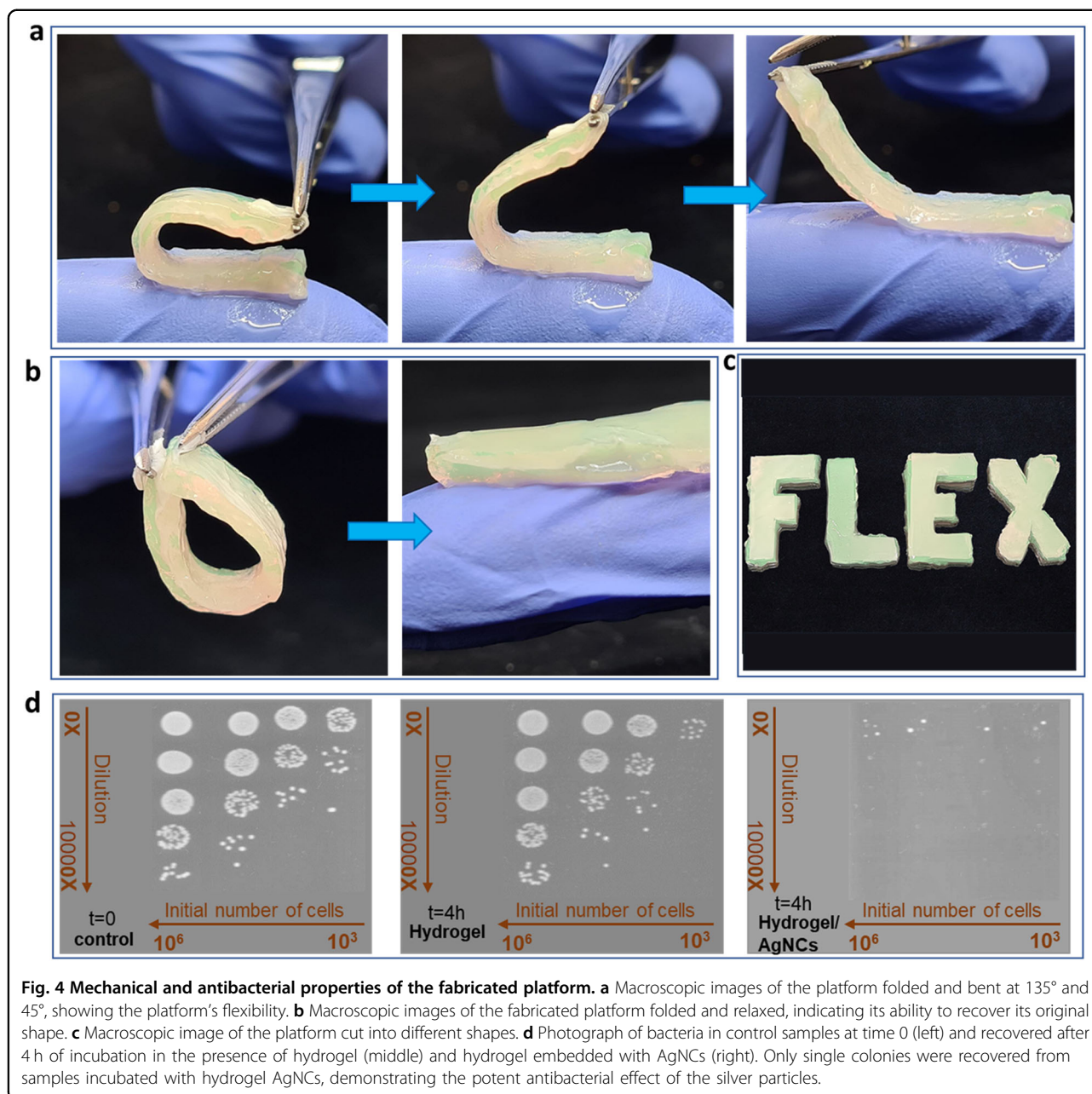


approximately 1 μm were successfully fabricated. The fibers obtained were uniform, regular, and bead-less, and they were randomly oriented and well distributed throughout the whole mat. They were also defect-free, showing no signs of breaking or deformation. In addition, the surface of these fibers was observed via AFM, as shown in Fig. 3c: the fibers appeared uniform and without defects. Figure 3d shows the TEM image of AgNCs in the final platform, confirming the presence of AgNCs in the hydrogel matrix. It can be observed that the nanoparticles are well dispersed throughout the hydrogel network; moreover, there is no sign of nanofiller aggregation. High-resolution TEM and EDS images in Fig. S7a, b show the high-magnification visualization of AgNCs in the hydrogel network. The uniform distribution and nonaggregation of AgNCs are confirmed here at nanometric scales. Fig. S8 shows the AFM topography of the composite, evidencing the presence of AgNCs on the surface of the hydrogel. There were no signs of fibers on the surface topography of the hydrogel composite, thus confirming

the homogeneous hydrogel layering on the platform. Figure 3e shows a top-view FE-SEM image of the platform, revealing a plain surface and the presence of AgNCs in the structure. Figure 3f shows an FE-SEM image of the platform's cross-section, highlighting the platform's layered structure composed of an electrospun fibrous mat placed between two layers of P(NIPAAm-co-NIPMAAm) hydrogel embedded with AgNCs. The nanometric scale interface and interpenetration of fibers in the hydrogel structure are visible in the cross-sectional FE-SEM image presented in Fig. 3g. The interpenetrated fibers in the cross-section support the idea of a compact platform and intimate anchorage between the layers (Fig. 3g), which play a crucial role in the mechanical properties and stability of the system.

Mechanical testing of the fabricated platform

Hydrogels possess poor mechanical properties due to their network structure and the retainment of significant amounts of water. Acrylate-based hydrogels are no



exception; thus, the high swelling ratio of PNIPAAm-based hydrogels results in very poor physical strength⁶⁴. This feature may not cause problems in applications in an aqueous state, but it is a major hurdle for applications such as biosensing, tissue engineering, and robotics⁶⁵. To overcome this limitation, we introduced a nanofibrous mat into the system so that its coupling with the hydrogel could boost the mechanical properties of the final system. The fabricated platform showed outstanding mechanical properties and flexibility, enabling it to be folded and bent at different angles without causing any material structural damage. Macroscopic images of the platform folded and

bent to 135° and 45° are shown in Fig. 4a. Furthermore, due to its flexibility, the platform can recover its original shape and size without any fractures from both physical and structural standpoints. Macroscopic images of the platform before and after removing a load are shown in Fig. 4b. This platform can be shaped into different designs, thus obtaining whatever shape is needed for other applications. A first example is shown in Fig. 4c, and another is presented in Figure S9. Mechanical tensile testing was also performed on the samples. Specimens were cut into the shape of dumbbells, placed between the grips of the mechanical testing machine, and subjected to

an extension rate of 5 mm min^{-1} . Figure S10 shows the sample's extension diagram, indicating the system's capacity for an extension up to 160% of its initial length. Additionally, the tensile strength of the specimens was calculated using Eq. 1. The tensile strength of the sample was calculated to be 0.32 N mm^{-1} , which appears reasonable for the system.

$$\text{Tensile strength} = \frac{\text{max load}}{\text{SA}} \quad (1)$$

where SA is the surface area of the sample.

Thus, fibers are integrated into the hydrogel network by compositing a layer of electrospun fibers between two hydrogel layers. This procedure results in a compact, stable, and easily handled platform.

Antibacterial properties of the composite platform

Silver compounds such as silver nitrate and silver sulfadiazine have been used to prevent bacterial growth in applications such as drinking water decontamination and burn care⁶⁶. Nanosilver is increasingly being introduced as an antibacterial agent in health care products^{67,68}. Nanocrystalline silver provides a very large specific surface area for the release of ionic silver, and even a small amount of silver can provide potent bactericidal action⁶⁹. Metallic silver has also been added to polymer fabrics and catheters to provide antibacterial properties⁷⁰.

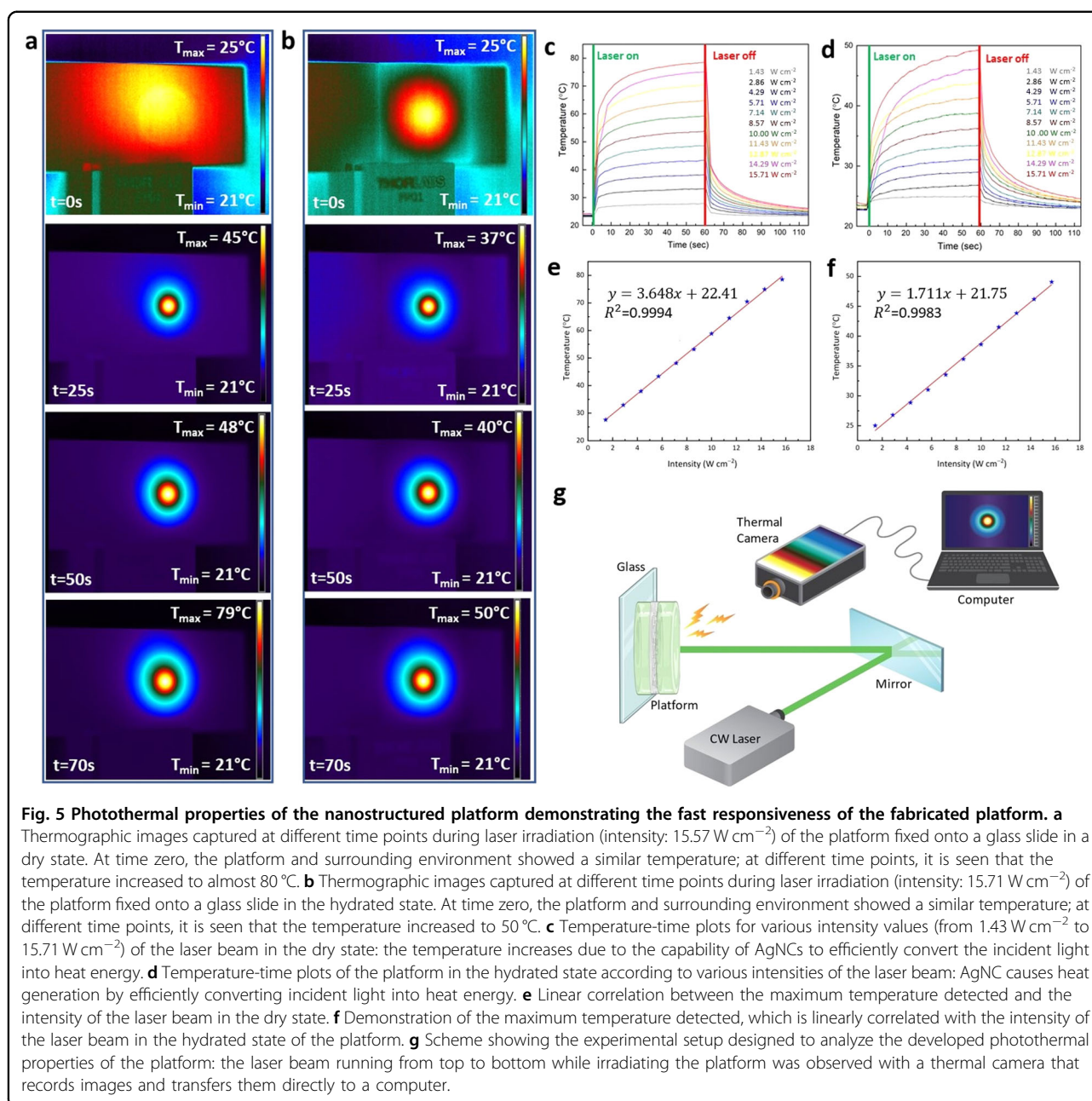
The antibacterial activity of the developed composite embedded with AgNCs was investigated by seeding *Staphylococcus aureus* (*S. aureus*) cells in phosphate-buffered saline (PBS) onto the sample surface. The bacterial cells were enumerated by serial dilutions at time zero and after 4 h of incubation. Figure 4d illustrates colonies grown from serial dilutions of bacteria at time zero and after four hours of incubation on the hydrogel samples without silver nanocubes and samples with 20 wt% AgNCs. As shown in the images, after 4 h of incubation on the surface of the platform, only single colonies could be recovered, while numerous bacteria were grown after incubation on the surface of samples without AgNCs. Taking these results into account, it was calculated that after 4 h of incubation, half of the initial number of bacterial cells was recovered from neat hydrogels, while silver-containing hydrogels eliminated over 99.9% of bacteria independent of the AgNC concentration (Supplementary Fig. S11).

It is possible to assess that the presence of AgNCs in the platform can provide a powerful antibacterial effect to the multifunctional platform. As the antibacterial properties of silver are well known, the reduced number of bacteria on P(NIPAAm-co-NIPMAAm)/AgNC composites after a relatively short incubation time (4 h) confirms the presence and successful embedding of AgNCs into the hydrogel structure.

Fast photothermal responsiveness of the composite

The thermoresponsive behavior of the plasmonic nano-platform was investigated using a green laser operating at 532 nm as a function of the laser intensity (from 1.43 W cm^{-2} to 15.71 W cm^{-2}). AgNCs show an intense absorption band in the visible region, and owing to their remarkable photothermal efficiency, the absorbed light can be converted into heat⁷¹. The AgNCs embedded in the final composite are also responsible for the intense absorption band in the visible region of the final nanostructured platform. When the heat from the converted energy from green laser irradiation at the absorption peak exceeds the hydrogel VPTT, a cascade-like series of stimulus/response events leads to a rapid shrinkage of the hydrogel and water evic-tion. These phenomena demonstrate the hydrogel's significant thermoresponsive properties.

Figure 5a, b show some thermographic images of the different hydration states and irradiation times of the platform after exposure to the laser beam at an intensity of 15.71 W cm^{-2} . Images taken with the thermal camera detected an immediate increase in the temperature of the platform, which is considered the direct rate of responsiveness. Although the neat P(NIPAAm-co-NIPMAAm)-based hydrogel has negligible photothermal responsivity (Fig. S12), plasmonic AgNCs make the composite hydrogel strongly responsive to visible light. As reported in Fig. 5a, exposure to laser irradiation for 70 s increased the temperature of dry samples to $\sim 80^\circ\text{C}$; the hydrated hydrogel tested under the same conditions reached $\sim 50^\circ\text{C}$. This difference is because the absorption peak varies, passing from hydrated to dry states and shifting the absorption peak in the case of a fully hydrated state (no longer centered on laser emissions), thus making the photoresponsivity less efficient. The different surrounding environments can also explain this phenomenon since air takes less time to reach high temperatures than water. Time-temperature profiles at different intensity values of the laser pump beam (from 1.43 W cm^{-2} to 15.71 W cm^{-2}) are shown in Fig. 5c, d. When the laser was ON, the temperature increased to almost 80°C in the dry state (Fig. 5c) and up to 50°C in the hydrated platform (Fig. 5d). In both cases, the temperature increase is attributed to the photothermal efficiency of AgNCs. When the laser was turned OFF, both samples cooled to room temperature in less than one minute. This behavior ensures the reusability of the system, as by increasing the temperature, the platform shrinks due to the LSCT nature of the hydrogel and expels the infiltrated solution. Removing the light source returns the hydrogel to its original state, and it is ready to be used again. A higher laser power could certainly lead to a faster heating efficiency of the sample. The linear correlation between the temperature and intensity of the laser can be seen in Fig. 5e, f for both hydrated and dry samples, respectively. Figure 5g shows



the experimental optical setup used for photothermal investigation of the platforms. A continuous-wave (CW) laser source operating at 532 nm irradiated the samples placed in a tailor-designed specimen holding the nanostructured platform after passing through a custom-designed optical patch. A side-view thermal camera recorded thermographic images with changes in the sample temperature at different irradiation times.

Glucose sensing

According to optical transducer/phenomena, optical glucose sensors are classified into four groups: surface plasmon

resonance (SPR), fluorescent, surface-enhanced Raman scattering (SERS), and photonic bandgap sensors. Our multifunctional platforms were investigated for glucose sensing due to their high sensitivity to changes in the surrounding refractive index. The readout of these sensors depended on the change detected in the resonant absorbed wavelength with glucose concentrations. Localized surface plasmon resonance (LSPR) is based on the surface plasmon resonance phenomenon in which metal electrons oscillate coherently in an electromagnetic field during surface conduction. This phenomenon can enhance the measurement sensitivity of the local environment on the metal nanostructure surface.

To first examine the sensing reliability of the AgNCs, nanocubes were tested dispersed in liquid solutions with different glucose concentrations. The shift of the wavelength of the main LSPR band can be seen in Fig. S13, which shows that the AgNCs are sensitive to glucose. Biosensors using plasmonic NPs have been mainly developed using techniques such as electrodeposition of nanoparticles to functionalize the surface of supporting materials. Although this technique allows good attachment of particles on the surface, the immobilization of nanoparticles on the supporting material surface greatly reduces the contact area between the nanomaterials and the tested analyte. To overcome this drawback, the incorporation of plasmonic nanoparticles into bulk hydrogels has been explored. Indeed, embedding nanoparticles into the hydrogel mass renders the entire nanoparticle surface available for exposure to the sample. This elegant strategy strongly improves the sensor sensitivity. In addition, particle encapsulation is an inexpensive and simple approach compared to the electrodeposition of nanoparticles.

Figure 6a shows a schematic illustration of the glucose-sensing procedure in human urine samples. As shown in this scheme and described in the materials and methods section, the analyzed human urine sample was added to various standard glucose solutions and infiltrated into the hydrogel/mat platform. The hydrogel samples were placed in a UV–Vis spectrophotometer, and the shift of the maximum LSPR band was detected.

Figure 6b shows the absorption spectra of P(NIPAAm-co-NIPMAAm)/AgNCs in three different infiltrating media: air, pure water, and an 8 mM D-glucose solution. The absorption spectrum of the composite in air shows an intense plasmonic peak centered at 551 nm, which is associated with the resonance of the (100) planes of AgNCs, along with two peaks at 410 nm and 352 nm, attributed to the edges and corners of AgNCs, respectively⁷². P(NIPAAm-co-NIPMAAm) hydrogels possess a refractive index ($n = 1.5$) higher than that of water ($n = 1.3$). Therefore, the position of the plasmonic peaks of the hydrogel samples embedded with AgNCs is shifted with respect to the plasmonic peaks of the colloidal dispersion of AgNCs (shown in Fig. 2c).

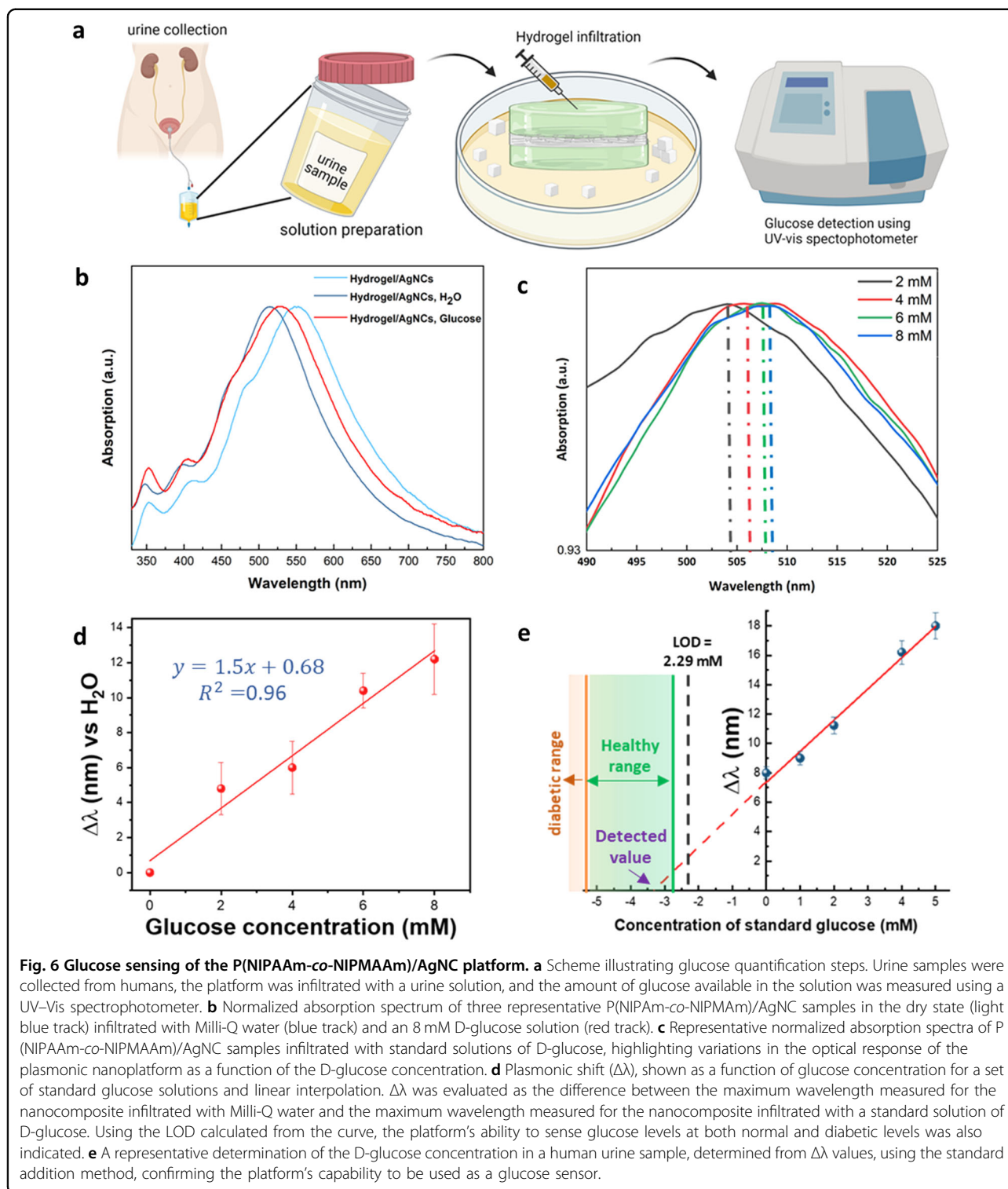
The infiltration of the P(NIPAAm-co-NIPMAAm)/AgNC nanocomposite with Milli-Q water resulted in a blueshift of 37 nm ($\Delta\lambda_T$) from the main plasmonic peak of AgNCs, as highlighted by the dark blue track in Fig. 6b. In comparison, a lower blueshift (31 nm) ($\Delta\lambda_S$) was measured following the infiltration of P(NIPAAm-co-NIPMAAm)/AgNC samples with an 8 mM D-glucose solution.

The spectral shift of the absorption spectrum of P(NIPAAm-co-NIPMAAm)/AgNC samples is due to variation in the refractive index surrounding AgNCs; the average refractive index is expected to decrease slightly

after Milli-Q water is introduced into the dried P(NIPAAm-co-NIPMAAm) sample⁷³. Accordingly, the decreased local refractive index value resulted in a blueshift of the plasmon bands of AgNCs in the P(NIPAAm-co-NIPMAAm)/AgNC sample. This significant $\Delta\lambda_T$ value can be further elucidated considering that the infiltration of P(NIPAAm-co-NIPMAAm)/AgNCs with Milli-Q water can alter the arrangement of the P(NIPAAm-co-NIPMAAm) molecules surrounding AgNCs. In particular, the P(NIPAAm-co-NIPMAAm) structure can change from a collapsed state (when the polymer is dry) to a swollen state following infiltration with Milli-Q water. Indeed, water is an optimal solvent for P(NIPAAm-co-NIPMAAm), as it minimizes attractive forces among polymer molecules, thus promoting polymer swelling. In the swollen state, the density of the polymer molecules embedded with AgNCs is lower than that of P(NIPAAm-co-NIPMAAm) molecules in the dried state. The lower density in the swollen state can reduce the refractive index value for P(NIPAAm-co-NIPMAAm), as demonstrated by Tagliazucchi et al.⁷⁴. Therefore, when the P(NIPAAm-co-NIPMAAm) sample was infiltrated with water, the density of the polymer molecules surrounding AgNCs decreased, leading to a consequent further decrease in the P(NIPAAm-co-NIPMAAm) refractive index value, thereby causing an intense blueshift of the AgNC plasmon band⁷⁵.

When the plasmonic nanoplatform was infiltrated with an 8 mM D-glucose solution, a less intense (31 nm) blueshift was measured. Indeed, the presence of D-glucose molecules in the infiltrating solution can produce an overall increase in the local refractive index value experienced by AgNCs (compared with Milli-Q water); this situation resulted in a less intense blueshift than the optical shift measured for the P(NIPAAm-co-NIPMAAm)/AgNC sample infiltrated with Milli-Q water.

Figure 6c shows the absorption spectra of the P(NIPAAm-co-NIPMAAm)/AgNC samples infiltrated with D-glucose standard solutions at different concentrations used to prepare a typical calibration curve and, in turn, to evaluate the limits of detection (LODs) of the system. As the D-glucose concentration decreased in the infiltrating solution, the peak in the corresponding absorption spectrum of the infiltrated sample shifted toward lower wavelengths due to a reduced average refractive index. Moreover, it is well known that if the concentration of D-glucose decreases, the viscosity of the infiltrating solution is reduced⁷⁶. Consequently, attractive interactions among P(NIPAAm-co-NIPMAAm) molecules decrease. Under these conditions, polymer swelling is progressively promoted (compared to polymer collapse), thus resulting in a progressively lower local refractive index value. This change results in a more intense blueshift of the AgNC plasmon band than that of the dry P(NIPAAm-co-NIPMAAm)/AgNC sample⁷⁴. The ability of



P(NIPAAm-co-NIPMAAm)/AgNC hydrogels to behave as plasmonic-based refractive index sensors was also evaluated by associating the plasmonic shift with the concentration of D-glucose standard solutions. The calibration curve obtained as described earlier shows a linear

correlation between the plasmonic shift ($\Delta\lambda$) and D-glucose concentration for the sensing of the platform (Fig. 6d). The limit of detection (LOD) of the system was calculated to be 2.29 mM, which is fully consistent with the typical detection limits of commercial urine strip

tests⁴⁶. This result emphasizes the sensitivity of P(NIPAAm-co-NIPMAAm)/AgNCs to variations in the local refractive index value. Indeed, based on the work published by Surendar et al. used to calculate the refractive index value of the D-glucose standard solutions⁷⁷, we were able to estimate a sensitivity of 433 nm/RIU (refractive index unit), which is also in agreement with the results previously reported in the literature for silver nanoparticles⁷⁸.

Finally, we tested our sensor's ability to analyze the D-glucose concentration in human urine samples by exploiting the method of standard additions. This method was used because although urine samples are relatively simple, it enabled avoiding any matrix effect and further sample preparation before performing tests⁷⁹. Additionally, it is worth mentioning that we avoided testing artificial urine in this protocol to verify the ability of the developed platform to test real human samples⁸⁰. As previously described, hydrogel composite samples were infiltrated with D-glucose standard solutions, and absorption wavelengths were measured. As shown in Fig. 6e, with the increase in the concentration of standard D-glucose solutions, the plasmonic shift redshifted in response to the change in the local reflective index, as previously reported and discussed for standard D-glucose solutions, according to the experimental results. Figure 6e shows a representative analysis of the developed method based on the use of the nanostructured platform, which permitted detection of a D-glucose amount of 3.7 ± 0.3 mM in the investigated sample. This technique was explored to detect glucose in urine as a proof-of-concept of the proposed noninvasive detection method, showing excellent detection of glucose levels within a wide range of concentrations. The glucose level in healthy people is between 2.78 and 5.5 mM and more than 5.5 mM for diabetic people⁸¹. This range of glucose concentrations is above the detection limit calculated by our system, which is reliable and reproducible considering the calculated standard deviation. All these results prove the sensor's ability to detect the desired glucose levels in urine. It is worth mentioning that the reusability of the platform is ensured by the photothermal responsivity of the system, which expels the liquid infiltrating the gel upon irradiation.

Conclusions

In this work, we successfully fabricated an antibacterial photothermal-responsive glucose-sensing platform inspired by the structure of chameleon skin. The multifunctional platform consists of a layer of PEO/PCL electrospun fibers enclosed by two layers of P(NIPAAm-co-NIPMAAm)-based hydrogels with embedded plasmonic nanoparticles, i.e., AgNCs with outstanding sensing performance. The P(NIPAAm-co-NIPMAAm) hydrogel is a

thermo-responsive hydrogel. Coupling this hydrogel with AgNCs made it possible to develop novel and unique functions of the platform. AgNCs endow the platform with antibacterial properties, promote the hydrogel's photothermal responsivity with plasmonic properties and, most importantly, enable the system's sensing feature. Several studies were performed using laser beam irradiation at 532 nm and a high-resolution thermal camera to demonstrate the photothermal behavior of the proposed platform. The presence of a PEO/PCL nanofibrous mat was a requisite for mechanical stability of the system. Indeed, hydrogel itself consists of 94% water and does not have suitable mechanical stability and physical properties for handling as a platform for sensing applications. The PEO/PCL nanofibrous mat gives the platform excellent mechanical properties to allow the system to be designed in various shapes and overcome mechanical failures during bending, twisting, and stretching, thus ensuring that the structure and uniformity of the platform are maintained. The presence of AgNCs imparted plasmonic properties to the proposed nanoplatfrom. The well-structured platform was tested as a biosensor to detect glucose in body fluids, presenting an accurate and reproducible procedure. The platform provided a fast and cost-effective glucose monitoring procedure as an LSPR sensor and was successfully tested for analysis of glucose in a human urine sample by following an accurate and reproducible procedure. The detection limit of this platform (2.29 mM) is lower than the glucose levels in both healthy and diabetic people; additionally, this method benefits from the fact that it is noninvasive. Optical detection is based on the difference in the refractive index of the surrounding environment with a linear coloration between the $\Delta\lambda$ and glucose concentration in urine samples. The presence of glucose causes a change in the reflective index of the surrounding medium, thus producing a shift in absorption peaks. Considering the platform's antibacterial properties and photothermal responsiveness, along with the sensing capability, our system has been proven to be a promising platform capable of detecting glucose levels in body fluids.

Acknowledgements

This study was partially supported by the First TEAM grant number POIR.04.04.00-00-5ED7/18-00, which is carried out within the framework of the First TEAM program of the Foundation for Polish Science (FNP), co-financed by the European Union under the European Regional Development Fund. The authors are also grateful for the support of this work by the National Agency for Academic Exchange (NAWA), grant no. PPI/APM/2018/1/00045/U/001. Chiara Rinoldi, Paweł Nakielski, and Filippo Pierini acknowledge financial support from the Polish Ministry of Science and Higher Education through scholarships for outstanding young scientists. Chiara Rinoldi was partially supported by the Foundation for Polish Science (FNP). Luciano De Sio acknowledges financial support from the Air Force Office of Scientific Research (AFOSR), Air Force Research Laboratory (AFRL) and U.S. Air Force grant no. FA9550-18-1-0038 (P.I.L. De Sio, EOARD 2017–2020) and the Materials and Manufacturing; the Sapienza University of Rome, under grant no. RM11816431206A2C (Progetto di Ateneo 2018, P.I.L. De Sio). Part of this

research was also carried out using apparatuses available thanks to EC structural funds within the framework of the Center for Preclinical Research and Technology (CePT), POIG No. 02.02.00-17-024/08-00.

Author details

¹Department of Biosystems and Soft Matter, Institute of Fundamental Technological Research, Polish Academy of Sciences, Warsaw 02-106, Poland. ²Institute of Crystallography CNR-IC, National Research Council of Italy, Via Salaria Km 29,300, 00015 Monterotondo - Rome, Italy. ³Mossakowski Medical Research Institute, Polish Academy of Sciences, 02-106 Warsaw, Poland. ⁴Innovation Center for Textile Science and Technology, Donghua University, West Yan'an Road 1882, Shanghai 200051, China. ⁵Department of Medico-Surgical Sciences and Biotechnologies - Research Center for Biophotonics, Sapienza University of Rome Corso della Repubblica 79, 04100 Latina, Italy. ⁶CNR-Lab. Licryl, Institute NANOTEC, Arcavacata di Rende 87036, Italy

Author contributions

Y.Z. fabricated the nanoplatfoms, performed the structural and mechanical characterization, and wrote the article. F.Pe. carried out the biosensing tests. C. R. developed the nanoplatfoms. P.N. performed the platform structural characterization. A.Z. fabricated the platform and carried out the structural characterization. T.A.K. performed the platform structural characterization. W.A. conducted the antibacterial studies. X.L. carried out the mechanical tests. A.C. performed the nanoplatfom optical characterization. I.S. carried out the antibacterial test. B.D. conducted the mechanical characterization. L.D.S. formulated the idea and conducted the photoresponsiveness experiments. F. Pi. conceived the idea, designed the experiments, and supervised the project. All authors discussed the results and revised the manuscript.

Data availability

The data that support the findings of this study are available from the corresponding author upon reasonable request.

Conflict of interest

The authors declare no competing interests.

Publisher's note

Springer Nature remains neutral with regard to jurisdictional claims in published maps and institutional affiliations.

Supplementary information The online version contains supplementary material available at <https://doi.org/10.1038/s41427-022-00365-9>.

Received: 29 October 2021 Revised: 31 December 2021 Accepted: 12 January 2022.

Published online: 4 March 2022

References

- Katlyar, N., Goel, G., Hawi, S. & Goel, S. Nature-inspired materials: emerging trends and prospects. *NPG Asia Mater.* **3**, 56 (2021).
- Perera, A. S. & Coppens, M.-O. Re-designing materials for biomedical applications: from biomimicry to nature-inspired chemical engineering. *Trans. R. Soc. A* **377**, 20180268 (2019).
- Kimovski, D., Ijaz, H., Saurabh, N. & Prodan, R. Adaptive nature-inspired fog architecture. *2018 IEEE 2nd International Confere* Washington, DC, 1–3 May 2018.
- Pfeifer, R., Lungarella, M. & Iida, F. Self-organization, embodiment, and biologically inspired robotics. *Science* **318**, 1088–1093 (2007).
- Chen, J. et al. Nature-inspired hierarchical protrusion structure construction for washable and wear-resistant superhydrophobic textiles with self-cleaning ability. *ACS Appl. Mater. Interfaces* **13**, 18142–18151 (2021).
- Xu, C. et al. Nature-inspired hierarchical materials for sensing and energy storage applications. *Chem. Soc. Rev.* **50**, 4856–4871 (2021).
- Xu, K., Lu, Y. & Takei, K. Multifunctional skin-inspired flexible sensor systems for wearable electronics. *Adv. Mater. Technol.* **4**, 1800628 (2019).
- Goel, G., Hélic-Nielsen, C., Upadhyaya, H. M. & Goel, S. A bibliometric study on biomimetic and bioinspired membranes for water filtration. *NPJ Clean. Water* **4**, 41 (2021).
- Zhu, C. et al. A nature-inspired, flexible substrate strategy for future wearable electronics. *Small* **15**, 1–11 (2019).
- Lee, S.-W. et al. NiCHE platform: nature-inspired catechol-conjugated hyaluronic acid environment platform for salivary gland tissue engineering. *ACS Appl. Mater. Interfaces* **12**, 4285–4294 (2020).
- Dong, Y. et al. Chameleon-inspired strain-accommodating smart skin. *ACS Nano* **13**, 9918–9926 (2019).
- Wang, Y., Cui, H., Zhao, Q. & Du, X. Chameleon-inspired structural-color actuators. *Matter* **1**, 626–638 (2019).
- Chou, H.-H. et al. A chameleon-inspired stretchable electronic skin with interactive colour changing controlled by tactile sensing. *Nat. Commun.* **6**, 1–10 (2015).
- Lee, G. H. et al. Chameleon-inspired mechanochromic photonic films composed of non-close-packed colloidal arrays. *ACS Nano* **11**, 11350–11357 (2017).
- Teyssier, J., Saenko, S., van der Marel, D. & Milinkovitch, M. C. Photonic crystals cause active colour change in chameleons. *Nat. Commun.* **6**, 6368 (2015).
- Kergoat, L., Piro, B., Berggren, M., Horowitz, G. & Pham, M. C. Advances in organic transistor-based biosensors: From organic electrochemical transistors to electrolyte-gated organic field-effect transistors. *Anal. Bioanal. Chem.* **402**, 1813–1826 (2012).
- Sun, C. et al. Preparation of novel electrochemical glucose biosensors for whole blood based on antibiofouling polyurethane-heparin nanoparticles. *Electrochim. Acta* **97**, 349–356 (2013).
- Bruen, D., Delaney, C., Florea, L. & Diamond, D. Glucose sensing for diabetes monitoring: recent developments. *Sensors* **17**, 1866 (2017).
- Wang, J. Electrochemical Glucose Biosensors. *Chem. Rev.* **108**, 814–825 (2008).
- Chen, C. et al. Recent advances in electrochemical glucose biosensors: a review. *RSC Adv.* **3**, 4473–449 (2013).
- Nery, E. W., Kundys, M., Jeleń, P. S. & Jönsson-Niedziółka, M. Electrochemical glucose sensing: Is there still room for improvement? *Anal. Chem.* **88**, 11271–11282 (2016).
- McNichols, R. J. & Coté, G. L. Optical glucose sensing in biological fluids: an overview. *J. Biomed. Opt.* **5**, 5–16 (2000).
- Makaram, P., Owens, D. & Aceros, J. Trends in nanomaterial-based non-invasive diabetes sensing technologies. *Diagnostics* **4**, 27–46 (2014).
- Lee, H. et al. Wearable/disposable sweat-based glucose monitoring device with multistage transdermal drug delivery module. *Sci. Adv.* **3**, e1601314 (2017).
- Zhang, W., Du, Y. & Wang, M. L. On-chip highly sensitive saliva glucose sensing using multilayer films composed of single-walled carbon nanotubes, gold nanoparticles, and glucose oxidase. *Sens. Bio-Sens. Res.* **4**, 96–102 (2015).
- Farandos, N. M., Yetisen, A. K., Monteiro, M. J., Lowe, C. R. & Yun, S. H. Contact lens sensors in ocular diagnostics. *Adv. Healthc. Mater.* **4**, 792–810 (2015).
- Saraoglu, H. M. & Mehmet, K. Determination of blood glucose level-based breath analysis by a quartz crystal microbalance sensor array. *IEEE Sens. J.* **10**, 104–109 (2010).
- Elsherif, M., Hassan, M. U., Yetisen, A. K. & Butt, H. Hydrogel optical fibers for continuous glucose monitoring. *Biosens. Bioelectron.* **137**, 25–32 (2019).
- Bartic, C. & Borghs, G. Organic thin-film transistors as transducers for (bio) analytical applications. *Anal. Bioanal. Chem.* **384**, 354–365 (2006).
- Wang, L., Fine, D., Sharma, D., Torsi, L. & Dodabalapur, A. Nanoscale organic and polymeric field-effect transistors as chemical sensors. *Anal. Bioanal. Chem.* **384**, 310–321 (2006).
- Ahmed, E. M. Hydrogel: Preparation, characterization, and applications: A review. *J. Adv. Res.* **6**, 105–121 (2015).
- Kopeček, J. Hydrogel biomaterials: A smart future? *Biomaterials* **28**, 5185–5192 (2007).
- Kamath, K. R. & Park, K. Biodegradable hydrogels in drug delivery. *Adv. Drug Deliv. Rev.* **11**, 59–84 (1993).
- Vashist, A., Vashist, A., Gupta, Y. K. & Ahmad, S. Recent advances in hydrogel based drug delivery systems for the human body. *J. Mater. Chem. B* **2**, 147–166 (2014).
- Sood, N., Bhardwaj, A., Mehta, S. & Mehta, A. Stimuli-responsive hydrogels in drug delivery and tissue engineering. *Drug Deliv.* **23**, 748–770 (2016).
- Kim, D., Kim, H., Lee, E., Jin, K. S. & Yoon, J. Programmable volume phase transition of hydrogels achieved by large thermal hysteresis for static-motion Bilayer Actuators. *Chem. Mater.* **28**, 8807–8814 (2016).

37. Xue, Q. et al. Nanostrip flexible microwave enzymatic biosensor for non-invasive epidermal glucose sensing. *Nanoscale Horiz.* **5**, 934–943 (2020).
38. Ruel-Gariépy, E. & Leroux, J. C. In situ-forming hydrogels - Review of temperature-sensitive systems. *Eur. J. Pharm. Biopharm.* **58**, 409–426 (2004).
39. Nakielski, P. et al. Multifunctional platform based on electrospun nanofibers and plasmonic hydrogel: a smart nanostructured pillow for near-infrared light-driven biomedical applications. *ACS Appl. Mater. Interfaces* **12**, 54328–54342 (2020).
40. Heskins, M. & Guillet, J. E. Solution Properties of Poly(N-isopropylacrylamide). *J. Macromol. Sci. Part A - Chem.* **2**, 1441–1455 (1968).
41. Haq, M. A., Su, Y. & Wang, D. Mechanical properties of PNIPAM based hydrogels: A review. *Mater. Sci. Eng. C.* **70**, 842–855 (2017).
42. Anker, J. N., et al. in *Nanosci. Technol. A Collect. Rev. from Nat. Journals* 308–319, https://doi.org/10.1142/9789814287005_0032 (World Scientific Publishing Co., 2009).
43. Sannomiya, T. & Vörös, J. Single plasmonic nanoparticles for biosensing. *Trends Biotechnol.* **29**, 343–351 (2011).
44. Guglielmelli, A. et al. Thermoplasmonics with gold nanoparticles: a new weapon in modern optics and biomedicine. *Adv. Photonics Res.* **2**, 2000198 (2021).
45. Dreaden, E. C., Alkildany, A. M., Huang, X., Murphy, C. J. & El-Sayed, M. A. The golden age: gold nanoparticles for biomedicine. *Chem. Soc. Rev.* **41**, 2740–2779 (2012).
46. Loiseau, A. et al. Silver-based plasmonic nanoparticles for and their use in biosensing. *Biosensors* **9**, 78 (2019).
47. Narayanan, R. & El-Sayed, M. A. Changing catalytic activity during colloidal platinum nanocatalysis due to shape changes: Electron-transfer reaction. *J. Am. Chem. Soc.* **126**, 7194–7195 (2004).
48. Lee, C. L., Chang, K. C. & Syu, C. M. Silver nanoplates as inkjet ink particles for metallization at a low baking temperature of 100 °C. *Colloids Surf. A Physicochem. Eng. Asp.* **381**, 85–91 (2011).
49. He, M., Wang, Q., Zhang, J., Zhao, W. & Zhao, C. Substrate-independent Ag-nanoparticle-loaded hydrogel coating with regenerable bactericidal and thermoresponsive antibacterial properties. *ACS Appl. Mater. Interfaces* **9**, 44782–44791 (2017).
50. Lannutti, J., Reneker, D., Ma, T., Tomasko, D. & Farson, D. Electrospinning for tissue engineering scaffolds. *Mater. Sci. Eng. C.* **27**, 504–509 (2007).
51. Sill, T. J. & von Recum, H. A. Electrospinning: applications in drug delivery and tissue engineering. *Biomaterials* **29**, 1989–2006 (2008).
52. Liu, M., Duan, X.-P., Li, Y.-M., Yang, D.-P. & Long, Y.-Z. Electrospun nanofibers for wound healing. *Mater. Sci. Eng. C.* **76**, 1413–1423 (2017).
53. Ren, G. et al. Electrospun poly(vinyl alcohol)/glucose oxidase biocomposite membranes for biosensor applications. *React. Funct. Polym.* **66**, 1559–1564 (2006).
54. Li, D., Frey, M. W. & Baeumner, A. J. Electrospun polylactic acid nanofiber membranes as substrates for biosensor assemblies. *J. Membr. Sci.* **279**, 354–363 (2006).
55. Liang, D., Hsiao, B. S. & Chu, B. Functional electrospun nanofibrous scaffolds for biomedical applications. *Adv. Drug Deliv. Rev.* **59**, 1392–1412 (2007).
56. Li, W. J., Laurencin, C. T., Caterson, E. J., Tuan, R. S. & Ko, F. K. Electrospun nanofibrous structure: A novel scaffold for tissue engineering. *J. Biomed. Mater. Res.* **60**, 613–621 (2002).
57. Yang, Q. et al. Highly sensitive and selective sensor probe using glucose oxidase/gold nanoparticles/graphene oxide functionalized tapered optical fiber structure for detection of glucose. *Optik* **208**, 164536 (2020).
58. Rinoldi, C. et al. Mechanical and biochemical stimulation of 3D multilayered scaffolds for tendon tissue engineering. *ACS Biomater. Sci. Eng.* **5**, 2953–2964 (2019).
59. Pawłowska, S. et al. Ultraviolet light-assisted electrospinning of core-shell fully cross-linked P(NIPAAm-co-NIPMAAm) hydrogel-based nanofibers for thermally induced drug delivery self-regulation. *Adv. Mater. Interfaces* **7**, 2000247 (2020).
60. Rinoldi, C. et al. Three-dimensional printable conductive semi-interpenetrating polymer network hydrogel for neural tissue applications. *Biomacromolecules* **22**, 3084–3098 (2021).
61. Nasajpour, A. et al. Cholesteryl ester liquid crystal nanofibers for tissue engineering applications. *ACS Mater. Lett.* **2**, 1067–1073 (2020).
62. Baker, B. M. et al. The potential to improve cell infiltration in composite fiber-aligned electrospun scaffolds by the selective removal of sacrificial fibers. *Biomaterials* **29**, 2348–2358 (2008).
63. Kupka, V. et al. Well-blended PCL/PEO electrospun nanofibers with functional properties enhanced by plasma processing. *Polymers* **12**, 1403 (2020).
64. Haq, M. A., Su, Y. & Wang, D. Mechanical properties of PNIPAM based hydrogels: a review. *Mater. Sci. Eng. C.* **70**, 842–855 (2017).
65. Yoon, C. et al. Functional stimuli responsive hydrogel devices by self-folding. *Smart Mater. Struct.* **23**, 094008 (2014).
66. Praveena, S. M., Karuppiah, K. & Than, L. T. L. Potential of cellulose paper coated with silver nanoparticles: a benign option for emergency drinking water filter. *Cellulose* **25**, 2647–2658 (2018).
67. Chen, X. & Schluesener, H. J. Nanosilver: a nanoparticle in medical application. *Toxicol. Lett.* **176**, 1–12 (2008).
68. Anjum, S. & Gupta, B. Bioengineering of functional nanosilver nanogels for smart healthcare systems. *Glob. Chall.* **2**, 1800044 (2018).
69. Fong, J. & Wood, F. Nanocrystalline silver dressings in wound management: a review. *Int. J. Nanomed.* **1**, 441–449 (2006).
70. Wei, D., Sun, W., Qian, W., Ye, Y. & Ma, X. The synthesis of chitosan-based silver nanoparticles and their antibacterial activity. *Carbohydr. Res.* **344**, 2375–2382 (2009).
71. Yin, Q. Q. et al. Plasmonic molybdenum oxide nanosheets supported silver nanocubes for enhanced near-infrared antibacterial activity: Synergism of photothermal effect, silver release and photocatalytic reactions. *Appl. Catal. B* **224**, 671–680 (2018).
72. Wang, B., Zhang, L. & Zhou, X. Synthesis of silver nanocubes as a SERS substrate for the determination of pesticide paraoxon and thiram. *Spectrochim. Acta - Part A Mol. Biomol. Spectrosc.* **121**, 63–69 (2014).
73. Pierini, F. et al. Thermoplasmonic-activated hydrogel based dynamic light attenuator. *Adv. Opt. Mater.* **8**, 2000324 (2020).
74. Tagliacuzzi, M., Blaber, M. G., Schatz, G. C., Weiss, E. A. & Szeifer, I. Optical properties of responsive hybrid Au@Polymer nanoparticles. *ACS Nano* **6**, 8397–8406 (2012).
75. Müller, M. B. et al. Plasmonic library based on substrate-supported gradiential plasmonic arrays. *ACS Nano* **8**, 9410–9421 (2014).
76. Telis, V. R. N., Telis-Romero, J., Mazzotti, H. B. & Gabas, A. L. Viscosity of aqueous carbohydrate solutions at different temperatures and concentrations. *Int. J. Food Prop.* **10**, 185–195 (2007).
77. Surendar, C. & Raju, D. Determination of refractive index of glucose solution using low cost fiber optic sensor. *Int. J. Eng. Sci. Res. Technol.* **5**, 155–159 (2016).
78. Martinsson, E., Otte, M. A., Shahjamali, M. M., Sepulveda, B. & Aili, D. Substrate effect on the refractive index sensitivity of silver nanoparticles. *J. Phys. Chem. C.* **118**, 24680–24687 (2014).
79. Burns, D. T. & Walker, M. J. Origins of the method of standard additions and of the use of an internal standard in quantitative instrumental chemical analyses. *Anal. Bioanal. Chem.* **411**, 2749–2753 (2019).
80. Sarigul, N., Korkmaz, F. & Kurultak, I. A new artificial urine protocol to better imitate human urine. *Sci. Rep.* **9**, 20159 (2019).
81. Miyashita, M. et al. Development of urine glucose meter based on micro-planer amperometric biosensor and its clinical application for self-monitoring of urine glucose. *Biosens. Bioelectron.* **24**, 1336–1340 (2009).

Supporting Information

Chameleon-inspired multifunctional plasmonic nanoplatfoms for biosensing applications

*Yasamin Ziai,[†] Francesca Petronella,[§] Chiara Rinoldi,[†] Paweł Nakielski,[†] Anna Zakrzewska,[†]
Tomasz A. Kowalewski,[†] Weronika Augustyniak,^{||} Xiaoran Li,[⊥] Antonella Calogero[‡], Izabela
Sabala,^{||} Bin Ding,[⊥] Luciano De Sio,^{‡,Δ*} Filippo Pierini^{†*}*

[†]Department of Biosystems and Soft Matter, Institute of Fundamental Technological Research,
Polish Academy of Sciences, Warsaw 02-106, Poland

[§]Institute of Crystallography CNR-IC, National Research Council of Italy, Via Salaria Km
29,300, 00015 Monterotondo - Rome, Italy

^{||} Mossakowski Medical Research Institute, Polish Academy of Sciences, Warsaw 02-106, Poland

[⊥] Innovation Center for Textile Science and Technology, Donghua University, West Yan'an Road
1882, Shanghai 200051, China

[‡] Department of Medico-Surgical Sciences and Biotechnologies - Research Center for
Biophotonics, Sapienza University of Rome Corso della Repubblica 79, 04100 Latina, Italy

^ΔCNR-Lab. Licryl, Institute NANOTEC, Arcavacata di Rende, 87036, Italy

*Corresponding authors` e-mail addresses: luciano.desio@uniroma1.it, fpierini@ippt.pan.pl

1. Morphological structure of the neat P(NIPAAm-*co*-NIPMAAm) hydrogel

The morphological structure of the P(NIPAAm-*co*-NIPMAAm) hydrogel without embedding any nanoparticle was studied using SEM. Figure S1 shows the cell-like structure of the hydrogel, with a pore size of an average of 10 μm .

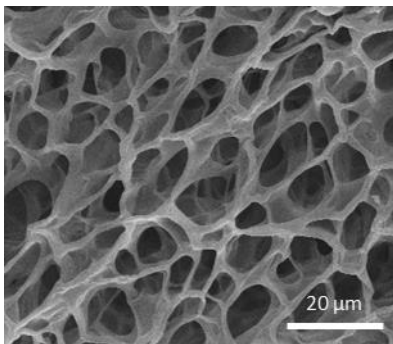


Figure S1. Characterization of nanostructured P(NIPAAm-*co*-PNIPMAAm) hydrogel. SEM image demonstrating the microstructure of the P(NIPAAm-*co*-NIPMAAm) hydrogel

2. Optical changes in the P(NIPAAm-*co*-NIPMAAm)/AgNCs hydrogel

When nanoparticles absorb light, the observer sees the light that is transmitted through the formulation, causing the observer to perceive the light of the complementary color to the absorbed color. When white light interacts with these particles, blue and green light is preferentially absorbed, and red light is transmitted through the material. Additionally, since plasmonic nanoparticles both scatter and absorb light, their perceived color is dependent on the perspective and the background. The reason why the plasmonic particles appear in different colors on different backgrounds is due to the fact that they have both scattering and absorption components within the same particle. In the case of silver nanoparticles, which have a plasmon

resonance in the blue region of the spectra, in the case of a lighter background more portion of the blue light will be absorbed, causing the change of the color to more green shades.

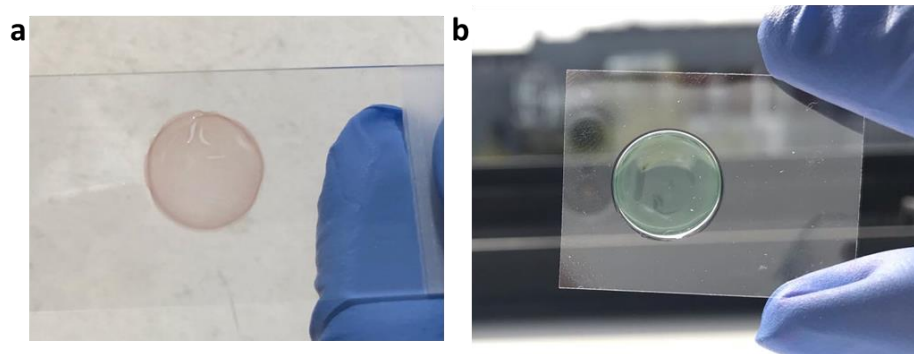


Figure S2. Optical observation of P(NIPAAm-*co*-NIPMAAm)/AgNCs. a) Image of the hydrogel with a solid white background, scattering most of blue light, showing a red-shade color. b) Hydrogel in natural light-absorbing the blue light and resulting in more blue-shade color.

3. Morphological structure of the P(NIPAAm-*co*-NIPMAAm) hydrogel embedded with different amounts of silver nanocubes (1:20-1:50)

AFM image of the P(NIPAAm-*co*-NIPMAAm) hydrogel embedded with AgNCs, showing the topography of the surface of the hydrogel containing silver cubes. Figure S3 shows the AFM images of the hydrogel containing two different concentrations of AgNCs. Images show the distribution of AgNCs in the hydrogel, where the difference is visible according to the average distance between nanoparticles.

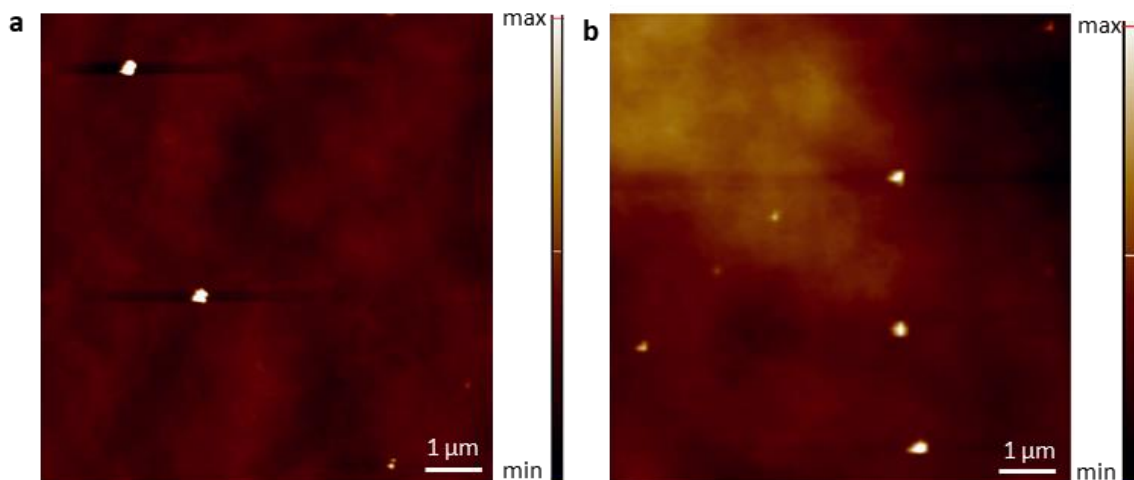


Figure S3. Characterization of nanostructured P(NIPAAm-*co*-PNIPMAAm) hydrogel embedded with AgNCs a) 2% wt b) 5% wt.

4. Antibacterial properties of P(NIPAAm-*co*-NIPMAAm) hydrogel embedded with AgNCs

Figure 4 presents the initial number of bacterial cells loaded onto hydrogel samples and enumerated by serial dilution after 4 hours of incubation on hydrogel samples with different concentrations of AgNCs. The number of bacterial cells incubated on hydrogels alone decreases by 50% after 4 hours of incubation, the really potent antibacterial activity is observed for samples with silver. In this case, over 99,9% of bacterial cells are eliminated. This drastic reduction in colony number demonstrates the potent antibacterial properties of the platform.

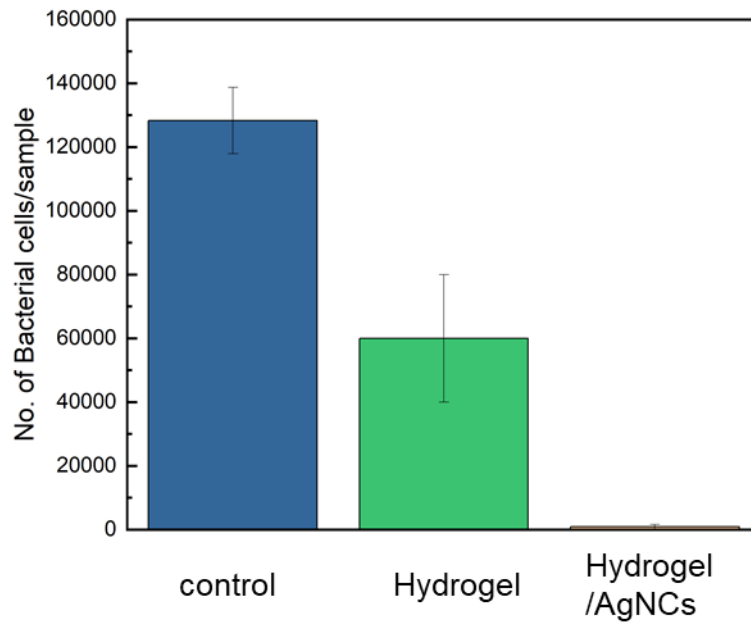


Figure S4. Antibacterial properties of the platform: average number of the colonies loaded on the samples and recovered after 4 hours of incubation on hydrogels alone and with AgNCs. The experiment was repeated three times with duplicates.

ARTICLE

Lysozyme-sensitive plasmonic hydrogel nanocomposite for colorimetric dry-eye inflammation biosensing

Yasamin Ziaj,^a Chiara Rinoldi^a, Francesca Petronella^b, Anna Zakrzewska^a, Luciano De Sio^c, Filippo Pierini^{*a}

https://www.google.com/imgres?q=ft-ir&imgurl=https%3A%2F%2Fuploa.d.wikimedia.org%2Fwikipedia%2Fcommons%2F1%2F1b%2FFFTIR_Spectrometer_%252B_ATR.jpg&imgrefurl=https%3A%2F%2Fen.wikipedia.org%2Fwiki%2FFourier-transform_infrared_spectroscopy&docid=w7DFRhaqFZYCSM&tbnid=hDULeqMmKL4F1M&vet=12ahUKEwjCk3SyKiFAxU0VvEDHdPTAJQMQ3oECDAQAA..i&w=776&h=599&hcb=2&ved=2ahUKEwjCk3SyKiFAxU0VvEDHdPTAJQMQ3oECDAQA
 Received 00th January 20xx,
 Accepted 00th January 20xx

DOI: 10.1039/x0xx00000x

Detection of lysozyme levels in ocular fluids is considered crucial for diagnosing and monitoring various health and eye conditions, including dry eye syndrome. Hydrogel-based nanocomposites have been demonstrated to be one of the most promising platforms for fast and accurate sensing of different biomolecules. In this work, hydrogel, electrospun nanofibers, and plasmonic nanoparticles are combined to fabricate a sensitive and easy-to-use biosensor for lysozyme. Poly(L-lactide-co-caprolactone)(PLCL) nanofibers were covered with silver nanoplates (AgNPLs), providing a stable plasmonic platform, where poly(N-isopropylacrylamide)-based hydrogel layer allows mobility and well-integration of the biomolecules. By integrating these components, the platform can also exhibit a colorimetric response to the presence and concentration of lysozyme, allowing for easy and non-invasive monitoring. Quantitative biosensing operates on the principle of localized surface plasmon resonance (LSPR) induced by plasmonic nanoparticles. Chemical, structural, thermal, and optical characterizations were performed on each platform layer, and the platform's ability to detect lysozyme at concentrations relevant to those found in tears of patients with dry eye syndrome and other related diseases was investigated by colorimetry and UV-Vis. This biosensor's sensitivity and rapid response time, alongside the easy detection by the naked eye, make it a promising tool for early diagnosis and treatment monitoring of eye diseases.

Introduction

Lysozyme, an essential protein in various body fluids, plays a pivotal role in the body's innate immune defense against bacterial infections¹. It has gained widespread recognition as a highly effective antibacterial agent, particularly renowned for its efficacy against Gram-positive bacteria due to its ability to break down their cell walls². Notably, c-type lysozyme exhibits presence in bodily fluids, with its concentration reaching its peak in tears and serum, ranging from 1 to 2 g.L⁻¹³, while being present at lower levels, around 1 to 10 µg.L⁻¹, in urine and cerebrospinal fluid⁴. Detecting elevated or dropped lysozyme levels can serve as a valuable non-specific indicator for various diseases in pathological conditions. For instance, heightened lysozyme levels have been associated with AIDS⁵, leukemia⁶, and dry eye disease (DED)⁷. As a result, monitoring lysozyme as a biomarker provides essential insights to track patients' health

status and make well-informed decisions regarding diagnosis, treatment, and disease progression.

Consequently, the escalating demand for affordable, rapid, and user-friendly biosensors enabling point-of-care diagnostics has led to developments in biosensing. Among the various affinity biosensors, those utilizing plasmonic materials have attracted significant attention due to their potential for studying surface plasmon resonance (SPR) signals resulting from lysozyme binding to receptors⁸. Plasmonic materials, notably noble metals like gold (Au) and silver (Ag), display an intriguing optical phenomenon when light excites from interactions between incident light and surface electrons, manifesting as an extinction spectrum⁹. Moving towards nanotechnology, noble nanoparticles have substantially enhanced biosensor sensitivity, enabling the detection of low concentrations of biomarkers and small biomolecules¹⁰. The optical properties of plasmonic materials, specifically the refractive index (RI) and resonance wavelength (λ_{max}), can be precisely controlled by manipulating factors such as nanoparticle shape, size, interparticle spacing, and the immediate surrounding environment. These attributes offer versatility across a broad spectral range, affording flexibility in designing biosensors for diverse applications.

Additionally, the ability to tailor the receptor environment further enhances the adaptability of plasmonic biosensors to

^a Department of Biosystems and Soft Matter, Institute of Fundamental Technological Research, Polish Academy of Sciences, Warsaw 02-106, Poland.

^b Institute of Crystallography CNR-IC, National Research Council of Italy, Via Salaria Km 29,300, 00015, Monterotondo - Rome, Italy

^c Department of Medico-Surgical Sciences and Biotechnologies, Sapienza University of Rome, Corso della Repubblica 79, 04100Latina, Italy

varying matrices^{11,12}. In conjunction with the precise LSPR biosensing methods, incorporating visual aids for rapid result determination can prove highly advantageous within practical applications. Visual colorimetry technique facilitates the rapid assessment of biomarker alterations resulting from nanoparticle aggregation¹³. Using the unique properties of plasmonic nanoparticles, a color change can be detected upon binding biomolecules to the surface of the nanoparticles. This phenomenon alters the absorption wavelength and scatter light. The intensity of the shift and color change can be directly correlated with the concentration of the target biomarker, offering a rapid and straightforward means of analysis^{14,15}.

Li et al. used a hybrid system comprising gold nanoparticles and ruthenate to detect lysozyme. In the absence of lysozyme, introducing ruthenate leads to particle aggregation, resulting in a visible color shift from red to blue. Conversely, in the presence of lysozyme, an electrostatic charge alteration induced by the interaction between plasmonic particles and ruthenate prevents aggregation, thereby preserving the original coloration¹⁶. A similar approach was undertaken by Castillo et al., who employed sodium chloride (NaCl) for lysozyme detection in urine samples. In this study, they harnessed the potential of particle aggregation, both in the presence and absence of lysozyme, as induced by NaCl¹⁷.

A suitable platform to carry the nanoparticles and provide a proper detecting matrix is necessary to maximize detection efficiency. Nanofibers, fabricated using the electrospinning technique, are promising candidates as substrates to carry plasmonic nanoparticles. Electrospinning involves applying an electric field to a polymer solution or melt, causing the polymer to elongate into ultrafine fibers with diameters ranging from nanometers to micrometers. This unique method enables the production of nanofibers with exceptional structural characteristics, including a high aspect ratio and interconnected porous network, alongside tunable mechanical properties¹⁸. Electrospun nanofibers from various natural and synthetic polymers have been widely used in biomedical applications such as tissue engineering¹⁹, wound dressing²⁰, drug delivery²¹, and biosensing²². Upon applying noble metal nanoparticles like gold or silver, the nanofibers can serve as ideal hosts for these nanoscale components due to their abundant surface area, enabling a higher loading capacity of plasmonic materials²³. From another point of view, focusing on enhancing the transport and detection of biomolecules and biomarkers within biosensing platforms, hydrogels have appeared as a promising class of materials, serving as carriers for these tiny particles²⁴. Hydrogels, characterized by their three-dimensional network structures, retain substantial amounts of water within their matrix. The high water capacity of hydrogels facilitates the efficient and controlled transport of biomolecules and biomarkers, allowing for enhanced interactions and improved sensitivity in biosensing assays. Their tunable and biocompatible nature further augments their suitability for accommodating diverse biomolecules and their feasibility for specific needs²⁵. Stimuli-responsive hydrogels exhibit reversible physical changes in response to minor alterations in their surrounding environment. Among these, poly(N-

isopropylacrylamide)-based hydrogels (PNIPAAm) stand out as a class of smart hydrogels with photothermal-responsive behavior²⁶. Incorporating recognition elements in the hydrogel structure allows for responsive reactions with specific chemical substances.

Consequently, these interactions trigger changes in the solubility or charge state of the hydrogel. Likewise, solubility changes can directly influence the hydrogel's volume response²⁷. Notably, these smart hydrogels demonstrate remarkable volume variations in response to even minor temperature fluctuations, making them particularly well-suited for various applications where precise temperature responsiveness is desirable²⁸.

Here in this research, we have fabricated a composite platform consisting of poly(L-lactide/ ϵ -caprolactone) (PLCL) nanofibers, Ag nanoplates (AgNPIs), and PNIPAAm hydrogel as a biosensor for lysozyme enzyme. AgNPIs were drop-casted onto the electrospun mat to provide a stable layer for detection, followed by the addition of hydrogel precursor. Penetration of the hydrogel into the structure of the mat before polymerization allows for the biomarkers to maneuver, resulting in facile recognition and efficient sensing. Each composite material component was investigated individually, and subsequently, an analysis of the entire composite was performed as a unified entity. A rapid colorimetry assay based on the aggregation of AgNPIs was also tested to check the system's applicability for naked-eye lysozyme detection. Photothermal responses and the sensing limits were examined, demonstrating the material's potential suitability as a viable candidate biosensor for lysozyme detection.

Materials and methods

Materials

N,N-isopropylacrylamide (NIPAAm, 97%, Sigma Aldrich, Poland), N-isopropylmethacrylamide (NIPMAAm, 97%, Sigma Aldrich, Poland), N,N'-methylene bisacrylamide (BIS-AAm, 99.5%, Sigma Aldrich, Poland), 2-Hydroxy-4'-(2-hydroxyethoxy)-2-methylpropiophenone (Irgacure 2959, 98%, Sigma Aldrich, Poland), silver nanoplates (AgNPIs, 53 nm, PVP, Nanocomposix, USA), Poly (L-lactide/ ϵ -caprolactone)(PLCL 70/30, Mn 80 kDa), Chloroform (CHCl₃, POCh, Poland), and N,N-dimethylformamide (DMF, POCh, Poland), Lysozyme human ($\geq 100,000$ units.mg⁻¹ protein, Sigma Aldrich, Poland) and Sodium chloride (NaCl, $\geq 99\%$, Sigma Aldrich, Poland) were used as received.

Electrospinning of PLCL

10% (w/w) of PLCL was dissolved into a chloroform/DMF solution mixture with a 90:10 (w/w) ratio. The solution was kept on stirring overnight using a magnetic stirrer prior to the electrospinning process. The electrospinning process was optimized to use a 15-kV positive voltage, 800 μ L.h⁻¹ flow rate, and a 26G needle tip at a distance of 15 cm from a rotating drum collector with 500 rpm speed to achieve favorable fibers. Electrospun nanofibers in the shape of a mat were collected

after using 2 mL of solution to achieve convenient thickness at room temperature (25°C) and 40% relative humidity.

Hydrogel precursor sol

A mixture of 578.13 mg NIPAAm, 15.63 mg NIPMAAm, 31.25 mg BIS-AAm, and 12.5 mg Irgacure 2959 was prepared. This mixture was dissolved in 10 mL of deionized water to reach 95.2 wt% of the solution. The sol was protected from light while stirred overnight using a magnetic stirrer up to its complete dissolution²².

Fabrication of the nanostructured platform

First, an aqueous solution of AgNPLs with 6.5% (v/v) was added onto the mat's surface via the drop-casting method to fabricate the nanocomposite structure. Kept under the hood, the water evaporated, and a composite of PLCL nanofibers loaded with AgNPLs was ready to use. Mats were cut in the favored size and shape and placed in the same shape mold, where hydrogel sol was added to the top. It is worth mentioning that argon bubbling must be applied to the sol before use to remove any oxygen in the mixture. The mold was placed in an ice bath and irradiated by an ultra-violet (UV) lamp (Dymax lamp with 400 W capacity and a power density of 225 mW cm⁻²) for 90 seconds.

Structural characterization

Field emission scanning electron microscopy (FE-SEM) and scanning electron microscopy (SEM) were performed with FEI Nova NanoSEM 450 and JEOL JSM-6390LV microscopes, respectively. Hydrogel discs and the final construct were frozen in liquid nitrogen before cutting the cross-section, and freeze-dried samples were obtained. Before imaging, samples were sputtered with gold layers around 8 nm thick using a SC7620 Polaron mini sputter coater (Quorum Technologies Ltd., Ashford, UK). Samples were freeze-dried, then the lyophilized materials were cut into small pieces, immersed in ethanol, and placed on a copper mesh with an amorphous carbon membrane. The size of nanofibers and hydrogel pores was then calculated using ImageJ. For transmission electron microscopy (TEM), samples were analyzed on an FEI Talos F200X TEM (acceleration voltage of 200 kV) after four hours of drying in a vacuum drier.

Energy-dispersive X-ray spectroscopy (EDX) analysis was also conducted using scanning transmission electron microscopy (STEM). This involved using a high-angle annular dark-field detector and a Super-X EDX system equipped with four silicon drift detectors (SDDs). The topography of the sample surface was examined using an atomic force microscope (AFM, Ntegra, NT-MDT) that featured a silicon cantilever (NSG01, NT-MDT, tip radius 10nm). These AFM measurements were carried out in semi-contact mode at a resonance frequency of 150 kHz, capturing 500x500 data points per image. The hydrodynamic size of the AgNPLs was determined through dynamic light scattering (DLS) using a Zetasizer Nano ZS analyser (Malvern Instruments). Aqueous dispersions containing 0.1% wt of AgNPLs were prepared, and the samples were placed into quartz micro-cuvettes for triple measurements to establish an average

size value. DLS was performed before and after sonication(500 W, 20 kHz, 3 min; Vibra-Cell™ Ultrasonic Liquid Processor).

Chemical characterization

A Multiskan GO spectrophotometer (Thermo Scientific, USA) was used to collect data on ultraviolet-visible (UV-Vis) spectra. UV-Vis spectrophotometer scanned from 400 nm to 1000 nm every 5 nm. Fourier-transform infrared (FT-IR) spectroscopy was used to characterize the functional groups in each layer. FT-IR analyses were conducted in an attenuated total reflectance (ATR) mode with a Bruker Vertex70 FT-IR Spectrometer and carried out in the wavenumber range of 400-4000 cm⁻¹ with a resolution of 2 cm⁻¹ and eight scans for each sample.

Photothermal-responsivity characterization

The near-infrared (NIR) light source utilized was a diode laser from CNI (Changchun New Industries Optoelectronics Technology Co., Ltd.), which operates within the absorption spectrum of AgNPLs (longitudinal plasmon band) and features a rectangular beam profile. To assess and visualize the spatial distribution of heat and the temperature profile during laser exposure, a high-resolution thermal camera (FLIR, A655sc) was used. This camera captures thermal images at a resolution of 640x480 pixels with a precision of ±0.2°C. Additionally, it integrates smoothly with the FLIR ResearchIR Max software, which handles and analyzes the collected thermal data.

Colorimetry

Visual colorimetric analysis was conducted on optimized solutions, considering the Lysozyme concentration in a single eye drop, AgNPLs concentration, and the utilization of commercially available 0.9% sodium chloride solution serum, commonly known as saline solution. Various concentrations of Lysozyme and AgNPLs mixtures were prepared, and each solution was subsequently augmented with saline solution. The alteration in coloration was documented using a standard smartphone camera, both before and after the addition of NaCl, with intermediate recordings captured at 10, 30, and 60-minute intervals. Simultaneously, a Multiskan GO spectrophotometer (Thermo Scientific, USA) was employed to record changes in the absorption spectra of each sample at the same time intervals. For the colorimetric analysis of the finalized platform, pre-fabricated platforms were air-dried and subsequently immersed in a lysozyme solution, allowing the hydrogel component of the platform to swell to its original dimensions for 2 hours. Following this, saline solution was introduced into the platform, with observable color changes manifesting within 15 minutes.

Lysozyme sensing tests

The absorption spectra of AgNPLs-based platforms were collected by using a UV-Vis spectrometer (Lambda 365, Perkin Elmer). The sensing ability of the AgNPLs-based platforms was tested by preparing standard solutions of lysozyme in water at the following concentrations: 2 mg. mL⁻¹, 1.5 mg. mL⁻¹, 1 mg. mL⁻¹, 0.5 mg. mL⁻¹

The samples were placed on a glass substrate, and then 200 μL of Lysozyme standard solution was cast on the nanostructured platform. They were kept at rest for 15 minutes to promote a uniform and complete distribution of the solution within the samples before evaluating the optical response.

At this stage, the excess of the lysozyme solution (not in direct contact with the sample) was carefully removed, and the wet nanoplatform was carefully placed in the sample holder to measure its absorption spectrum.

Each absorption spectrum was mathematically converted into its first-order derivative to determine the wavelength of the plasmon peak of AgNPIs (λ_{max}).

After that, the optical shift ($\Delta\lambda$) was calculated as the difference between the λ_{max} value measured after ($\lambda_{\text{max_lyso}}$) and before (λ_{max}) the contact with the lysozyme solution, respectively.

$$\Delta\lambda = \lambda_{\text{max}} - \lambda_{\text{max_lyso}} \quad (1)$$

The $\Delta\lambda$ values were plotted against the lysozyme concentration to obtain the calibration curve, and the experimental points were interpolated using a linear fit.

The sensing limits was calculated as three times the standard deviation of the blank. It was calculated by performing five times the absorption spectrum of the sample soaked with water and multiplying by three the standard deviation of the average $\Delta\lambda$ value.

A standard addition method was also employed to monitor the lysozyme concentration in human tears samples. A defined concentration of lysozyme solutions was added to the collected human tear samples before and after wearing contact lenses for 5 hrs (written and signed agreement has been obtained from the volunteer for the experiment.). These solutions infiltrated the nanoplatforms, and the resulting optical shift was detected. The lysozyme concentration in human tears was calculated using the standard addition plot.

Results and discussion

Silver nanoparticles (AgNPIs). AgNPIs were selected as the plasmonic entities in this experimental platform with an average dimension of 40 ± 15 nm. The dimension specified here refers to an average, as the particles, despite having consistent sizes, exhibit various shapes. The choice of these particular particles is strategic; the optical properties of nanoparticles are influenced by their shape and size. Even though these particles are of uniform size, the presence of diverse shapes with sharp and round edges enhances the precision and sensitivity of the biosensor²⁹. The morphological diversity of platelet-shaped AgNPIs is precisely captured through Transmission electron microscopy (TEM) images in **Figure 1a-c**, each offering a different shape and controlled thickness. Dynamic light scattering (DLS) measurements were conducted on the nanoparticles before and after sonication. The nanoparticles' average size was also calculated using DLS, where they are reported to be an average of 57.2 ± 0.53 nm. Although the difference between the size resulted from the TEM and DLS method due to the hydrodynamic radius is a known fact, having different shapes of the nanoplates offering a more diverse

hydrodynamic radius has its effect in this case. The observation that their average size remained consistent throughout sonication is additional evidence of their stability and resistance to aggregation (**Figure S1, S2**). An example of representative particle dispersion is also visually presented in the TEM image in **Figure 1d**, confirming the stability of nanoparticles and the absence of inter-particle aggregation phenomena.

Further insight into the features of these nanoparticles is offered by energy-dispersive spectroscopy (EDS) elemental mapping, as shown in **Figure 1e**, highlighting the structural shape of the nanoparticles with the average size and distribution. Morphological characterization continues via Field-Emission Scanning Electron Microscopy (FE-SEM) visualization, as shown in **Figure 1f**, showing a comprehensive understanding of the plasmonic nanoparticles' topographical dispersion. As can be seen, AgNPIs are well-distributed, and there are no signs of aggregation between them, confirming their stability in the system.

Fabrication of multi-layer nanostructured platform. The stepwise procedure of fabrication of the final nanostructure is illustrated in **Figure 2a**. In the initial step, the electrospinning technique was used to fabricate the poly (L-lactide/ ϵ -caprolactone) (PLCL) nanofibrous mat. Several critical parameters, including voltage, flow rate, working distance, and needle gauge size, were optimized to attain the desired uniform nanofibers. The nanofibrous mat was subsequently sectioned into well-plate dimensions using a cork borer. In each well, precise aliquots of AgNPIs with a defined concentration of $65 \mu\text{L}\cdot\text{mL}^{-1}$ were introduced with a drop-casting methodology. The well plate was then sealed and incubated overnight in darkness to facilitate particle deposition within the network as the solvent gradually evaporated. Notably, a visible visual transition, from white to blue, was observed upon AgNPIs introduction, confirming their presence within the system. A solution of hydrogel precursor, prepared as outlined in the materials and methods section, was then added to the plasmonic nanofibers. This solution incorporated NIPAAm and NIPMAAm monomers along with Irgacure as a photoinitiator, necessitating UV irradiation to initiate photo-polymerization. Before polymerization, the precursor solution underwent a brief period of argon bubbling to deplete oxygen content effectively. Subsequently, the precursor solution was uniformly dispensed onto each plasmonic nanofiber within the well plate. The entire assembly was carefully immersed in an ice bath when UV irradiation was applied for 60 seconds to complete the hydrogel polymerization process. Utilizing an ice bath is imperative so that the temperature does not exceed the material's characteristic lower critical solution temperature (LCST) during UV irradiation. Each part of the platform was characterized separately.

Material characterization involved atomic force microscopy (AFM) topographic analysis of PLCL fibers, presented in **Figures 2b and 2c**. These images provide an illustrative representation of the surface topography of the fibers, offering insights into their size and morphology. **Figures 2a and 2b**, with $5 \mu\text{m}$ and $2.5 \mu\text{m}$ Z-scale bars, respectively, represent the vertical changes in

cantilever position over the sample. This Z-scale, denoting sensor height topography, is an indicator of surface properties. As can be seen, AFM images were also done after particle drop-casting. However, as a result of the size and well-dispersion of the particles, no sign of the particles was seen in the AFM images regarding the magnification. Fourier Transform Infrared (FT-IR) spectroscopy, as depicted in **Figure S3**, shows the chemical composition of nanofibers with and without AgNPs. Notably, there is no sign of the silver content within the electrospun fiber network which is a sign of no aggregation of the nanoparticles and their stability in the system.

Remarkably, a transition in wettability features is detected through contact angle measurements (Figure 2d,e). Specifically, the contact angle of the fibers is dropped from 128.8° to 71.3°, indicating a shift from hydrophobicity to hydrophilicity. This can happen due to changes in the surface charge and energy of the mat which is also known as nanoparticle-induced hydrophilicity³⁰. This alteration in surface characteristics is of great significance, particularly concerning following fabrication steps involving adding a hydrogel precursor solution composed mainly of aqueous content. The increased hydrophilicity of the fibers facilitates solution permeation throughout the fibrous network, thereby fostering superior integration, anchorage efficacy, and consequent structural stability within the final platform³¹. As shown in the FE-SEM image in Figure 2f, nanofibers are in the same shape and diameter, uniform and continuous with an average diameter of $1.478 \pm 0.183 \mu\text{m}$. Figure 2g shows the interconnected porous 3D structure of hydrogel, where the pore sizes have a 2-5 μm dimension. This image has been taken from pure hydrogel prepared separately after freeze-drying to show precisely the intra-structure of the hydrogel. Finally, Figures 2h and 2i show the intersection between the hydrogel and fiber layers and their anchorage and penetration. These images confirm the hydrogel's stable structure and full fiber penetration. This platform feature helps the following application regarding biosensing of lysozyme, as it allows biomolecule transition into the network, offering more sensing area.

Fast photothermal responsiveness of the nanocomposite. The NIR-induced photothermal-responsive characteristics of the plasmonic nanoplatforms were explored using a red laser operating at 808 nm wavelength with an intensity of 1500 mW cm^{-2} . The presence of AgNPs within the platform is a distinctive absorption peak within the visible spectrum, showing exceptional photothermal efficiency by converting absorbed light into thermal energy. As the generated heat from the NIR laser, operating at the absorption peak surpasses the hydrogel's VPTT, a cascade-like series of stimulus-response events happen, resulting in a shrinkage of the hydrogel and subsequent expulsion of water. These phenomena are the significant thermo-responsive properties inherent to the hydrogel.

Figure 3a illustrates the experimental setup used for the photothermal assessment of the composite platform. A continuous-wave (CW) laser source emits an 808 nm wavelength laser beam, which irradiates upon the composite platform following passage through a custom-designed optical

apparatus. Thermographic imaging, capturing variations in sample temperature throughout different irradiation durations, is recorded by a thermal camera positioned orthogonally to the sample.

In Figure 3b, thermal images corresponding to various hydration levels and irradiation durations of the platform are presented. Employing thermal imaging technology, we observed an immediate temperature elevation in both dry and hydrated states of the platform, indicating a direct responsiveness to the applied stimuli. Notably, compared to pure NIPAAm-based hydrogels lacking photothermal responsiveness, the introduction of plasmonic AgNPs modifies the composite into a highly responsive platform. Dry samples exposed to laser irradiation for 300 seconds exhibited a temperature rise to approximately 48°C, while under identical conditions, hydrated platforms reached a maximum temperature of 39.7°C. This disparity arises from variations in the absorption peak between hydrated and dry states, causing a shift in the absorption profile when in a fully hydrated state, no longer optimally aligned with laser emissions, thus reducing photoresponsivity. This phenomenon can also be attributed to differences in the surrounding media; notably, considering the immediate vicinity of the plasmonic particles, water has higher thermal capacity, leading to minor changes in temperature. These findings are presented as time-temperature profiles in Figure 3c. While the laser remained active, prompt temperature elevations of nearly 50°C in the dry state and up to 40°C in the hydrated state were evident. In both scenarios, the temperature escalation can be attributed to the photothermal efficiency of AgNPs. Following the deactivation of the laser and removing the pump beam, the samples swiftly returned to room temperature, taking less than one minute. This property can be beneficial in the reusability of the nanoplatforms, as they can easily be washed, and using just a high temperature of water and changes in the volume, the platform can be washed and used again.

Visual colorimetry

Using NaCl as an aggregating agent, visual colorimetry was employed in both the solutions and the final platform. Following the methods detailed earlier, we conducted visual colorimetry on previously optimized solutions comprising plasmonic particles, lysozyme, and saline. Given that a healthy lysozyme concentration typically falls between 1-2 mg mL^{-1} , with levels under 1 mg mL^{-1} considered indicative of unhealthy conditions, we chose to test various lysozyme concentrations of 0, 0.5, 1, 1.5, and 2 mg mL^{-1} . **Figure 4a** shows the schematic of the principle behind colorimetry using NaCl as a salt. The system containing the same amount of silver is exposed to various concentrations of lysozyme, ranging from unhealthy to healthy. Upon adding the lysozyme to the system, the biomolecule tends to attach to the surface of the nanoparticles. Visual colorimetry happens when using a standard concentration of NaCl available in saline serum. By infiltrating the platforms with the saline solution, due to the changes in the surface charges of nanoparticles, they tend to aggregate. In the healthy range of lysozyme presence, they will act as shields and do not let the aggregation occur, whereas, in the non-sufficient amount of

lysozyme, they can not defeat NaCl. This will result in the aggregation of nanoparticles, which will appear as a change in absorbance peak and visual color. Figures 4b and 4c depict the absorption spectra of the samples immediately after NaCl addition and after 60 minutes. The peak wavelengths initially showed subtle shifts, indicating limited particle aggregation, particularly in samples 2 and 5. However, after 60 minutes, as shown in Figure 4c, more significant shifts in absorption wavelengths were evident, leading to visible color changes.

Changes in the absorption spectra of the solution were measured using UV-Vis at other time points like 10 and 30 mins (Figure S4, S5). Using these data, Figure S6 presents the correlation between lysozyme concentration and changes in maximum absorption wavelengths, revealing a linear trend. This underscores that in our optimized system, higher lysozyme concentrations yield smaller $\Delta\lambda$ values, resulting in more stable color shades compared to the prominent color changes observed at lower concentrations, as illustrated in Figure S6. Figure 4d demonstrates the result of NaCl addition at four different time points. Initially, when lysozyme was added to the aqueous AgNPLs solution, all samples exhibited the same blue coloration. However, upon the addition of the designated amount of NaCl, noticeable color changes were observed. Samples 1 and 2, representing lysozyme concentrations below the healthy range, exhibited a rapid shift to a more purple hue. Over time, these color changes became even more pronounced at the 30 and 60-minute intervals, while samples 4 and 5, containing healthy lysozyme levels, remained stable. This reaffirms the viability of our method for visual colorimetry. The changes in the wavelength $\Delta\lambda$ were also described in a bar chart provided in Figure 4e. As seen in this demonstration, samples below the healthy region underwent enormous $\Delta\lambda$; In contrast, those with a healthy amount of lysozyme stayed in the same wavelength region with minimal change.

Moreover, we extended our investigations to assess potential color changes on the final platform. It's noteworthy that due to the extended travel time of particles within the porous hydrogel structure, it takes more time for color changes to become apparent. After applying the requisite amount of lysozyme and NaCl as specified in the methods section, we observed a visible color change in the sample with $0.5 \text{ mg}\cdot\text{mL}^{-1}$ of lysozyme, indicating the potential practicality of the platform (Figure S7).

Lysozyme biosensing

The absorption spectrum of the Ag nanoplates-based platform is reported in Figure 5a. The spectrum shows an increasing absorption range from 500 nm to 1000 nm, with a shoulder appearing at 540 nm. To better identify this absorption signal, the spectrum was converted to its first derivative, as depicted in the red line of Figure 5a. By differentiating the spectrum, we can appreciate the rate of absorbance change as a function of the wavelength. It allows the identification of minor spectral features, removing the effects of the matrix and the background. Indeed, the first derivative absorption spectrum points out an absorption deep at 540 nm. This absorption signal can be safely associated with the plasmon band of AgNPLs, and the broad peak indicates the effect of different shapes of the

nanoparticles, where they have the same size. The position of the AgNPLs plasmon band is blue-shifted with respect to the maximum of the plasmon band of Ag nanoplates dispersed in water due to the variation of the refractive index of the medium³².

Experimental results reported in Figure 5b highlight the spectroscopic behavior of the Ag-based nanoplatforms as a function of the surrounding refractive index. The sample showed an absorption deep at 605 nm; however, when it is soaked with pure water or lysozyme, the deep shifts to 557 nm and 534 nm, respectively. The spectral blue shift of the absorption spectrum can be ascribed to a variation in the refractive index surrounding Ag nanoplates. After the milli-Q water is introduced into the dried sample, the average refractive index is expected to decrease slightly, probably due to the alteration of the density of polymer molecules. Accordingly, the decreased local refractive index value resulted in a blue shift of 48 nm of the plasmon bands of AgNPLs. Also, the introduction of lysozyme solution determined a 71 nm-blueshift of the Ag nanoplates plasmon band. The sensitivity of the plasmon wavelength position is exploited to use the AgNPLs-based platforms as a biosensing system for lysozyme quantification.

To investigate the possibility of detecting the lysozyme from bodily fluids, we have first to assess the potential and limit of detection of the nanoplatforms. The AgNPLs-based samples were soaked with solutions with different concentrations of lysozyme ranging from $0 \text{ mg}\cdot\text{mL}^{-1}$ to $2.5 \text{ mg}\cdot\text{mL}^{-1}$. The absorption spectrum is collected and mathematically converted in its first derivative to measure the λ_{max} . At this stage, the $\Delta\lambda$ is calculated with equation 1 and reported as a function of the lysozyme concentration (Figure 5c).

The next set of experiments was conducted to examine the possibility of nanoplatforms being used to detect the human eye's tears and the amount of lysozyme. Figure 5d shows the experiment's procedure, starting with collecting tears from a normal eye and an eye in a non-healthy condition. As described in the material and methods section, these drops were added to the standard lysozyme solutions prepared before. AgNPLs-based nanoplatforms were infiltrated with these solutions, and after careful placement in the holder, their absorbance was detected. Figure 5e shows the results of this experiment. Analysis of the experimental data using tears revealed a blue shift of 26 nm. Based on the linear interpolation in Figure 5c, this shift corresponds to a lysozyme concentration of $3.6 \text{ mg}\cdot\text{mL}^{-1}$. The donor wore contact lenses for over 5 hours and stimulated lacrimation. This elevated concentration suggests a potential inflammatory state, which can be detected using the developed AgNPLs-based nanoplatform.

Conclusions

In this work, we have successfully designed and fabricated a soft nanocomposite platform by integrating PLCL nanofibers covered with AgNPLs and a PNIPAAm hydrogel. PLCL nanofibers with high surface area provide physical stability to the system and, with their unique structural properties, provide a stable

substrate to carry nanoparticles. Silver nanoplates, a type of plasmonic nanoparticle, were added to the system with the aim of colorimetry and LSPR biosensing of lysozyme. A NIPAAm-based hydrogel layer was added to the system to offer a more available matrix for the final purpose of the nanoplates. Hydrogels, with their high water content, will provide a transportable matrix for nanoparticles and biomolecules, making biosensing more efficient and sensitive. The design of AgNPLs-based nanoplates represents a significant advancement in the non-invasive and efficient detection of lysozyme levels in ocular fluids. Comprehensive chemical, optical, and structural characterization of layers of nanoplates was conducted, ensuring a well-fabricated and stable platform. Photothermal characterization of the platforms using a thermal camera confirms the possibility of reusability of the system, benefiting from the synergy effect of NIPAAm-based hydrogel and AgNPLs. The possibility of visual colorimetry was tested on the system, showing the color change from blue to purple hue in the case of dry-eye condition. The innovative approach of colorimetry using saline serum, available to everyone, makes this system an accessible and non-invasive method for examining their health. The LSPR phenomenon induced by plasmonic nanoparticles was done to make the biosensing more quantitative and underscore its capability to accurately detect lysozyme concentrations in conditions such as dry eye syndrome. The biosensor's notable sensitivity, rapid response time, and simplicity of visual detection reveal its potential as a valuable tool for the early diagnosis and ongoing management of various eye-related health issues.

Author Contributions

Y. Z. designed the experiments and fabricated the nanoplates. Y. Z. performed the morphological and chemical characterization of nanofibers. A.Z. performed FE-SEM and TEM analyses. Y.Z. and C.R. performed the colorimetry experiments. F.Pe and L.D. performed the biosensing experiments with human tears. Y.Z. wrote the manuscript. F. Pi. conceived the idea and supervised the project. All authors discussed the results and commented on the manuscript.

Conflicts of interest

There are no conflicts to declare.

Acknowledgments

This work was supported by the National Science Centre (NCN) SONATA BIS Project No. 2020/38/E/ST5/00456. Figures 2, 3, 4, and 5 were partially created with BioRender. C.R. and F.P. acknowledge the financial support from the Polish Ministry of Science and Higher Education through scholarships for outstanding young scientists.

References

- 1 T. Jesse Joel, S. Suguna S. and S. R. Steffi, *Asian J. Pharm. Res. Heal. Care*, 2016, **8**, 42–46.
- 2 G. Leśniewski and T. Yang, *Trends Food Sci. Technol.*, 2021, **107**, 333–342.
- 3 R. L. Pietsch and M. E. Pearlman, *Arch. Ophthalmol.*, 1973, **90**, 94–96.
- 4 J. Hankiewicz and E. Swierczek, *Clin. Chim. Acta*, 1974, **57**, 205–209.
- 5 M. H. Grieco, M. M. Reddy, H. B. Kothari, M. Lange, E. Buimovici-Klein and D. William, *Clin. Immunol. Immunopathol.*, 1984, **32**, 174–184.
- 6 P. Venge, T. Foucard, J. Henriksen, L. Håkansson and A. Kreuger, *Clin. Chim. Acta*, 1984, **136**, 121–130.
- 7 Z. Jia, W. Wei, K. Tu, B. Fang, M. Zhang and L. Shi, *Sensors Actuators B Chem.*, 2023, **378**, 133179.
- 8 G. Melinte, G. Selvolini, C. Cristea and G. Marrazza, *Talanta*, 2021, **226**, 122169.
- 9 Y. Ziai, C. Rinoldi, P. Nakielski, L. De Sio and F. Pierini, *Curr. Opin. Biomed. Eng.*, DOI:10.1016/j.cobme.2022.100413.
- 10 T. Špringer, M. L. Ermini, B. Špačková, J. Jabloňkú and J. Homola, *Anal. Chem.*, 2014, **86**, 10350–10356.
- 11 T. Xu and Z. Geng, *Biosens. Bioelectron.*, 2021, **174**, 112850.
- 12 M. Cottat, N. Thioune, A. M. Gabudean, N. Lidgi-Guigui, M. Focsan, S. Astilean and M. Lamy de la Chapelle, *Plasmonics*, 2013, **8**, 699–704.
- 13 X. Wang, Y. Xu, Y. Chen, L. Li, F. Liu and N. Li, *Anal. Bioanal. Chem.*, 2011, **400**, 2085–2091.
- 14 M. S. Verma, J. L. Rogowski, L. Jones and F. X. Gu, *Biotechnol. Adv.*, 2015, **33**, 666–680.
- 15 Y. Song, W. Wei, X. Qu, Y. Song, W. Wei and X. Qu, *Adv. Mater.*, 2011, **23**, 4215–4236.
- 16 J. Li, X. Mu, K. C. Chan, C. C. Ko and M. J. Li, *Microchim. Acta*, 2018, **185**, 1–6.
- 17 P. M. Castillo, F. J. Fernández-Acejo, J. M. Carnerero, R. Prado-Gotor and A. Jimenez-Ruiz, *Nanomater.* 2021, Vol. 11, Page 612, 2021, **11**, 612.
- 18 P. Nakielski, C. Rinoldi, M. Pruchniewski, S. Pawłowska, M. Gazińska, B. Strojny, D. Rybak, K. Jezierska-Woźniak, O. Urbanek, P. Denis, E. Sinderewicz, W. Czelejewska, J. Staszkiwicz-Chodor, M. Grodzik, Y. Ziai, M. Barczewska, W. Maksymowicz and F. Pierini, *Small*, 2022, **18**, 2104971.
- 19 C. Rinoldi, A. Fallahi, I. K. Yazdi, J. Campos Paras, E. Kijeńska-Gawrońska, G. Trujillo-De Santiago, A. Tuoheti, D. Demarchi, N. Annabi, A. Khademhosseini, W. Swieszkowski and A. Tamayol, *ACS Biomater. Sci. Eng.*, 2019, **5**, 2953–2964.
- 20 D. Rybak, Y. C. Su, Y. Li, B. Ding, X. Lv, Z. Li, Y. C. Yeh, P. Nakielski, C. Rinoldi, F. Pierini and J. M. Dodda, *Nanoscale*, 2023, **15**, 8044–8083.
- 21 K. Goodarzi, F. Jonidi Shariatzadeh, A. Solouk, S. Akbari and H. Mirzadeh, *Eur. Polym. J.*, 2020, **139**, 109992.
- 22 Y. Ziai, F. Petronella, C. Rinoldi, P. Nakielski, A. Zakrzewska, T. A. Kowalewski, W. Augustyniak, X. Li, A. Calogero, I. Sabała, B. Ding, L. De Sio and F. Pierini, *NPG Asia Mater.*, DOI:10.1038/S41427-022-00365-9.
- 23 C. Cleeton, A. Keirouz, X. Chen and N. Radacsi, *ACS*

- Biomater. Sci. Eng.*, 2019, **5**, 4183–4205.
- 24 H. R. Culver, J. R. Clegg and N. A. Peppas, *Acc. Chem. Res.*, 2017, **50**, 170–178.
- 25 Y. Ziai, C. Rinoldi, P. Nakielski, L. De Sio and F. Pierini, *Curr. Opin. Biomed. Eng.*, 2022, **24**, 100413.
- 26 G. Li, L. Zhang, Q. Han, T. Zheng, L. Wu, W. Guan, S. Sun and Y. Yang, *Compos. Part B Eng.*, 2023, **254**, 110551.
- 27 N. Sood, A. Bhardwaj, S. Mehta and A. Mehta, *Drug Deliv.*, 2016, **23**, 758–780.
- 28 S. Pawłowska, C. Rinoldi, P. Nakielski, Y. Ziai, O. Urbanek, X. Li, A. Kowalewski, B. Ding and F. Pierini, *Wiley Online Libr. Pawłowska, C Rinoldi, P Nakielski, Y Ziai, O Urbanek, X Li, TA Kowalewski, B Ding* *Advanced Mater. Interfaces*, 2020 • *Wiley Online Libr.*, , DOI:10.1002/admi.202000247.
- 29 M. Shabaninezhad and G. Ramakrishna, *J. Chem. Phys.*, 2019, **150**, 144116.
- 30 N. Gao, Y. Yan, X. Chen and D. J. Mee, *Langmuir*, 2012, **28**, 12256–12265.
- 31 Y. Ziai, M. Lanzi, C. Rinoldi, S. S. Zargarian, A. Zakrzewska, A. Kosik-Kozioł, P. Nakielski and F. Pierini, *Nanoscale Adv.*, 2024, **6**, 1246–1258.
- 32 F. Rojas, C. O.-A. chimica acta and undefined 2009, *ElsevierFS Rojas, CB Ojeda* *Analytica Chim. acta*, 2009 • *Elsevier*.

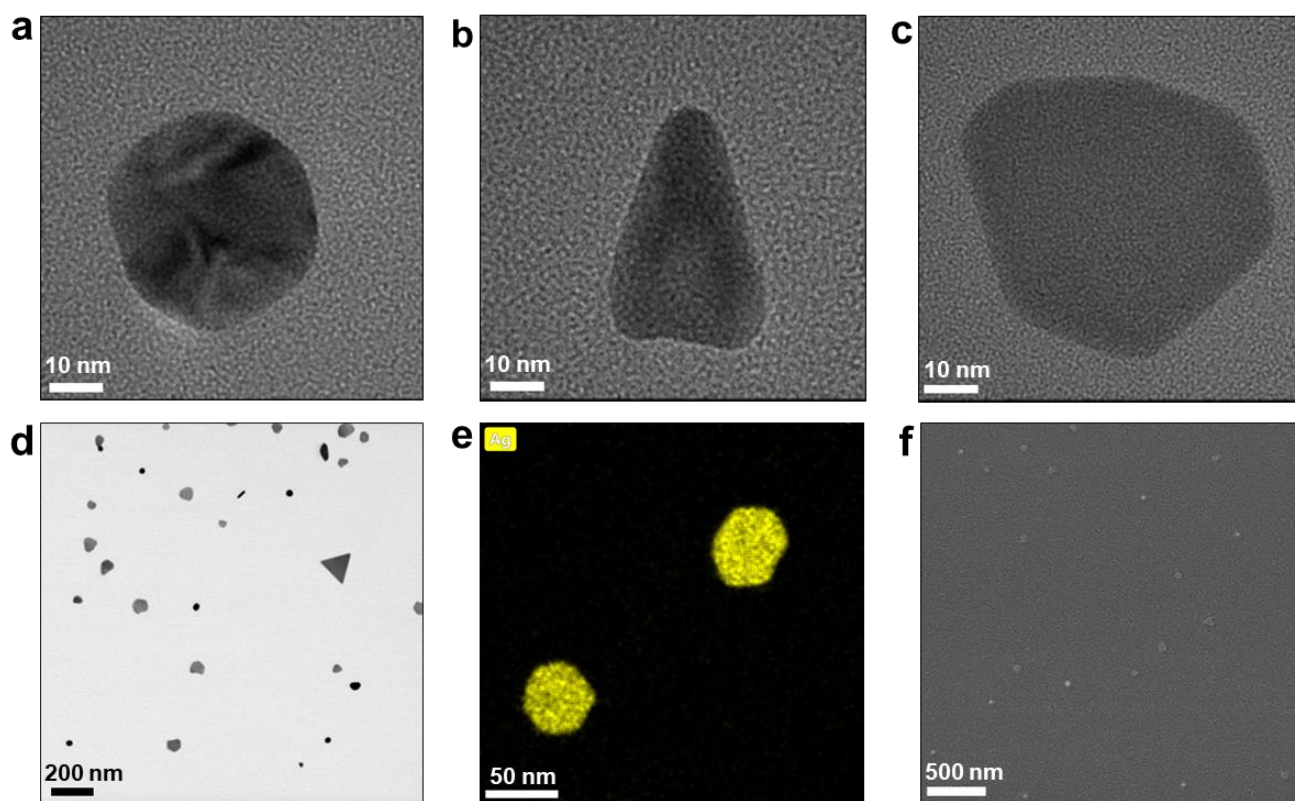


Figure 1. Characterization of silver nanoplates. a-c) TEM images of the AgNPIs show the different shapes of the particles, consisting of circular, triangle, and polygonal, with the same average dimension. e) TEM image with lower resolution showing the dispersity of the particles, indicating their stability in the system without aggregation. f) EDS mapping of the particles showing the average size and distribution of particles. g) FE-SEM of the particles, showing their distribution and stability.

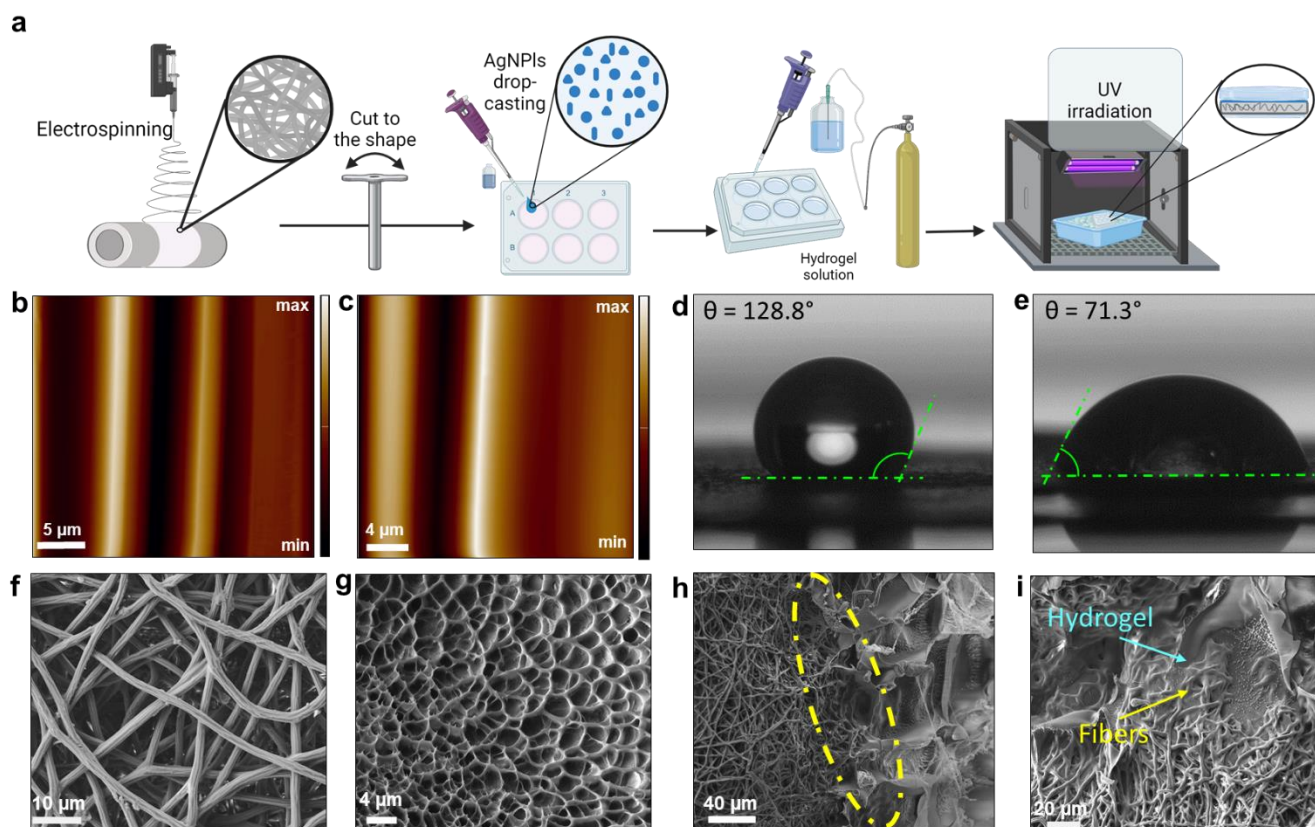


Figure 2. Nanoplatfrom fabrication and characterization. a) Scheme of the fabrication process of the nanoplatforms, electrospinning was done, and the PLCL nanofibers were cut into the desired shape. AgNPIs were added to each sample, and then hydrogel solution was added to the top of each layer. The whole structure was irradiated under UV light to complete polymerization. b-c) AFM images of the PLCL nanofibers before and after applying nanoparticles show no changes in the size and shape of the fibers, showing no changes in the surface of nanofibers. d) contact angle of the PLCL fibers before applying the silver particles, showing high hydrophobicity with the contact angle of 129° and e) contact angle of PLCL nanofibers after the addition of nanoparticles, which enhanced the hydrophilicity of the fibers, making them more appropriate for layering with hydrogel. f) SEM image of PLCL nanofibers showing their regular defect-free shape, with the average size of $1.478 \pm 0.183 \mu\text{m}$. g) SEM images of the porous NIPAAm-based hydrogel layer with the average pore size of $3.067 \pm 0.06 \mu\text{m}$. h) FE-SEM image of the cross-section of the layers, showing the incorporation of the fibers into the hydrogel matrix and i) FE-SEM of the cross-section showing the stable and robust engagement of the layers, making a steady nanoplatfrom.

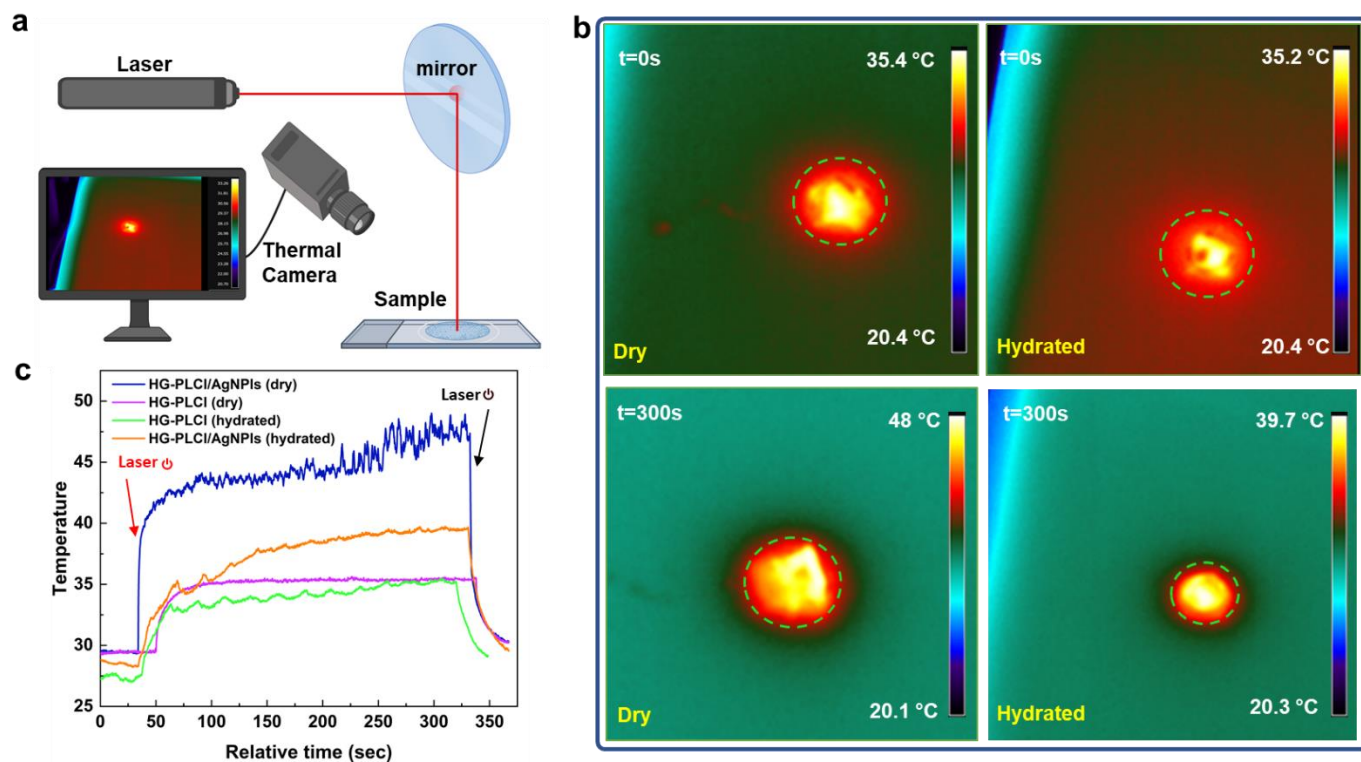


Figure 3. Thermo-responsive properties of the nanoplateforms. **a)** schematic of the procedure, using a laser and a thermal camera to heat up and record the changes in the temperature. **b)** Thermal images of the samples in both dry and hydrated states show the system's temperature rise at the same time point. **c)** Temperature vs. time graphs for the samples, showing the fast photothermal responsiveness upon turning on and off the laser.

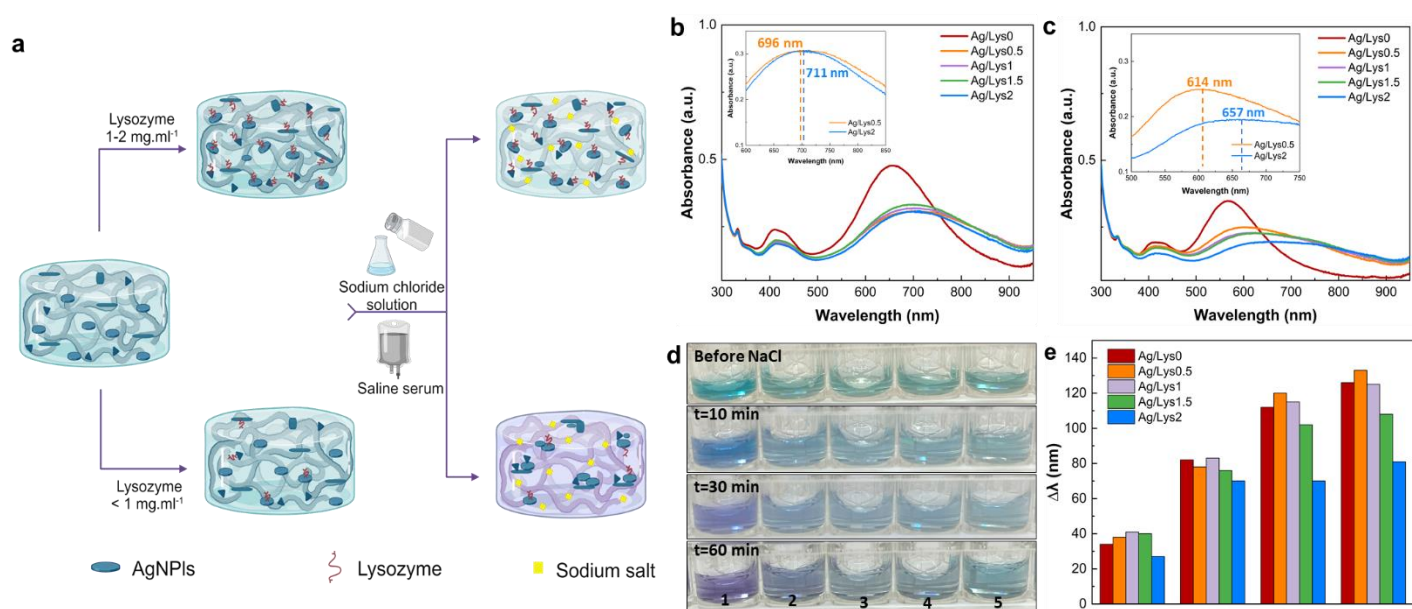


Figure 4. Colorimetry assay. **a)** Scheme of the procedure explaining the chemistry of colorimetry detection mechanism upon the addition of NaCl salt. **b-c)** Absorbance vs. wavelength of the samples with different amounts of lysozyme before and after adding salt. There are no changes in the peak wavelength before the presence of salt in various concentrations, but after the addition of NaCl, there is a shift of around 75 nm in the peaks of the sample with less than a healthy amount of lysozyme, where the solutions containing more lysozyme in the healthy range, remain with minor changes. **d)** Photographs of the aqueous solutions containing silver nanoplates show the color change of the solutions upon the addition of salt over time. **e)** $\Delta\lambda$ is shown with respect to the measured time points. The rate of the changes for each of the samples containing different amounts of lysozyme is shown in the bar chart.

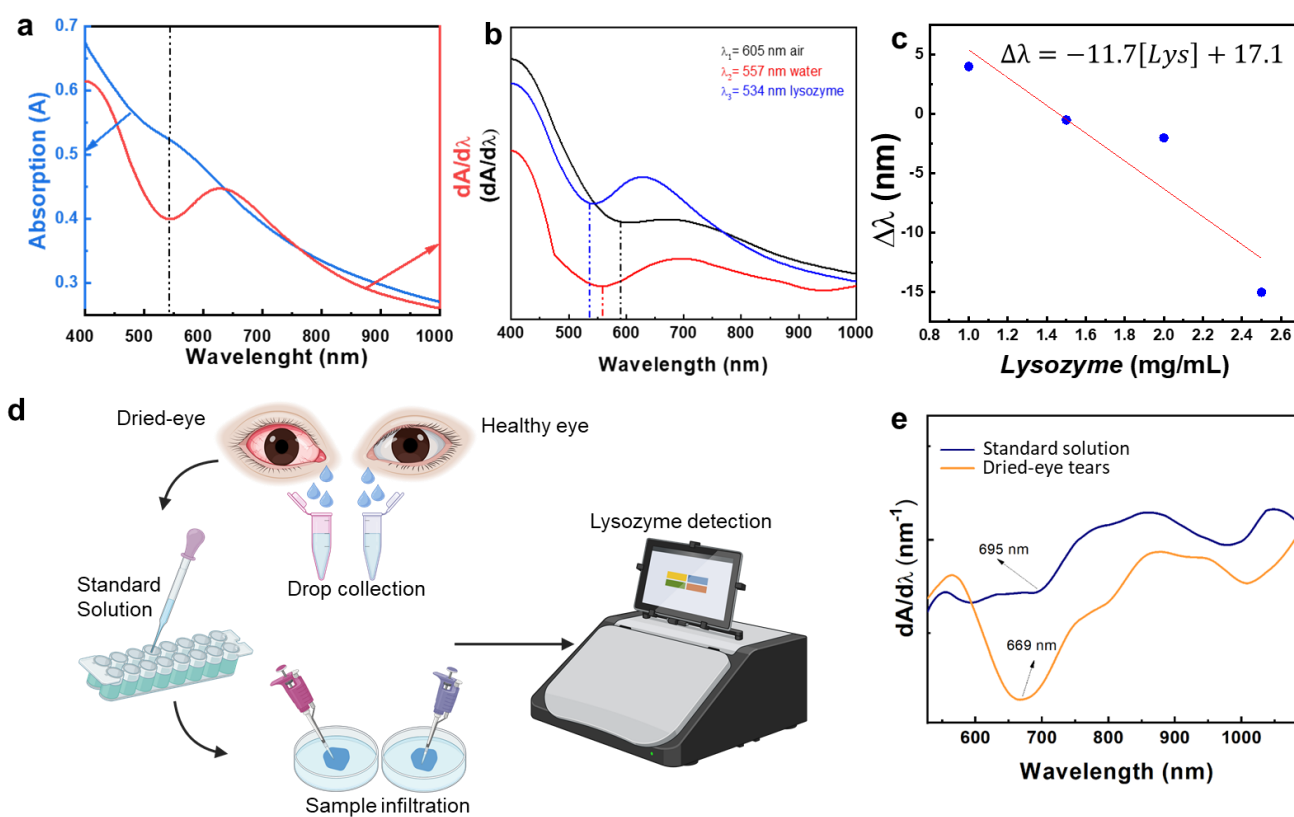


Figure 5. LSPR-based lysozyme biosensing of the nanostructures for dry eye application. **a)** The Absorption spectra of silver nanostructures and their first derivative show the peak and depth at around 540 nm. **b)** First, derivate absorption spectra of the platform in various environments, and the blue shift observed changes from air to water and lysozyme. **c)** Linear correlation between the $\Delta\lambda$ and lysozyme concentration. **d)** Schematic of sensing procedure from real human tears, starting with collecting drops from human eyes, adding to standard solutions, and infiltrating the nanostructures. Then, the amount of lysozyme was detected and calculated using a spectrophotometer. **e)** First derivative of the absorption and blue shift of the peaks from human tears.

[Supplementary Information]

Lysozyme-sensitive plasmonic hydrogel nanocomposite for colorimetric dry-eye inflammation biosensing

Yasamin Ziai,^a Chiara Rinoldi,^a Francesca Petronella,^b Anna Zakrzewska,^a
Luciano De Sio,^c Filippo Pierini^{a*}

- a. Department of Biosystems and Soft Matter, Institute of Fundamental Technological Research, Polish Academy of Sciences, Warsaw 02-106, Poland.
- b. Institute of Crystallography CNR-IC, National Research Council of Italy, Via Salaria Km 29,300, 00015, Monterotondo - Rome, Italy
- c. Department of Medico-Surgical Sciences and Biotechnologies, Sapienza University of Rome, Corso della Repubblica 79, 04100 Latina, Italy

*corresponding author: fpierini@ippt.pan.pl

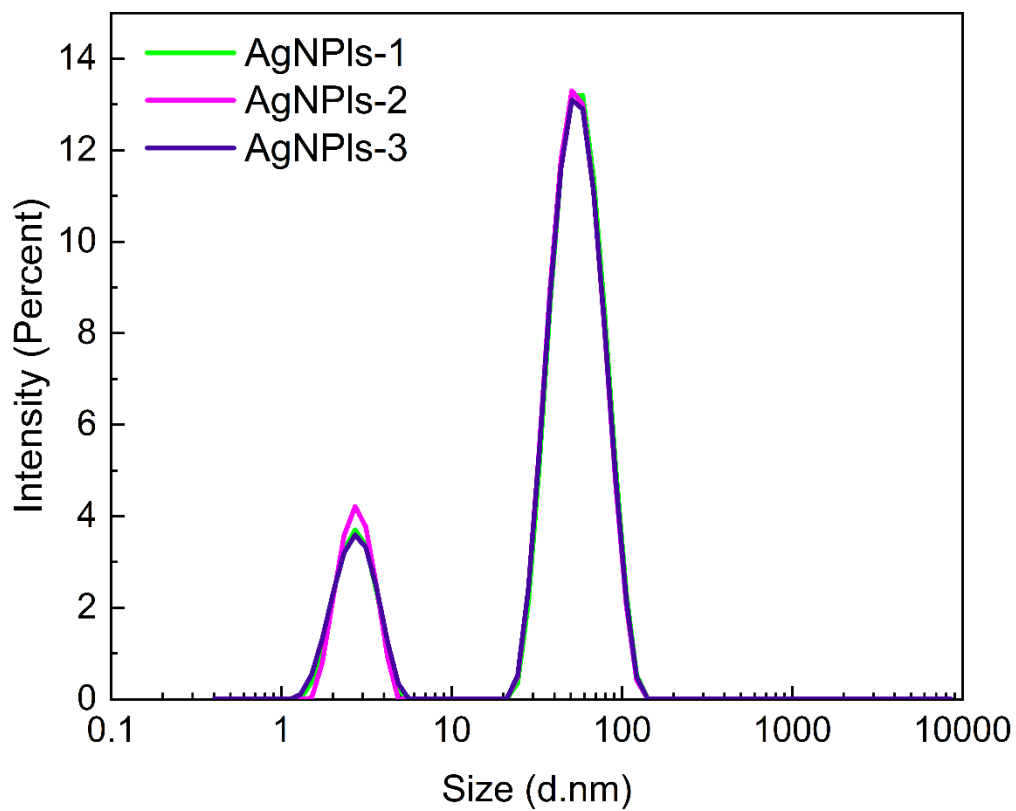


Figure S1. DLS measurements of the AgNPIs showing their average size before sonication (average size of 57.2 ± 0.53 nm).

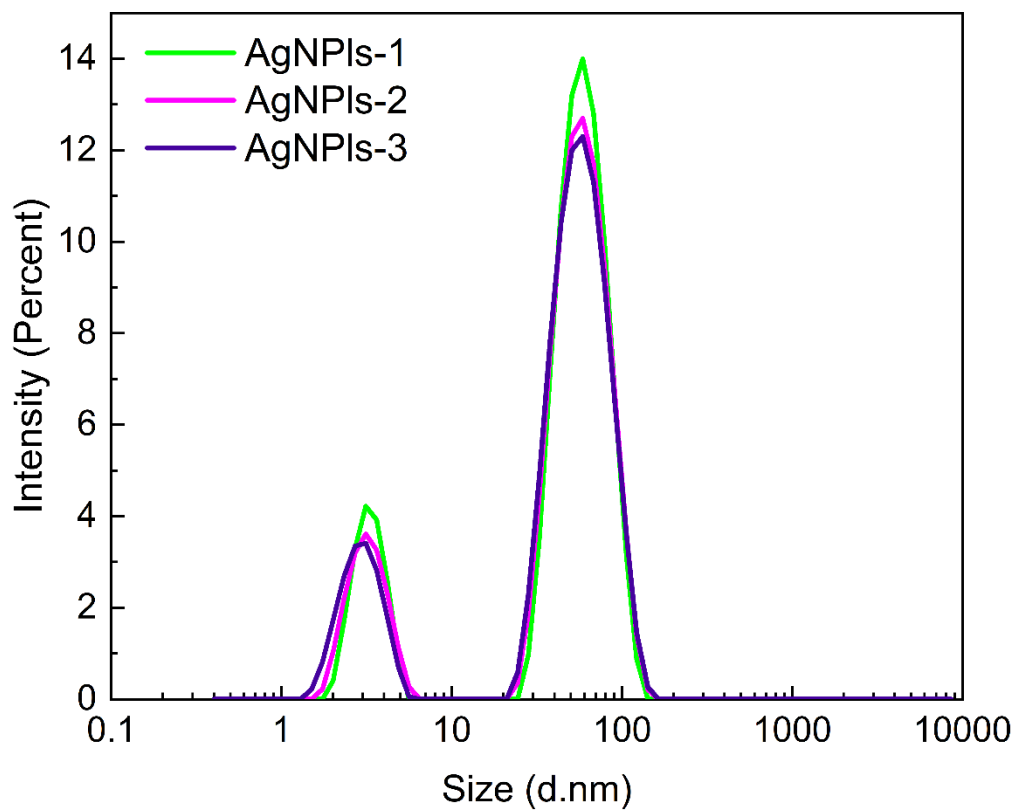


Figure S2. DLS measurements of the AgNPIs displaying their average size before sonication (average size of 60.89 ± 0.31 nm), which proves the nanoparticles' stability before and after the sonication.

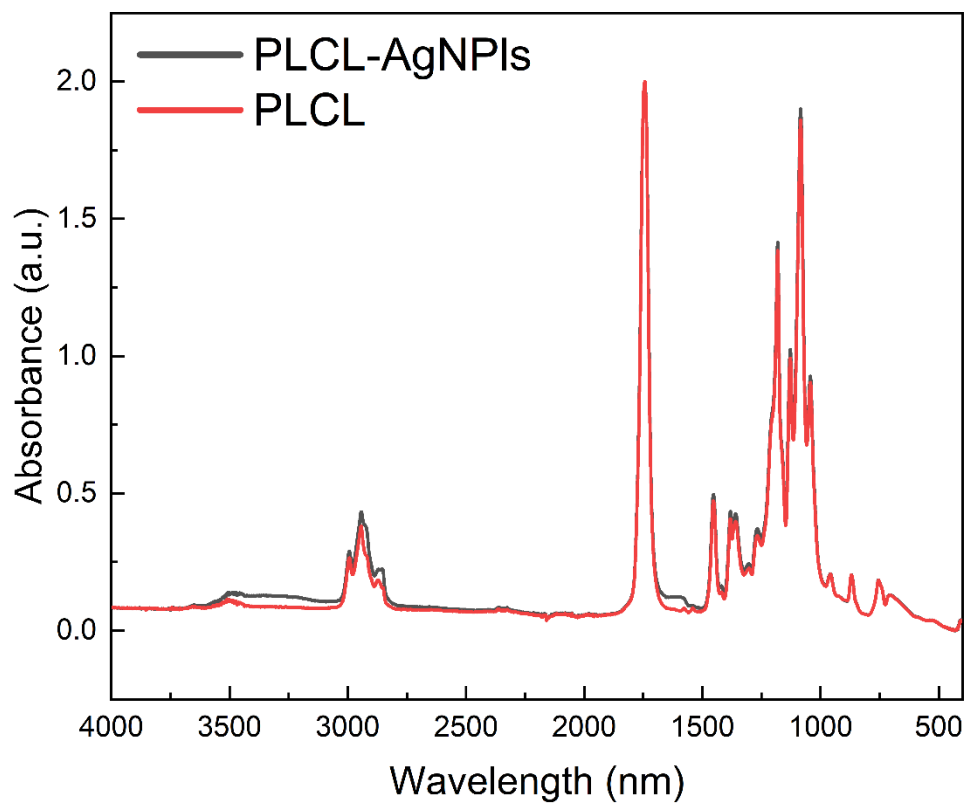


Figure S3. FT-IR spectrum of PLCL nanofibers before and after integrating silver nanoparticles in the system.

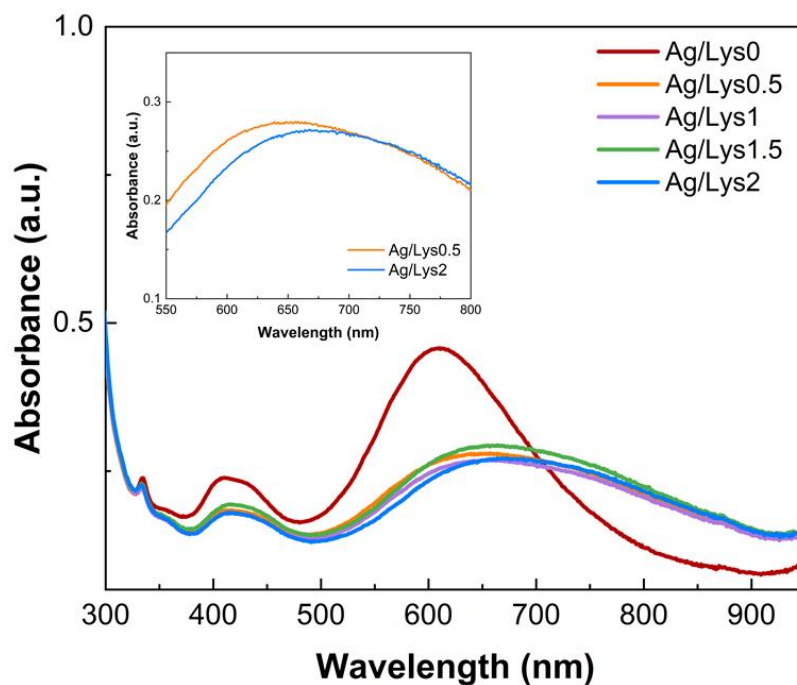


Figure S4. Absorbance spectra of the AgNPI sols after 10 minutes of incubation with lysozyme and NaCl.

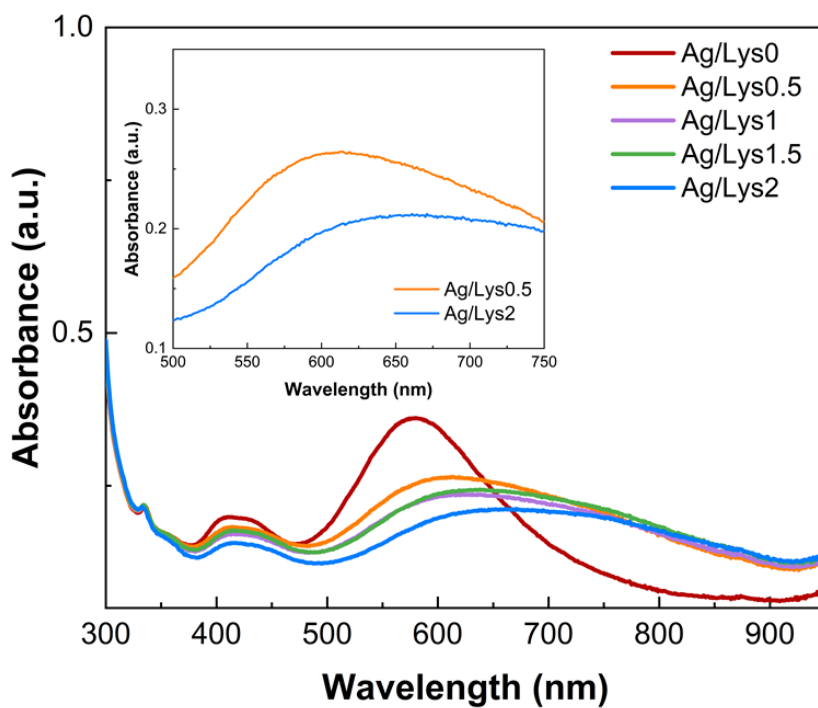


Figure S5. Absorbance spectra of the AgNPIs sols after 30 minutes of incubation with lysozyme and NaCl.

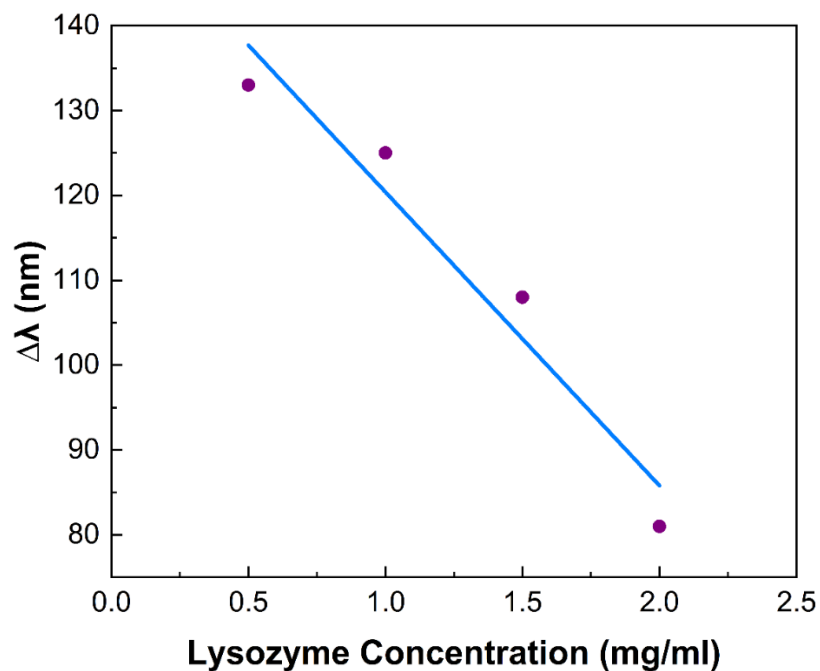


Figure S6. Linear correlation between the changes in the lysozyme concentration and changes in the wavelength.

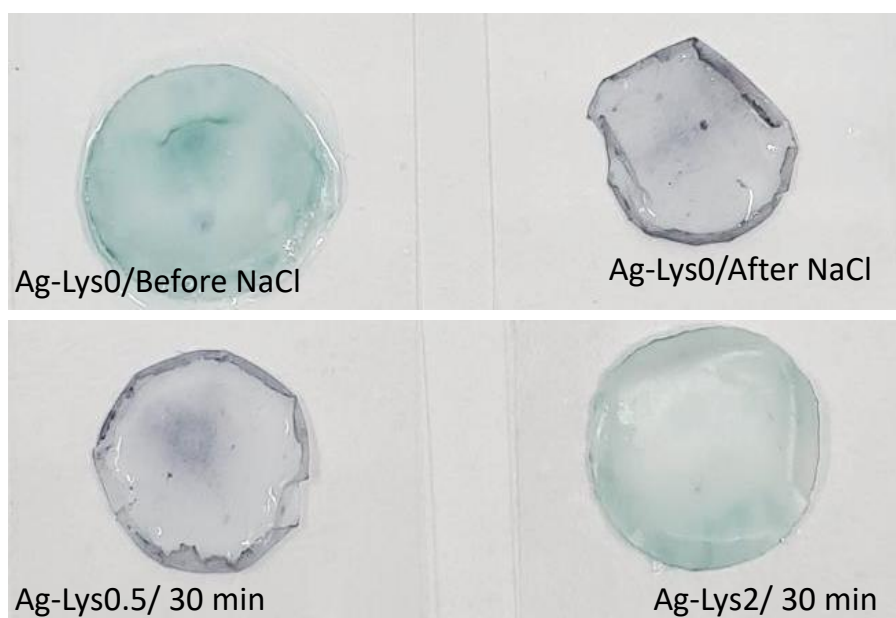
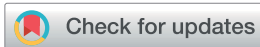


Figure S7. Photos of the color change of the samples before and after applying the lysozyme to the samples with and without NaCl. The color change for the samples in the non-healthy range of lysozyme, changing from blue to purple, confirms the potential detection by the naked eye.

Cite this: *Nanoscale Adv.*, 2024, 6, 1246

Developing strategies to optimize the anchorage between electrospun nanofibers and hydrogels for multi-layered plasmonic biomaterials†

Yasamin Ziai,^a Massimiliano Lanzi,^b Chiara Rinoldi,^a Seyed Shahrooz Zargarian,^a Anna Zakrzewska,^b Alicja Kosik-Kozioł,^a Paweł Nakielski^b and Filippo Pierini^b*^a

Polycaprolactone (PCL), a recognized biopolymer, has emerged as a prominent choice for diverse biomedical endeavors due to its good mechanical properties, exceptional biocompatibility, and tunable properties. These attributes render PCL a suitable alternative biomaterial to use in biofabrication, especially the electrospinning technique, facilitating the production of nanofibers with varied dimensions and functionalities. However, the inherent hydrophobicity of PCL nanofibers can pose limitations. Conversely, acrylamide-based hydrogels, characterized by their interconnected porosity, significant water retention, and responsive behavior, present an ideal matrix for numerous biomedical applications. By merging these two materials, one can harness their collective strengths while potentially mitigating individual limitations. A robust interface and effective anchorage during the composite fabrication are pivotal for the optimal performance of the nanostructures. Nanostructures are subject to varying degrees of tension and physical alterations depending on their specific applications. This is particularly pertinent in the case of layered nanostructures, which require careful consideration to maintain structural stability and functional integrity in their intended applications. In this study, we delve into the influence of the fiber dimensions, orientation and surface modifications of the nanofibrous layer and the hydrogel layer's crosslinking density on their intralayer interface to determine the optimal approach. Comprehensive mechanical pull-out tests offer insights into the interfacial adhesion and anchorage between the layers. Notably, plasma treatment of the hydrophobic nanofibers and the stiffness of the hydrogel layer significantly enhance the mechanical effort required for fiber extraction from the hydrogels, indicating improved anchorage. Furthermore, biocompatibility assessments confirm the potential biomedical applications of the proposed nanostructures.

Received 20th November 2023
Accepted 28th January 2024

DOI: 10.1039/d3na01022h

rsc.li/nanoscale-advances

Introduction

Recent years have witnessed remarkable progress in the field of biomedical materials, leading to the development of structures and platforms tailored for specific applications. These advancements aimed to harness the unique capabilities of various materials while addressing their inherent limitations. A particularly promising approach involves using composite materials, which combine the strengths of multiple materials within a single platform.^{1,2} Among these composites, hydrogel/fiber combinations have garnered substantial attention because they offer the potential to synergize the benefits of hydrogels and fibers while mitigating their respective shortcomings.^{3,4}

Hydrogels, characterized by their three-dimensional structures with significant water content, biocompatibility, and tuneable mechanical characterizations, are particularly suitable for various biomedical applications,⁵ including drug delivery,⁶ tissue engineering,⁷ wound healing,⁸ *etc.* One of the most significant advantages of hydrogels is their resemblance to the natural extracellular matrix (ECM), which allows cells to proliferate, differentiate, and migrate within these structures. This ECM-mimicking property is particularly beneficial in tissue engineering, where hydrogels can provide a supportive environment for cells to grow and form new tissues.^{9,10} Due to hydrogels' interconnected porous structure, they have been considered to be one of the best substrates to carry plasmonic nanoparticles for different applications. Due to their unique optical properties arising from interactions with incident light, plasmonic nanoparticles have been extensively explored in various fields. Noble metals, notably gold (Au) and silver (Ag) which are recognized as the most significant plasmonic materials, are characterized by the occurrence of surface plasmon resonance (SPR) at distinct resonance frequencies within both

^aDepartment of Biosystems and Soft Matter, Institute of Fundamental Technological Research, Polish Academy of Sciences, Warsaw 02-106, Poland. E-mail: fpierini@ippt.pan.pl

^bDepartment of Industrial Chemistry, University of Bologna, 40136 Bologna, Italy

† Electronic supplementary information (ESI) available. See DOI: <https://doi.org/10.1039/d3na01022h>



the visible and near-infrared (NIR) spectra.¹¹ When these metals are utilized in the form of nanoparticles, a phenomenon known as localized surface plasmon resonance (LSPR) is observed. This LSPR can be effectively tuned by manipulating the size and shape of the nanoparticles to suit specific applications. Such tunability offers versatility in customizing their optical properties, thereby expanding their applicability in various applications.¹²

When incorporated into hydrogels, these nanoparticles can leverage their solid and tunable optical responses, enabling the manipulation of photothermal effects upon external light exposure. This combination has been particularly advantageous for biomedical applications such as biosensing¹² and photothermal therapy.¹³ The engagement of hydrogels and nanoparticles has led to the development of advanced nanocomposite hybrid platforms, which benefit from both hydrogels and nanoparticles, offering stimuli-responsive features and expanding their range of applications.^{14,15} Plasmonic hydrogels can offer precise biosensing platforms, with low detection limits due to their biorecognition efficiency.¹⁶ Upon exposure to near-infrared (NIR) light, these nanoparticles can rapidly heat up, leading to a localized temperature rise. Combined with biocompatible and flexible hydrogels, these materials can be used in a wide range of applications such as photothermal therapy,¹⁷ targeted drug delivery systems,¹⁸ wound dressing,¹⁹ *etc.* However, as the majority of materials, hydrogels present some limitations. One of the primary shortcomings of hydrogels is their relatively low mechanical properties in terms of modulus. While some hydrogels can be engineered for specific mechanical strengths, many naturally derived hydrogels lack the robustness and durability required for certain bio-applications, especially in load-bearing tissues like cartilage or bone.²⁰ One of the effective procedures to reinforce hydrogels from a mechanical point of view is proposed to be the integration of fibers into a hydrogel network.^{21,22}

The electrospinning technique is a well-established method for fabricating fibrous biomaterials and has been widely studied by numerous research groups.²³ This process involves the use of a high-voltage power supply to create nanofibers with a broad range of diameters, from the micro-to nanoscale. Researchers can optimize various processing parameters, such as voltage, working distance, needle size, and flow rate, to tailor the material's properties to specific needs.²⁴ Nanofibers have found applications in various biomedical fields, including tissue engineering,^{25,26} drug delivery,²⁷ cell carriers,²⁸ wound healing,²⁹ biosensing,³⁰ *etc.* They offer a range of advantageous features, including a large surface area, tuneable porosity, a possibility for easy surface functionalization, and sufficient mechanical properties. One of the notable advantages of nanofibers is their ability to provide an ideal biocompatible substrate for culturing many types of cells. This is due to their high interconnected porosity, gas permeability, and capacity for fluid absorption.³¹ However, challenges arise regarding the infiltration of cells within the matrix, mainly due to the two-dimensional nature of electrospun mats, where there is a lack of cell-recognition sites especially in synthetic polymers.

Moreover, tissues with lower mechanical strength, such as brain tissue, pose unique challenges that electrospun fibers alone may not adequately address.³² Incorporating nanofibers into hydrogels has been investigated widely due to the reinforcement and enhancements the nanofibers introduce in terms of mechanical properties. There are several techniques to add these components, although the layering technique, where the two layer are in direct contact, can remodel the structures of tissues and develop adaptable platforms for different required load bearings.³³

Hydrogel/fiber composites represent a compelling fusion of electrospun nanofibers and hydrogels, offering a platform that benefits from both materials' strengths while overcoming their weaknesses. Nakielski *et al.* have introduced a layered nanocomposite inspired by the natural structure of mesoglea of jellyfish bells for drug delivery purposes. This layered structure consists of two layers of electrospun poly(L-lactide) nanofibers loaded with Rhodamine B, and a layer of poly(*N*-isopropylacrylamide) (PNIPAAm)-based hydrogel with plasmonic gold nanorods. The hydrogel layer has been placed between two layers of nanofibers, allowing for controlled, rapid, and reversible structural changes upon NIR light irradiation. The mechanical contraction of the composite, triggered by temperature increases from plasmonic hydrogel-light interactions, can lead to rapid water expulsion, showing the importance of having a solid interface keeping the platform in shape while changing. This action, in conjunction with the temperature rise, stimulates the release of molecules from the nanofibers, making it an efficient platform for controlled drug delivery.³⁴ In another work, Mohabatpour *et al.*, have developed a novel nanocomposite hydrogel scaffold by incorporating electrospun PLA (poly-lactic acid) nanofibers within alginate-grafted-hyaluronate (Alg-*g*-HA) hydrogel. The hydrogel scaffold demonstrated enhanced mechanical properties and reduced water uptake due to the embedded PLA nanofibers. Furthermore, the scaffold exhibited cytocompatibility, with chondrocytes maintaining their morphology and producing cartilage-specific matrix components, suggesting its potential application in cartilage tissue engineering.³⁵

In this study, we have investigated a crucial aspect of these composites: ensuring a robust attachment between the fibrous mats and plasmonic hydrogel layers. In this work, polycaprolactone (PCL) was chosen as a representative biopolymer with a wide range of bio-applications. The study explores the influence of fibers' dimensions, alignment, and surface modifications on the fabricated fibrous mats' wettability, structural, and mechanical aspects. Polyacrylamide-based hydrogels with the incorporation of plasmonic gold nanorods have been introduced as the hydrogel layer. From this point of view, the effect of crosslinking density on integrating two layers was studied.

Additionally, biocompatibility tests were conducted on the developed platforms to assess the platforms' potential for biomedical applications. This research contributes to the evolving hydrogel/fiber composites field, offering valuable insights into multi-layer biofabrication. Structural, chemical, morphological, and mechanical enhancements in each layer



and their impact on having a strong interface have been investigated.

Materials and methods

Materials

To prepare the nanoplatfoms, polycaprolactone (PCL, Mn 80 kDa), *N,N*-dimethylformamide (DMF), chloroform (99%), *N,N*-isopropylacrylamide (NIPAAm, 97%), *N*-isopropylmethacrylamide (NIPMAAm, 97%), *N,N'*-methylene bisacrylamide (BIS-AAm, 99.5%), 2-hydroxy-4'-(2-hydroxyethoxy)-2-methylpropiofenone (Irgacure 2959, 98%), ammonium persulfate (APS, 98%), *N,N,N',N'*-tetramethylethylenediamine (TEMED, 99%) were bought from Sigma-Aldrich (Poland). Gold nanorods (AuNRs, $\lambda = 800$ nm, OD = 50, $C = 0.88$ mg mL⁻¹) from nanoComposix (USA) were used as received.

To perform biocompatibility tests, L929 murine fibroblasts, bovine serum albumin (BSA), phosphate buffer saline (PBS), Triton X, and DAPI were obtained from Sigma-Aldrich (Poland). Dulbecco's modified Eagle's medium (DMEM), fetal bovine serum (FBS), penicillin-streptomycin (PS), and EDTA-trypsin were bought from Gibco Invitrogen (USA). Alexa Fluor 488 Phalloidin, PrestoBlue reagent and live/dead cytotoxicity kit assay were purchased from Thermo-Fisher Scientific (USA).

Electrospinning

Solutions containing PCL at concentrations of 10% and 14% w/v were prepared in a solvent mixture comprising chloroform and DMF (9 : 1) for the electrospinning process. Through a series of optimizations, nanofibers were successfully generated, with key electrospinning parameters set as follows: a flow rate of 0.5 mL h⁻¹, employment of a 26 G needle featuring an outer diameter of 0.45 mm, and an applied voltage of 12.5 kV. In order to collect the resulting nanofibers in either a random or aligned configuration, a flat collector and a drum collector with a rotating speed of 2000 rpm were employed, positioned at a working distance of 15 cm from the electrospinning needle, respectively. Temperature of 20 °C, 40% relative humidity, and these optimized parameters were thoughtfully chosen to yield the desired nanofibers' morphology and alignment while ensuring the effectiveness of the electrospinning process. Nanofibers with 10% aligned (PCL 10A) and random orientation (PCL 10R) and 14% aligned (PCL 14A) and random orientation (PCL 14R) were fabricated and used for further studies.

Surface functionalization

Diener Zepto oxygen plasma generator machine was used for surface modification of the nanofibrous layer. Nanofibers were cut in the desired shapes as rectangles and placed in the chamber for plasma treatment with a generator with a frequency of 40 MHz and power of 100 W for 2 minutes.

Preparation of the hydrogel precursor solution

For the formulation of the hydrogel precursor solution with a concentration of 4.8 wt%, a precise combination of components was executed. This included the addition of 578.1 mg of

NIPAAm, 15.6 mg of NIPMAAm, 31.2 mg of BIS-AAm, and 12.5 mg of Irgacure 2959. This composition was introduced into 10 mL of deionized water. This solution was used to prepare hydrogels *via* photo-polymerization (Ph-P).

0.1 wt% APS solution and 0.04% v/v of TEMED were added to the precursor solution to add the effect of chemical polymerization (Ph-P + C-P). To safeguard the solution from the effects of light, the mixture was securely enveloped in aluminum foil and subjected to continuous stirring overnight until complete dissolution was achieved.

This careful preparation ensured the uniformity and stability of the hydrogel precursor solution, setting the stage for subsequent experimental procedures.

Fabrication of the nanoplatfoms

Nanofibers were carefully tailored to the 3 × 0.5 cm × cm and were positioned into a mould with the dimension of 4 × 1 cm × cm. A 2% w/v solution of gold nanorods was introduced into each hydrogel precursor solution before the polymerization process. To facilitate photo polymerization, argon gas was introduced into the solution for a duration of 10 minutes, effectively displacing oxygen. 200 µl of each type of hydrogel precursor solution was then gently added over the nanofibers within the mould. The mould was carefully immersed in an ice bath to maintain the temperature at a controlled level below 15 °C during the UV irradiation process. Following this step, the mould, was exposed to UV light (Dymax lamp with 400 W capacity and a power density of 225 mW cm⁻²). The exposure time to UV irradiation was precisely adjusted, varying from 60 to 120 seconds, contingent upon the quantity of hydrogel material present.

Table 1 shows the list of the materials tested, with their acronyms.

Chemical and morphological analysis

Contact angle measurements were done using an OCA 15EC goniometer. Droplets of 1 µl were placed on the surface of the PCL nanofibers, and the contact angle of 10 drops was measured and averaged using ImageJ.

Fourier transform infrared (FT-IR) spectroscopy was used to characterize the functional groups in each layer. FT-IR analyses were conducted in attenuated total reflectance (ATR) mode with a Bruker Vertex70 FT-IR spectrometer and carried out in the wavenumber range of 400–4000 cm⁻¹ with a resolution of 2 cm⁻¹ and eight scans for each sample.

Molecular weights were determined at room temperature by gel permeation chromatography (GPC) using CHCl₃ solutions on an Agilent PL-GPC 50 apparatus equipped with a mixed bed column Waters Styragel HR 4E at a 1 mL min⁻¹ flow rate.

Field emission scanning electron microscopy (FE-SEM) and scanning electron microscopy (SEM) were performed with FEI Nova NanoSEM 450 and JEOL JSM-6390LV microscopes, respectively. Hydrogel disks and layered constructs were frozen in liquid nitrogen before cross-sectional cutting and then freeze-dried. Before imaging, samples were sputtered with an approximately 8 nm thick gold layer using a SC7620 Polaron mini sputter coater (Quorum Technologies Ltd, Ashford, UK).



Table 1 Samples description and acronyms

	PCL concentration (%)	Nanofibers orientation	Plasma surface treatment	Ph-P hydrogel	Ph-P + C-P hydrogel
10A/Ph-P	10	Aligned	No	Yes	No
10R/Ph-P	10	Random	No	Yes	No
14A/Ph-P	14	Aligned	No	Yes	No
14R/Ph-P	14	Random	No	Yes	No
10A + plasma/Ph-P	10	Aligned	Yes	Yes	No
10R + plasma/Ph-P	10	Random	Yes	Yes	No
14A + plasma/Ph-P	14	Aligned	Yes	Yes	No
14R + plasma/Ph-P	14	Random	Yes	Yes	No
10A/Ph-P + C-P	10	Aligned	No	Yes	Yes
10R/Ph-P + C-P	10	Random	No	Yes	Yes
14A/Ph-P + C-P	14	Aligned	No	Yes	Yes
14R/Ph-P + C-P	14	Random	No	Yes	Yes
10A + plasma/Ph-P + C-P	10	Aligned	Yes	Yes	Yes
10R + plasma/Ph-P + C-P	10	Random	Yes	Yes	Yes
14A + plasma/Ph-P + C-P	14	Aligned	Yes	Yes	Yes
14R + plasma/Ph-P + C-P	14	Random	Yes	Yes	Yes

Fiber dimension distribution analysis was done using ImageJ software, investigating 50 fiber diameters for each condition. The same software was used to measure the contact angle of the droplets, examining ten droplets per condition.

Mechanical tests

Both plasma-treated and untreated PCL specimens were tested to measure tensile strength. Rectangular samples of electrospun nanofibers, measuring 4.0 cm by 1.0 cm, were crafted for this purpose. These samples were secured within the clamps of the tensile testing device using a CTX Texture Analyzer (Brookfield Ametek), setting a gauge length of 10 mm. Data acquisition occurred at a rate of 50 readings per second. The actual testing commenced when the load reached 0.1 N. Samples were stretched at a rate of 1 mm s⁻¹ until rupture in triplicates for each scenario; force–displacement graphs were plotted using the Texture Pro V1.0 Build 19 software. The results were plotted as stress–strain graphs, considering stress as the force-to-initial area ratio and strain as the relative change in sample length. Subsequently, Young's modulus was determined for each specimen, representing the stress-to-strain ratio in the linear elasticity region (under 10% strain), indicating its deformation response to external forces.

Compression tests were conducted on Ph-P and Ph-P + C-P hydrogels using CTX Texture Analyzer from Brookfield Ametek in compression mode. Disc-shaped hydrogels with a diameter of 1 cm and a height of 1 cm were prepared and placed on a flat surface. The load cell of 5 kg was used to apply the load with the speed of 0.1 mm s⁻¹. Data acquisition occurred at a rate of 50 readings per second. The actual testing commenced when the load reached 0.1 N. Samples were compressed until destruction. Force-displacement graphs were plotted in triplicate for each scenario using the Texture Pro V1.0 Build 19 software.

Fiber pull-out tests were performed on the nanoplateforms of hydrogel/fiber. To prepare samples suitable for this test, fibrous mats cut in the dimensions of 5 cm by 0.5 cm were immersed in the bulk of hydrogel in a way that 3 cm of the fibers remained

out of the mould. To secure the position of fibers in the middle of hydrogel, a layer of precursor solution with a volume of 3 mL was first poured into the mould, followed by 30 seconds of UV irradiation. Fibers were then placed on top of the hydrogel layer, and 3 mL more of the precursor solution was poured gently over the fibrous layer and finally irradiated by UV light for 90 seconds. 3D printing was used to fabricate a customized holder to measure the adherence of the non-woven fabric to the hydrogels. With the help of Autodesk Inventor software, a 12 × 7 mm² cubic container with a height of 20 mm was designed, along with a matching lid with a 2 × 5 mm² rectangular hole in the middle. The printer was a Zortrax Inventure printing with PLA polymer and standard printing parameters ($T = 200$ °C, printing speed 20 mm s⁻¹). Prepared platforms were placed inside the holder and placed into the CTX Texture Analyzer from Brookfield Ametek in tensile mode. The fibers were secured within the top clamp of the tensile testing device, setting a gauge length of 10 mm. Data acquisition occurred at a rate of 50 readings per second. The actual testing commenced when the load reached 0.10 N, and the samples were stretched at a rate of 0.1 mm s⁻¹ until they were pulled entirely out of the hydrogel bulk. Stress–strain and work graphs were plotted in duplicate for each condition using the Texture Pro V1.0 Build 19 software and Origin Pro.

In vitro biological studies

Culture and seeding of L929 fibroblast cells. L929 murine fibroblast cells were cultured in DMEM supplemented with 10% FBS and 1% PS and placed in an incubator at 37 °C and 5% CO₂. The culture medium was refreshed every two days. Cell passaging was performed when the confluence of cells reached ~80%. For seeding, cells were detached by adding 0.05% EDTA-trypsin for 3 min and incubating the cells at 37 °C and 5% CO₂. Subsequently, cells were collected in a Falcon tube and centrifuged at 1200 rpm for 5 min. After centrifuging, a pellet of cells was visible at the bottom of the tube. Cells were then resuspended in a 1 mL culture medium and counted. Finally, the cell



suspension was further diluted in culture media to achieve a convenient cell density for seeding the samples. For the cytocompatibility indirect test, L929 fibroblast cells were seeded in 96 well tissue culture plates and incubated for 24 hours in modified DMEM at a density of 10 000 cells per well.

Sample sterilization and extract medium collection. Plasma-treated and untreated 14% random PCL nanofibers layered with both hydrogel types, and each side was sterilized for 30 minutes under UV light. DMEM modified with 10% FBS and 1% PS medium was added to each sample and incubated for 24 hours. The medium collected from each sample was filtered using 0.22 μm filters. Subsequently, the extracts were used to replace the culture medium in contact with the seeded cells in the tissue culture plates. The control condition was also tested by culturing the cells in a fresh medium. Cells were cultured for up to 7 days.

Cell viability. The viability of cells was measured by PrestoBlue assay. Cells cultured with DMEM in contact with PCL 14R/PNIPAAm hydrogel samples and fresh DMEM were treated with a solution of 10% (v/v) PrestoBlue reagent in culture medium and incubated for one hour at 37 °C and 5% CO₂. Three replicates of each sample were analyzed at three selected time points: 1, 3, and 7 days after contact with sample extract mediums. After one hour of incubation, 100 μL aliquots of the PrestoBlue solution were transferred to a 96-well plate and analyzed at excitation 530 nm and emission at 620 nm by using a fluorometer plate reader (Fluoroskan Ascent TM Microplate Fluorometer, Thermo Scientific).

Cells were stained using a live/dead assay kit to investigate the viability of L929 fibroblasts in contact with sample extract mediums. On days 1 and 3 of culture, the samples were washed with PBS and treated with the Live/Dead staining solution composed of 0.5 μL of calcein (for staining the viable cells in green color) and 2 μL of ethidium homodimer (for red staining of dead cells) in 1 mL of PBS. Three replicates of each sample were soaked in the staining solution and incubated for 10 min at 37 °C and 5% CO₂. Then, scaffolds were washed three times in PBS and imaged using a confocal microscope (Leica). Percentages of viable cells were counted using the Cell Counter plugin of ImageJ (National Institute of Health, USA).

Cell morphology was evaluated by a confocal microscope. Actin staining was performed on three replicates per each condition at 3 and 7 days after contact with sample extract mediums. Cell cytoskeleton and nuclei were stained by fixing the samples in 4% paraformaldehyde for 15 min at room temperature. Samples were then washed three times in PBS and treated with a solution of 0.3% (v/v) Triton X-100 for 15 min. After washing, a solution of 1% (w/v) BSA in PBS was added to the samples for 30 min. The constructs were incubated in Alexa Fluor 488 Phalloidin solution (1 : 40) and placed in the dark for 40 min. Lastly, the staining of nuclei was performed by adding 1 : 500 DAPI solution for 10 min. Samples were washed thrice in PBS and imaged with a confocal microscope (Leica).

Statistical analysis

Data are reported in terms of mean \pm standard deviation. One-way ANOVA test was assessed, and statistically significant

differences are reported when p -value ≤ 0.05 : * $p \leq 0.05$, ** $p \leq 0.01$, *** $p \leq 0.001$, **** $p \leq 0.0001$.

Results and discussion

Electrospun nanofibrous layer and surface treatments

PCL stands as a prominent biomaterial frequently employed across various applications. Recognized for its biocompatibility, PCL's molecular weight exhibits significant versatility, making it adaptable for specific uses. Its semi-crystalline and hydrophobic characteristics render it ideal for applications necessitating a gradual degradation rate, complemented by its superior mechanical attributes. However, its hydrophobicity can pose challenges, leading to suboptimal wettability and hindered cell adhesion. Given the high water content of hydrogels, it becomes imperative to modify the fibers to enhance wettability in the context of hydrogel/fiber composites to improve the hydrogel-fiber bond, ensuring a cohesive and stable final product.³⁶

Modulating the fiber diameter size and alignment is a viable approach to enhance the wettability of fibers and strengthen their incorporation into the hydrogel structure.³⁷ Factors in electrospinning, such as solution concentration, flow rate, solvent system varieties, working distance, and applied voltage, influence fiber dimensions. Notably, solution concentration predominantly dictates fiber size.³⁸ While chloroform is a popular solvent, it restricts dimensions to the microscale. We opted for adding DMF to chloroform, facilitating the generation of both nano- and micro-scale fibers.³⁸ It is worth noting that there is a threshold to solution concentration to ensure the production of continuous, bead-free fibers. For this purpose, solutions of 8%, 10%, 12%, and 14% pf PCL in the same solvent system were tested, where SEM images of 8% and 12% nanofibers are shown in Fig. S1.† As it can be seen from the SEM images, 8% of nanofibers are continuous, but a lot of beads and imperfections can also be seen. By increasing the solution concentration, the fibers diameter is also increasing and beadless nanofibers are achieved. The average diameter size of 8% nanofibers was the smallest with 242 ± 43 nm, where they increased to 766 ± 92 nm for 10%, 1084 ± 140 nm for 12% and 1319 ± 102 nm for 14%. To be able to compare the effects of fiber diameter on wettability, we have selected nanofibers from 10% and 14% solutions for our study. Fig. 1a–d displays SEM images of the fibers from 10% and 14% concentration, with both random and aligned orientations, illustrating the distribution of fibers in each image. The associated data from the analysis is presented in Table 2. As evident from the SEM images and corroborated by the calculations, PCL 10A nanofibers exhibit smaller dimensions, whereas PCL 14R exhibits the biggest diameter size. As it can be seen, PCL10 nanofibers in each orientation show smaller diameters compared to nanofibers of PCL14 in the same orientation. This variation highlights the influence of solution concentration on fiber size. Aligned fibers, across both concentrations, possess reduced dimensions attributed to fiber stretching during collection for alignment. The pronounced disparity in diameter between random and aligned fibers of identical concentration is a consequence of the collector's elevated rotational speed. The



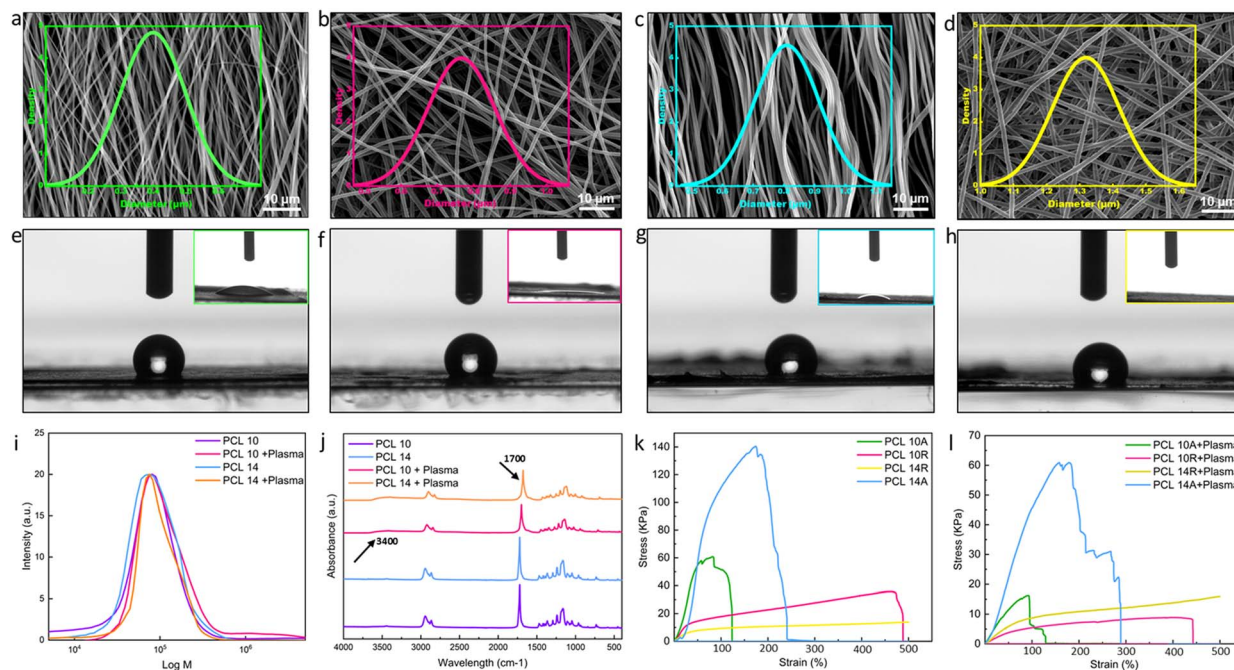


Fig. 1 Electrospun nanofibers characteristics. SEM and fiber diameter distribution of (a) PCL 10A with average diameter of 450 nm, (b) PCL 10R with average diameter of 766 nm, (c) PCL 14A with average diameter of 809 nm, (d) PCL 14R with average diameter of 1319 nm, show in the increase of average diameter with the increase in concentration of electrospinning solution. Random fibers in each concentration are greater in size in comparison to aligned ones. Contact angle of fibers before plasma treatment and inset image of contact angle 60 minutes after plasma treatment were also reported for (e) PCL 10A, (f) PCL 10R, (g) PCL 14A, (h) PCL 14R demonstrating the hydrophilicity of nanofibers after plasma treatment, where the signs of hydrophilicity can again be seen after around 60 minutes. (i) GPC test of nanofibers before and after plasma shows no sign of destruction in the chains of PCL. (j) FT-IR of PCL10 and PCL14 before and after plasma treatment showing changes in the absorption peaks as a result of the introduction of functional groups. (k) Stress-strain graph of fibers before plasma treatment. The graph shows the enhanced yield stress for aligned fibers and increased elongation at rate for random fibers, both values elevated in case of larger fiber dimensions. (l) Stress-strain graph of fibers post plasma treatment, showing the reduced values in the mentioned conditions in comparison to pre-treatment samples.

Table 2 Fibers characterization before and after plasma treatment

	10A	10R	14A	14R
Fiber diameter (nm)	449 ± 100	766 ± 92	809 ± 105	1319 ± 102
CA before plasma (°)	136.9 ± 3.2	128.6 ± 2.7	131.8 ± 1.3	126.2 ± 1.7
CA after plasma $t = 60$ min	≤10	≤10	≤10	0

correlation between fiber diameter and wettability is depicted in the contact angle visuals in Fig. 1e–h and Table 2. Larger diameter fibers with random orientation (PCL14R) appear to exhibit a tendency for hydrophilicity, potentially due to their increased surface area facilitating more interactions with water molecules. The influence of fiber alignment on dimensions and wettability can be understood by considering both the SEM visuals (Fig. 1a–d) and contact angle images (Fig. 1e–h). Contact angle measurements in Table 2 indicate a slight alteration in fiber wettability transitioning from aligned to random fibers, though the variations are minimal and may not translate to significant surface modifications.

Plasma treatment, a recognized technique for surface activation, can be executed by exposing materials to different gases such as O₂, N₂, and inert gases. As a result of exposure, the covalent bonds of the surface can break, actively reacting with

the functional groups. Oxygen, in particular, is a common approach to enhance interfacial adhesion in fibers, as highlighted in the literature.³⁹ Good adhesion is paramount in many tissue engineering applications, as the functionality of the device is mostly dependent on the stability of the interface of the tissue under tension. This highlights the importance of stable and strong anchorage in the multi-layer structures. Due to our final goal of fabricating multi-layer nanostructures with nanofibers and hydrogels, plasma treatment was selected as one of the most efficient methods to improve the wettability of nanofibers.⁴⁰ Plasma treatment can graft different functionalities (*e.g.*, NH₂, OH, COOH) at the surface, making them more hydrophilic.⁴¹ To enhance the wettability of fibers, they were subjected to plasma treatment for a duration of 2 minutes. The chemical modification of the surface can fade quickly due to the presence of air, necessitating prompt layering. The immediate



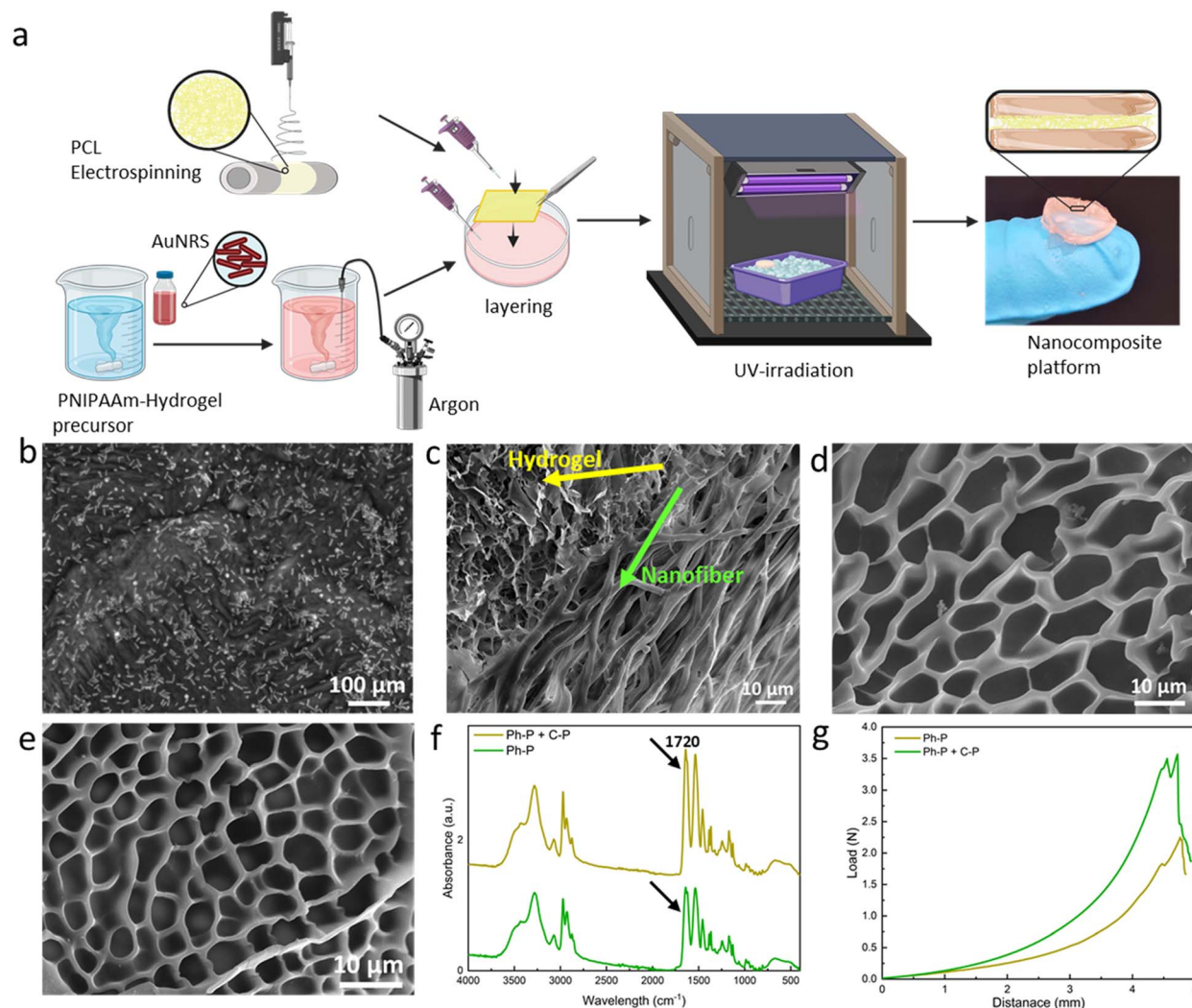


Fig. 2 Fabrication steps of the platform and hydrogel characterization. (a) Scheme of the fabrication of the layered nanoplatform. Briefly, the fabrication steps provide the addition of gold nanorods to the hydrogel precursor solution, argon bubbling prior to layering, addition of treated/untreated PCL nanofibers and crosslinking *via* UV-irradiation. (b) TEM micrograph of AuNRs in the hydrogel matrix. (c) Cross-section FE-SEM image of the platform, showing the incorporation of fibers into the hydrogel network. (d) FE-SEM images of the Ph-P hydrogel (e) FE-SEM of Ph-P + C-P hydrogel showing smaller pores. (f) FT-IR spectra of both hydrogels, confirming the increased crosslinking density of Ph-P + C-P hydrogel. (g) Force-displacement curves of hydrogels, showing enhanced toughness of the Ph-P + C-P hydrogel in comparison to C-P hydrogel.

post-plasma treatment contact angle of the fibers, as presented in the insets of Fig. 1e–h and Table 2, indicates a complete shift toward hydrophilicity with no difference among the tested conditions. This change remains stable for at least 60 minutes, at which initial signs of minor hydrophobicity begin to appear in samples. One of the important matters while fabrication is to act fast enough and add the hydrogel layer in the time frame in which the functional groups are present. Upon adding the hydrogel layer with high water content, hydrogen bonds and other polar interactions with the hydrogel matrix will form. These covalent linkages, which are a result of interaction of polymer chains of the hydrogel with the functional groups of the nanofibers, are permanent and irreversible.⁴² While executing plasma treatment, it is crucial to ensure that the surface modification has not compromised the polymer chain structure. The GPC test on samples, as visualized in Fig. 1i,

indicates neglectable changes in the molecular weight, suggesting the polymer chain remains almost intact. FT-IR analyses on varying PCL concentration samples pre- and post-plasma revealed peak intensity changes, signifying new functional group presence. Specific absorption peaks attributed to the formation of O–H groups are introduced to the spectrum for the samples after plasma treatment at the wavelength of 3400 cm^{-1} . The peak around 1720 cm^{-1} have become broader due to the interaction of carbonyl groups with the oxygen-contained groups.⁴³ All these changes showing the formation of some new bonds as a result of introduction of oxygen to the surface of the nanofibers, although there are no changes in the chemical backbone of the PCL nanofibers (Fig. 1j).

Mechanical testing on untreated and plasma-treated PCL samples assessed their Young's modulus and elongation at break. Fig. 1k presents typical stress–strain curves for pre-



plasma samples. Aligned fibers, across both concentrations, exhibited superior stress and Young's modulus values (Fig. S2†), while random fibers demonstrated enhanced strain rates.

Fiber alignment greatly affects the mechanical properties of the nanofibers; this impact shows itself in the random fibers in the elevated strain rates and in aligned fibers in enhanced young modulus and yield stress. The superior strength of aligned fibers is attributed to efficient load distribution along fiber lengths, minimizing stress concentration points and breakage susceptibility.⁴⁴ Consequently, the Young's modulus, indicative of material deformation resistance, increases. In random fibers, strain rates and the elongation at break are affected *via* alignment, as the random orientation of the fibers allows it to distribute the load unevenly between the fibers, making them more load-bearing. Also, in the case of random nanofibers, the breakage does not happen simultaneously, as fibers not in the direction of the load need to reorient for load bearing, where the voids between fibers will give them space.⁴⁵ Fiber diameter also has an impact on the performance of the nanofibers under tensile. In both aligned and random fibers, PCL 14 shows elevated characteristics than PCL 10. In random nanofibers, PCL 14R, offers longer elongation rates than PCL 10R, where PCL 14A exhibits larger shear strength in comparison the PCL 10A. The reason lies in the fact that fibers with lower diameters tend to have more imperfections in the microstructure, which can lead to their faster breakage.⁴⁶ Post-plasma tensile property alterations are illustrated in Fig. 11, where all the samples show lower characteristics than pre-plasma ones. Young modulus values associated with all conditions are also reported in Fig. S2.† Young's modulus displayed reductions in all samples, likely due to the introduction of functional groups, which can weaken polymer chain intermolecular forces, resulting in diminished tensile properties.⁴⁷

Plasmonic hydrogel layer

Hydrogels based on acrylamide have gained significant attention in the field of biomedical applications due to their unique properties. These hydrogels are crosslinked polymeric networks that possess the ability to swell and retain a significant fraction of water within their structure without dissolving. This water retention capability arises from the hydrophilic functional groups attached to the polymeric backbone. The intrinsic resistance to dissolution is attributed to crosslinks between network chains. Such hydrogels can be responsive to external stimuli like temperature, pH, or the ionic strength of the surrounding medium, making them "smart hydrogels". They can undergo significant volume variations in response to minor changes in environmental factors, which can be harnessed for sensing applications. One of the notable acrylamide-based hydrogels is the poly(*N*-isopropylacrylamide) or PNIPAAm-based hydrogel. When crosslinked to form hydrogels, the behaviour of these thermo-responsive polymers is significantly influenced by the volume phase transition temperature (VPTT). Above the VPTT, the polymer network shrinks, expelling the water contained within the hydrogel. The incorporation of the plasmonic particles into the PNIPAAm-hydrogel network has

been studied to evaluate potential enhancement in thermo-responsive properties of the material. The improved smart properties of this materials have been used in many applications, such as biosensing applications¹⁶ and photothermal therapy.⁴⁸

Fig. 2a illustrates the fabrication methodology of the fiber/hydrogel nanoplatform using a layering technique. The hydrogel precursor solution was prepared and stirred overnight before the integration of gold nanorods. Prior to layering, it is required to bubble the precursor solution with argon to eliminate oxygen. This step is needed due to the chain reaction for polymerization which can be induced *via* Irgacure as photoinitiator. Optionally, APS (as chemical initiator) and TEMED (as catalyst) can be introduced to increase the hydrogel's crosslinking density. APS, upon heating, liberates sulfate radicals capable of breaking acrylamide's double bonds, thus creating crosslinking sites. Concurrently, TEMED accelerates radical formation even at reduced temperatures. Subsequently, untreated/treated PCL nanofibers are positioned within a specified mould over which the precursor solution is poured. The mould is then cooled in an ice bath to regulate temperature during UV exposure, and the full hydrogel crosslinking is achieved within 90 seconds of UV irradiation. The composite's final architecture is visually represented in the accompanying schematic (Fig. 2a).

Gold nanorods' incorporation within the hydrogel matrix is validated through FE-SEM analysis, as depicted in Fig. 2b. The nanorods exhibit an average length of 55 ± 18 nm and a thickness of 15 ± 5 nm. Fig. 2c presents FE-SEM images of the composite's cross-section, revealing a stratified structure with seamless integration of fibers within the hydrogel matrix. FE-SEM images of the layered platform, showing the nanofibrous layer between two layers of hydrogel is shown in Fig. S3.† Evidently, the precursor solution permeates the fiber layers, resulting in a sturdy cross-section post-crosslinking. Fig. 2d shows a hydrogel formed solely through photo-polymerization (Ph-P) with an average pore size of 11.05 ± 1.96 μm . In contrast, Fig. 2e highlights a hydrogel synthesized using photo-polymerization and chemical polymerization (Ph-P + C-P) with APS and TEMED where the pore sizes have an average dimension of 5.16 ± 0.68 μm . The influence of APS and TEMED on hydrogels' degree of polymerization is discernible in these FE-SEM images. Higher crosslinking density manifests as reduced pore sizes, leading to a more rigid network.⁴⁹ This densification is further corroborated by FT-IR analysis of lyophilized samples, as shown in Fig. 2f. Peaks at 2900 and 2740 cm^{-1} correspond to asymmetrical and symmetrical C-H stretching, respectively, while the peak at 1720 cm^{-1} is attributed to the C=O stretching vibration of the carboxyl group in acrylic acid. The pronounced peak intensity at 1720 cm^{-1} is indicative of elevated crosslinking. Mechanical properties, assessed through compression tests on hydrogels with varying crosslinking densities, are depicted in Fig. 2g. The curve's gradient, representing the elastic modulus, is steeper for hydrogels synthesized using Ph-P + C-P. Both the yield and ultimate strengths are markedly higher for Ph-P + C-P.



Mechanical pull-out test

A customized mechanical test, known as the fiber pull-out test, was devised to assess the adhesion strength between a fiber bundle (acting as the reinforcing material) and the encompassing matrix material, such as a hydrogel. This test serves as a valuable tool for evaluating the interfacial bonding within the layers. The test procedure involves partially embedding a filament or bundle of fibers within the hydrogel matrix and subsequently applying a force to extract the fiber from the matrix.⁵⁰ The fiber pull-out test offers critical information into the strength and integrity of the fiber–matrix interface and, by extension, the overall performance of the composite material. The level of adhesion between these two components provides a practical indicator of the composite's load-bearing capacity and deformation resistance, reflecting the effectiveness of their integration.⁵¹

To facilitate this test, a custom-made setup was designed, as shown in Fig. 3a. Overcoming one of the primary challenges of this test, such as securing the hydrogel within the tensile machine, required innovative approach. To achieve this, a 3D-printed holder was designed to distribute the pressure exerted by the tensile grips without imposing stress on the hydrogel.

Additionally, the inherent tendency of the hydrogel to displace along with the embedded fibers under tension necessitated to address a few more requirements. A lid was created for the holder, featuring a hole specifically designed to the size of the fiber, as can be seen in Fig. 3a. The holder was then fixed into the lower grip of the tensile machine while the upper grip securely held the fiber bundle. The test proceeded until a complete separation of the two materials was achieved. Fig. 3b–e shows the stress–strain curves for all the samples in different conditions, where Fig. 3f shows the work of adhesion, needed for the fiber pull-out for each sample and group. Parameters which can affect this investigation are the fiber dimension, alignment and surface treatment, and toughness of hydrogel. With a quick glance, it can be stated that samples featuring Ph-P + C-P hydrogel, which is a stiffer hydrogel compared to Ph-P hydrogel, exhibit a higher work of adhesion. The results indicate that the force needed to pull the fibers is not solely the force for separating fibers from the hydrogel but is predominantly associated with the force required to fracture the hydrogel network in close proximity to the interface. This observation is supported by the fact that the fiber bundles extracted from the hydrogel matrix consistently, retain traces of

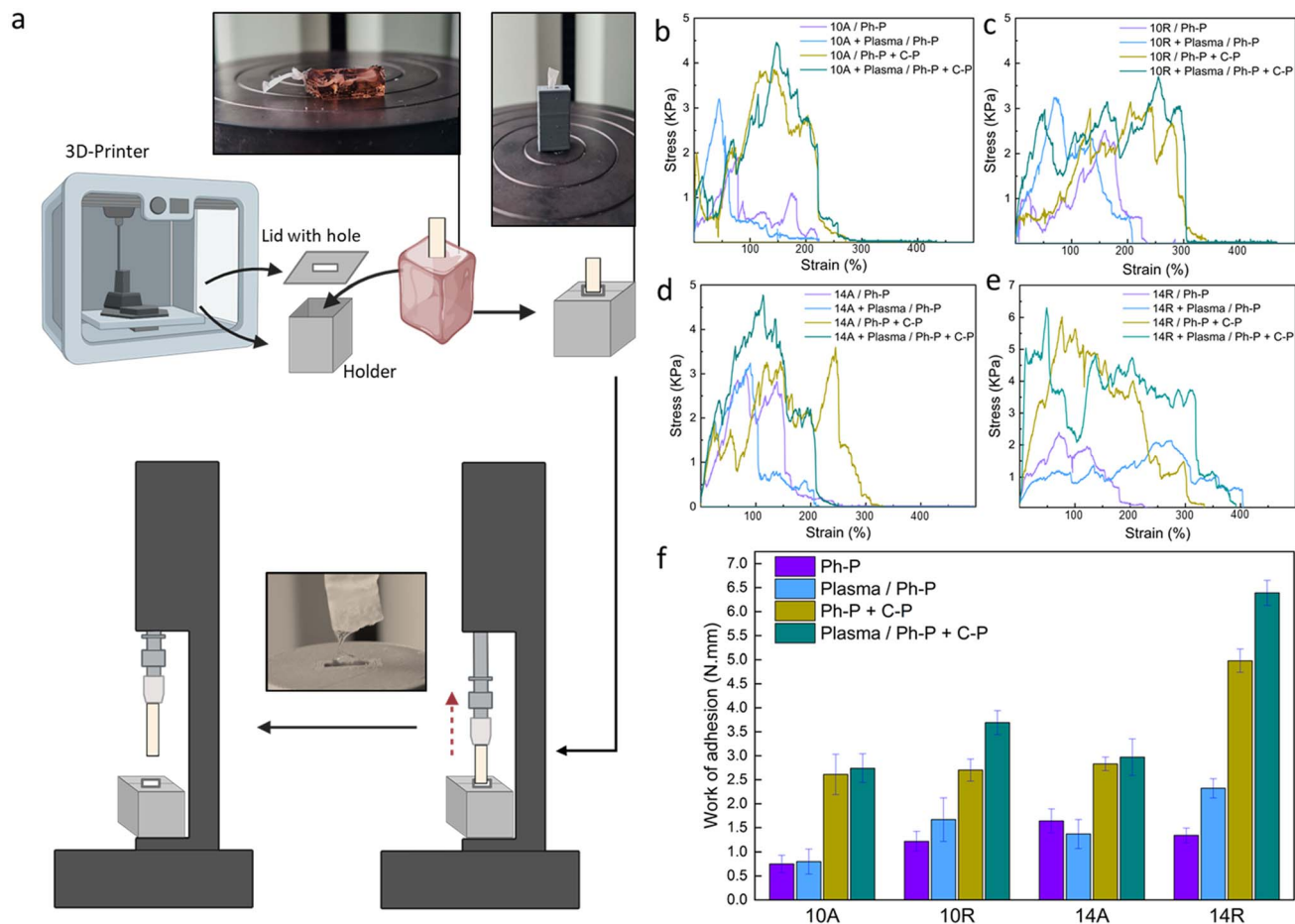


Fig. 3 Fiber pull-out test. (a) Scheme of the customized 3D-printed holder for the nanoplateforms and the test steps. (b–e) Stress–strain curves for (b) PCL10A, (c) PCL10R, (d) PCL14A, (e) PCL14R paired with hydrogel in all the conditions. (f) Nanoplateforms' toughness, measured by calculating the work per unit volume for each group set as an indicative value of the adhesion and incorporation of interfaces.



hydrogel on their surfaces, showing the robust integration of fibers into the hydrogel network (Fig. S4†).

While plasma treatment enhanced the wettability of the PCL nanofiber surfaces, promoting an expected increased intra-layer adhesion based on the previous results, the impact of plasma treatment in the fiber pull-out test is much less than the hydrogel part. Samples with plasma treatment in each group of

aligned nanofibers show very small increase compared to the not treated ones. This difference is shown to be much more in the case of samples with randomly oriented nanofibers. This can be because of the more exposed sites on random fibers in the procedure of plasma treatment.⁵² As discussed previously, fiber diameter and orientation, as other parameters, have some effects on the adhesion of nanocomposite. PCL 14R, with the

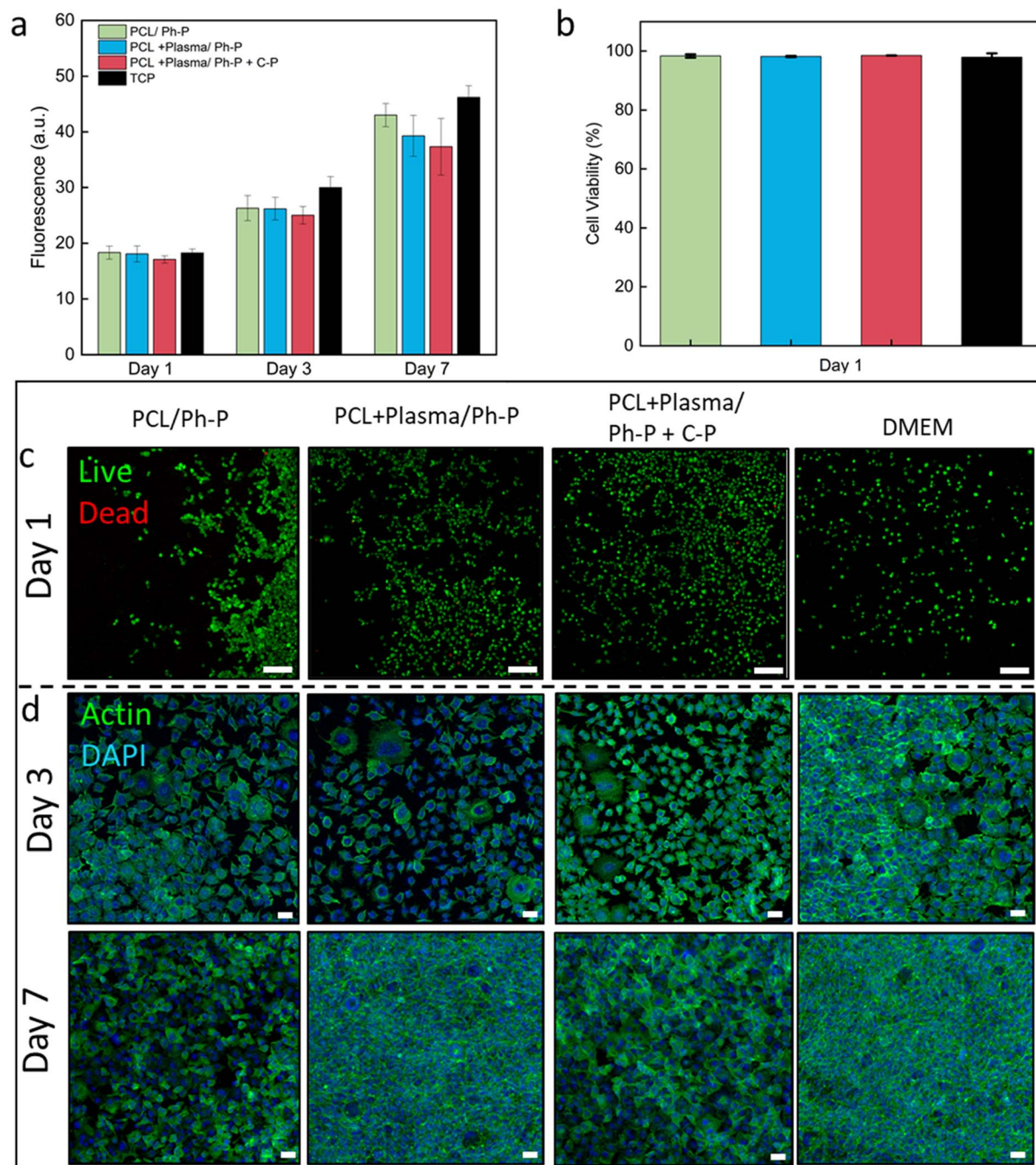


Fig. 4 *In vitro* biological response of L929 fibroblasts seeded on TCP and cultured with extracted medium of PCL14R nanofibers/hydrogel in different conditions. (a) Increasing trend of cell viability up to 7 days of culture tested. (b) Percentage of cell viability calculated from live and dead images, showing $\geq 97\%$ cell viability at day 1 of culture. (c) Live and dead images showing live cells (green) and dead cells (red) at day 1 of the culture. Scale bar: 50 μm . (d) Confocal images of samples stained with Actin (green) and DAPI (blue), visualizing cell cytoskeleton and nuclei, respectively. Scale bar: 50 μm .



most larger diameter size, has the greatest work of adhesion, whereas PCL 10A has the lowest values in pre- and post-treated samples. As mentioned before, PCL14, with a bigger fiber diameter, offers more strong fibers and randomly aligned nanofibers, offer more void and space for the precursor solution to penetrate, which can provide a more robust interface.

In summary, the mechanical response of PCL nanofibers within the composite system is profoundly influenced by the crosslink density and toughness of the hydrogel in all situations. Fiber diameter and orientation also play important roles as they will offer more space for penetration of the hydrogel layer. Finally, the plasma treatment, especially in randomly aligned nanofibers, can influence the required force and, hence the work of adhesion. The fiber pull-out test reveals that the force required for fiber extraction is intrinsically tied to the resilience of the hydrogel network near the interface, highlighting the importance of this interfacial region in composite materials.

Biocompatibility of nanoplatforms

To evaluate the biological properties of the nanoplatforms and verify their potential for biomedical applications, the material interaction with L929 fibroblast cells was investigated.⁵³ According to the mechanical tests, PCL14R nanofibers showed the most robust interface and hence were selected as a representative to assess the biocompatibility of nanoplatforms.

The viability of L929 cells seeded on TCP and cultured using extracted medium was evaluated and compared to control samples cultured with fresh medium. Linear cell growth is reported in Fig. 4a, showing increasing signals at each time point (1, 3, and 7 days) for all conditions. No significant difference between the conditions was measured at any time, confirming the indirect cytocompatibility of nanoplatforms, either with plasma-treated nanofibers or having additional C-P reagents for denser crosslinking.

Utilizing a Live/Dead assay kit, cells seeded on the culture plate were stained, with live cells appearing green and dead cells showing in red. This observation shows the predominant presence of viable green cells cultured in the presence of sample extracts, as shown in Fig. 4b and Table S1,[†] affirming the employed materials' indirect cytocompatibility. Illustrative Live/Dead images from day 1 and day 3 of culture are reported in Fig. 4c and S5,[†] respectively. Across the evaluated conditions, no significant variations were identified at any given time interval.

Confocal microscopy images of samples stained with Actin/DAPI showed the cell cytoskeleton and nuclei after 3 and 7 days of culture (Fig. 4d). The images allow the visualization of the elongated morphology of L929 fibroblasts, exhibiting a characteristic spindle shape from the early phase and evident cell proliferation and population at the later stage of culture, with no significant difference between conditions.

Conclusions

In this work, we investigated factors that could potentially result in a more robust interface between the plasmonic hydrogel

layer and electrospun nanofibers in multi-layer nanocomposites. The nanofibrous mats of PCL were successfully fabricated from 10% and 14% solutions, offering nanofibers with an average diameter of below and above 1 μm , respectively, in random and aligned orientations. O₂ plasma treatment was applied to the nanofibers' surface to enhance the materials' hydrophilicity. Morphological and mechanical investigations showed each parameter's impact on the nanofibers' wettability and hydrophilicity, which can influence their interface for further compositing steps. Fiber diameter and orientation have a neglectable effect on the nanofibers' hydrophilicity while applying plasma treatment makes them completely wettable for at least 60 min. Orientation and fiber diameter influence the mechanical tests, as random nanofibers offer more elongation at break in tensile and aligned fibers can bear higher shear stress. These mechanical values were significantly decreased post-plasma treatment due to the presence of new functional groups and reduced intramolecular forces. AuNRs were added to PNIPAAm hydrogel precursors with Ph-P (Irgacure as a photoinitiator) and Ph-P + C-P (Irgacure as photoinitiator and APS and TEMED as chemical initiator and catalyst) polymerization routes, then layered to nanofibrous layer to achieve a multi-layer nanocomposite. Morphological illustrations confirm the presence and distribution of AuNRs in the hydrogel layer. FE-SEM images and mechanical compression tests proved the increased crosslinking density in the Ph-P + C-P hydrogel due to smaller pore sizes and higher yield and toughness. A mechanical pull-out test was performed on all the samples, as the adhesion and robustness of the interface are crucial in layered smart platforms to provide stable construct within all changes and alterations. For this purpose, a custom-made 3D holder for the samples was printed, and the work of adhesion was calculated for all the sample sets. Nanofibers with larger diameters and random orientation had a more considerable work of adhesion, and this work was reduced by decreasing the fiber diameter and aligning. The impact of plasma treatment for aligned fibers was neglectable, whereas in random fibers, there is a noticeable increase in the adhesion of layers. The most significant alterations were noticed with the increase of the crosslinking density of the hydrogel, as the values increased for all the sample sets. It can be concluded that the impact of hydrogel stiffness is more significant, making it visible that the adhesion energy is mainly attributed to the force to break the hydrogel network near the fiber interface. Finally, cytocompatibility indirect tests with L929 fibroblasts show cell viability and proliferation in all conditions, proving that the nanoplatforms can be an ideal candidate for biomedical applications.

Author contributions

F. P. conceived the idea. Y. Z. designed the experiments, fabricated the nanoplatforms. Y. Z. performed the morphological characterization of nanofibers. M. L. tested the GPC of nanofibers before and after treatment. Y. Z. and A. Z. performed the morphological characterization of hydrogels. Y. Z. and S. S. Z. tested mechanical pull-out experiments. P. N. printed a 3D holder for the mechanical tests. Y. Z., C. R. and A. K. K.



conducted cell studies. Y. Z. wrote the manuscript. All authors discussed the results and commented on the manuscript. F. P. supervised the project.

Conflicts of interest

There are no conflicts to declare.

Acknowledgements

This work was supported by the National Science Centre (NCN) SONATA BIS Project No. 2020/38/E/ST5/00456. Fig. 2 and 3 were partially created with BioRender. C. R., and F. P. acknowledge the financial support from the Polish Ministry of Science and Higher Education through scholarships for outstanding young scientists. SSZ acknowledges the support of the European Union's Horizon 2021 research and innovation program under the Marie Skłodowska-Curie grant agreement no. 101068036, "SuSCoFilter".

References

- G. Kaur, R. Adhikari, P. Cass, M. Bown and P. Gunatillake, *RSC Adv.*, 2015, **5**, 37553–37567.
- C. Rinoldi, E. Kijeńska-Gawrońska, M. Heljak, J. Jaroszewicz, A. Kamiński, A. Khademhosseini, A. Tamayol and W. Swieszkowski, *ACS Mater. Au.*, 2023, 636–645.
- R. Ansar, S. Saqib, A. Mukhtar, M. B. K. Niazi, M. Shahid, Z. Jahan, S. J. Kakar, B. Uzair, M. Mubashir, S. Ullah, K. S. Khoo, H. R. Lim and P. L. Show, *Chemosphere*, 2022, **287**, 131956.
- A. Kosik-Kozioł, M. Costantini, T. Bolek, K. Szöke, A. Barbetta, J. Brinchmann and W. Świąszkowski, *Biofabrication*, 2017, **9**, 044105.
- H. Kamata, X. Li, U. Il Chung and T. Sakai, *Adv. Healthcare Mater.*, 2015, **4**, 2360–2374.
- M. Vigata, C. Meinert, D. W. Hutmacher and N. Bock, *Pharmaceutics*, 2020, **12**, 1188.
- C. Rinoldi, Y. Ziai, S. S. Zargarian, P. Nakielski, K. Zembrzycki, M. A. H. Bayan, A. B. Zakrzewska, R. Fiorelli, M. Lanzi, A. Kostrzevska-Księżyk, R. Czajkowski, E. Kublik, L. Kaczmarek and F. Pierini, *ACS Appl. Mater. Interfaces*, 2023, **15**, 6283–6296.
- N. Asadi, H. Pazoki-Toroudi, A. R. Del Bakhshayesh, A. Akbarzadeh, S. Davaran and N. Annabi, *Int. J. Biol. Macromol.*, 2021, **170**, 728–750.
- K. Goodarzi and S. S. Rao, *J. Mater. Chem. B*, 2021, **9**, 6103–6115.
- A. M. Rosales and K. S. Anseth, *Nat. Rev. Mater.*, 2016, **1**, 1–15.
- S. S. Hinman, K. S. McKeating and Q. Cheng, *Anal. Chem.*, 2018, **90**, 19.
- Y. Ziai, C. Rinoldi, P. Nakielski, L. De Sio and F. Pierini, *Curr. Opin. Biomed. Eng.*, 2022, **24**, 100413.
- J. H. Ha, H. H. Shin, H. W. Choi, J. H. Lim, S. J. Mo, C. D. Ahrberg, J. M. Lee and B. G. Chung, *Lab Chip*, 2020, **20**, 3354–3364.
- P. Lavrador, M. R. Esteves, V. M. Gaspar, J. F. Mano, P. Lavrador, M. R. Esteves, V. M. Gaspar and J. F. Mano, *Adv. Funct. Mater.*, 2021, **31**, 2005941.
- J. Guo, Z. Luo, F. Wang, H. Gu and M. Li, *Smart Med.*, 2022, **1**, e20220003.
- Y. Ziai, F. Petronella, C. Rinoldi, P. Nakielski, A. Zakrzewska, T. A. Kowalewski, W. Augustyniak, X. Li, A. Calogero, I. Sabała, B. Ding, L. De Sio and F. Pierini, *NPG Asia Mater.*, 2022, **14**, 1–17.
- F. Howaili, E. Özliseli, B. Küçüktürkmen, S. M. Razavi, M. Sadeghizadeh and J. M. Rosenholm, *Front. Chem.*, 2021, 602941.
- L. Moretti, A. Mazzanti, A. Rossetti, A. Schirato, L. Polito, F. Pizzetti, A. Sacchetti, G. Cerullo, G. Della Valle, F. Rossi and M. Maiuri, *Nanophotonics*, 2021, **10**, 247–257.
- A. Milanese, G. Magni, S. Centi, G. Schifino, A. Aluigi, B. N. Khlebtsov, L. Cavigli, A. Barucci, N. G. Khlebtsov, F. Ratto, F. Rossi and R. Pini, *J. Biophotonics*, 2020, **13**, e202000135.
- W. Wang, Y. Shi, G. Lin, B. Tang, X. Li, J. Zhang, X. Ding and G. Zhou, *Macromol. Biosci.*, 2023, **23**, 2200539.
- C. Rinoldi, A. Fallahi, I. K. Yazdi, J. Campos Paras, E. Kijeńska-Gawrońska, G. Trujillo-De Santiago, A. Tuoheti, D. Demarchi, N. Annabi, A. Khademhosseini, W. Swieszkowski and A. Tamayol, *ACS Biomater. Sci. Eng.*, 2019, **5**, 2953–2964.
- X. Liu, Y. Liu, J. Du, X. Li, J. Yu and B. Ding, *Eng. Regen.*, 2021, **2**, 63–69.
- G. Xia, B. Song and J. Fang, *Research*, 2022, 9896274.
- C. J. Angamma and S. H. Jayaram, *Part. Sci. Technol.*, 2016, **34**, 72–82.
- M. Polak, K. Berniak, P. K. Szewczyk, J. E. Karbowniczek, M. M. Marzec and U. Stachewicz, *Appl. Surf. Sci.*, 2023, **621**, 156835.
- J. Mu, D. Luo, W. Li and Y. Ding, *Biomed. Technol.*, 2024, **5**, 60–72.
- Z. J. Krysiak and U. Stachewicz, *Wiley Interdiscip. Rev.: Nanomed. Nanobiotechnol.*, 2023, **15**, e1829.
- Y. C. Kim, Y. H. Kim, J. W. Kim and K. Y. Ha, *J. Korean Med. Sci.*, 2016, **31**, 1373–1382.
- H. T. Bui, O. H. Chung, J. Dela Cruz and J. S. Park, *Macromol. Res.*, 2014, **22**, 1288–1296.
- A. H. Squires, J. S. Hersey, M. W. Grinstaff and A. Meller, *J. Am. Chem. Soc.*, 2013, **135**, 16304–16307.
- R. Rasouli, A. Barhoum, M. Bechelany, A. R. Dufresne, Rasouli, A. Barhoum, M. Bechelany and A. Dufresne, *Macromol. Biosci.*, 2019, **19**, 1800256.
- L. A. Bosworth, L. A. Turner and S. H. Cartmell, *Nanomed.: Nanotechnol. Biol. Med.*, 2013, **9**, 322–335.
- B. Pei, W. Wang, Y. Fan, X. Wang, F. Watari and X. Li, *Regener. Biomater.*, 2017, **4**, 257–268.
- P. Nakielski, S. Pawłowska, C. Rinoldi, Y. Ziai, L. De Sio, O. Urbanek, K. Zembrzycki, M. Pruchniewski, M. Lanzi, E. Salatelli, A. Calogero, T. A. Kowalewski, A. L. Yarin and F. Pierini, *ACS Appl. Mater. Interfaces*, 2020, **12**, 54328–54342.
- F. Mohabatpour, A. Karkhaneh and A. M. Sharifi, *RSC Adv.*, 2016, **6**, 83135–83145.



- 36 A. Cipitria, A. Skelton, T. R. Dargaville, P. D. Dalton and D. W. Huttmacher, *J. Mater. Chem.*, 2011, **21**, 9419–9453.
- 37 L. Vogt and A. R. Boccaccini, *Eur. Polym. J.*, 2021, **160**, 110772.
- 38 R. Ghobeira, M. Asadian, C. Vercruyssen, H. Declercq, N. De Geyter and R. Morent, *Polymer*, 2018, **157**, 19–31.
- 39 J. Đureje, Z. Prošek, J. Trejbal, Š. Potocký and P. Tesárek, *Acta Polytech. CTU Proc.*, 2022, **34**, 11–14.
- 40 D. Yan, J. Jones, X. Y. Yuan, X. H. Xu, J. Sheng, J. C. M. Lee, G. Q. Ma and Q. S. Yu, *J. Biomed. Mater. Res., Part A*, 2013, **101A**, 963–972.
- 41 A. Martins, E. D. Pinho, S. Faria, I. Pashkuleva, A. P. Marques, R. L. Reis and N. M. Neves, *Small*, 2009, **5**, 1195–1206.
- 42 F. A. Formica, E. Öztürk, S. C. Hess, W. J. Stark, K. Maniura-Weber, M. Rottmar, M. Zenobi-Wong, F. A. Formica, E. Öztürk, M. Zenobi-Wong, S. C. Hess, W. J. Stark, K. Maniura-Weber and M. Rottmar Biointerfaces Empa, *Adv. Healthcare Mater.*, 2016, **5**, 3129–3138.
- 43 M. Sivan, D. Madheswaran, M. Asadian, P. Cools, M. Thukkaram, P. Van Der Voort, R. Morent, N. De Geyter and D. Lukas, *Surf. Coat. Technol.*, 2020, **399**, 126203.
- 44 D. Yan, J. Jones, X. Yuan, X. Xu, J. Sheng, J. C.-M. Lee, G. Ma and Q. Yu, *J. Med. Biol. Eng.*, 2013, **33**, 171–178.
- 45 H. A. Lynch, W. Johannessen, J. P. Wu, A. Jawa and D. M. Elliott, *J. Biomech. Eng.*, 2003, **125**, 726–731.
- 46 H. H. Kim, M. J. Kim, S. J. Ryu, C. S. Ki and Y. H. Park, *Fibers Polym.*, 2016, **17**, 1033–1042.
- 47 M. Asadian, S. Grande, R. Morent, A. Nikiforov, H. Declercq and N. De Geyter, *J. Phys.: Conf. Ser.*, 2017, **841**, 012018.
- 48 C. Bermúdez-Jiménez, M. G. Romney, S. A. Roa-Flores, G. Martínez-Castañón and H. Bach, *Nanomed.: Nanotechnol. Biol. Med.*, 2019, **22**, 102093.
- 49 N. Seddiki and D. Aliouche, *Bull. Chem. Soc. Ethiop.*, 2013, **27**, 447–457.
- 50 J. L. Holloway, A. M. Lowman, M. R. Vanlandingham and G. R. Palmese, *Acta Biomater.*, 2014, **10**, 3581–3589.
- 51 L. Ferreira, M. B. Evangelista, M. C. L. Martins, P. L. Granja, J. L. Esteves and M. A. Barbosa, *Polymer*, 2005, **46**, 9840–9850.
- 52 R. Ghobeira, C. Philips, L. Liefoghe, M. Verdonck, M. Asadian, P. Cools, H. Declercq, W. H. De Vos, N. De Geyter and R. Morent, *Appl. Surf. Sci.*, 2019, **485**, 204–221.
- 53 P. Nakielski, C. Rinoldi, M. Pruchniewski, S. Pawłowska, M. Gazińska, B. Strojny, D. Rybak, K. Jezierska-Woźniak, O. Urbanek, P. Denis, E. Sinderewicz, W. Czelejewska, J. Staszkiwicz-Chodor, M. Grodzik, Y. Ziai, M. Barczewska, W. Maksymowicz and F. Pierini, *Small*, 2022, **18**, 2104971.



ARTICLE

Developing strategies to optimize the anchorage between electrospun nanofibers and hydrogel for multi-layered plasmonic biomaterials

Yasamin Ziai,^a Massimiliano LANZI^b, Chiara Rinoldi^a, Seyed Shahrooz Zargarian^a, Anna Zakrzewska^a, Alicja Kosik-Kozioł^a, Paweł Nakielski^a, and Filippo Pierini^{*a}

Supplementary Information

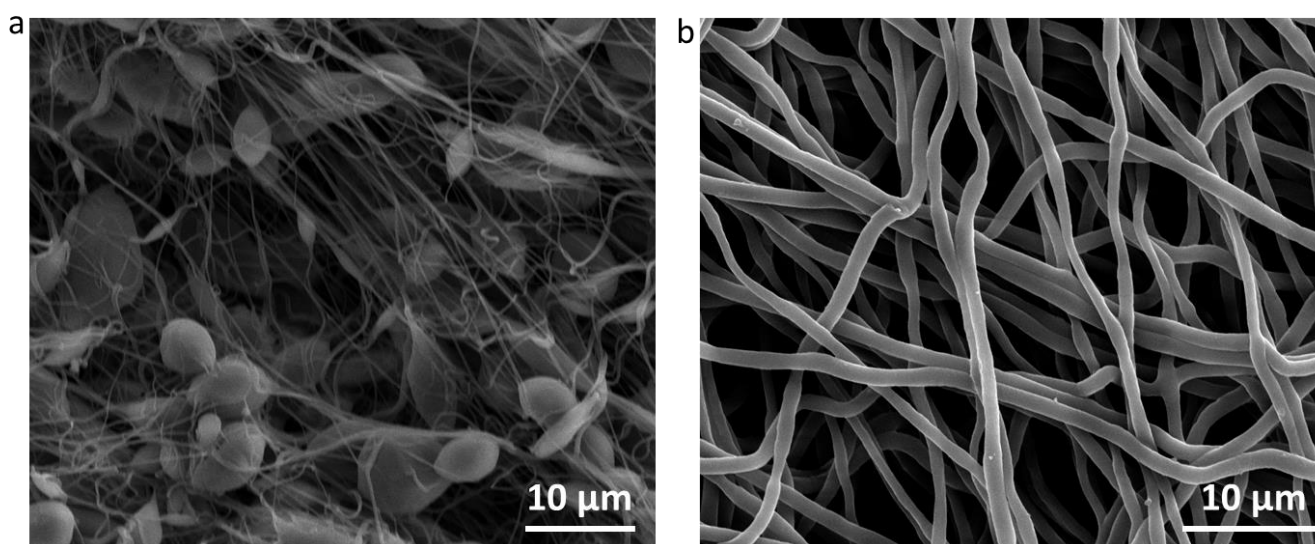


Figure S1. SEM images of PCL nanofiber. a) 8% concentration with an average diameter of 242 ± 43 nm, beads in the nanofibers, b) 12% concentration with an average diameter of 1084 ± 0.14 nm, continuous nanofibers.

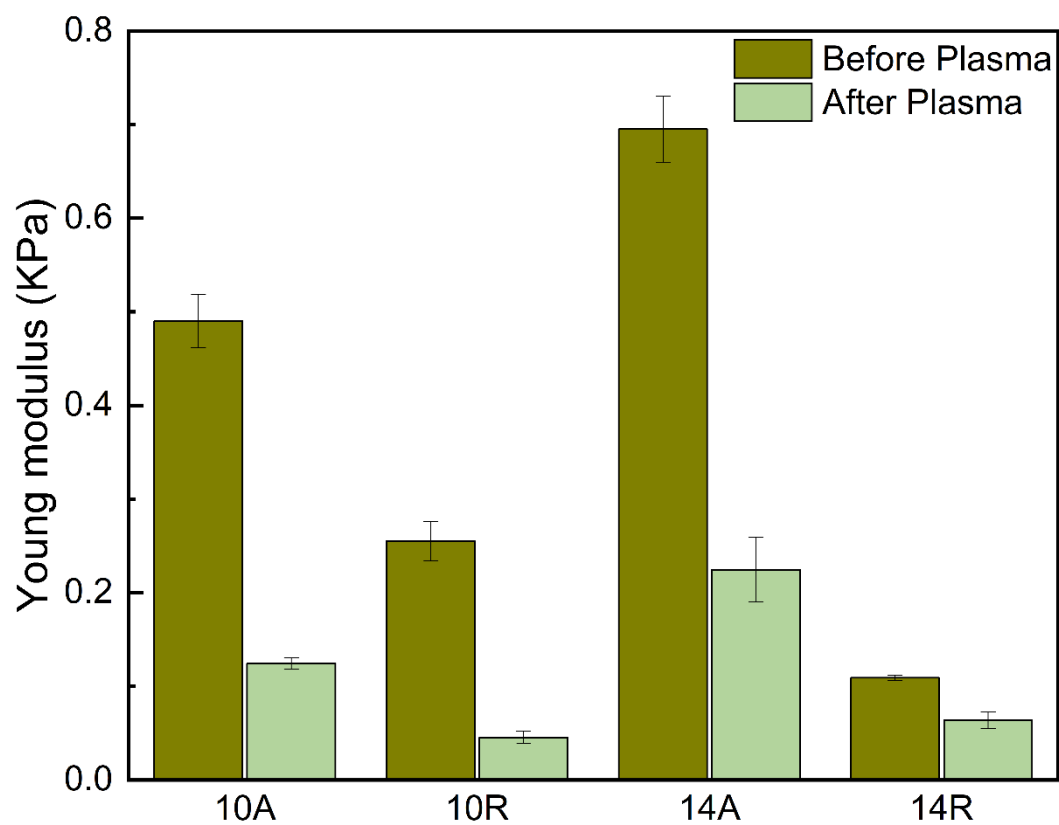


Figure S2. Young modulus of PCL nanofibers before and after plasma treatment

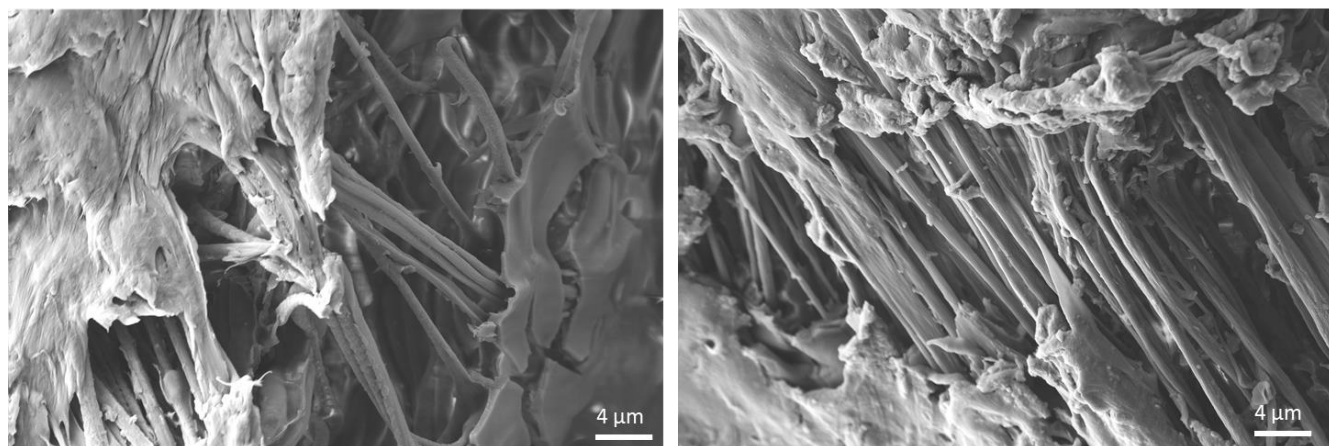


Figure S3. FE-SEM images of nanocomposite cross-section, showing the layered structure of the platform, with a layer of nanofibers between two layers of hydrogel.

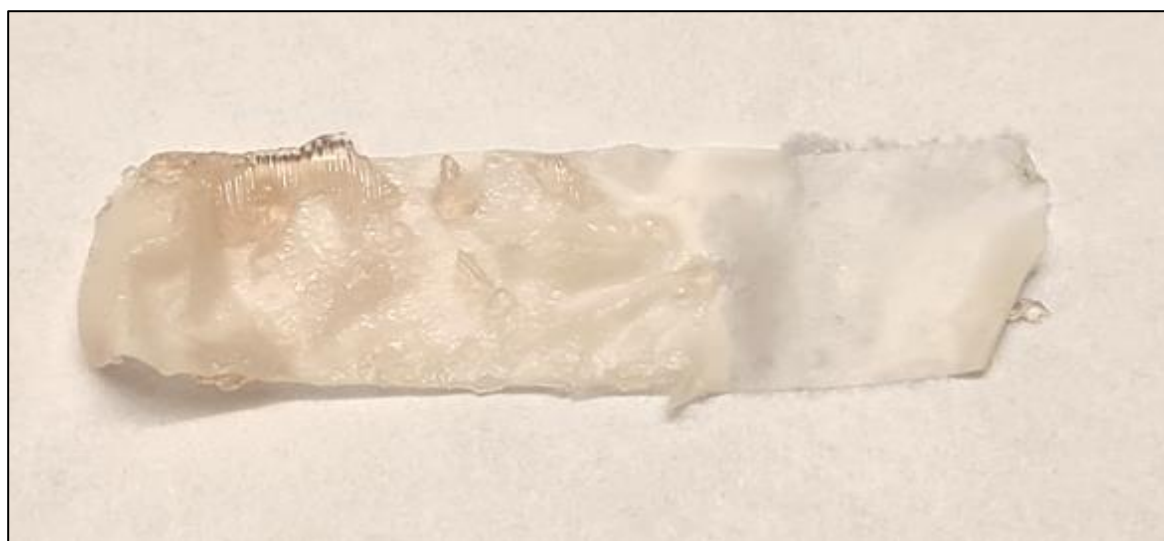


Figure S4. Image of the fiber bundle after pull-out test. The traces of the hydrogel remaining on the surface of the fibers, indicate the stable interface between the layers of the nanocomposite. This image also confirms the fact that the force required for the pull-out test is mostly spent on the destruction of the hydrogel network very close to the interface with the fibrous layer.

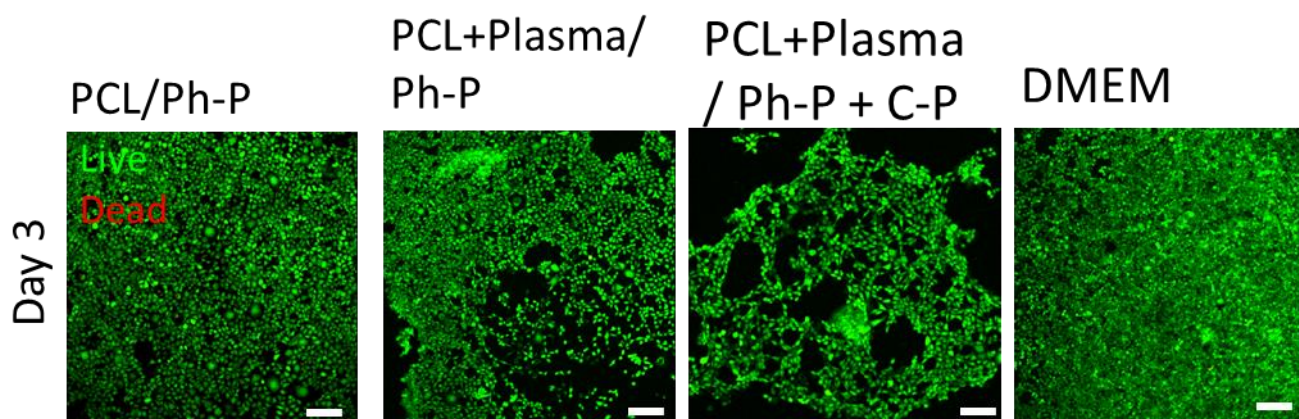


Figure S54. *In vitro* biological response of L929 fibroblasts seeded on TCP and cultured with the extracted medium of PCL14R nanofibers/hydrogel platforms in the form of Live and dead images. Live cells (green) and dead cells (red) on day 3 of the culture. Scale bars: 50 μm

Samples	Cell viability (%)
PCL/Ph-P	97.96
PCL+Plasma/Ph-P	94.02
PCL+Plasma/ Ph-P + C-P	94.84
DMEM	98.45

Table S1. *In vitro* biological response of L929 fibroblasts seeded on TCP and cultured with the extracted medium of PCL14R nanofibers/hydrogel platforms in the form of Live and dead image analysis on day 3 of culture.

Conducting polymer-based nanostructured materials for brain–machine interfaces

Yasamin Ziai¹  | Seyed Shahrooz Zargarian¹ | Chiara Rinoldi¹ |
 Paweł Nakielski¹ | Antonella Sola² | Massimiliano Lanzi³ |
 Yen Bach Truong² | Filippo Pierini¹ 

¹Department of Biosystems and Soft Matter, Institute of Fundamental Technological Research, Polish Academy of Sciences, Warsaw, Poland

²Commonwealth Scientific and Industrial Research Organisation (CSIRO), Manufacturing Business Unit, Clayton, Victoria, Australia

³Department of Industrial Chemistry “Toso Montanari”, University of Bologna, Bologna, Italy

Correspondence

Filippo Pierini, Department of Biosystems and Soft Matter, Institute of Fundamental Technological Research, Polish Academy of Sciences, Warsaw 02-106, Poland.
 Email: fpierini@ippt.pan.pl

Funding information

Fundacja na rzecz Nauki Polskiej, Grant/Award Number: POIR.04.04.00-00-5ED7/18-0; HORIZON EUROPE Marie Skłodowska-Curie Actions, Grant/Award Number: 101068036; European Regional Development Fund; Polish Ministry of Science and Higher Education; Polish National Agency for Academic Exchange (NAWA) under Bekker NAWA Programme, Grant/Award Number: BPN/BEK/2021/1/00161

Edited by: Gareth Williams, Associate Editor and Nils G. Walter, Co-Editor-in-Chief

Abstract

As scientists discovered that raw neurological signals could translate into bioelectric information, brain–machine interfaces (BMI) for experimental and clinical studies have experienced massive growth. Developing suitable materials for bio-electronic devices to be used for real-time recording and data digitalizing has three important necessities which should be covered. Biocompatibility, electrical conductivity, and having mechanical properties similar to soft brain tissue to decrease mechanical mismatch should be adopted for all materials. In this review, inorganic nanoparticles and intrinsically conducting polymers are discussed to impart electrical conductivity to systems, where soft materials such as hydrogels can offer reliable mechanical properties and a biocompatible substrate. Interpenetrating hydrogel networks offer more mechanical stability and provide a path for incorporating polymers with desired properties into one strong network. Promising fabrication methods, like electrospinning and additive manufacturing, allow scientists to customize designs for each application and reach the maximum potential for the system. In the near future, it is desired to fabricate biohybrid conducting polymer-based interfaces loaded with cells, giving the opportunity for simultaneous stimulation and regeneration. Developing multi-modal BMIs, Using artificial intelligence and machine learning to design advanced materials are among the future goals for this field.

This article is categorized under:

Therapeutic Approaches and Drug Discovery > Nanomedicine for Neurological Disease

KEYWORDS

3D printing, brain–machine interface, conductive hydrogels, electrospinning, neural recording

1 | INTRODUCTION

Bioelectronic signals are among the principal activities of our body's routine function, including electrophysiological and biochemical stimulation (Yao et al., 2020). In particular, electronic signals within the nervous system regulate

several biological activities, from simple skeletal muscle movements to complex brain functions such as thinking and remembering (Miller et al., 2020). Regular brain activities provide the coordinated transmission, oscillation, and synchronization of neural signals, involving a considerable part of the nervous tissue. However, in the case of neurological injuries, disorders, and degenerative processes, the neural population shows an insufficient capacity for self-repairing and regeneration, leading to permanent brain dysfunctions (Rinoldi, Zargarian, et al., 2021). Neurological trauma caused by accidents can provoke injuries in the brain tissue, nerves, or spine and subsequently affect several body functions, including vital organs, blood vessels, and musculoskeletal activities. Car, bike, and sports accidents, as well as accidental falls, are the most common situations which lead to neurological damage (Pichiorri & Mattia, 2020). On the other hand, neurological illness may occur in any person worldwide, regardless of gender, age, education, or wealth, and it has been estimated as 1 billion cases yearly (World Health Organization, WHO; WHO report, 2007). The high incidence results in several billions of Euros spent annually to sustain the costs related to neurological disease treatments (Y Liu et al., 2021). For this reason, the effective detection of neural signals is crucial for obtaining bioelectronic information about cognitive processes and pathways as well as diagnosing and treating related diseases (e.g., schizophrenia, autism, epilepsy, Parkinson, and Alzheimer's; McGlynn et al., 2021; Oldroyd & Malliaras, 2022). Therefore, several electrically conductive devices have been lately researched and developed for the fabrication of bioelectronic devices, including brain-machine interfaces (BMIs; S. M. Won et al., 2018; Zhao et al., 2022). These systems are designed to serve as implantable interface electrodes to record and digitize the brain signals in real-time by directly transferring them to a computer for final visualization and analysis (Song et al., 2020). Approaches for brain signal recording can be divided into three main categories: (i) recording on the top of the scalp (i.e., electroencephalography, EEG); (ii) recording under the skull, on the brain cortex surface (i.e., electrocorticography, ECoG); and (iii) intracortical recording into the brain tissue (i.e., local field potential, LFP; Figure 1a; Alahi et al., 2021). According to the position of the related electrodes, EEG, ECoG, and LFP differentiate for two main factors: the invasiveness and the amplitude of acquired potentials (M. Lee et al., 2019; Sung et al., 2020). EEG is a noninvasive strategy and has—consequently—the lowest acquired potentials ($\sim 1 \mu\text{V}$) and spatial resolution. On the other hand, among the invasive approaches, ECoG shows a high signal-to-noise ratio and good spatial resolution. Additionally, it is less invasive than LFP, but it registers signal at lower amplitudes ($\sim 100 \mu\text{V}$ for ECoG vs. $\sim 1 \text{ mV}$ for LFP) (Figure 1b; Milin Zhang et al., 2020).

In this frame, recent advances are aimed at improving the efficiency and functionalities of BMIs in terms of recording, monitoring, and stimulation of bioelectronic signals (Polikov et al., 2005; N. Wu et al., 2021). When designing an ideal electronic device, one should consider inducing minimal traumas during implantation, along with avoiding micro-motions by guaranteeing the possibility of deformation according to the native tissue movements (Choi et al., 2018). However, nowadays, many of these proposed devices (e.g., metal- and silicon-based) have the limitation of mismatching the mechanical properties with the brain tissue, which is particularly crucial for successful device implantation (Yuk et al., 2019; Sunwoo et al., 2020). Indeed, the intrinsic difference between soft, high water-containing brain tissues (1–100 kPa) and stiff, brittle and dry synthetic devices (with mechanical characteristics in the order of GPa) can result in injuries and poor coupling and integration at the implantation site (Llerena Zambrano et al., 2021; Shur et al., 2020). This may introduce chronic inflammation reactions and interfacing issues, resulting in an increase in impedance—due to the formation of astrocytic scars and microglia populations—and a decrease in detection and stimulation efficiency—because of delamination phenomena (Figure 1c; Dhawan & Cui, 2022; X. Wu & Peng, 2019). The ideal material for BMI applications should observe three main requirements: (i) it should be highly biocompatible to minimize the immunological and inflammatory response; (ii) it should be compatible at physical and chemical levels in order not to induce any damage or injury to the brain tissue; and (iii) it should have high electric conductive characteristics for improving the acquisition of signals (Khan et al., 2021; Shur et al., 2020).

For this reason, researchers are dedicating considerable efforts to designing a new generation of soft and compatible devices at chemical, physical, and biological levels, investigating conducting polymer (CP)-based nanostructured systems (Cuttaz et al., 2021; Dalrymple et al., 2020; Y. Wu et al., 2020; Yuk et al., 2019). Biocompatible CPs are considered great candidates for electronic devices such as BMIs, because of their suitable biological response as well as tunable electrical, optical, and mechanical properties (Goding et al., 2019; S. Lee, Ozlu, et al., 2020; Y. Park et al., 2022; Yuk et al., 2020). Indeed, compared to metal and silicon-based devices, CPs offer a large room for improvements in terms of modification and optimization of the final system. For instance, they have the great ability to modulate their stiffness by applying hierarchical nano-structuration and providing the use of soft hydrogel networks. Thus, CPs can potentially resemble the brain tissue characteristics, avoiding mechanical mismatching while guaranteeing excellent electrical conductivity for the efficient transduction of brain signals (Rylie Green, 2019; Goding et al., 2019; M. Wang et al., 2017). The biocompatibility and adhesiveness of those systems can lead to a minimum gap between biological tissues and

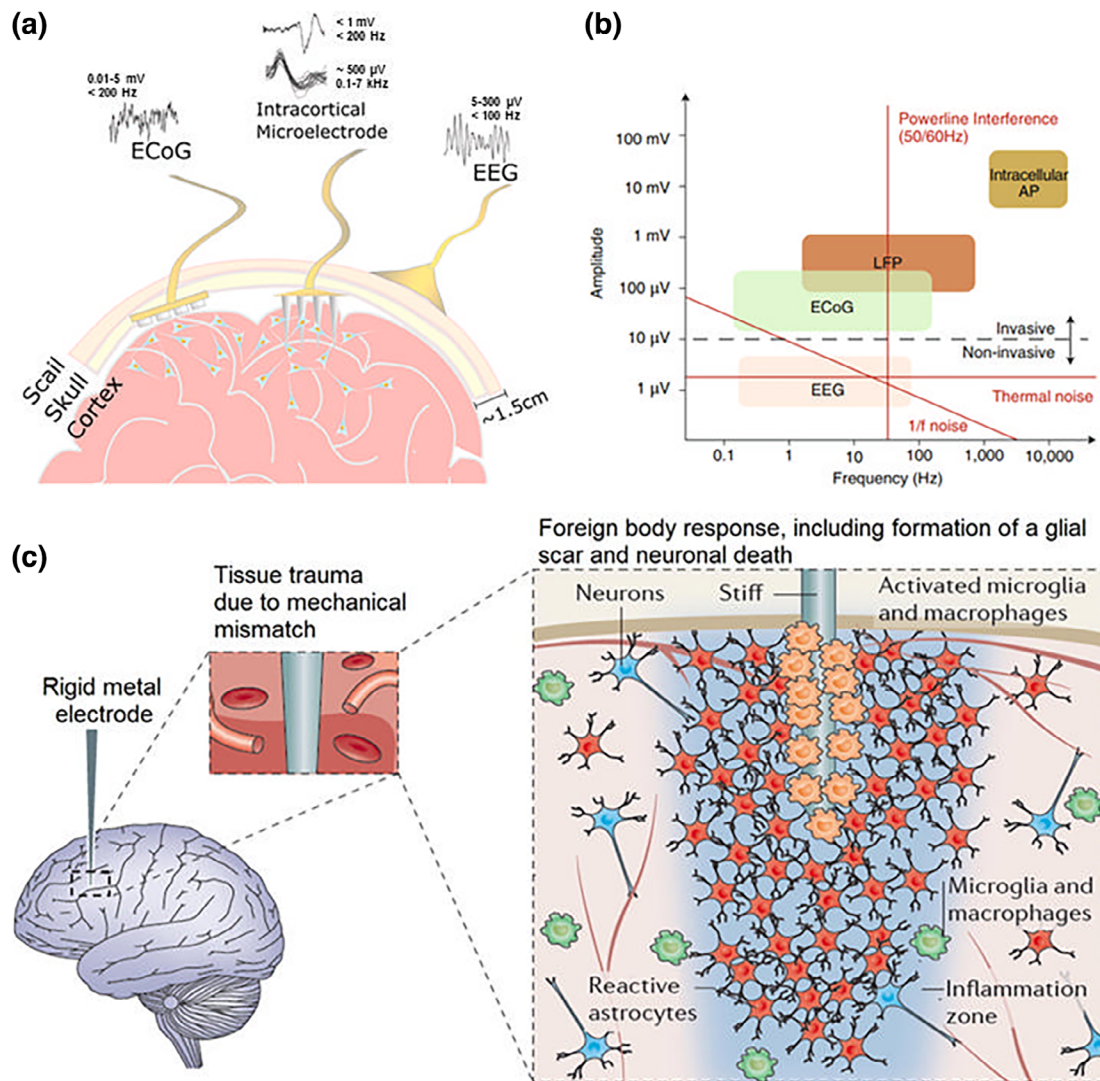


FIGURE 1 Characteristics and features of brain–machine interface. (a) Schematic representation of different brain signal recording approaches, including ECoG, EEG, and LFP (intracortical microelectrode). Reprinted with permission from Alahi et al. (2021). (b) Differences in acquired signal amplitude in the case of different recording strategies. Reprinted with permission from Milin Zhang et al. (2020). (c) Schematic illustration of neuroinflammation occurring during the implantation of rigid metal electrodes. Reprinted with permission from X. Wu et al. (2019).

electrodes, thus minimizing their relative movements and guaranteeing an intimate electrode–tissue contact (N. Wu et al., 2021). Additionally, they have the great advantage of reducing the interfacial impedance, which is crucial in biomedical applications since biological signals are alternating currents transmitted (Parashar et al., 2020). All these great properties have led CPs to be used to fabricate biocompatible devices and also as coatings for some BMIs, enhancing their functionalities. Applied coating can increase the geometric surface area and electrochemical properties of the probes, lower the modulus of the surface, and, most importantly, integrate advanced therapeutic functions if required. Coatings are also beneficial in the matter of custom-designing and specific applications, to achieve the desired properties in an easier and cost-effective manner (L. C. Wang et al., 2019; P. Yin et al., 2021).

This review presents and critically discusses the most recent scientific literature on CP-based nanostructured materials for BMIs. Our focus includes systems based on inorganic nanomaterials and composites—as carbon nanotubes, graphene, graphene oxide, and reduced graphene oxide-, intrinsically CPs and blends—like polyaniline, polypyrrole, and polythiophene-, and conductive interpenetrating polymer hydrogel networks—such as semi-IPNs and IPNs. The advantages and limitations of the reported devices have been highlighted, along with the challenges of fabrication and

nanostructuring methods (including electrospinning and additive manufacturing). Finally, new trends and future perspectives of the BMI field have been discussed.

2 | INTRINSICALLY CPS AND BLENDS

The term “polymers” refers to molecules of high molecular weight (macromolecules) formed by chains of smaller molecules called monomers, which therefore represent their structural units (Young & Lovell, 2011). When obtained by chemical reaction, usually from petrochemical industry products, they have commonly named “plastics.” In general, plastics are universally considered electrical insulating materials: in fact, they are widely used for surrounding metal wires to prevent the passage of electricity to/from the environment (Brydson, 1999). However, in the late 1970s years, scientists discovered that a synthetic polymer, polyacetylene (PA), when in its trans configuration and doped with bromine or iodine vapors, achieved an electrical conductivity of 3000 S/m, a value slightly lower than that shown by common metals (Heeger, 2001). After the discovery of polyacetylene, an enormous number of scientific articles were published related to the new conductive polymers since this family of macromolecules, which combines the properties of organic polymers (structural versatility, lightness, flexibility, and low cost) with the electroconductivity typical of metals, was undoubtedly very intriguing. A new term was even coined to describe these new materials: synthetic metals.

The common feature of these polymers is the presence of unsaturated bonds in the main chain, which gives rise to a delocalization of electrons due to conjugation. Indeed, they are also called indifferently conjugated polymers or CPs.

Irrespective of the method adopted for their synthesis, the main CPs (polyacetylene, polyaniline, polypyrrole, and polythiophene) are not entirely soluble in common organic solvents, infusible, and generally intractable materials (Quijada, 2020). Substituted analogs were then polymerized to obtain more processable polymers with side groups linked to the conjugated backbone through flexible oligomethylenic side chains (Nalwa, 2000). Functionalized CPs have been extensively studied during the last three decades and are always in the limelight owing to their high conductivity, easy synthesis, structural versatility, good mechanical properties (this is particularly true for their composites with inorganic materials), and effortless fabrication of final devices (Namsheer & Rout, 2021). They have also successfully been employed in biomedical applications, including biomaterials and biosensors (Nezakati et al., 2018) and as electrodes between biological tissues and electronic devices, being flexible and capable of both electronic and ionic conductions (Ouyang, 2021).

2.1 | Polyaniline

Polyaniline (PANI), also known as “aniline black,” has been known since the XIX century. It was first used as a dye for the tissues of priests' cassocks and then was prepared with a procedure based on the oxidation of aniline using mineral acids and oxidants like chlorate, dichromate, and persulfate (Cohen, 1887). PANI exists in different oxidation states: reduced (leukoemeraldine), partially oxidized (emeraldine), and fully oxidized (pernigraniline). Emeraldine form has an equal ratio of benzoid and quinoid repeating units and, when protonated, becomes conductive (emeraldine salt), reaching a specific electrical conductivity of 10^3 S/cm (Boeva & Sergeyev, 2014). This kind of “protonic acid doping” is a peculiarity of polyaniline, since no oxidation or reduction has to be made on emeraldine to make it conducting. High-quality PANI can be prepared by chemical oxidation of aniline using an equimolar amount of hydrochloric or sulfuric acid in the presence of ammonium peroxydisulfate (Blinova et al., 2007), or by electrochemical oxidation of aniline to emeraldine. Interfacial polymerization is also used to prepare polyaniline: in this method, green nanofibers of PANI are formed at the interface between an aqueous solution of HCl and $\text{NH}_4\text{S}_2\text{O}_8$ and an organic phase composed by a solution of the aniline monomer in CHCl_3 (Abdolahi et al., 2012). Electrospun hollow-core PANI nanofibers with high conductivity and solubility have recently been prepared with the same reagents used for interfacial polymerization.

Garrudo et al. investigated the fabrication of poly (caprolactone) (PCL) electrospun nanofibers with PANI for neural stem cell growth and electrical stimulation. By optimizing the doping mechanism and solvent system, fibers diameter, conductivity, and softness of the electrode were possible to be tuned. Cell adhesion was enhanced, and cell differentiation was successful, while electrical stimulation using AC improved neural expression (Garrudo et al., 2021). In another study, an EEG dry electrode from stainless steel was covered with PANI, showing a significant reduction in impedance compared to the metal electrode (Figure 2a). This reduction occurred because of the porous structure of the PANI,

while the intrinsic electrical conductivity allowed for efficient charge transfer. The structure of the PANI coating showing the porous network was investigated in the work of Aghazadeh et al. (2021).

Another system was designed by Manouchehri et al. (2019) to investigate the effect of oligoaniline load on reducing the impedance for brain signal recording. A conductive coating for neural electrodes was introduced based on chitosan-oligoaniline hydrogel, which was later epoxidized. By incorporating oligoaniline into the system, the conductivity was increased to the range of 10^{-2} – 10^{-4} which is adequate for cellular activity. Also, a decrease in the impedance at the frequency of 1 kHz was seen in the system, which is essential for the neuronal action potentials.

2.2 | Polypyrrole

Polypyrrole (PPy) is a CP that can be easily synthesized by oxidative polymerization of the corresponding monomer (pyrrole) in organic solvents or aqueous systems (water and mineral acids) in the presence of FeCl_3 . Although some other synthesis methods, such as electropolymerization, ultrasonic irradiation-assisted polymerization, vapor-phase polymerization, and photopolymerization have been recently proposed, chemical oxidative polymerization is the preferred system for industrial applications. The reason can be its cost-effectiveness and the possibility of obtaining the final polymer in highly conductive (oxidized) form (Pang et al., 2020). Acting on the preparation method, conducting PPy has been obtained in many different forms: bulk, films, nanoparticles, nanotubes, wires used to prepare light-

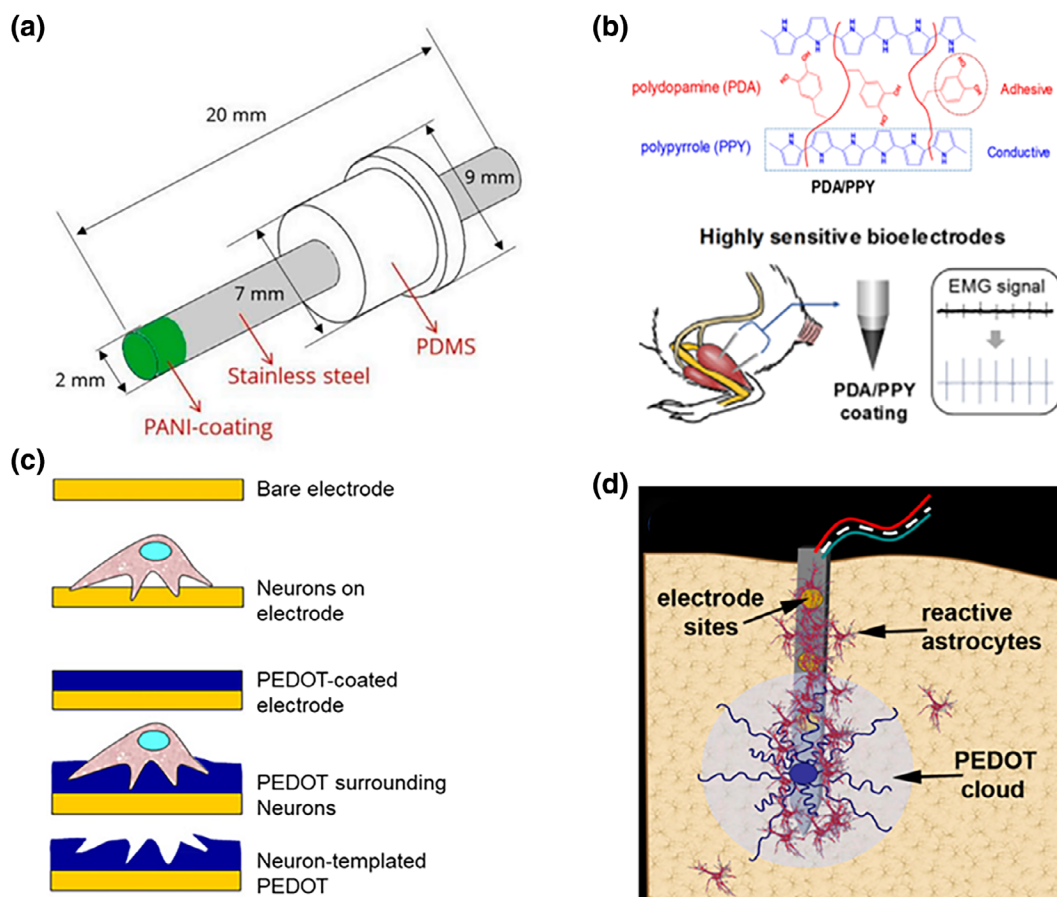


FIGURE 2 Use of intrinsically conducting polymers for BMI application. (a) Digital image of PANI@SS used for brain signal recording. Reprinted with permission from Aghazadeh et al. (2021). (b) Schematic of the electrochemical copolymerization (PDA/PPY) of dopamine and pyrrole and the use of PDA/PPY as a high-performance biomaterial for highly sensitive bioelectrode. Reprinted with permission from S. Kim et al. (2018). (c) Bare electrode, neural cells on the bare electrode, PEDOT-coated electrode, neural cells embedded in PEDOT matrix, and neural cell-templated PEDOT. Reprinted with permission from Richardson-Burns, Hendricks, Foster, et al. (2007) (d) Diagram representing the process of polymerizing PEDOT directly into brain tissue from a neural electrode device to bypass the surrounding glial scar. Reprinted with permission from Richardson-Burns, Hendricks, & Martin (2007).

emitting diode (LED), supercapacitors, diodes, transistors, and chemical sensors. For example, recently electrochromic pH and CO₂ sensors have been designed using conducting PPy thin films on indiumtin oxide (ITO) glass (Ratautaite et al., 2019). PPy, in combination with Bi₂WO₆ as a catalyst, has been used for the photocatalytic reduction of CO₂ to CH₃OH and CH₃CH₂OH in the water, while PPy-CdS composites have revealed great activity in the photocatalytic production of hydrogen starting from water solutions of sodium sulfite (Shanmugam et al., 2022). PPy nanocomposites have been successfully employed for tissue engineering scaffolds, drug delivery systems, and photo-thermal therapy (PTT) (Pierini et al., 2018; Zare et al., 2021) thanks to their biological properties due to the excellent cell adhesion and growth properties on their surface.

PPy as a coating for neural interfaces was investigated in the work done by George et al., in this case with different dopants like polystyrene-sulfonate (PSS) and dodecylbenzenesulfonate (NaDBS). Using PPy with different dopants can benefit many applications, from neural substrates to electrode coatings. Their study has shown that the biocompatibility of the electrodes has been increased compared with Teflon implants, and positive surface interactions have been noticed in the interface (George et al., 2005). A combination of SWCNT with PPy composite films was designed and used as electrode materials by Xiao et al. the pore size of the structure was tuned by controlling the concentration of the metal ions, and the PPy ultrathin layer was obtained by pulsed electropolymerization. Using this technique, SWCNTs are immobilized on the electrode surface; hence the adhesion was improved while the larger electrode-electrolyte interface was also obtained; therefore, the ion transfer can happen faster within the bulk film. The system's impedance showed a significant decrease; at the same time, the new electrodes showed excellent biocompatibility for neural cells for long-term applications (H. Xiao et al., 2015).

Polydopamine (PDA) has been used in many applications to promote the adhesion of the substrates and can be used with other materials as robust coatings for biomedical applications. According to the previous studies, coatings prepared from PDA/PPy are adhesive and conductive; *in vivo* and *in vitro* studies were also done on the electrodes to check further potentials (Figure 2b). Culturing myoblasts and PC12 neuronal cells showed that these electrodes can significantly encourage the growth and differentiation of neuronal cells. At the same time, electrical stimulation showed the neurite outgrowth of the PC12 cells. Even with the thick layers of the coating, good electrochemical properties were seen, and by *in vivo* experiments, EMG signals with high sensitivity were recorded (S. Kim et al., 2018).

2.3 | Polythiophene

The preparation of conductive polythiophene (PT) started at the beginning of the 1980s, and since then, it has progressively gained a prominent place in the CP field thanks to its structural versatility, high conductivity, and thermal and environmental stability. The literature on PT and its derivatives is very extensive, with a tremendous increase in the number of articles published in the last few years. Indeed, they can show a dramatic color shift in response to changes in solvent (solvatochromism), temperature (thermochromism), applied potential (electrochromism), presence of other molecules (affinochromism), or ions (ionochromism), paving the way for the production of high-speed and inexpensive chromic sensors (Kaloni et al., 2017).

Moreover, the electronic structure (and then the color) of polythiophene is also influenced by the steric repulsion between substituents or, when directly linked to the thiophene ring, by their electron-withdrawing or donating effects, making chromism widely tunable. Bulk heterojunction (BHJ) solar cells based on photoactive layers of polythiophene derivatives as electron-donors have reached power conversion efficiencies up to 10% (Guo et al., 2013) and PT-based organic light emitting diodes (OLED) have shown high intensity of emission and tunable colors by simply varying substituents employed on the thiophene unit (Grimsdale et al., 2009). One of the most important PT derivatives is undoubtedly the poly(3,4-ethylenedioxythiophene) (PEDOT) thanks to its high conductivity, thermal stability and easy processability when doped with PSS. PEDOT has high electroconductivity (around 500 S/cm), sufficient to allow the production of organic LEDs, electrochromic devices and polymeric solar cells and is well soluble in water. It can be easily obtained with spontaneous solid-state polymerization of 5-bromo-2,3-dihydro-thieno[3,4-b][1,4]dioxine by simple heating (Y. Yin et al., 2013). PEDOT is currently considered as neural interface for the communication between neurons and machines, including neuroprosthetic devices, cochlear implants, cardiac pacemakers, and vision prostheses (R Green & Abidian, 2015). In a work done by Richardson-Burns et al., a novel biomaterial based on PEDOT has been designed for cell-templated neural probe coating. This material can also be used as a CP-live neural cell electrode. PEDOT has been electrochemically deposited around neurons cultured on electrodes, where cells embedded within the polymer matrix remain viable for 120 h after

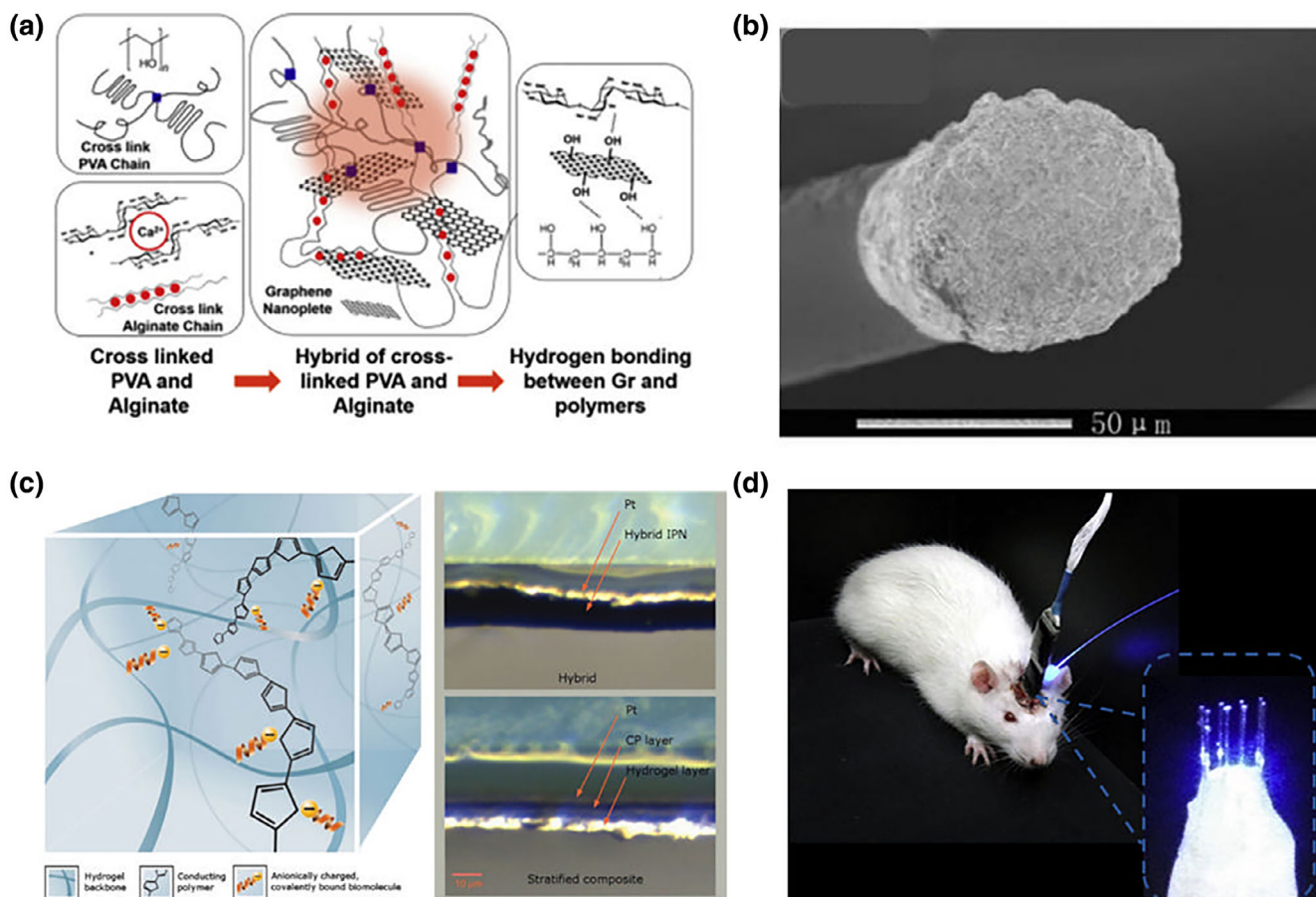


FIGURE 3 Hydrogels as soft materials for BMI applications. (a) Schematic illustration of the formation of PVA:SA interpenetrating network, via physical crosslinking of PVA by heat treatment and chemical crosslinking of Alginate by CaCl_2 solution. Hydrogen bonding between Gr nanosheets and polymer matrix is also shown, leading to significantly promoted mechanical properties. Reprinted with permission from Golafshan et al. (2017). (b) TEM image of alginate/PCNT hydrogel. Reprinted with permission from Kun Wang et al. (2018) copyright (www.tandfonline.com). (c) Scheme of ideal hybrid configuration (left) and photo comparison of hybrid material created by using a bound dopant, compared to stratified composite produced by using a free dopant (right). Both material samples are hydrated. Reprinted with permission from Green et al. (2012). (d) Tip of optrode array with the light on when optical stimulation and electrical recording using optrode array implanted in freely moving animal is happening. Reproduced with permission from Lu et al. (2012).

polymerization (Figure 3c; Richardson-Burns, Hendricks, Foster, et al., 2007). Indeed, due to the soft nature of this polymer, a conductive layer of PEDOT on a metallic substrate can lower the mechanical mismatch between the electrode and the tissue, thus reducing the risk of gliosis or inflammation. PEDOT can be also directly polymerized within the brain tissue, leading to a conductive network of polymeric chains as it can be seen in Figure 2d (Richardson-Burns, Hendricks, Foster, et al., 2007). Self-assembled monolayering (SAM) is an alternative fabrication method that can overcome the problems of electrodeposition. SAMs containing conductive polymers can offer high conductivity and can be customized by different functional groups. This characteristic is of great importance, as it can allow to have the self-assembly on metals, thus improving the effective surface and lowering the impedance. This opportunity was investigated in the work of Widge et al., where they have designed pTh-based SAMs. Neural stimulating and recording through electrodes has been improved and the biocompatibility of the electrodes tested to be successful (Widge et al., 2007).

To summarize, CPs and especially PEDOT are among the most effective categories of materials exploited to gain high quality signal recordings and electrical stimulation. CPs have high mechanical flexibility which allows fabricating adjustable constructs, at the same time, they have low cost. Addition of CPs into the substrate of the polymers can enhance their electrochemical properties and biocompatibility (Ouyang, 2021). There are challenges regarding the use of these materials in neural interfaces, such as designing a long-term effective implant. Researches show that although

using CPs can increase surface area and roughness of the electrode, but poor electroactive stability can affect their application (R. A. Green et al., 2008; Rossetti et al., 2021).

3 | CONDUCTIVE INTERPENETRATING POLYMER HYDROGEL

Development of materials which can cover the three required criteria for the BMI application has been the purpose of the research for many scientists in this field. Designing a material which has mechanical properties similar to soft tissues, as well as conductivity, has been very challenging. The majority of conventional electrode materials (e.g., silicon, gold, platinum, titanium nitride, iridium, tungsten, and tin) exhibit very high Young's moduli over 1 GPa, which are several orders of magnitude higher than that of neural tissues. In the last decade, a number of novel materials and laboratory-level devices have been developed to minimize the biomechanical dissimilarities between electronics and biology. For example, polymeric materials such as plastics (e.g., polycarbonate, polyimide [PI], and parylene C) and elastomers (e.g., epoxy, PDMS, and polyurethane [PU]) have been adopted to reduce the modulus gap. However, their Young's moduli (typically 1 MPa to 1 GPa) are still much higher than those of neural tissues ($E \sim 10$ kPa) and not sufficient to provide truly mechanically matching interfaces. While numerous materials as mentioned in previous sections have been studied for BMI technology in the past, innovative nanomaterials with low modulus and low electrical impedance are developed vastly. Hydrogels as three-dimensional (3D) polymeric networks can meet the requirements of this area and have been widely used in recent years due to their highly tailorable structures. Their characteristics make them perfect candidates to be used in biomedical applications such as biosensing (Ziai et al., 2022), drug delivery (Nakielski et al., 2020), tissue engineering (Quint et al., 2022; Rinoldi et al., 2019), wearable electronic (Deng et al., 2020), and BMI (X. Wang et al., 2022).

These hydrophilic networks with extremely high water intake have perfect resemblance to the mechanical properties of the extracellular matrix (ECM; Hoffman, 2001). As a result, they endow a promising route to ameliorating the biomechanical mismatch at tissue–electrode interfaces. Unlike other dry electrode materials, the water- and ion-rich hydrogels have the potential to offer unconventional but improved stimulation/recording performance via integrative use of both electronic and ionic activities (Yuk et al., 2019). Hydrogels have lattice-like intra-structure, with interconnected pores, which not only can retain high water content, but also, other materials can be incorporated in their structure. As a result, they can also be used for other purposes in neural bioelectronics, like drug delivery and active electrode coatings. Using CPs to form hydrogels as well as the incorporation of conducting molecules, polymeric chains, and nanomaterials into the hydrogel matrix are popular approaches toward the goal of having conducting hydrogels (Deng et al., 2021). These materials have been investigated to have specific characterizations such as self-healing and stimuli-responsiveness. Tailoring these properties make it possible to use them in many applications especially wearable electronics devices (Deng et al., 2018, 2019). Meanwhile, pure hydrogels—as single network materials with weak mechanical properties—are very difficult to handle practically as the sole material to be used for the final application. In order to enhance the mechanical properties, stability, and other aspects of hydrogel networks, blended structures were introduced.

Polymers can be blended in systems using mechanical blends and graft copolymers. In mechanical blends there is no chemical bonding between the components, while primary bonds can be seen between the components in graft copolymers (Zoratto & Matricardi, 2018). Interpenetrating polymer networks, known as IPNs, are networks consisting of two polymers polymerized in the presence of each other, while there are no chemical bonds between different components. According to the presence and type of crosslinking of the polymeric chains, they are classified into subclasses such as block copolymers, semi-IPNs and full IPNs (Zoratto & Matricardi, 2018). By having an interpenetrated network of more than one polymer, enhanced mechanical stability can be developed, and no phase separation will occur under tensile or shear stress. Moreover, using combinations of natural and synthetic polymers in one system offers tailorable chemical properties, where synergetic properties of both polymers can be acquired. This combination is of key importance in BMI application, where a CP can be introduced into the devices, with preserved conductivity along with properties of the hydrogel structure.

3.1 | Semi-IPNs

Semi-IPNs are defined as systems where there is one fully crosslinked network along with one or more linear or branched polymeric macromolecules interpenetrated inside the first network. There are two main crosslinking pathways of semi-IPN networks: in situ and sequential. In none of these cases, bonds between the different components of the system are present.

In the in-situ approach, all of the reagents needed to polymerize the first polymer, will be added at the same time with the already polymerized chains of the other components. Crosslinking of the first polymer will take place in the presence of other polymers. Conversely, in the sequential method, the first polymer will be polymerized and then impregnated with the chains of the second polymer (Chikh et al., 2011). Using intrinsically CPs as an additive in the network of hydrogels is one of the main strategies for providing electrical conductivity to BMI platforms.

In the work of Golafshan et al. a semi-IPN hydrogel based on alginate and poly(vinyl alcohol) (PVA) was investigated for neural applications. The hydrogel network was incorporated with graphene to develop electrical conductivity, and then optimized to obtain fibrous scaffolds using the electrospinning technique (Figure 3a) (Golafshan et al., 2017). As a result of this fabrication design, considerable improvements in the electrical and mechanical properties of the system were reported. Adding Gr nanosheets not only introduced conductivity to the system, but also enhanced the strength and toughness of the device.

Siddhanta et al. introduced linear polyaniline (PAn) into the nanostructured gel network of poly (2-acrylamido-2-methyl propane sulphonic acid) (PAMPS). While the in-situ polymerization of the polyaniline chains took place, a semi-IPN hydrogel with suitable electrical properties was achieved (Siddhanta & Gangopadhyay, 2005). The electrical conductivity of the system was increased from $\leq 10^{-5}$ S/cm for pure PAMPS to ~ 0.21 S/cm for the system loaded with PAn. Studies on the systems confirmed that all the conductivity gained by the system is attributed to the electrical conductivity caused by PAn, as the ionic conductivity is negligible. Chitosan, a biocompatible polysaccharide, was also used alongside with conductive PAn and then crosslinked in the presence of agarose to form a semi-IPN hydrogel to form a conductive material for neural applications. The electrical conductivity of the samples was measured $\sim 10^{-4}$ S/cm, which lies in the proper range for biological signal detection. The use of PAn in this structure was also important to microstructurization of the system by changing it from honeycomb to aligned. Aligned structure not only shows better mechanical properties, but also enhances cell activities. Release of dexamethasone (DX) was also studied and effect of PAn was studied. Due to the interaction of PAn with DX, drug release was decreased in the beginning, but by electrical stimulation, an on-demand controlled release was achieved (Bagheri et al., 2019).

Another system of a semi-IPN hydrogel was designed by Rinoldi et al. where poly(*N*-isopropylacrylamide-*co*-*N*-isopropylmethacrylamide) (P(NIPAm-*co*-NIPMAm)) was used as the hydrogel network. In contrast, sodium poly [6-(3-thienyl) hexanesulfonate] (P3HT6S) was added as a conductive polymer to provide the system with good electrical properties. Electrical tests were performed on the construct, demonstrating the notable decrease in the impedance of the semi-IPN platform compared to the pristine hydrogel. The culture of neural progenitor cells (NPCs) onto the hydrogels showed the platform's suitability to support the survival and neural differentiation of the central nervous system cell line (Rinoldi, Lanzi, et al., 2021).

Hydrophobic poly (3-hydroxybutyrate-*co*-3-hydroxyvalerate) (PHBV) formed a semi-IPN with hydrophilic PVA, where PPy was added as a conductive nanoparticle incorporated into the matrix. Preparing the network with a ratio of 70/30 provided structural reinforcement while preserving the hydrogel properties; thus, the system could be quickly introduced and function in aqueous environments. Improved electrical properties were measured as a result of embedding PPy nanoparticles, revealing the system's potential for BMI application (Aparicio-Collado et al., 2020).

3.2 | IPNs

A simple definition of the IPN is a polymer network consisting of two or more structures interlaced with no covalent bonds. There is no possibility of separating them unless breaking the chemical bonds of each system. In other words, IPNs are a combination of at least two polymer networks, each in the lattice form, where each lattice is crosslinked in the immediate presence of the other. No covalent bonds present between them (Soman et al., 2015). They can also be described as alloys of crosslinked polymers (Dragan, 2014). Like the semi-IPNs, IPNs can be synthesized through two main pathways. In the in-situ pathway, all the reactants of all polymers are mixed before crosslinking, although they may or may not start simultaneously. Sequential synthesis, also known as impregnation synthesis, on the other hand, is a process where the first polymeric network will be synthesized. Then all the reagents needed for polymerizing the second network will be added to the system. Morphological properties of the first system are controlled by both polymers simultaneously and can be manipulated by altering the proportions, the order, and the rate of polymerization. However, latterly, morphology is mainly determined by the properties of the first network (Chikh et al., 2011). The presence of hydrogels at the tissue-electrode interfaces can potentially compromise electrical performance despite enhanced biomechanical interactions. Introducing improved electrical properties (e.g., lower interfacial impedance and higher

charge injection capacity) without compromising their desirable biomechanical features (e.g., low mechanical modulus and biocompatibility) can provide opportunities to improve tissue–electrode further interfaces. One of the most popular ways of modifying the properties is to use CPs such as PEDOT and PPy. Using these materials not only improves the final material's electrical conductivity but can also further facilitate tissue integration by immobilizing biomolecules. Use of the CPs can be solemnly or by combining them in the network of the hydrogel. As a result of its soft mechanical properties, it was proposed that the hydrogel can reduce the mechanical mismatch between the tissue and the electrode material and can act to stabilize the otherwise brittle CP. The hydrogel can also serve as an anti-biofouling surface, preventing unwanted adhesion of proteins or inflammatory cells.

There are significant advancements in the use of hydrogel-based IPNs for different applications. Physical phase separation cannot occur between the components due to the infinite zero-viscosity of the hydrogel, resulting in considerably higher stability of the system. Also, due to the fact that at least two crosslinked networks are entangled in the system, the mechanical properties of the final network are enhanced remarkably (Soman et al., 2015).

There are three main approaches to fabricating conductive hydrogel networks; the most common is electrochemically depositing the CP within the hydrogel network (B. C. Kim et al., 2000; Lira & Córdoba De Torresi, 2005). Other approaches include chemical crosslinking of the CP in an already polymerized hydrogel network or simultaneous polymerization of all the components (Dai et al., 2009, 2010).

PEDOT:PSS was treated with CNTs and evenly dispersed in an alginate solution to be electrodeposited on a neural electrode. This specific structure was investigated by Wang et al. and was used to record *in vivo* signals and noise floor, TEM image shown in Figure 3b. Improved electroconductivity and charge capacity of the IPN hydrogels were studied, and mechanical characterizations also showed that the material has enough stiffness to penetrate the brain in the dry state without inflammation after swelling (Kun Wang et al., 2018).

Kleber et al. synthesized an IPN system composed of P(DMAA-co-5%MABP-co-2,5%SSNa) (PDMAAp) hydrogel, with PEDOT conductive chains propagating inside the hydrogel network, making a full IPN as a matrix. PEDOT was successfully integrated into the already patterned hydrogel matrix through a combination of electropolymerization and the establishment of ionic interactions between the negative charges of the sulfonate in the hydrogel and the positive charges of PEDOT. This kind of promising design addressed the requirement for making possible a homogeneous coating on the electrode substrate. Significant higher stability and impedance reduction confirmed the beneficial effect of PEDOT in hydrogel matrix (Kleber et al., 2017). Abidian et al. designed a hybrid interface for neural electrodes with the capability of controlling drug release. The construct consisted of a layer of nanofibers for regulating the drug release, topped with a hydrogel platform embedding conducting nanotubes, acting as a mechanical buffer in the interface between probe and tissue. PEDOT was polymerized on the electrode sites and inside the hydrogel, making an IPN. In order to minimize the damage during implantation, the electrodes were used in a dry state and were rehydrated inside the brain. Electrodes proved to improve the electrical conductivity of the metal electrode (Abidian & Martin, 2009).

A conducting IPN hydrogel was fabricated using PEDOT as CP crosslinked in the network of an anionic hydrogel of PVA and heparin (Figure 3c). Mechanical properties of the system were improved vs. pure hydrogel, and at the same time, their electroactivity was significantly raised from metal electrodes (R. A. Green et al., 2012). Poly(vinyl alcohol)/poly(acrylic acid) IPNs were prepared by Lu et al. (2009), showing that the ionic conductivity was maintained for electrode-neural interfaces. Excellent stability was observed after 6 weeks of implantation, as well as a homogenous coating. The same system was also used to improve the interface and stability after chronic implantation, as shown in Figure 3d. PEDOT:PSS was electrochemically deposited into the network as the conductive component. The higher capacitance and lower impedance due to the presence of the conductive material were observed, where higher mechanical properties due to the IPN network were obtained compared to the polymer films. Chronically optogenetic modulation and electrophysiology recordings were performed, showing stable and improved outcomes compared to bare electrodes, making the system a promising candidate for BMI applications (Lu et al., 2012).

Summary of studied systems in the shape of semi-IPN and IPN hydrogel systems, marking their components and special features has been presented in Table 1.

4 | INORGANIC NANOMATERIALS AND THEIR COMPOSITES

The most common devices implanted in the brain are electrodes (Jia & Rolandi, 2020). Several inorganic materials have been considered, studied, and used as structural materials for these electrodes (Scaini & Ballerini, 2018; N. Wu et al., 2021; Yang et al., 2010). Among them, noble metal particles have been explored extensively due to their excellent

TABLE 1 Examples of the conductive semi-IPN and IPN systems, their components and recognizable features.

Hydrogel system	Polymer base	Conducting element	Features	References
Semi-IPN	Poly(2-acrylamido-2-methyl propane sulphonic acid) (PAMPS)	Polyaniline (PAn)	Electrical conductivity ~ 0.21 S/cm	(Siddhanta & Gangopadhyay, 2005)
Semi-IPN	Chitosan/agarose	Polyaniline (PAn)	Electrical conductivity $\sim 10^{-4}$ S/cm	(Bagheri et al., 2019)
Semi-IPN	Poly(<i>N</i> -isopropylacrylamide-co- <i>N</i> -isopropylmethacrylamide) P(NIPAm-co-NIPMAAm)	Poly[6-(3-thienyl)-hexanesulfonate] (P3HT6S)	Electrical impedance $\sim 30 \Omega$	(Rinoldi, Lanzani, et al., 2021)
Semi-IPN	Poly(3-hydroxybutyrate-co-3-hydroxyvalerate) (PHBV)/polyvinyl alcohol (PVA)	Poly pyrrole (PPy)	Electrical conductivity ~ 6.35 mS/m	(Aparicio-Collado et al., 2020)
IPN	P(DMAA-co-5%MABP-co-2.5%SSNa)	Poly(3,4-ethylenedioxythiophene) (PEDOT)	Impedance decrease and 2.5 fold increase in CSC	(Kun Wang et al., 2018)
IPN	PLLA, PLGA, Alginate	Poly(3,4-ethylenedioxythiophene) (PEDOT)	Impedance to $\sim 2.5 \Omega$	(Abidian & Martin, 2009)
IPN	Poly(vinyl alcohol) (PVA)/heparin methacrylate (Hep-MA)	Poly(3,4-ethylenedioxythiophene) doped with para- toluenesulfonate (PEDOT/pTS)	Electrical conductivity ~ 1.1 S/cm	(R. A. Green et al., 2012)
IPN	Poly(vinyl alcohol)/poly (acrylic acid) (PVA/PAA)	Ionic conductivity	Ionic conductivity ~ 0.18 mS/cm	(Lu et al., 2009)
IPN	Poly(vinyl alcohol)/poly (acrylic acid) (PVA/PAA)	Poly(3,4-ethylenedioxythiophene)/poly(styrene sulfate)(PEDOT/PSS)	Electrical impedance $\sim 2.73 \Omega$	(Lu et al., 2012)

electrical conductivity, chemical stability, and good biocompatibility (S. M. Won et al., 2018). For instance, gold nanoparticles (Au NPs) have gained large popularity because of their capability to be easily bio-conjugated with various biomolecules and create biomimetic architectures (Wellman et al., 2018).

To mimic the topographical cues of the brain, electrode fabrication using metallic materials with nanoscale geometries has evolved (Aurand et al., 2018). In this frame, carbon nanotubes (CNTs) and graphene were introduced into this arena, showing improved stability and longevity as new microfabrication technologies emerged (John et al., 2015).

Notwithstanding the high electrical conductivity and ease of surface modification of CNTs and graphene, using these nanomaterials in direct contact with human tissue has faced many challenges (Saleemi et al., 2021; Z. Wang et al., 2021). By reviewing the experimental endeavors, it can be deduced that the reduction in the probe functionality over time and the appearance of glial scarring in the implanted tissue are the most cited problems (Dong et al., 2021; Spencer et al., 2017; Zou et al., 2021). In other words, an inflammatory response coupled with the degradation of the probe properties happens during the extended utilization of the rigid probes comprised of inorganic nanomaterials (Pavone et al., 2020). This observation magnifies the importance of electrode biocompatibility for BMI.

The gap in the literature between 2012 and 2017 vividly shows the period of rethinking and redesigning the strategies for implementing CNTs in biological applications (*Web of Science*). The same trend can be observed for pristine graphene (PG), graphene oxide (GO), and reduced graphene oxide (rGO) (Wen et al., 2015).

An evolving promising solution is to restrain the inorganic materials inside a polymeric substrate (Kozai et al., 2012; Woods et al., 2020). The polymeric composites fabricated from different nanostructures of metals or carbon allotropes bring about the functional properties of both components and overcome the performance limits by increasing the longevity and stability of the neural interface. Furthermore, the presence of a polymeric material in a neural probe's substrate adds flexibility to the structure and compliance with the surrounding bio environment (Kozai et al., 2012). The match between the mechanical properties of the brain tissue and the neural probes are considered the second prompt of the vast utilization of inorganic nanomaterials in BMI application. In turn, the compatibility between the inorganic materials and polymeric matrix plays a vital role in the coating's final mechanical, thermal, and electrical properties (Pumera, 2013; Smith et al., 2019).

Studies on brain tissue disruption during the chronic implantation of BMI devices comprised of inorganic nanomaterials are still at an early stage. Nevertheless, the excellent properties of these nanomaterials justify deeper and more dedicated investigations, which can provide a way out of the current uncertainties.

4.1 | Carbon nanotubes

Carbon nanotubes (CNTs) are 2D carbon sheets rolled into a cylinder with a hollow interior, constituting a carbon nanotube. Their excellent physical properties and electrical conductivity favor the foundation of desired electrical settings (Feng et al., 2021; Pavone et al., 2020). Combined with their unique structural properties, CNTs have become promising in many scientific fields, including energy storage, wearable electrodes, and neuroscience (Y. Wu et al., 2020; Q. Zhang et al., 2013). The single-walled (SW) and multiwalled (MW) forms of CNTs have different thermal properties, conductivity, and electrical percolation thresholds (Moisala et al., 2006; Sandler et al., 2003). These hollow cylinders of carbon layers were introduced to the traditional transition metals utilized in fabricating microelectrode arrays to lower their impedance and unfavorable electrochemical reactions. For instance, the advantages of SWCNTs over platinum for prolonged chronic use of electrocorticographic electrodes have been evaluated (Pavone et al., 2020). With some reservation, platinum's biostability is low as delamination occurs on the explanted arrays (Grabiec et al., 2013; Vomero et al., 2017). On the contrary, it can be deduced that the biocompatibility and biostability of SWCNTs are higher than platinum since limited delamination and degeneration of neurons were observed for the arrays coated with these nanotubes.

The proper distribution and restraining of CNTs inside a polymeric substrate have the potential to diminish their coincidental accumulation inside living tissue. In this context, incorporating CNTs into a polymeric substrate may support the formation of neurons' functional networks and guides axonal growth. It was shown that the presence of MWCNTs in a polydimethylsiloxane (PDMS) elastomeric construct reconnects the segregated explants and guides the regeneration of axons (Aurand et al., 2018). Tissue integration of the interface was also highlighted in this study. The pure polymeric substrates had limited interaction with the surrounding brain tissue, and as a result, the integration of these substrates failed. This was in contrast to the implantation results of PDMS/MWCNTs brain interface where neurons infiltrated into the probe construct.

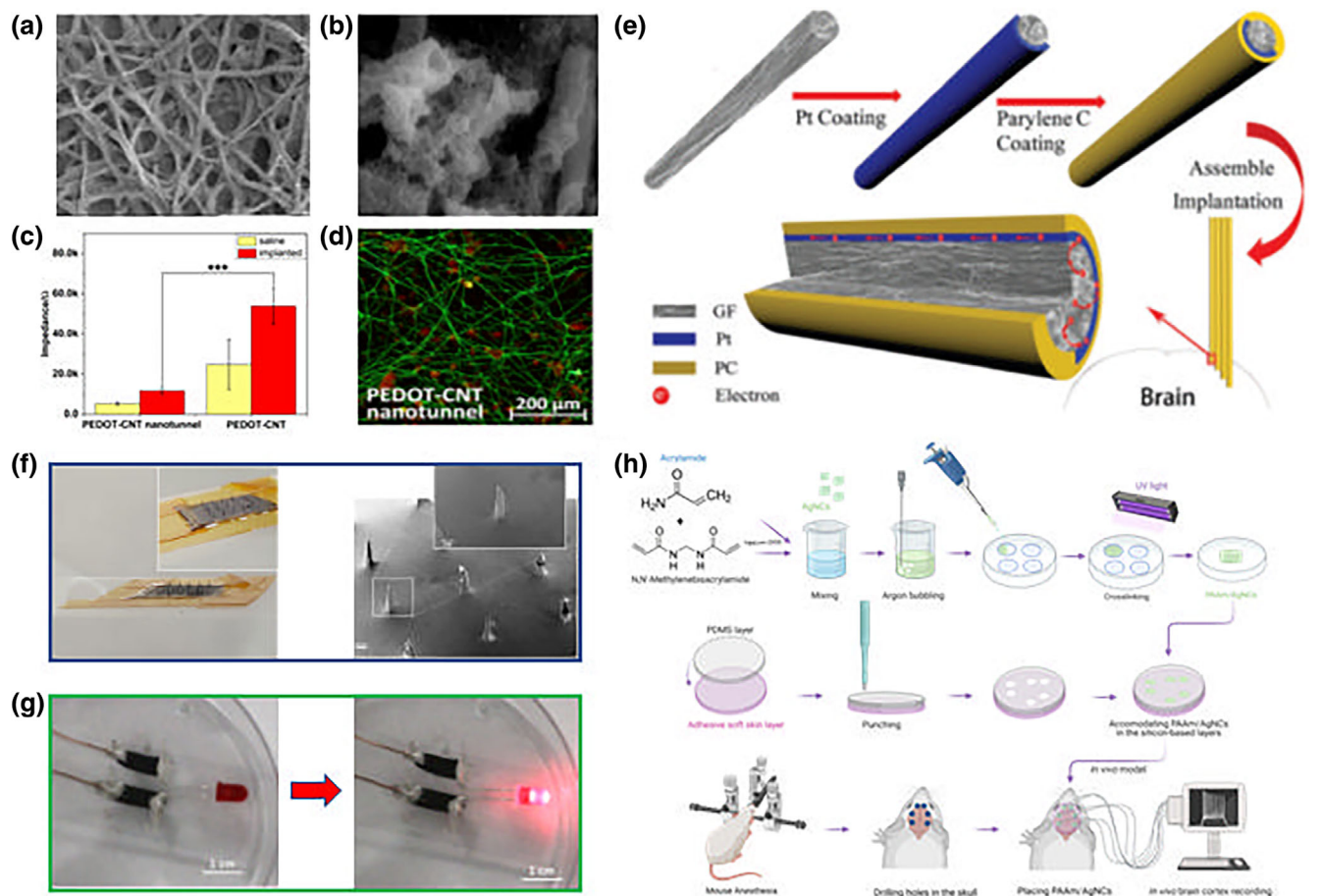


FIGURE 4 Brain-machine interfaces based on inorganic nanomaterials and their composites. (a–d) Tunnel-like electrode coating comprising of CNTs and PEDOT for highly sensitive neural recording: (a,b) SEM images of PEDOT-CNT nanotunnel deposited on the electrode site at different magnifications; scale bar for (a) is 10 μm , and for (b) is 1 μm ; (c) impedance of the electrodes coated with PEDOT-CNT nanotunnel and PEDOT-CNT in saline and after implantation during acute signal recording from the rat's peripheral nerve. Statistical significance is indicated using *** for $p < 0.001$; (d) image related to the immunostaining of rat's neurons and glial cells cultured on PEDOT-CNT nanotunnel substrate. Cells were isolated for the staining on the fourth day of the *in vitro* studies. The green represents the neurons, while the red represents the glial cells. Reprinted with permission from N. Chen et al. (2020) Copyright 2020, American Chemical Society. (e) Durable microelectrodes comprised of graphene fibers coated with platinum and parylene-C: schematic illustration of graphene microelectrode fabrication and its application as a recording interface during intracortical implantation. Platinum sputter coating on one side of the microfibers was performed to increase the conductivity of the interface and reduce the adverse effect of the length on the electric resistance of graphene fibers. The coating of the final polymeric layer served to increase the dielectric property, flexibility, and biocompatibility of the graphene-based electrode. Reprinted with permission from Kezhong Wang et al. (2019). Reproduced with permission. Copyright 2019, Wiley-VCH. (f,g) Neural interfacing construct based on pristine graphene and collagen: (f) collagen/pristine graphene (CpG) composite was used to fabricate a 5×5 microneedle array set via dry cast method. The height of the needles was 2.5 mm narrowing at the tip with a diameter of 40–80 μm . The array set under the SEM showed the sharp bore and tips for each needle. (g) The composite was then modified to serve as a printable bio-ink. A controllable 3D printing process was optimized to create complex geometries. An LED was powered through a printed circuit to demonstrate the composite conductivity. Reprinted with permission from Maughan et al. (2022). Copyright 2022, Elsevier. (h) Hydrogel-nanoparticle composite fabrication and application scheme. The hydrogel was formed based on acrylamide using a photoinitiator in deionized water. AgNCs were added to the hydrogel precursor before UV cross-linking. For *in vivo* study, six hydrogels were placed into dedicated holes punched through layers of soft skin adhesive and PDMS. The final system was placed on the mouse skull with stereotactically drilled holes through which hydrogel could reach the brain cortex and permit a specific ECoG signal acquisition. Reprinted with permission from Rinoldi et al. (2022). Copyright 2022, American Chemical Society.

In another work authored by Chen et al., CNTs in combination with poly(3,4-ethylene dioxothiophene) (PEDOT) were electrodeposited on sacrificial polymeric nanofibers (N. Chen et al., 2020). The achieved structure was in the form of nanotunnels (Figure 4a,b) and used as an electrode coating for neural recordings. The authors reported improved

adhesion of the coating after the incorporation of CNTs into the structure. Moreover, the topology of the CNTs-PEDOT composite played a significant role in decreasing the impedance of the electrode (Figure 4c) and increasing its electrical fidelity. As CNTs were well anchored in the PEDOT substrate, the diffusion of CNTs into the tissue was reported to be negligible in this study, and with that, the inflammation risk was minimized (Figure 4d). The mentioned advantages of these nanotubes persuaded Ding et al. to develop a biocompatible hydrogel comprising functionalized CNTs as a neural electrode (Ding et al., 2022). In their work, CNTs were used to compensate for the polymeric hydrogels' low conductivity and high impedance. Furthermore, to enhance the dispersion and the affinity of CNTs toward the hyaluronic acid and silk fibroin hydrogel, tyramine monomers were chemically grafted onto the surface of CNTs. This modification allowed the formation of a percolation network with high conductivity and low impedance.

Summarizing, it is difficult to reach a solid conclusion on the safety of CNTs. There is inconsistency in the practiced methods and evaluated biological systems. Their toxicity is an open-ended subject, the mechanism behind it is still being debated, and the suppression methodologies are still being investigated (Mohanta et al., 2019; Salemi et al., 2021). However, considering the low impedance, high conductivity, flexibility, and surface compliance of CNTs, the arrays comprised of these nanotubes can still pass the basic requirements for BMI chronic implantation when mixed into a polymeric substrate.

4.2 | Graphene

The unique arrangement of carbon atoms in a two-dimensional (2D) honeycomb structure of graphene turns it into one of the most exciting allotropes of carbon (Jie Li et al., 2021; Smith et al., 2019). This nanomaterial exhibits excellent thermal conductivity, possesses great electron transport capability, and has a high surface area. These 2D carbon sheets have excellent flexibility and can be used in polymeric conformal coatings (Y. Zhang et al., 2022).

The undisruptive functionalization of PG has been recently explored. Such functionalization includes microfabrication (Jie Li et al., 2021), complexation with biomolecules (Maughan et al., 2022), and structural repatterning (M. Xiao et al., 2020). PG shielding using a polymeric layer can potentially decrease the adverse effect related to tissue compatibility. For instance, a microelectrode array bearing a PG fiber core was constructed to serve as a recording device (Kezhong Wang et al., 2019). The surface of these fibers was coated with a layer of platinum, and the whole construct was protected further with a sheet of Parylene-C (Figure 4e). The latter was proven to have good biocompatibility and electrical properties. Although the polymeric sheet prohibited direct contact between the brain tissue and PG, the chronic studies showed the delamination of Parylene-C, exposure of the core material to the implanted region, and, ultimately, the device failure. Recently, a nanostructured biocomposite was fabricated from collagen and PG (Maughan et al., 2022). Type-I collagen used in this study prevented direct cellular contact with PG and enhanced the biocompatibility of the construct. The electrical conductivity of PG severely diminished but stayed at physiologically required electrical properties. A microneedle array was fabricated to establish the processability of the mentioned nanostructured material in electrocorticography (Figure 4f). Moreover, a circuit was printed using the PG-chitosan, demonstrating the ability of the nanomaterial to be used as a printable bio-ink (Figure 4g). The first report of a conductive bioink comprised of graphene was also achieved through complexation with a hyperbranched polymer (Cheng et al., 2018). This bioink showed excellent electrical properties and was suspendable and processable in an aqueous solution. In another study, M. Xiao et al. (2020) developed a free-standing ordered graphene network. It was shown that the nanopatterned surface of graphene could encode geometrical cues for the neuronal ordered growth and alignment. The wrinkles and ripples in this 3D structure favored astrocytes, bipolar neurons, and neuronal network activity. Another approach was also practiced to benefit from the patterned graphene. A single-layer PG (SLPG) was deposited on a copper foil via the chemical vapor deposition (CVD) process and was further moved on a glass cover using a two-step growth procedure (Zummo et al., 2021). Although this single layer had previously been shown to support neural activity (Pampaloni et al., 2018), it was further revealed that the synapses on SLPG can maintain their structural functionality while boosting the neuronal activity of the tissue residing in proximity. Interestingly, the authors showed that upon the functionalization of SLPG with phenylacetic acid, the cell stiffness and focal adhesion severely changed, and the electrical activity decreased. Their findings show the extent of unknowns for a chemically functionalized PG utilized for BMI.

Benefiting from their abundant functional groups, GO and rGO can maintain or improve the mechanical property of a polymeric composite (Phiri et al., 2018). However, the structural distortion of the PG after the modification process and the formation of surface oxides severely hampers the conductivity of GO and, to a lesser extent, rGO, making them

unattractive for BMI. The PG's high electrical and thermal properties on the one hand, and the excellent mechanical properties and biocompatibility of its modified forms, on the other, complicated the selection procedure for the BMI applications.

4.3 | Metal nanoparticles

The veteran structural material for electrodes is noble metals. This group is vast, including Au (Zhang et al.), Ag (Krukiewicz et al.), and Pt (Minev et al.), to name a few. The nano structuration of noble metals has been extensively studied and developed for BMI. Several groups developed different methods of obtaining electrodes with Au NPs to study the cellular response to electrical stimuli. To observe nerve cell response *in vitro*, J. S. Park et al. (2009) used 20 nm Au NPs adsorbed to the positively charged cover glass coated with polyethyleneimine (PEI). The PC12 cells extended neurites with a mean length of 98.5 μm on the Au NPs in the presence of electrical stimulation (250 mV for 1 h). In contrast, the neurite outgrowth length without electrical stimulation was approximately 10–20 μm . Studies with libraries of nanoporous gold coatings showed that small (~ 30 nm) features reduce astrocytic surface coverage by inhibiting focal adhesion formation (Chapman et al., 2017).

More advanced works confirmed that nanoparticles could be applied in neural tissue engineering to develop neural prosthetic devices and bioelectronic interfaces. One of the methods of using nanoparticles is to form a coating layer over the electrode, which can increase the electrochemical surface area (ESA). Nanostructuration of the electrode surface significantly improves the electrochemical properties of the microelectrodes while the geometric surface area (GSA) remains constant. Due to the introduction of nanoscale features, the roughness and porosity of the surface increase charge transfer with a surrounding electrolyte and decrease the impedance.

One of the methods used for nanoporous surface preparation is a selective de-alloying procedure of silver–gold (Ag–Au) (Y. H. Kim et al., 2015; Seker et al., 2010). Such nanoporous arrays can tune cell adhesion and provide a high spatial resolution of electrical recording and stimulation. Besides porous nanosphere-like structures, nanoclusters (Shah et al., 2013), or nanorods (Ganji et al., 2018; Jang et al., 2022) can further increase the electrode surface area. Zhou et al. show that the Au nanorods layer (70 nm in diameter and 500 nm in length) on a flexible PI has approximately 25 times lower interface impedance than conventional planar electrodes (1.85 vs. 50 k Ω at 1 kHz), which corresponds well with the increase in surface area (Hong-Bo Zhou et al., 2009).

Another approach involves the electrochemical or layer-by-layer deposition of Au, Ag, or IrOx to create nanoparticles (Bao et al., 2019; Chan et al., 2021; D. Lee et al., 2018; H. Zhang et al., 2012) or nanograins (R. Kim et al., 2013) on the electrode surface. Zhang et al. used a layer-by-layer technique to deposit CNTs or Au NPs in poly(diallyl dimethylammonium chloride) (PDDA) on the electrode (H. Zhang et al., 2012). The impedance values were about one order of magnitude lower for the electrodes of pure nanoporous Au. Compared with CNT films, AuNPs films showed increased charge storage capacity (1.32 vs. 0.173 mC/cm²), lower impedance (2.68 vs. 9.65 k Ω), and comparable electrochemical stability.

Metallic neural electrodes have certain limitations due to the mismatch between rigid metals and soft neural tissues. The softer electrically conductive electrodes could promote chronic device function. For this purpose, composite materials combining Au NPs and polymers could improve their electrochemical properties for neural stimulation and recording. One of the examples includes the formation of percolating networks in soft polymer matrices. Minev et al. (2015) formed PDMS loaded with platinum (Pt) nanoparticles (0.5–1.2 μm diameter), resulting in low impedances (≈ 4 k Ω at 1 kHz). Moreover, the electrochemical and electromechanical responses were robust and stable when subjected to tensile stretching. Krukiewicz et al. (2018) compared the electrical percolation threshold for CNTs, silver nanowires, and poly(hydroxymethyl 3,4-ethylenedioxythiophene) microspheres (MSP) in poly(*e*-decalactone) (EDL) matrix. These soft and conducting composites exhibited favorable electrochemical characteristics: EDL/CNT—the lowest resistance (1.2 ± 0.3 k Ω) and EDL/AgNW—the highest charge storage capacity (10.7 ± 0.3 mC/cm²). During *in vitro* study, all the films reduced the presence of reactive astrocytes relative to control electrodes. The electrical properties of such systems can be improved by replacing PDMS or EDL with a conductive polymer such as PEDOT (S. Chen et al., 2013). After electrochemical conditioning, a multilayered PEDOT/Au electrode made by combinational sputter and spin-coating formed fractal-like assemblies of gold particles. Finally, the electrical impedance was 30 ± 2 Ω at 1 kHz. Electrodes formed by electrodeposition of PEDOT mixed with MWCNTs resulted in 8 mC/cm² of charge injection limit and impedance of ~ 10 k Ω at 1 kHz.

The percolating neural interfaces formed with hydrogels further improve the mechanical matching between the electrode and the brain. Due to their high water content, ionic transfer through hydrogel allows for fast ionic conduction. Rinoldi et al. developed a soft and flexible neural interface from polyacrylamide (PA) loaded with silver nanocubes (Figure 2h; Rinoldi et al., 2022). The mechanical parameters of the hydrogel-nanoparticle composite were chosen to minimize the mismatch between the nerve tissue and the biomaterial (Young's modulus <10 kPa). The electrically conductive hydrogel composite had a low electrical impedance (100 Ω at 1 kHz). Moreover, the soft and flexible electrodes were placed directly on the mouse's cortical surfaces enabling a stable long-term neural recording.

In summary, neural interfaces utilizing nanoparticles have been observed to induce advantageous effects on neurons' outgrowth, alignment, and orientation *in vitro*. However, consideration of type, size, concentration, and capping agents is necessary since released nanoparticles can cause frustrated phagocytosis and apoptosis (Wellman et al., 2018).

5 | FABRICATION AND NANOSTRUCTURE

Choosing the materials needed for a specific application is followed by the next step, which is to single out the best fabrication method which can provide all the aspects of the final device. Ideal BMI devices should be able to reach out to neurons and successfully sense and transmit the signals throughout the system. The device's feature size, shape, and dimension can vary depending on the application. For instance, deep brain stimulation electrodes have a size of 4–8 mm; on the other hand, in the case of neural recording, the size is reduced to 10–100 μm . In some cases, multi-electrode arrays would be the best option, but their specific shape and design need to be appropriately implemented (Lebedev & Nicolelis, 2006). Electrospinning and 3D printing are considered two of the most promising fabrication methods to obtain the desired nanostructures.

Electrospinning is known as a technique that can provide materials in the form of nanofibers with tunable properties and can be applied to a variety of polymers. One of the essential features of this technique for biomedical applications, especially BMI, is that the fibers produced with this technique have a high surface-to-volume ratio (Liguori et al., 2022). This property makes them perfect candidates for neural interfaces by enhancing the quality of the record of neural signals and promoting cell integration (Sampson et al., 2014). Many studies have shown that using nanofibers can induce cell growth and proliferation in the desired way. Low prices and easy processing are the other aspects of this technique that have gained more and more attention.

Additive manufacturing has been applied in many applications since its invention, as it allows the creation of complex geometries, which cannot be obtained via conventional fabrication techniques. The use of 3D printing methods for BMI application has been prompted by the possibility of developing biomimetic tissue constructs, soft robots, and customized drug delivery systems with extremely high precision (S. M. Won et al., 2018).

5.1 | Electrospinning

In the past couple of decades, electrospinning (Nayak et al., 2012) has become a popular technique for the fabrication of materials and biomaterials for a range of applications such as drug delivery (Pawłowska et al., 2020), tissue engineering (Rinoldi et al., 2018), cell carriers (Nakielski et al., 2022), wound healing (Rieger et al., 2013), and so on. The electrospinning technique produces continuous nanoscale fibers with diameters in the sub-micrometer to nanometer range using a high-voltage power supply (Zargarian et al., 2019). This leads to materials with high surface area and potential for alignment, giving rise to a range of applications such as filtration and thermal insulation and in the manufacture of protective clothing, sensors, conducting devices and a range of biomedical applications. Electrospun nanofibers can be tailored by selecting processing parameters such as flow rate of the solution flowing through the needle, inner diameter of the needle, voltage and working distance. Additionally, the effect of environmental conditions is not negligible. The ability of depositing nanofibers on a flat or rotating drum collector also offers great opportunities to obtain aligned or random nanofibers, which are impactful on the structural properties of the nanofibers. Further applications, specially cell growth and proliferation are dependent on these properties (Stachewicz et al., 2015). The capability of the technique to use different types of natural (collagen, chitosan, alginate, etc.) and synthetic (PLA, PCL, PLGA, PVA, PAAm) polymers, is another recognizable advantage of electrospinning. Each material category offers certain benefits to the system as natural polymers have outstanding biocompatibility properties, while synthetic polymers outperformed in miming mechanical properties of ECM and processability. Electrospinning make it possible to process

and enhance the base-materials to reach desired properties for target purpose (Amini et al., 2021; Krysiak & Stachewicz, 2023). A review published 15 years ago focusing on the electrospinning technique to fabricate materials for biomedical applications from a range of nonconducting natural, and synthetic polymers showed a few types of fiber morphologies (Agarwal et al., 2008). Nowadays, the electrospinning technique can produce nanofibers with a range of different morphologies and microstructures (X. X. Wang et al., 2021) from conducting and nonCPs.

CP-based nanostructured materials can be fabricated using different variants of electrospinning techniques. Conductive polymers (CPs) are promising organic semiconductors for many essential applications because of their tunable physical/chemical properties, mechanical flexibility, low weight, reversible doping, good biocompatibility, and scalable production.

Direct or neat electrospinning of CPs is difficult to achieve as they tend to have rigid backbones, low molecular weights, and low degrees of chain entanglement, which make them unsuitable for electrospinning purposes. There have been limited reports of successful electrospinning and nanofiber formation from pure CP solutions.

One of the earliest direct electrospinning of a CP was published in 2006 using poly-pyrrole (Chronakis et al., 2006) as the CP to produce pure poly-pyrrole conductive nanofibers by electrospinning organic solvent soluble poly-pyrrole using the functional doping agent di(2-ethylhexyl) sulfosuccinate sodium salt. The authors reported that the electrical conductivity of the nanofiber web was about 2.7×10^{-2} S/cm but did not demonstrate an application. In a more recent article, direct electrospinning of polyaniline has been shown via doped polyaniline solutions in common organic solvents, which were processed into nanofibers using a convenient single-nozzle electrospinning technique (Spiers et al., 2021) with nanofibrous membranes generated substrates subsequently employed in colorimetric gas sensing for ammonia. These substrates demonstrated response linearity upon exposure to 50–5500 ppm ammonia at ambient ($50 \pm 10\%$ RH) and high (80% RH) humidity. These limitations are the main reasons why CPs have not achieved their expected application potential in conventional processing forms. Due to the drawbacks of CPs, novel strategies are necessary to fabricate nanostructured materials. Different electrospinning approaches, including direct or neat electrospinning of CPs into fibers, co-electrospinning with a carrier polymer to give blended fibers, co-axial electrospinning, and coating of electrospun fiber, have been developed.

Co-electrospinning with a carrier polymer has been a common approach to overcoming the spinnability of CPs. Numerous publications are using this approach to produce blended electrospun fibrous materials. The research group of Nobel Prize winner Alan MacDiarmid conducted some of the early investigations into electrospun CPs utilizing carrier polymers. They electrospun blends of doped PANI with PEO (Norris et al., 2000) and found that the fiber diameter varied with the concentration and nature of the carrier polymer. In a separate article by the same group, PS was used as a carrier polymer (MacDiarmid et al., 2001). However, a clear disadvantage of employing the co-electrospinning approach is that it causes significant reductions in the electrical conductivity of the final materials.

Coaxial electrospinning (Yoon et al., 2018) or electrospinning with a two-capillary spinneret (Yu et al., 2004) is another approach that can be used to fabricate continuous core-shell CP composite fibers and pure CP nanotubes. To overcome problems associated with electrospinning PANI, Zhang and Rutledge (2012) utilized coaxial electrospinning to generate PANI/PMMA nanofibers, using emeraldine base PANI dissolved in chloroform for the inner core and poly(methyl methacrylate) dissolved in *N,N*-dimethylformamide as the outer shell. Smooth and continuous PANI/PMMA nanofibers were obtained with diameters of 1.44 μm . The PMMA outer shell could be removed via immersion in an isopropanol solution for 1 h to yield neat PANI nanofibers with decreased diameters of ca. 620 nm and conductivities of 50 S/cm^{-1} .

Another approach to producing CP-based nanostructured materials is coating the CP onto a substrate. Electrospun nanofibers can be used as a template substrate for fabricating coaxial CP fibers. Both organic or inorganic electrospun fibers can provide a robust and stable template during the growth of one-dimensional (1D) nanostructures of various CPs. Remarkably, the nanofiber template can be removed during or after the polymerization process of CPs. Presently, two methods are used to grow CPs on electrospun fiber templates: solution-deposition polymerization and vapor deposition polymerization. Dip coating has been demonstrated to produce conductive polymeric materials by Ding et al. for a textile application. They coated electrospun PU with PEDOT:PSS. The conductivity of the PU nonwovens increased relative to the number of dip coatings applied. The samples, which were dip-coated three times, yielded a conductivity of 2 S/cm.

In another interesting example that uses the coating approach, electrically conductive biomaterial was produced in two stages (J. Y. Lee et al., 2009). The authors first electrospun poly(lactic-co-glycolic acid) (PLGA) and then coated the PLGA meshes with poly-pyrrole. They found that electrical stimulation of PC12 cells on these conductive fibers improved neurite outgrowth compared to nonstimulated cells.

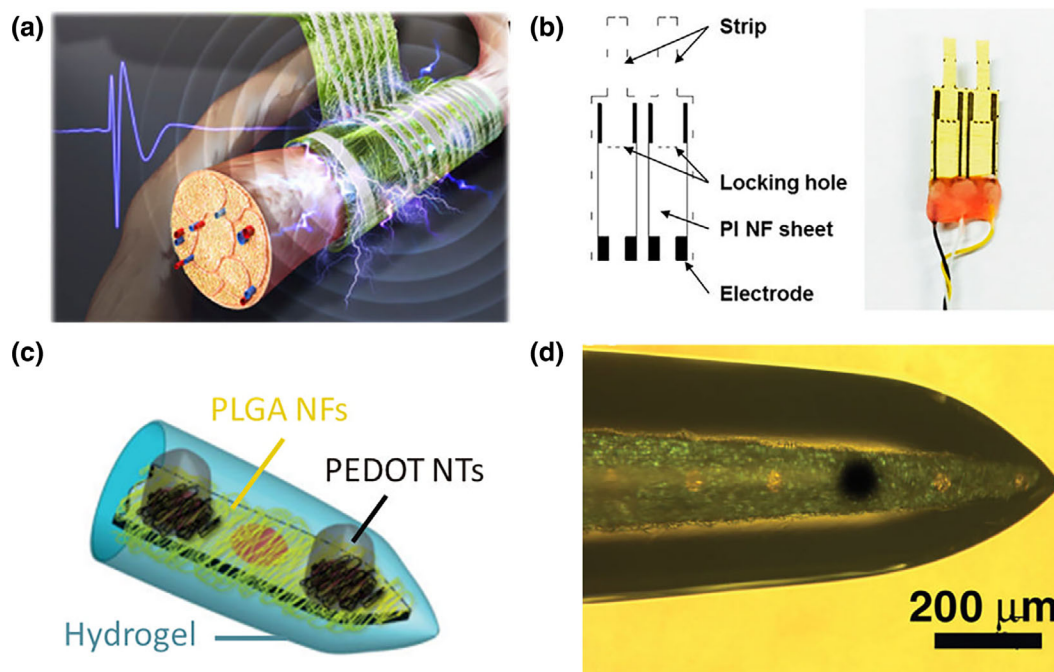


FIGURE 5 Electrospinning technique for BMI application. (a) Illustration of the structure of soft electrodes after *in vivo* implantation, (b) concept design and the image of the fabricated electrode. Reprinted with permission from Heo et al. (2017) (Heo et al., 2017). (c) Schematic of electrodes PEDOT NTs and cloudy PEDOT embedded inside the alginate hydrogel on the electrodes covered previously with PLGA nanofibers, (d) optical micrograph of the described electrode from the top view. Reprinted with permission from Abidian and Martin (2009).

It is possible to produce CP-based nanostructured materials by overcoming the barriers of CP electrospinning using different approaches. These CP electrospun materials find applications in many other areas, including the biomedical field, where the high surface areas of electrospun nanofibers often prove advantageous. Two of the approaches, co-axial electrospinning, and coating postelectrospinning, may prove to be challenging when large volumes of materials are needed for the applications such as filtration media or textiles. The volume required for biomedical purposes is much smaller than other industrial applications, and current electrospinning approaches should provide sufficient material. In another study by Kim et al., a highly aligned electrospun material was designed to coat a nerve conduit. As shown in Figure 5a, external and internal layers of random-aligned fibers are rolled to form the coating. This is because the internal part with growth factor embedded aligned fibers is expected to improve nerve regeneration. In contrast, the external layer of random fibers increases mechanical strength (J. I. Kim et al., 2016). PCL was also combined with conductive copolymer PAT which is a mixture of aniline tetramer (AT), dopamine (DOPA), and polyethylene glycol (PEG), used for electrospinning as shown in Figure 5b. The effects of nanofiber structure on the proliferation and differentiation of neural stem cells were studied by Yan et al. (2020).

In order to reduce neural tissue damage and more stable neural communication, Heo et al. (2017) investigated soft materials such as PI for neural electrodes. Electrospun fibers of the PI can offer more mechanical match compared to other polymers, where conductive polymers can be embedded inside the polymer. Also, these electrospun nanofibers have more surface contact area, which increases neural compression. In this context, AgNPs were used as an electronic connection pad, and PEDOT:PSS was layered to ensure conductivity. Patterned flexible electrode cuffing around the nerves and a detailed structure of the whole structure is shown in Figure 5a,b. After implanting the electrodes *in vivo*, long-term biocompatibility was seen, where neural signals were recorded for an extended period.

Electrospun fibers can also be used as coatings on neural electrodes to contain anti-inflammatory drugs such as dexamethasone (DX). However, these drugs cannot be incorporated into the continuous coatings as they are insulators and will affect the electrode's functionality. PLGA nanofibers are good candidates for releasing such drugs in a controlled manner. Abidian et al. fabricated a multi-step construct to be used potentially as the neural interface for any BMI application. Silicon-based microelectrodes were coated with DX-incorporated PLGA nanofibers in the first step.

The diameter of these fibers was in a range of 50–100 nm with porous structures. An alginate hydrogel layer was crosslinked onto the probe and covered the entire shank of microelectrodes. PEDOT was also electropolymerized to induce electrical conductivity. An illustration of this platform can be seen in Figure 5c, while in Figure 5d, a detailed SEM image of the tip of the electrode is demonstrated. The electrical conductivity of the electrodes was increased significantly, alongside a decrease of about two orders of magnitude in the impedance at 1 kHz. PLGA NFs controlled the drug release of DX with the help of the hydrogel layer. This multilayered structure provides all the requirements for further use for BMI application (Abidian & Martin, 2009).

5.2 | Additive manufacturing

According to the standard ISO-ISO/ASTM 52900 (2015), additive manufacturing (AM), commonly known as 3D printing, is the “process of joining materials to make parts from 3D model data, usually layer upon layer”. This synthetic definition conveys the fundamental idea that starting from a digital model, which can be a computer-aided design (CAD) file or a 3D scan of a physical sample, AM builds up the targeted object by means of the progressive addition of material. AM also known as 3D printing or rapid prototyping, have distinctive techniques such as stereo lithography (SLA), digital light processing (DLP), electron beam melting (EBM), selective laser sintering (SLS), fusion deposition modeling (FDM), and multi-jet 3D printing and laminated object manufacturing (LOM). In all the techniques, variety of materials as plastics, metals, powder, liquids or even living cells are utilized in similar principles to form the target in a layer by layer manner (Kumar et al., 2021). This is in stark contrast to conventional fabrication methods, which either change the shape of the bulk of material through melting and casting or through solid-state plastic deformation (formative methods), or rely on the progressive removal of material where it is not needed (subtractive methods) (Onuh & Yusuf, 1999).

AM is gradually progressing from being a rapid prototyping tool to playing a fundamental role in the Industry 4.0 revolution. The adoption of AM offers key advantages, especially in the biomedical field. If body scans are fed in as the digital model, implants can be fabricated to reproduce the anatomy of the patient exactly. Moreover, since AM is a moldless technology, the printed geometry can be easily changed job by job without incurring additional costs. This ultimately enables the timely and cost-effective obtainment of biomedical devices that conform to the patient's physical structure and physiology (Shidid et al., 2016). Faithful reproductions of organs and anatomical details can also be helpful in presurgical planning and training (Bibb et al., 2009). The selective deposition of material where it is needed according to a computer-controlled toolpath opens the way for fabricating extremely complicated architectures, including lattices and topologically optimized structures. 3D models that reproduce the intricacy of natural constructs are crucial in tissue engineering. They create a biomimetic environment for cell growth and tissue regeneration *in vitro* and *in vivo* (Chandrasekaran et al., 2017). AM is also poised to be a game-changer in the production of implantable sensors, including optogenetic probes, as 3D printing does not necessarily require expensive materials, long processing times, and special cleanroom machines as often seen with conventional microfabrication procedures (Parker et al., 2022).

Historically, research in AM has been focused on structural materials, with the final target being the optimization (i.e., the maximization) of the mechanical stiffness and strength of the printed object. Driven by the increasing need for appropriate interfaces with neural tissue, it has only been very recently that attention has also been paid to extra-soft and compliant printable materials (Shur et al., 2020). However, some AM technologies are intrinsically unsuitable for processing extra-soft and compliant materials because of their very functioning mechanism. In fused filament fabrication (FFF), for example, the feedstock, which is typically a thermoplastic material, cannot be printed if the ratio between (compressive) modulus and molten viscosity is lower than a critical value in the range of 3×10^5 – 5×10^5 s⁻¹ (considering a print nozzle of 508 μm; Venkataraman et al., 2000) and this explains why thermoplastic elastomers having a stiffness in the order of several MPa (10^6 – 10^9 Pa) are currently the “softest” materials printable by FFF (Awasthi & Banerjee, 2021). Even provided that extra-soft and compliant materials can be printed, they are likely to collapse. For this reason, extra-soft and compliant materials are often 3D printed with the structural support of a stiffer material to avoid sagging (Pati et al., 2014) or processed in a hydrogel- or granular gel-based bath that counteracts the force of gravity (“embedded printing”) (Kajtez et al., 2022). Bi-dimensional electrode coatings can be directly screen-printed on stretchable substrates such as polydimethylsiloxane (PDMS) (Shur et al., 2020).

Another obstacle is represented by the printing temperature. Many AM methods require heating the feedstock material to induce inter-layer bonding, a precondition for fabricating a solid object (Sola, 2022). The input of thermal energy, either through direct heating or through interaction with a high-power laser or electron beam, is incompatible

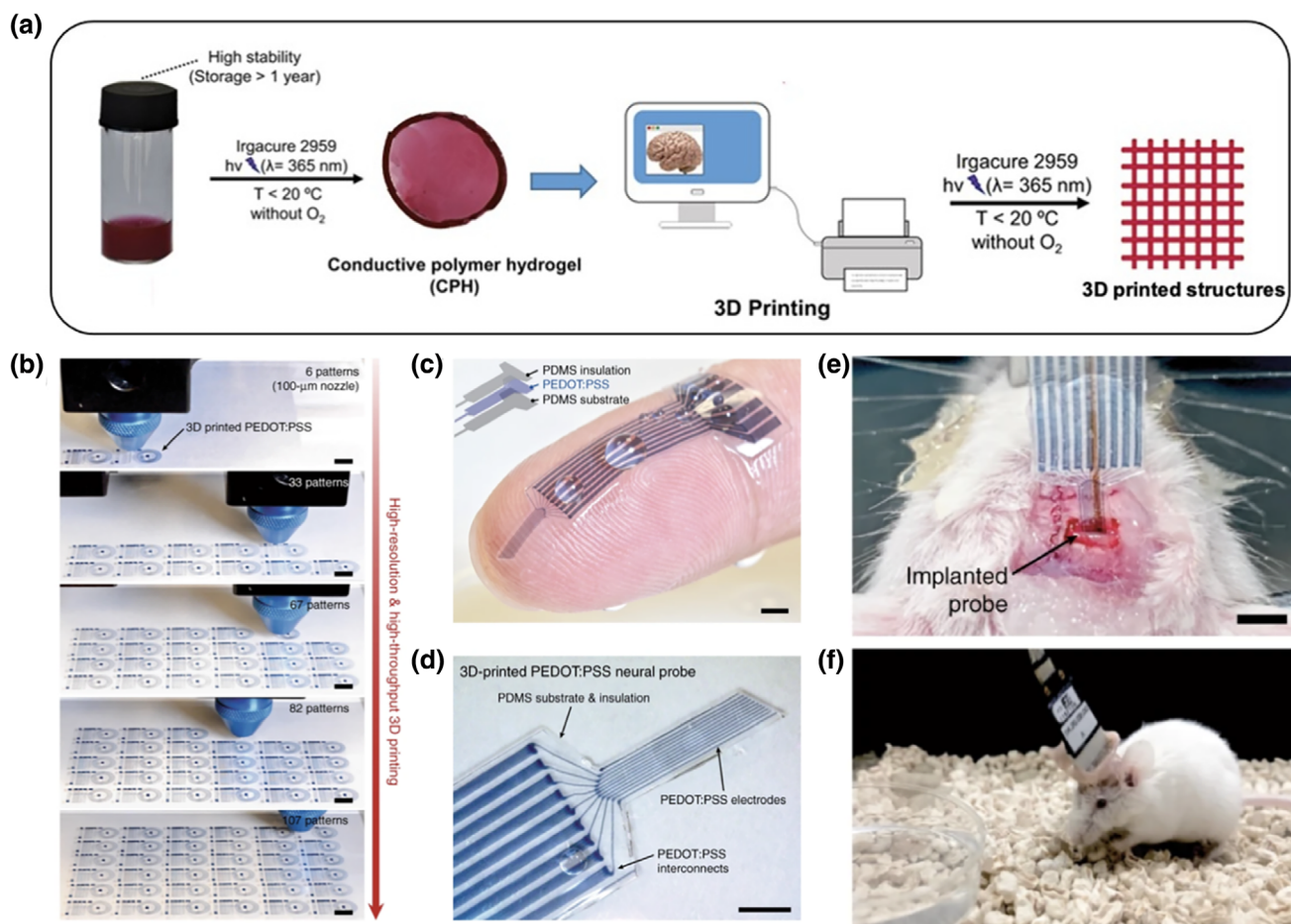


FIGURE 6 Additive manufacturing of flexible structures by vat photopolymerization (VPP) of extra-soft and conductive hydrogels: (a) Schematic representation of the manufacturing workflow. Reproduced with permission from Rinoldi, Lanzi, et al. (2021), (b–f) additive manufacturing of conducting polymer devices by material extrusion (MEX) of PEDOT:PSS-based inks: (b) high throughput fabrication of high-density flexible electronic circuit patterns (scale bar: 5 mm); (c,d) 3D-printed soft neural probe with 9-channels as seen at (c) low magnification and (d) high magnification (scale bars: 1 mm); (e,f) in vivo testing of the probe in a mouse model, showing (e) the craniotomy site (scale bar: 2 mm) and (f) a freely moving mouse with the implanted probe. Reproduced with permission from Yuk et al. (2020).

with cell-laden bioprinting. Consequently, cells must be seeded on the part's surface after printing, as opposed to being co-printed and thus spatially distributed within the scaffold's architecture, as would be the case with living tissues (Jipeng Li et al., 2016). While relatively uninfluential when printing neural probes, the ability to co-print living cells becomes very important for neural tissue engineering. Moreover, the melt-to-solid transition is typically accompanied by a substantial increase in stiffness, which may undermine the mechanical compatibility with neural tissue.

Presently, few AM techniques exist that are able to cope with these obstacles. 3D printing of soft materials compatible with neural tissue has been mainly accomplished either via vat photopolymerization (VPP: light-based approach) or via material extrusion (MEX: ink-based approach) (Y. Park et al., 2022). For example, as for VPP methods, Rinoldi et al. combined a soft and biocompatible hydrogel based on poly(*N*-isopropylacrylamide-co-*N*-isopropylmethacrylamide) with polythiophene, an intrinsically conductive polymer (ICP), to obtain a printable semi-IPN with good electrical properties. In vitro tests proved that the new hybrid hydrogel was highly compatible with neurons and astrocytes and could even promote the differentiation of neural cells. Figure 6a illustrates the printing workflow, where scaffolds could be successfully built up with feature sizes as small as 3 µm via UV light-based stereolithography (SLA) (Rinoldi, Lanzi, et al., 2021).

Since AM affords on-the-fly design customization, Lee et al. developed scalable optogenetic probes based on SLA substrates whose size and layout could be easily adapted to mammalian brain models with different sizes (J. Lee et al., 2020). After printing, the substrates, whose surface was micro-grooved, received a silver paste coating to build the interconnects and a microscale inorganic light-emitting diode. Finally, the shanks were coated with a PDMS/parylene

C bilayer to impart biocompatibility, chemical inertness, and waterproofing. Owing to the high print accuracy enabled by SLA, the substrates were just 60 μm thick, which is comparable to the thickness of a human hair. This enhanced the flexibility of the probes for biomechanical compatibility with soft brain tissue. Meanwhile, the probes were stiff enough to penetrate phantom brain tissue without bending. In a mice model, the bare probes without parylene coating produced significantly larger lesions than conventional probes. However, parylene coating reduced the inflammatory response to levels comparable to fiber implants. Moreover, the new probes are suitable for implementing wireless functionality, which allows neural activity to be monitored in freely behaving animals (Parker et al., 2022).

Even if the spatial resolution is lower concerning VPP, MEX-based AM is a viable option for printing probes and electrodes for neural interfaces owing to its compatibility with a wide range of materials, high throughput (example in Figure 6b), and multi-material printing capability (Y. Park et al., 2022). For instance, Yuk et al. formulated a conductive polymer ink based on PEDOT:PSS. In order to achieve appropriate rheological properties for 3D printing, an aqueous solution of PEDOT:PSS was freeze-dried in a cryogenic condition and then redispersed in water and dimethyl sulfoxide (DMSO) mixture (Yuk et al., 2022). After printing, the free-standing PEDOT:PSS structures needed drying and annealing to remove the solvents and facilitate the establishment of a conductive percolation pathway. The resultant dry parts could be easily converted into a pure PEDOT:PSS hydrogel (equilibrium water content $\sim 87\%$; Young's modulus below 1.1 MPa) by swelling in a wet environment, as shown in Figure 6c,d. PEDOT:PSS hydrogel electronic circuits were co-printed with PDMS ink for insulating encapsulation. In this way, a flexible neural probe could be readily fabricated in less than 20 min in a single-step process. As illustrated in Figure 6e,f, *in vivo* tests demonstrated the capability of the probe to record continuous neural activity in a freely moving mouse.

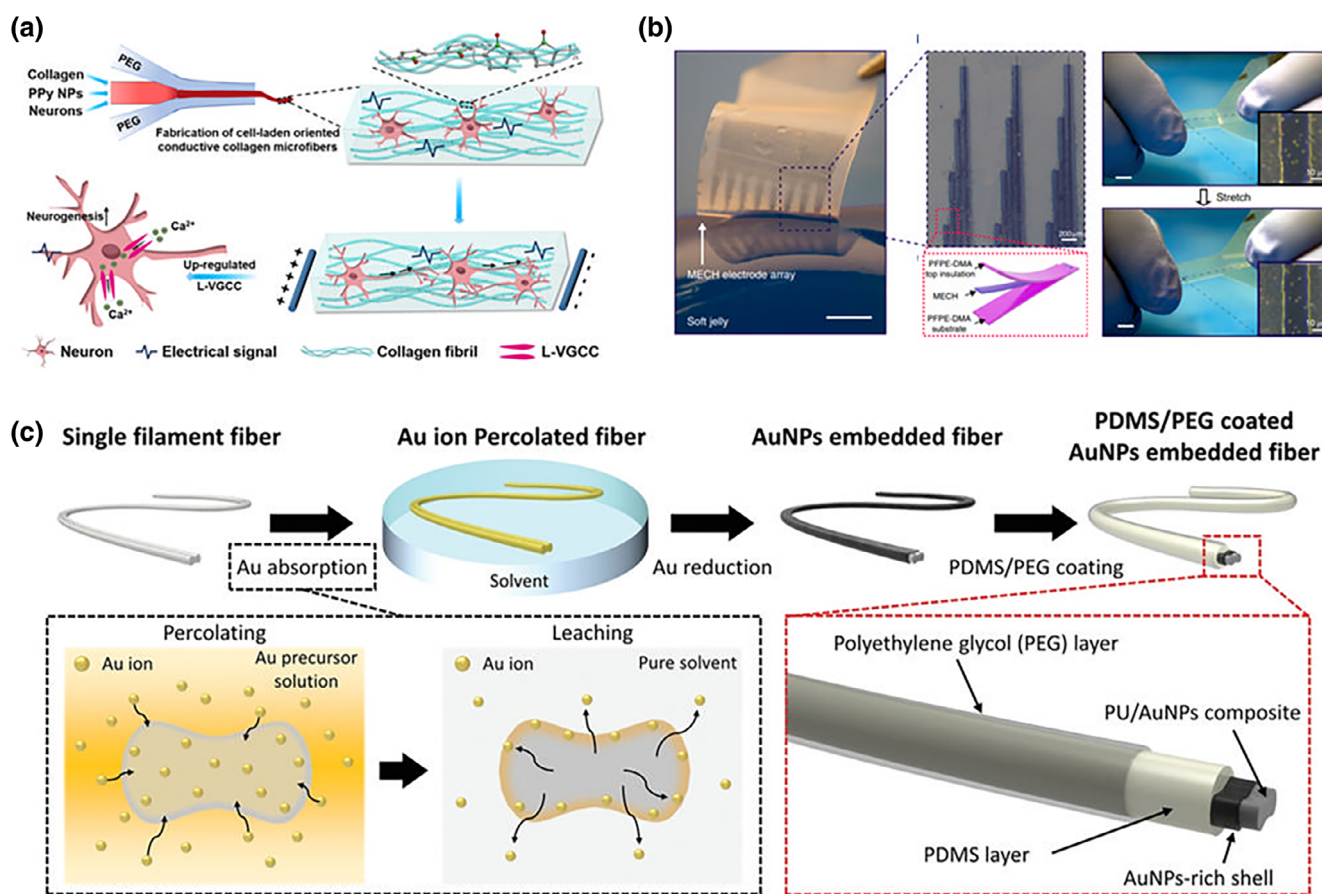


FIGURE 7 New trends in conducting polymer-based systems for brain-machine interfaces. (a) Electrical conducting hydrogels consisting of cell-laden collagen-PPy NPs hybrid hydrogels having the shape of a microfiber for promoting cell alignment and electrical conductivity. Reprinted with permission from Wu et al. (2019). (b) Lithographically micropatterned electrically conductive hydrogels with high resistance to mechanical tensile stretching (up to 20% strain). Reprinted with permission from Liu et al. (2019). (c) Schematic representation of neural probes made of PDMS/PEG-coated AuNPs-embedded fiber. Reprinted with permission from Won et al. (2022).

6 | NEW TRENDS

Nowadays, novel strategies and approaches for designing more efficient, reliable, and functional BMIs have been explored. In order to guarantee stable contact and long-term communication with the neural tissue, the improvement of biocompatibility, the enhancement of electrical properties, and the decrease of mechanical characteristics are considered the most crucial aspects in the new generation of neural interfaces (Choi et al., 2018). Indeed, properly tuning each of these key properties might result in higher fidelity and quality of signal transmission between the brain and machines.

Current progress includes developing biomimetic interfaces which can enhance cell adhesion and induce specific cell spreading. In this frame, efforts in designing CP materials that can be loaded with cells are crucial to increase the biocompatibility of the proposed devices. The housing cultured cells have the function of promoting the integration of the implant in the host tissue, thus improving the quality, fidelity, and long-term stability of the brain tissue-electrode interface (Rochford et al., 2020). Wu et al. produced a biomimetic extracellular matrix for neurogenesis composed of electroconductive polypyrrole (PPy) nanoparticles embedded in collagen hydrogel microfibers loaded with PC12 cells (Figure 7a; C. Wu et al., 2019). The particles were modified to obtain higher hydrophilicity, thus achieving a uniform dispersion into the hydrogel network. The final system was created by using microfluidic technology, resulting in a conductive, biocompatible, and highly-oriented 3D structure that can mimic the neural microenvironment and transfer electrical signals. In another work, a tissue-inspired CP multinet network hydrogel was developed to reproduce the native extracellular matrix properties. Intrinsically conducting PEDOT was polymerized in situ with PA hydrogel loaded with nanoclay Laponite (Tondera et al., 2019). The hydrogel was then coated with a layer of adhesive peptide and polysaccharide dextran sulfate to improve the biocompatibility and suitability of the system for human induced pluripotent stem cell attachment and differentiation. Additionally, the resulting neural electrode showed adequate electrical conductivity (i.e., 26 S/m)—thanks to the presence of PEDOT doped with Laponite-, stretchability (i.e., 800%), and elastic modulus comparable with the one of native tissue (i.e., 15 kPa)—imparted by the PA hydrogel-, revealing its potential as tissue-mimetic BMI.

Biomedical fields—and more specifically neural and BMI application—can benefit significantly from well-defined structures and precise designs, which cannot be fully achieved in nanofibrous materials using conventional electrospinning methods. Techniques such as draw spinning can offer exceptional mechanical properties and alignments, which can be useful for cell differentiation. The high specific surface ratio leads to rapid evaporation of the solvent and yet, formation of solid fibers (A. Liu et al., 2018). Microfluidic spinning considered one of the new approaches to obtain fibers with more homogeneous structure in mild pressure and temperature, better mimicking the human tissue (Wei et al., 2023; Mengfan Zhang et al., 2022). For instance, conductive hollow fibers of sodium alginate/ Ca^{2+} (SC) and PA were fabricated and conducting PPy was added to induce electrical conductivity to the system. The electrical conductivity of $\sim 3 \times 10^{-3}$ S/cm provided requirements for both drug loading into sciatic nerves and also bioelectrical signal transduction (Jiao et al., 2021).

Several efforts in reducing the mechanical characteristics of BMIs have been made in order to narrow the mechanical mismatch with the brain tissue and prevent severe neuroinflammatory reactions (Osmani et al., 2020). For this purpose, the choice of using CP-based nanostructured hydrogels as materials for producing BMIs has become more and more popular in recent years due to their unique softness and flexibility, which can induce minimal stress on the brain tissue and stability of the implants in the long-term (Yuk et al., 2022). In this frame, Wang et al. have developed a bioadhesive ultrasoft interface composed of dopamine methacrylate-hybridized PEDOT nanoparticles embedded in a hydrogel structure. The system showed comparable modulus with the brain tissue and negligible host immune response, permitting an efficient and long-term acquisition of biosignals (X. Wang et al., 2022). By targeting the same goal, Liu et al. developed a conductive hydrogel-based electrode with high stretchability (20%) and Young's modulus values similar to the native tissue (in the order of kPa). A final thin-film “elastronic” electrode array was produced using the micropatterning technique by photopatterning a micropatterned electrically conductive PEDOT:PSS hydrogel with two elastomeric external layers of dimethacrylate-functionalized perfluoropolyether, resulting in a promising system for soft tissue-like BMI (Figure 7b) (Yuxin Liu et al., 2019). On the other hand, recent studies have demonstrated that matching the viscoelastic properties might also be beneficial for improving the functionality, long-term stability, and biocompatibility of BMIs. Xiong et al. fabricated a conductive multilayered graphene hydrogel membrane, showing the role of viscoelasticity in decreasing nerve compression during implantation while inducing only a mild inflammatory response in the long-term (i.e., 8 weeks; Xiong et al., 2022).

Besides, it is worth underlining how crucial it is to overcome the trade-off between mechanical and electrical characteristics of materials and identify a proper balance of the mechanoelectrical properties. This is probably the biggest challenge in the field and has recently motivated researchers to explore and propose new solutions (P. Wang et al., 2020). Won et al. designed a novel neural probe with a core-shell fiber structure, where the core is made of Au-embedded PU-based filament and a shell of PDMS and PEG polymers (Figure 7c) (C. Won et al., 2022). The resulting fiber showed excellent electrical conductivity of 7.68×10^4 S/m and impedance of $2.88 \times 10^3 \Omega$ at a physiologically relevant frequency (i.e., 1 Hz), while the mechanical properties were comparable to the brain tissue characteristics (in the order of kPa; i.e., 170 kPa). The system was implanted in vivo in a mouse model, reporting stable long-term signal acquisition for up to 4 months (both spontaneous and evoked potentials) with minimal immune response. Similarly, Krukiewicz et al. proposed a few BMI core-shell systems composed of soft poly(*ε*-decalactone) filled with conductive particles such as CNTs, Ag nanowires (AgNWs) or microspheres made of poly(hydroxymethyl 3,4-ethylenedioxythiophene, P(EDOT-OH)) (Krukiewicz et al., 2021). Data showed that: (i) the addition of CNTs led to lower resistance (1.2 ± 0.3 k Ω); (ii) the presence of AgNWs resulted in the highest charge storage capacity (10.7 ± 0.3 mC cm⁻²); and (iii) the composite with P(EDOT-OH) microspheres possessed the highest interphase capacitance (1478.4 ± 92.4 μ F cm⁻²). Authors reported in vitro data to demonstrate the cytocompatibility of the systems, revealing the potential of the proposed materials as BMIs.

Finally, researchers have recently dedicated increasing efforts to developing advanced CP-based materials for producing shape memory and stimuli-responsive BMI systems. Indeed, shape memory materials can be tuned to have 2D geometry and stiff characteristics for easier implantation, while recovering in a 3D shape with softer mechanical features after being implanted in the human body at 37°C (Sadeghi et al., 2023). On the other hand, stimuli-responsive materials possess outstanding characteristics as they can intelligently respond to different stimuli, including electrical, optical, mechanical, ultrasonic, and magnetic stimuli. This trend has the potential to achieve wireless, direct, and reciprocal interactions with the nervous system, avoiding invasive wiring and the implantation of energy sources (Sadeghi et al., 2023).

6.1 | Conclusion and future perspectives

Current progress and advancements in neuroscience and neurotechnology have been strongly related to the growing interest in researching novel and more efficient BMI systems. The promising potential of BMIs has been explored to acquire and study brain signals, stimulate brain tissue, and develop strategies for neurological disease treatments. Up to date, CPs are considered among the best candidates as materials for BMI fabrication since they have the unique advantage of being easily tuned and optimized to obtain desired and convenient characteristics. For this reason, CPs-based BMIs can simultaneously offer sufficient electrical properties, mechanical features similar to native tissue, and excellent biocompatibility, highlighting their extraordinary potential for this application. Thanks to these outstanding features, those systems are able to maintain stable and intimate contact at the electrode-tissue interface and reduce the foreign body response in terms of scarring and neuroinflammation, enabling an efficient recording of high-quality neural signals in the long term. The field has grown enormously in recent years, providing devices with ameliorated electrical and mechanical properties while improving their biocompatibility. Nowadays, several different CP-based nanostructured systems have been reported in the literature, including BMIs formed from (i) inorganic nanomaterials and composites (e.g., CNTs, graphene, GO, and rGO); (ii) intrinsically CPs (i.e., polyaniline, polypyrrole, polythiophene); (iii) conductive interpenetrating polymer hydrogels (i.e., semi-IPNs and IPNs). Different production and fabrication methods to obtain BMIs have also been deeply explored (e.g., electrospinning and additive manufacturing). In this frame, intrinsically CPs evidence higher potential than polymers embedded with conductive nanofillers, showing enhanced electrical and mechanical properties. Designing BMIs with balanced mechano-electrical properties seems to be, nowadays, the direction of this research area, while high-resolution miniaturizing of devices is considered the most probable future perspective for enhancing the spatial resolution. Besides, the possibility of loading and releasing anti-inflammatory drugs from BMIs in a controlled manner holds a high potential to suppress the foreign body response.

Furthermore, the development of smart CP-based materials (e.g., thermo-responsive and shape memory materials) looks promising for BMI applications. Shape memory materials will provide easy-to-handle systems during the implantation procedure. Advanced thermo-responsive materials will play as a wireless neural transducer, preventing the use of invasive wires and the implantation of energy sources. The development and design of more diverse materials with suitable properties for specific applications in BMIs is a growing field. Piezoelectric surfaces have been found to be

responsible for surface charges leading to generating electrical signals, miming physiological micro-environments (Ura & Stachewicz, 2022). Cellular interactions and cell adhesion can be enhanced by changing the type of charges accumulated on the surface by alternating polarity using techniques like electrospinning (Polak et al., 2023). Electrical stimulation caused by triboelectric materials has proven to be helpful in cell differentiation and proliferation (Khandelwal et al., 2020; Pan et al., 2018).

We believe that the future of the field may also include high-resolution integrated technologies and nanotechnologies to develop multi-modal high-performing BMIs with the ability to detect electrical and optical signals simultaneously. Additionally, it is foreseen that artificial intelligence and machine learning will also assist in the modeling and designing of novel advanced materials for BMI fabrication with outstanding properties in the near future (Sadeghi et al., 2023).

Finally, we believe that the next generation of neural interfaces will provide the combination of CP-based BMI with cell transplantation to restore and repair neurological function in the most effective manner. Indeed, it is well known that both approaches are of crucial importance for successful clinical translational neuromodulation therapies. This might pave the way for novel treatment opportunities by recording/stimulating signals while regenerating the damaged neural tissue. Thus, we expect that the concept of biohybrid CP-based interfaces will take over the field in the near future, offering conductive implantable interfaces loaded with cells that will be integrated into the host tissue. This will result in highly promising systems that would be able to detect or stimulate signals while promoting the regeneration of the tissue, thus controlling and restoring neural functions.

AUTHOR CONTRIBUTIONS

Yasamin Ziai: Writing – original draft (lead); writing – review and editing (lead). **Seyed Shahrooz Zargarian:** Writing – original draft (supporting); writing – review and editing (supporting). **Chiara Rinoldi:** Writing – original draft (supporting); writing – review and editing (supporting). **Paweł Nakielski:** Writing – original draft (supporting); writing – review and editing (supporting). **Antonella Sola:** Writing – original draft (supporting); writing – review and editing (supporting). **Massimiliano Lanzi:** Writing – original draft (supporting); writing – review and editing (supporting). **Yen Bach Truong:** Writing – original draft (supporting); writing – review and editing (supporting). **Filippo Pierini:** Conceptualization (lead); funding acquisition (lead); resources (lead); supervision (lead); writing – original draft (supporting); writing – review and editing (supporting).

ACKNOWLEDGMENTS

This study was supported by the First TEAM grant number POIR.04.04.00-00-5ED7/18-00, which is carried out within the framework of the First TEAM program of the Foundation for Polish Science (FNP), co-financed by the European Union under the European Regional Development Fund and the Polish National Agency for Academic Exchange (NAWA) under Bekker NAWA Programme, grant number: BPN/BEK/2021/1/00161. Chiara Rinoldi, Paweł Nakielski, and Filippo Pierini acknowledge the financial support from the Polish Ministry of Science and Higher Education through scholarships for outstanding young scientists. Seyed Shahrooz Zargarian was partially from the European Union's Horizon 2021 research and innovation programme under the Marie Skłodowska-Curie grant agreement No. 101068036 (SuSCoFilter). [Correction added on 13 May 2023, after first online publication: The acknowledgement statement has been updated to include missing funding information from NAWA.].

CONFLICT OF INTEREST STATEMENT

The authors declare no competing financial interest.

DATA AVAILABILITY STATEMENT

Data sharing is not applicable to this article as no new data were created or analyzed in this study.

ORCID

Yasamin Ziai  <https://orcid.org/0000-0002-0648-761X>

Filippo Pierini  <https://orcid.org/0000-0002-6526-4141>

RELATED WIREs ARTICLES

[Recent progress of electroactive interface in neural engineering](#)

REFERENCES

- Abdolahi, A., Hamzah, E., Ibrahim, Z., & Hashim, S. (2012). Synthesis of uniform polyaniline nanofibers through interfacial polymerization. *Materials*, *5*, 1487–1494.
- Abidian, M. R., & Martin, D. C. (2009). Multifunctional nanobiomaterials for neural interfaces. *Advanced Functional Materials*, *19*(4), 573–585. <https://doi.org/10.1002/ADFM.200801473>
- Agarwal, S., Wendorff, J. H., & Greiner, A. (2008). Use of electrospinning technique for biomedical applications. *Polymer*, *49*(26), 5603–5621. <https://doi.org/10.1016/J.POLYMER.2008.09.014>
- Aghazadeh, H., Yazdi, M. K., Kolahi, A., Yekani, M., Zarrintaj, P., Ramsey, J. D., Ganjali, M. R., Stadler, F. J., Saeb, M. R., & Mozafari, M. (2021). Synthesis, characterization and performance enhancement of dry polyaniline-coated neuroelectrodes for electroencephalography measurement. *Current Applied Physics*, *27*, 43–50. <https://doi.org/10.1016/J.CAP.2021.04.003>
- Alahi, M. E. E., Liu, Y., Xu, Z., Wang, H., Wu, T., & Mukhopadhyay, S. C. (2021). Recent advancement of electrocorticography (ECoG) electrodes for chronic neural recording/stimulation. *Materials Today Communications*, *29*, 102853. <https://doi.org/10.1016/J.MTCOMM.2021.102853>
- Amini, S., Salehi, H., Setayeshmehr, M., & Ghorbani, M. (2021). Natural and synthetic polymeric scaffolds used in peripheral nerve tissue engineering: Advantages and disadvantages. *Polymers for Advanced Technologies*, *32*(6), 2267–2289. <https://doi.org/10.1002/PAT.5263>
- Aparicio-Collado, J. L., Novoa, J. J., Molina-Mateo, J., Torregrosa-Cabanilles, C., Serrano-Aroca, Á., & Sabater I Serra, R. (2020). Novel semi-interpenetrated polymer networks of poly(3-hydroxybutyrate-co-3-hydroxyvalerate)/poly (vinyl alcohol) with incorporated conductive polypyrrole nanoparticles. *Polymers*, *13*(1), 57. <https://doi.org/10.3390/POLYM13010057>
- Aurand, E. R., Usmani, S., Medelin, M., Scaini, D., Bosi, S., Rosselli, F. B., Donato, S., Tromba, G., Prato, M., & Ballerini, L. (2018). Nanostructures to engineer 3D neural-interfaces: Directing axonal navigation toward successful bridging of spinal segments. *Advanced Functional Materials*, *28*(12), 1700550. <https://doi.org/10.1002/adfm.201700550>
- Awasthi, P., & Banerjee, S. S. (2021). Fused deposition modeling of thermoplastic elastomeric materials: Challenges and opportunities. *Additive Manufacturing*, *46*, 102177. <https://doi.org/10.1016/J.ADDMA.2021.102177>
- Bagheri, B., Zarrintaj, P., Surwase, S. S., Baheiraei, N., Saeb, M. R., Mozafari, M., Kim, Y. C., & Park, O. O. (2019). Self-gelling electroactive hydrogels based on chitosan–aniline oligomers/agarose for neural tissue engineering with on-demand drug release. *Colloids and Surfaces B: Biointerfaces*, *184*, 110549. <https://doi.org/10.1016/J.COLSURFB.2019.110549>
- Bao, B., Ji, B., Wang, M., Gao, K., Yang, B., Chen, X., Wang, X., & Liu, J. (2019). Development and characterisation of electroplating silver/silver chloride modified microelectrode arrays. *Micro & Nano Letters*, *14*(3), 299–303. <https://doi.org/10.1049/mnl.2018.5113>
- Bibb, R., Eggbeer, D., Evans, P., Bocca, A., & Sugar, A. (2009). Rapid manufacture of custom-fitting surgical guides. *Rapid Prototyping Journal*, *15*(5), 346–354. <https://doi.org/10.1108/13552540910993879/FULL/XML>
- Blinova, N. V., Stejskal, J., Trchova, M., Prokes, J., & Omastová, M. (2007). Polyaniline and polypyrrole: A comparative study of the preparation. *European Polymer Journal*, *43*, 2331–2341 Retrieved from <https://www.sciencedirect.com/science/article/pii/S0014305707002017>
- Boeva, Z., & Sergeev, V. (2014). Polyaniline: Synthesis, properties, and application. *Polymer Science Series C*, *56*(1), 144–153. <https://doi.org/10.1134/S1811238214010032>
- Brydson, J. A. (1999). *Plastics materials*. Retrieved from https://books.google.pl/books?hl=en&lr=&id=OlGSAEZYmmoC&oi=fnd&pg=PP1&dq=plastics&ots=CIK-gb25No&sig=rK42weKrv2hYHZj7FdQxPdQLcAQ&redir_esc=y#v=onepage&q=plastics&f=false
- Chan, F., Syu, H., Wang, T., Tang, Z., Huang, C., Lee, J., Burnouf, T., Hu, S. H., Chen, P. C., & Huang, W. C. (2021). Iridium oxide nanoparticle–protein corona neural interfaces with enhanced electroactivity and bioactivity enable electrically manipulatable physical and chemical neuronal activation. *Advanced Materials Interfaces*, *8*(16), 2170086. <https://doi.org/10.1002/ADMI.202170086>
- Chandrasekaran, A., Avci, H. X., Ochalek, A., Rösingh, L. N., Molnár, K., László, L., Bellák, T., Téglási, A., Pesti, K., Mike, A., Phanthong, P., Biró, O., Hall, V., Kitiyanant, N., Krause, K. H., Kobolák, J., & Dinnyés, A. (2017). Comparison of 2D and 3D neural induction methods for the generation of neural progenitor cells from human induced pluripotent stem cells. *Stem Cell Research*, *25*, 139–151. <https://doi.org/10.1016/J.SCR.2017.10.010>
- Chapman, C. A. R., Wang, L., Chen, H., Garrison, J., Lein, P. J., & Seker, E. (2017). Nanoporous gold biointerfaces: Modifying nanostructure to control neural cell coverage and enhance electrophysiological recording performance. *Advanced Functional Materials*, *27*(3), 1604631. <https://doi.org/10.1002/adfm.201604631>
- Chen, N., Luo, B., Patil, A., Wang, J., Gammad, G., Yi, Z., Liu, X., Yen, S.-C., Ramakrishna, S., & Thakor, N. V. (2020). Nanotunnels within poly (3, 4-ethylenedioxythiophene)-carbon nanotube composite for highly sensitive neural interfacing. *ACS Nano*, *14*(7), 8059–8073. <https://doi.org/10.1021/acs.nano.0c00672>
- Chen, S., Pei, W., Gui, Q., Tang, R., Chen, Y., Zhao, S., Wang, H., & Chen, H. (2013). PEDOT/MWCNT composite film coated microelectrode arrays for neural interface improvement. *Sensors and Actuators A: Physical*, *193*, 141–148. <https://doi.org/10.1016/j.sna.2013.01.033>
- Cheng, C., Zhang, J., Li, S., Xia, Y., Nie, C., Shi, Z., Cuellar-Camacho, J. L., Ma, N., & Haag, R. (2018). A water-processable and bioactive multivalent graphene nanoink for highly flexible bioelectronic films and nanofibers. *Advanced Materials*, *30*(5), 1705452. <https://doi.org/10.1002/adma.201705452>
- Chikh, L., Delhorbe, V., & Fichet, O. (2011). (Semi-)interpenetrating polymer networks as fuel cell membranes. *Journal of Membrane Science*, *368*(1–2), 1–17. <https://doi.org/10.1016/j.memsci.2010.11.020>
- Choi, J. R., Kim, S. M., Ryu, R. H., Kim, S. P., & Sohn, J. W. (2018). Implantable neural probes for brain-machine interfaces? Current developments and future prospects. *Experimental Neurobiology*, *27*(6), 453–471. <https://doi.org/10.5607/EN.2018.27.6.453>

- Chronakis, I. S., Grapenson, S., & Jakob, A. (2006). Conductive polypyrrole nanofibers via electrospinning: Electrical and morphological properties. *Polymer*, 47(5), 1597–1603. <https://doi.org/10.1016/J.POLYMER.2006.01.032>
- Cohen, J. B. (1887). Aniline black; its history and its application in dyeing and printing. *Journal of the Society of Dyers and Colourists*, 3(7), 104–112. <https://doi.org/10.1111/J.1478-4408.1887.TB00770.X>
- Cuttaz, E. A., Chapman, C. A. R., Syed, O., Goding, J. A., & Green, R. A. (2021). Stretchable, fully polymeric electrode arrays for peripheral nerve stimulation. *Advanced Science*, 8(8), 2004033. <https://doi.org/10.1002/advs.202004033>
- Dai, T., Qing, X., Lu, Y., & Xia, Y. (2009). Conducting hydrogels with enhanced mechanical strength. *Polymers*. Retrieved from <https://www.sciencedirect.com/science/article/pii/S0032386109007824>, 50, 5236–5241.
- Dai, T., Qing, X., Zhou, H., Shen, C., Wang, J., & Lu, Y. (2010). Mechanically strong conducting hydrogels with special double-network structure. *Synthetic Metals* Retrieved from <https://www.sciencedirect.com/science/article/pii/S0379677910000354>, 160, 791–796.
- Dalrymple, A. N., Robles, U. A., Huynh, M., Nayagam, B. A., Green, R. A., Poole-Warren, L. A., Fallon, J. B., & Shepherd, R. K. (2020). Electrochemical and biological performance of chronically stimulated conductive hydrogel electrodes. *Journal of Neural Engineering*, 17(2), 026018. <https://doi.org/10.1088/1741-2552/AB7CFC>
- Deng, Z., Guo, Y., Zhao, X., Ma, P. X., & Guo, B. (2018). Multifunctional stimuli-responsive hydrogels with self-healing, high conductivity, and rapid recovery through host-guest interactions. *Chemistry of Materials*, 30(5), 1729–1742. https://doi.org/10.1021/ACS.CHEMMATER.8B00008/SUPPL_FILE/CM8B00008_SI_006.AVI
- Deng, Z., Hu, T., Lei, Q., He, J., Ma, P. X., & Guo, B. (2019). Stimuli-responsive conductive nanocomposite hydrogels with high stretchability, self-healing, adhesiveness, and 3D printability for human motion sensing. *ACS Applied Materials and Interfaces*, 11(7), 6796–6808. https://doi.org/10.1021/ACSAMI.8B20178/SUPPL_FILE/AM8B20178_SI_006.AVI
- Deng, Z., Wang, H., Ma, P. X., & Guo, B. (2020). Self-healing conductive hydrogels: Preparation, properties and applications. *Nanoscale*, 12(3), 1224–1246. <https://doi.org/10.1039/C9NR09283H>
- Deng, Z., Yu, R., & Guo, B. (2021). Stimuli-responsive conductive hydrogels: Design, properties, and applications. *Materials Chemistry Frontiers*, 5(5), 2092–2123. <https://doi.org/10.1039/D0QM00868K>
- Dhawan, V., & Cui, X. T. (2022). Carbohydrate based biomaterials for neural interface applications. *Journal of Materials Chemistry B*, 10(25), 4714–4740. <https://doi.org/10.1039/D2TB00584K>
- Ding, J., Chen, Z., Liu, X., Tian, Y., Jiang, J., Qiao, Z., Zhang, Y., Xiao, Z., Wei, D., Sun, J., Luo, F., Zhou, L., & Fan, H. (2022). A mechanically adaptive hydrogel neural interface based on silk fibroin for high-efficiency neural activity recording. *Materials Horizons* Retrieved from <https://pubs.rsc.org/en/content/articlehtml/2022/mh/d2mh00533f>, 9, 2215–2225.
- Dong, R., Wang, L., Hang, C., Chen, Z., Liu, X., Zhong, L., Qi, J., Huang, Y., Liu, S., Wang, L., Lu, Y., & Jiang, X. (2021). Printed stretchable liquid metal electrode arrays for in vivo neural recording. *Small*, 17(14), e2006612. <https://doi.org/10.1002/sml.202006612>
- Dragan, E. S. (2014). Design and applications of interpenetrating polymer network hydrogels: A review. *Chemical Engineering Journal*, 243, 572–590. <https://doi.org/10.1016/J.CEJ.2014.01.065>
- Feng, J., Chen, C., Sun, X., & Peng, H. (2021). Implantable fiber biosensors based on carbon nanotubes. *Accounts of Materials Research*, 2(3), 138–146. <https://doi.org/10.1021/accountsmr.0c00109>
- Ganji, M., Hossain, L., Tanaka, A., Thunemann, M., Halgren, E., Gilja, V., Devor, A., & Dayeh, S. A. (2018). Monolithic and scalable Au nanorod substrates improve PEDOT-metal adhesion and stability in neural electrodes. *Advanced Healthcare Materials*, 7(22), e1800923. <https://doi.org/10.1002/adhm.201800923>
- Garrudo, F. F. F., Mikael, P. E., Rodrigues, C. A. V., Udangawa, R. W., Paradiso, P., Chapman, C. A., Hoffman, P., Colaço, R., Cabral, J. M. S., Morgado, J., Linhardt, R. J., & Ferreira, F. C. (2021). Polyaniline-polycaprolactone fibers for neural applications: Electroconductivity enhanced by pseudo-doping. *Materials Science and Engineering: C*, 120, 111680. <https://doi.org/10.1016/J.MSEC.2020.111680>
- George, P. M., Lyckman, A. W., LaVan, D. A., Hegde, A., Leung, Y., Avasare, R., Testa, C., Alexander, P. M., Langer, R., & Sur, M. (2005). Fabrication and biocompatibility of polypyrrole implants suitable for neural prosthetics. *Biomaterials*, 26(17), 3511–3519. <https://doi.org/10.1016/J.BIOMATERIALS.2004.09.037>
- Goding, J., Vallejo-Giraldo, C., Syed, O., & Green, R. (2019). Considerations for hydrogel applications to neural bioelectronics. *Journal of Materials Chemistry B*, 7(10), 1625–1636. <https://doi.org/10.1039/C8TB02763C>
- Golafshan, N., Kharaziha, M., & Fathi, M. (2017). Tough and conductive hybrid graphene-PVA: Alginate fibrous scaffolds for engineering neural construct. *Carbon*, 111, 752–763. <https://doi.org/10.1016/J.CARBON.2016.10.042>
- Grabiec, P., Domanski, K., Szmigiel, D., & Hodgins, D. (2013). Electrode array design and fabrication for implantable systems. In *Implantable sensor systems for medical applications* (pp. 150–182). Woodhead Publishing. <https://doi.org/10.1533/9780857096289.1.150>
- Green, R., & Abidian, M. R. (2015). Conducting polymers for neural prosthetic and neural interface applications. *Advanced Materials*, 27(46), 7620–7637. <https://doi.org/10.1002/ADMA.201501810>
- Green, R. A., Hassarati, R. T., Goding, J. A., Baek, S., Lovell, N. H., Martens, P. J., & Poole-Warren, L. A. (2012). Conductive hydrogels: Mechanically robust hybrids for use as biomaterials. *Macromolecular Bioscience*, 12(4), 494–501. <https://doi.org/10.1002/MABI.201100490>
- Green, R. A., Lovell, N. H., Wallace, G. G., & Poole-Warren, L. A. (2008). Conducting polymers for neural interfaces: Challenges in developing an effective long-term implant. *Biomaterials*, 29(24–25), 3393–3399. <https://doi.org/10.1016/J.BIOMATERIALS.2008.04.047>
- Green, R. (2019). Elastic and conductive hydrogel electrodes. *Nature Biomedical Engineering*, 3(1), 9–10. <https://doi.org/10.1038/s41551-018-0342-7>

- Grimsdale, A. C., Chan, K. L., Martin, R. E., Jokisz, P. G., & Holmes, A. B. (2009). Synthesis of light-emitting conjugated polymers for applications in electroluminescent devices. *Chemical Reviews*, *109*(3), 897–1091. <https://doi.org/10.1021/CR000013V>
- Guo, X., Zhou, N., Lou, S. J., & Tice, D. (2013). Polymer solar cells with enhanced fill factors. *Nature Photonics*, *7*, 825–833. <https://doi.org/10.1038/nphoton.2013.207>
- Heeger, A. J. (2001). Nobel lecture: Semiconducting and metallic polymers: The fourth generation of polymeric materials. *Reviews of Modern Physics*, *73*(3), 681–700. <https://doi.org/10.1103/REVMODPHYS.73.681>
- Heo, D. N., Kim, H. J., Lee, Y. J., Heo, M., Lee, S. J., Lee, D., do, S. H., Lee, S. H., & Kwon, I. K. (2017). Flexible and highly biocompatible nanofiber-based electrodes for neural surface interfacing. *ACS Nano*, *11*(3), 2961–2971. <https://doi.org/10.1021/acsnano.6b08390>
- Hoffman, A. (2001). Hydrogels for biomedical applications. *Advanced Drug Delivery Reviews*, *944*, 62–73. <https://doi.org/10.1111/j.1749-6632.2001.tb03823.x>
- International Organization for Standardization/American Society of Testing and Materials – standard No. ISO/ASTM 52900 (2015). <https://www.iso.org/standard/74514.html>
- Jang, H., Yoon, D., & Nam, Y. (2022). Enhancement of thermoplasmonic neural modulation using a gold nanorod-immobilized polydopamine film. *ACS Applied Materials & Interfaces*, *14*(21), 24122–24132. <https://doi.org/10.1021/acami.2c03289>
- Jia, M., & Rolandi, M. (2020). Soft and ion-conducting materials in bioelectronics: From conducting polymers to hydrogels. *Advanced Healthcare Materials*, *9*(5), 1901372. <https://doi.org/10.1002/adhm.201901372>
- Jiao, J., Wang, F., Huang, J. J., Huang, J. J., Li, Z. A., Kong, Y., & Zhang, Z. J. (2021). Microfluidic hollow fiber with improved stiffness repairs peripheral nerve injury through non-invasive electromagnetic induction and controlled release of NGF. *Chemical Engineering Journal*, *426*, 131826. <https://doi.org/10.1016/J.CEJ.2021.131826>
- John, A. A., Subramanian, A. P., Vellayappan, M. V., Balaji, A., Mohandas, H., & Jaganathan, S. K. (2015). Carbon nanotubes and graphene as emerging candidates in neuroregeneration and neurodrug delivery. *International Journal of Nanomedicine*, *10*, 4267–4277. <https://doi.org/10.2147/IJN.S83777>
- Kajtez, J., Wessler, M. F., Birtele, M., Khorasgani, F. R., Rylander Ottosson, D., Heiskanen, A., Kamperman, T., Leijten, J., Martínez-Serrano, A., Larsen, N. B., Angelini, T. E., Parmar, M., Lind, J. U., & Emnéus, J. (2022). Embedded 3D printing in self-healing annealable composites for precise patterning of functionally mature human neural constructs. *Advanced Science*, *9*(25), 2201392. <https://doi.org/10.1002/ADVS.202201392>
- Kaloni, T. P., Giesbrecht, P. K., Schreckenbach, G., & Freund, M. S. (2017). Polythiophene: From fundamental perspectives to applications. *Chemistry of Materials*, *29*(24), 10248–10283. <https://doi.org/10.1021/ACS.CHEMMATER.7B03035>
- Khan, Z. M., Wilts, E., Vlasisavljevich, E., Long, T. E., & Verbridge, S. S. (2021). Electroresponsive hydrogels for therapeutic applications in the brain. *Macromolecular Bioscience*, *22*(2), e2100355. <https://doi.org/10.1002/mabi.202100355>
- Khandelwal, G., Maria Joseph Raj, N. P., & Kim, S. J. (2020). Triboelectric nanogenerator for healthcare and biomedical applications. *Nano Today*, *33*, 100882. <https://doi.org/10.1016/J.NANTOD.2020.100882>
- Kim, B. C., Spinks, G. M., Wallace, G. G., & John, R. (2000). Electroformation of conducting polymers in a hydrogel support matrix. *Polymer*, *41*(5), 1783–1790. [https://doi.org/10.1016/S0032-3861\(99\)00308-0](https://doi.org/10.1016/S0032-3861(99)00308-0)
- Kim, J. I., Hwang, T. I., Aguilar, L. E., Park, C. H., & Kim, C. S. (2016). A controlled design of aligned and random nanofibers for 3D bi-functionalized nerve conduits fabricated via a novel electrospinning set-up. *Scientific Reports*, *6*(1), 1–12. <https://doi.org/10.1038/srep23761>
- Kim, R., Hong, N., & Nam, Y. (2013). Gold nanograin microelectrodes for neuroelectronic interfaces. *Biotechnology Journal*, *8*(2), 206–214. <https://doi.org/10.1002/biot.201200219>
- Kim, S., Jang, L. K., Jang, M., Lee, S., Hardy, J. G., & Lee, J. Y. (2018). Electrically conductive polydopamine-polypyrrole as high performance biomaterials for cell stimulation in vitro and electrical signal recording in vivo. *ACS Applied Materials and Interfaces*, *10*(39), 33032–33042. https://doi.org/10.1021/ACSAMI.8B11546/SUPPL_FILE/AM8B11546_SI_001.PDF
- Kim, Y. H., Kim, G. H., Kim, A. Y., Han, Y. H., Chung, M.-A., & Jung, S.-D. (2015). In vitro extracellular recording and stimulation performance of nanoporous gold-modified multi-electrode arrays. *Journal of Neural Engineering*, *12*(6), 66029. <https://doi.org/10.1088/1741-2560/12/6/066029>
- Kleber, C., Bruns, M., Lienkamp, K., Rühle, J., & Asplund, M. (2017). An interpenetrating, microstructurable and covalently attached conducting polymer hydrogel for neural interfaces. *Acta Biomaterialia*, *58*, 365–375. <https://doi.org/10.1016/J.ACTBIO.2017.05.056>
- Kozai, T. D. Y., Langhals, N. B., Patel, P. R., Deng, X., Zhang, H., Smith, K. L., Lahann, J., Kotov, N. A., & Kipke, D. R. (2012). Ultrasmall implantable composite microelectrodes with bioactive surfaces for chronic neural interfaces. *Nature Materials*, *11*(12), 1065–1073. <https://doi.org/10.1038/nmat3468>
- Krukiewicz, K., Britton, J., Więclawska, D., Skorupa, M., Fernandez, J., Sarasua, J. R., & Biggs, M. J. P. (2021). Electrical percolation in extrinsically conducting, poly(ϵ -decalactone) composite neural interface materials. *Scientific Reports*, *11*(1), 1–10. <https://doi.org/10.1038/s41598-020-80361-7>
- Krukiewicz, K., Chudy, M., Vallejo-Giraldo, C., Skorupa, M., Więclawska, D., Turczyn, R., & Biggs, M. (2018). Fractal form PEDOT/Au assemblies as thin-film neural interface materials. *Biomedical Materials*, *13*(5), 54102. <https://doi.org/10.1088/1748-605X/aabced>
- Krysiak, Z. J., & Stachewicz, U. (2023). Electrospun fibers as carriers for topical drug delivery and release in skin bandages and patches for atopic dermatitis treatment. *Wiley Interdisciplinary Reviews: Nanomedicine and Nanobiotechnology*, *15*(1), e1829. <https://doi.org/10.1002/WNAN.1829>

- Kumar, R., Kumar, M., & Chohan, J. S. (2021). The role of additive manufacturing for biomedical applications: A critical review. *Journal of Manufacturing Processes*, 64, 828–850. <https://doi.org/10.1016/J.JMAPRO.2021.02.022>
- Lebedev, M. A., & Nicoletis, M. A. L. (2006). Brain–machine interfaces: Past, present and future. *Trends in Neurosciences*, 29(9), 536–546. <https://doi.org/10.1016/J.TINS.2006.07.004>
- Lee, D., Moon, H. C., Tran, B.-T., Kwon, D.-H., Kim, Y. H., Jung, S.-D., Joo, J. H., & Park, Y. S. (2018). Characterization of tetrodes coated with Au nanoparticles (AuNPs) and PEDOT and their application to thalamic neural signal detection in vivo. *Experimental Neurobiology*, 27(6), 593–604. <https://doi.org/10.5607/en.2018.27.6.593>
- Lee, J., Parker, K. E., Kawakami, C., Kim, J. R., Qazi, R., Yea, J., Zhang, S., Kim, C. Y., Bilbily, J., Xiao, J., Jang, K. I., McCall, J. G., & Jeong, J. W. (2020). Rapidly customizable, scalable 3D-printed wireless optogenetic probes for versatile applications in neuroscience. *Advanced Functional Materials*, 30(46), 2004285. <https://doi.org/10.1002/ADFM.202004285>
- Lee, J. Y., Bashur, C. A., Goldstein, A. S., & Schmidt, C. E. (2009). Polypyrrole-coated electrospun PLGA nanofibers for neural tissue applications. *Biomaterials*, 30(26), 4325–4335. <https://doi.org/10.1016/J.BIOMATERIALS.2009.04.042>
- Lee, M., Shim, H. J., Choi, C., & Kim, D. H. (2019). Soft high-resolution neural interfacing probes: Materials and design approaches. *Nano Letters*, 19(5), 2741–2749. <https://doi.org/10.1021/ACS.NANOLETT.8B04895>
- Lee, S., Ozlu, B., Eom, T., Martin, D. C., & Shim, B. S. (2020). Electrically conducting polymers for bio-interfacing electronics: From neural and cardiac interfaces to bone and artificial tissue biomaterials. *Biosensors and Bioelectronics*, 170, 112620. <https://doi.org/10.1016/J.BIOS.2020.112620>
- Li, J., Zeng, H., Zeng, Z., Zeng, Y., & Xie, T. (2021). Promising graphene-based nanomaterials and their biomedical applications and potential risks: A comprehensive review. *ACS Biomaterials Science & Engineering*, 7(12), 5363–5396. <https://doi.org/10.1021/acsbomaterials.1c00875>
- Li, J., Chen, M., Fan, X., & Zhou, H. (2016). Recent advances in bioprinting techniques: Approaches, applications and future prospects. *Journal of Translational Medicine*, 14(1), 1–15. <https://doi.org/10.1186/S12967-016-1028-0>
- Liguori, A., Pandini, S., Rinoldi, C., Zaccheroni, N., Pierini, F., Focarete, M. L., & Gualandi, C. (2022). Thermoactive smart electrospun nanofibers. *Macromolecular Rapid Communications*, 43(5), 2100694. <https://doi.org/10.1002/MARC.202100694>
- Lira, L. M., & Córdoba De Torresi, S. I. (2005). Conducting polymer–hydrogel composites for electrochemical release devices: Synthesis and characterization of semi-interpenetrating polyaniline–polyacrylamide networks. *Electrochemistry Communications*, 7(7), 717–723. <https://doi.org/10.1016/J.ELECOM.2005.04.027>
- Liu, A., Zhu, H., Liu, G., Noh, Y.-Y., Fortunato, E., Martins, R., & Shan, F. (2018). Draw spinning of wafer-scale oxide fibers for electronic devices. *Advanced Electronic Materials*, 4(6), 1700644. <https://doi.org/10.1002/AELM.201700644>
- Liu, Y., Feig, V., & Bao, Z. (2021). Conjugated polymer for implantable electronics toward clinical application. *Advanced Healthcare Materials*, 10(17), 2001916. <https://doi.org/10.1002/adhm.202001916>
- Liu, Y., Liu, J., Chen, S., Lei, T., Kim, Y., Niu, S., Wang, H., Wang, X., Foudeh, A. M., Tok, J. B. H., & Bao, Z. (2019). Soft and elastic hydrogel-based microelectronics for localized low-voltage neuromodulation. *Nature Biomedical Engineering*, 3(1), 58–68. <https://doi.org/10.1038/s41551-018-0335-6>
- Llerena Zambrano, B., Renz, A. F., Ruff, T., Lienemann, S., Tybrandt, K., Vörös, J., & Lee, J. (2021). Soft electronics based on stretchable and conductive nanocomposites for biomedical applications. *Advanced Healthcare Materials*, 10(3), 2001397. <https://doi.org/10.1002/ADHM.202001397>
- Lu, Y., Li, Y., Pan, J., Wei, P., Liu, N., Wu, B., Cheng, J., Lu, C., & Wang, L. (2012). Poly(3,4-ethylenedioxythiophene)/poly(styrenesulfonate)-poly(vinyl alcohol)/poly(acrylic acid) interpenetrating polymer networks for improving optrode-neural tissue interface in optogenetics. *Biomaterials*, 33(2), 378–394. <https://doi.org/10.1016/J.BIOMATERIALS.2011.09.083>
- Lu, Y., Wang, D., Li, T., Zhao, X., Cao, Y., Yang, H., & Duan, Y. Y. (2009). Poly(vinyl alcohol)/poly(acrylic acid) hydrogel coatings for improving electrode–neural tissue interface. *Biomaterials*, 30(25), 4143–4151. <https://doi.org/10.1016/J.BIOMATERIALS.2009.04.030>
- MacDiarmid, A. G., Jones, W. E., Norris, I. D., Gao, J., Johnson, A. T., Pinto, N. J., Hone, J., Han, B., Ko, F. K., Okuzaki, H., & Llaguno, M. (2001). Electrostatically-generated nanofibers of electronic polymers. *Synthetic Metals*, 119(1–3), 27–30. [https://doi.org/10.1016/S0379-6779\(00\)00597-X](https://doi.org/10.1016/S0379-6779(00)00597-X)
- Manouchehri, S., Bagheri, B., Rad, S. H., Nezhad, M. N., Kim, Y. C., Park, O. O., Farokhi, M., Jouyandeh, M., Ganjali, M. R., Yazdi, M. K., Zarrintaj, P., & Saeb, M. R. (2019). Electroactive bio-epoxy incorporated chitosan-oligoaniline as an advanced hydrogel coating for neural interfaces. *Progress in Organic Coatings*, 131, 389–396. <https://doi.org/10.1016/J.PORGCOAT.2019.03.022>
- Maughan, J., Gouveia, P., Gonzalez, J., & Leahy, L. (2022). Collagen/pristine graphene as an electroconductive interface material for neuronal medical device applications. *Applied Materials*, 29, 101629. Retrieved from <https://www.sciencedirect.com/science/article/pii/S2352940722002633>
- McGlynn, E., Nabaei, V., Ren, E., Galeote-Checa, G., das, R., Curia, G., & Heidari, H. (2021). The future of neuroscience: Flexible and wireless implantable neural electronics. *Advanced Science*, 8(10), 2002693. <https://doi.org/10.1002/adv.202002693>
- Miller, K., Hermes, D., & Focus, N. S. (2020). The current state of electrocorticography-based brain–computer interfaces. *Neurosurgical Focus*, 49(1), E2. <https://doi.org/10.3171/2020.4.FOCUS20185>
- Minev, I. R., Wenger, N., Courtine, G., & Lacour, S. P. (2015). Research update: Platinum-elastomer mesocomposite as neural electrode coating. *APL Materials*, 3(1), 014701. <https://doi.org/10.1063/1.4906502>
- Mohanta, D., Patnaik, S., Sood, S., & Das, N. (2019). Carbon nanotubes: Evaluation of toxicity at biointerfaces. *Journal of Pharmaceutical Analysis*, 9. Retrieved from <https://www.sciencedirect.com/science/article/pii/S2095177918305458>, 293–300.

- Moisala, A., Li, Q., Kinloch, I. A., & Windle, A. H. (2006). Thermal and electrical conductivity of single- and multi-walled carbon nanotube-epoxy composites. *Composites Science and Technology*, 66(10), 1285–1288. <https://doi.org/10.1016/j.compscitech.2005.10.016>
- Nakielski, P., Pawłowska, S., Rinoldi, C., Ziai, Y., de Sio, L., Urbanek, O., Zembrzycki, K., Pruchniewski, M., Lanzi, M., Salatelli, E., Calogero, A., Kowalewski, T. A., Yarin, A. L., & Pierini, F. (2020). Multifunctional platform based on electrospun nanofibers and plasmonic hydrogel: A smart nanostructured pillow for near-infrared light-driven biomedical applications. *ACS Applied Materials and Interfaces*, 12(49), 54328–54342. <https://doi.org/10.1021/acsami.0c13266>
- Nakielski, P., Rinoldi, C., Pruchniewski, M., Pawłowska, S., Gazińska, M., Strojny, B., Rybak, D., Jezierska-Woźniak, K., Urbanek, O., Denis, P., Sinderewicz, E., Czelejewska, W., Staszkiwicz-Chodor, J., Grodzik, M., Ziai, Y., Barczewska, M., Maksymowicz, W., & Pierini, F. (2022). Laser-assisted fabrication of injectable nanofibrous cell carriers. *Small*, 18(2), 2104971. <https://doi.org/10.1002/SMLL.202104971>
- Nalwa, H. (2000). *Handbook of advanced electronic and photonic materials and devices, Ten-volume Set*. Retrieved from [https://books.google.com/books?hl=en&lr=&id=a9s4WrI-014C&oi=fnd&pg=PR17&dq=H.+S.+Nalwa,+Handbook+of+advanced+electronic+and+photonic+materials+and+devices,+2001+Academic+Press,+San+Diego+\(CA\),+USA,+ISBN:+0-12-513758-3\)+121-126&ots=fh9OWXRc29&sig=LxE2prj2o](https://books.google.com/books?hl=en&lr=&id=a9s4WrI-014C&oi=fnd&pg=PR17&dq=H.+S.+Nalwa,+Handbook+of+advanced+electronic+and+photonic+materials+and+devices,+2001+Academic+Press,+San+Diego+(CA),+USA,+ISBN:+0-12-513758-3)+121-126&ots=fh9OWXRc29&sig=LxE2prj2o)
- Namsheer, K., & Rout, C. (2021). Conducting polymers: A comprehensive review on recent advances in synthesis, properties and applications. *RSC Advances*, 11(10), 5659–5697. <https://doi.org/10.1039/D0RA07800J>
- Nayak, R., Padhye, R., Kyrtzis, I. L., Truong, Y. B., & Arnold, L. (2012). Recent advances in nanofibre fabrication techniques. *Textile Research Journal*, 82(2), 129–147. https://doi.org/10.1177/0040517511424524/ASSET/IMAGES/10.1177_0040517511424524-IMG2.PNG
- Nezakati, T., Seifalian, A., Tan, A., & Seifalian, A. M. (2018). Conductive polymers: Opportunities and challenges in biomedical applications. *Chemical Reviews*, 118(14), 6766–6843. <https://doi.org/10.1021/ACS.CHEMREV.6B00275>
- Norris, I. D., Shaker, M. M., Ko, F. K., & MacDiarmid, A. G. (2000). Electrostatic fabrication of ultrafine conducting fibers: Polyaniline/polyethylene oxide blends. *Synthetic Metals*, 114(2), 109–114. [https://doi.org/10.1016/S0379-6779\(00\)00217-4](https://doi.org/10.1016/S0379-6779(00)00217-4)
- Oldroyd, P., & Malliaras, G. G. (2022). Achieving long-term stability of thin-film electrodes for neurostimulation. *Acta Biomaterialia*, 139, 65–81. <https://doi.org/10.1016/J.ACTBIO.2021.05.004>
- Onuh, S. O., & Yusuf, Y. Y. (1999). Rapid prototyping technology: Applications and benefits for rapid product development. *Journal of Intelligent Manufacturing*, 10(3), 301–311. <https://doi.org/10.1023/A:1008956126775/METRICS>
- Osmani, B., Schiff, H., Vogelsang, K., Guzman, R., Kristiansen, P. M., Crockett, R., Chacko, A., Bucher, S., Töpfer, T., & Müller, B. (2020). Hierarchically structured polydimethylsiloxane films for ultra-soft neural interfaces. *Micro and Nano Engineering*, 7, 100051. <https://doi.org/10.1016/J.MNE.2020.100051>
- Ouyang, J. (2021). Application of intrinsically conducting polymers in flexible electronics. *SmartMat*, 2(3), 263–285. <https://doi.org/10.1002/smm2.1059>
- Pampaloni, N. P., Lottner, M., Giugliano, M., Matruggio, A., D'Amico, F., Prato, M., Garrido, J. A., Ballerini, L., & Scaini, D. (2018). Single-layer graphene modulates neuronal communication and augments membrane ion currents. *Nature Nanotechnology*, 13(8), 755–764. <https://doi.org/10.1038/s41565-018-0163-6>
- Pan, R., Xuan, W., Chen, J., Dong, S., Jin, H., Wang, X., Li, H., & Luo, J. (2018). Fully biodegradable triboelectric nanogenerators based on electrospun polylactic acid and nanostructured gelatin films. *Nano Energy*, 45, 193–202. <https://doi.org/10.1016/J.NANOEN.2017.12.048>
- Pang, A., Arsal, A., & Ahmadipour, M. (2020). Synthesis and factor affecting on the conductivity of polypyrrole: A short review. *Polymers for Advanced Technologies*, 32(4), 1428–1454. <https://doi.org/10.1002/pat.5201>
- Parashar, K., Prajapati, D., McIntyre, R., & Kandasubramanian, B. (2020). Advancements in biological neural interfaces using conducting polymers: A review. *Industrial and Engineering Chemistry Research*, 59(21), 9707–9718. https://doi.org/10.1021/ACS.IECR.0C00174/ASSET/IMAGES/MEDIUM/IE0C00174_0005.GIF
- Park, J. S., Park, K., Moon, H. T., Woo, D. G., Yang, H. N., & Park, K.-H. (2009). Electrical pulsed stimulation of surfaces homogeneously coated with gold nanoparticles to induce neurite outgrowth of PC12 cells. *Langmuir: The ACS Journal of Surfaces and Colloids*, 25(1), 451–457. <https://doi.org/10.1021/la8025683>
- Park, Y., Chung, T. S., Lee, G., & Rogers, J. A. (2022). Materials chemistry of neural interface technologies and recent advances in three-dimensional systems. *Chemical Reviews*, 122(5), 5277–5316. https://doi.org/10.1021/ACS.CHEMREV.1C00639/ASSET/IMAGES/MEDIUM/CR1C00639_0020.GIF
- Parker, K. E., Lee, J., Kim, J. R., Kawakami, C., Kim, C. Y., Qazi, R., Jang, K. I., Jeong, J. W., & McCall, J. G. (2022). Customizable, wireless and implantable neural probe design and fabrication via 3D printing. *Nature Protocols*, 18(1), 3–21. <https://doi.org/10.1038/s41596-022-00758-8>
- Pati, F., Jang, J., Ha, D. H., Won Kim, S., Rhie, J. W., Shim, J. H., Kim, D. H., & Cho, D. W. (2014). Printing three-dimensional tissue analogues with decellularized extracellular matrix bioink. *Nature Communications*, 5(1), 1–11. <https://doi.org/10.1038/ncomms4935>
- Pavone, L., Moyanova, S., Mastroiacovo, F., Fazi, L., Busceti, C., Gaglione, A., & Senesi, R. (2020). Chronic neural interfacing with cerebral cortex using single-walled carbon nanotube-polymer grids. *Journal of Neural Engineering*, 17(3), 36032. <https://doi.org/10.1088/1741-2552/ab98db>
- Pawłowska, S., Rinoldi, C., Nakielski, P., Ziai, Y., Urbanek, O., Li, X., Kowalewski, T. A., Ding, B., & Pierini, F. (2020). Ultraviolet light-assisted electrospinning of core-shell fully cross-linked P(NIPAAm-co-NIPMAAm) hydrogel-based nanofibers for thermally induced drug delivery self-regulation. *Advanced Materials Interfaces*, 7(12), 2000247. <https://doi.org/10.1002/ADMI.20000247>

- Phiri, J., Johansson, L.-S., Gane, P., & Maloney, T. (2018). A comparative study of mechanical, thermal and electrical properties of graphene-, graphene oxide- and reduced graphene oxide-doped microfibrillated cellulose nanocomposites. *Composites Part B: Engineering*, *147*, 104–113. <https://doi.org/10.1016/j.compositesb.2018.04.018>
- Pichiorri, F., & Mattia, D. (2020). Brain-computer interfaces in neurologic rehabilitation practice. *Handbook of Clinical Neurology*, *168*, 101–116. <https://doi.org/10.1016/B978-0-444-63934-9.00009-3>
- Pierini, F., Nakielski, P., Urbanek, O., Pawłowska, S., Lanzi, M., De Sio, L., & Kowalewski, T. A. (2018). Polymer-based nanomaterials for photothermal therapy: From light-responsive to multifunctional nanoplateforms for synergistically combined technologies. *Biomacromolecules*, *19*(11), 4147–4167. <https://doi.org/10.1021/acs.biomac.8b01138>
- Polak, M., Berniak, K., Szewczyk, P. K., Karbowniczek, J. E., Marzec, M. M., & Stachewicz, U. (2023). PLLA scaffolds with controlled surface potential and piezoelectricity for enhancing cell adhesion in tissue engineering. *Applied Surface Science*, *621*, 156835. <https://doi.org/10.1016/J.APSUSC.2023.156835>
- Polikov, V., Tresco, P., & Reichert, W. (2005). Response of brain tissue to chronically implanted neural electrodes. *Journal of Neuroscience Methods*. Retrieved from <https://www.sciencedirect.com/science/article/pii/S0165027005002931>, *148*, 1–18.
- Pumera, M. (2013). Electrochemistry of graphene, graphene oxide and other graphenoids: Review. *Electrochemistry Communications*, *36*, 14–18. <https://doi.org/10.1016/j.elecom.2013.08.028>
- Quijada, C. (2020). Special issue: Conductive polymers: Materials and applications. *Materials*, *13*(10), 2344. <https://doi.org/10.3390/MA13102344>
- Quint, J. P., Samandari, M., Abbasi, L., Mollocana, E., Rinoldi, C., Mostafavi, A., & Tamayol, A. (2022). Nanoengineered myogenic scaffolds for skeletal muscle tissue engineering. *Nanoscale*, *14*(3), 797–814. <https://doi.org/10.1039/D1NR06143G>
- Ratautaite, V., Bagdzianas, G., Ramanavicius, A., & Ramanaviciene, A. (2019). An application of conducting polymer polypyrrole for the design of electrochromic pH and CO₂ sensors. *Journal of the Electrochemical Society*, *166*(6), B297–B303. <https://doi.org/10.1149/2.1221904JES/META>
- Richardson-Burns, S. M., Hendricks, J. L., Foster, B., Povlich, L. K., Kim, D. H., & Martin, D. C. (2007). Polymerization of the conducting polymer poly(3,4-ethylenedioxythiophene) (PEDOT) around living neural cells. *Biomaterials*, *28*(8), 1539–1552. <https://doi.org/10.1016/J.BIOMATERIALS.2006.11.026>
- Richardson-Burns, S. M., Hendricks, J. L., & Martin, D. C. (2007). Electrochemical polymerization of conducting polymers in living neural tissue. *Journal of Neural Engineering*, *4*(2), L6–L13. <https://doi.org/10.1088/1741-2560/4/2/L02>
- Rieger, K. A., Birch, N. P., & Schiffman, J. D. (2013). Designing electrospun nanofiber mats to promote wound healing—A review. *Journal of Materials Chemistry B*, *1*(36), 4531–4541. <https://doi.org/10.1039/C3TB20795A>
- Rinoldi, C., Fallahi, A., Yazdi, I. K., Campos Paras, J., Kijęńska-Gawrońska, E., Trujillo-de Santiago, G., Tuoheti, A., Demarchi, D., Annabi, N., Khademhosseini, A., Swieszkowski, W., & Tamayol, A. (2019). Mechanical and biochemical stimulation of 3D multilayered scaffolds for tendon tissue engineering. *ACS Biomaterials Science and Engineering*, *5*(6), 2953–2964. <https://doi.org/10.1021/acsbiomaterials.8b01647>
- Rinoldi, C., Kijęńska, E., Chlanda, A., Choinska, E., Khenoussi, N., Tamayol, A., Khademhosseini, A., & Swieszkowski, W. (2018). Nanobead-on-string composites for tendon tissue engineering. *Journal of Materials Chemistry B*, *6*(19), 3116–3127. <https://doi.org/10.1039/C8TB00246K>
- Rinoldi, C., Lanzi, M., Fiorelli, R., Nakielski, P., Zembrzycki, K., Kowalewski, T., Urbanek, O., Grippo, V., Jezierska-Woźniak, K., Maksymowicz, W., Camposeo, A., Bilewicz, R., Pisignano, D., Sanai, N., & Pierini, F. (2021). Three-dimensional printable conductive semi-interpenetrating polymer network hydrogel for neural tissue applications. *Biomacromolecules*, *22*(7), 3084–3098. <https://doi.org/10.1021/acs.biomac.1c00524>
- Rinoldi, C., Zargarian, S. S., Nakielski, P., Li, X., Liguori, A., Petronella, F., Presutti, D., Wang, Q., Costantini, M., de Sio, L., Gualandi, C., Ding, B., & Pierini, F. (2021). Nanotechnology-assisted RNA delivery: From nucleic acid therapeutics to COVID-19 vaccines. *Small Methods*, *5*(9), 2100402. <https://doi.org/10.1002/SMTD.202100402>
- Rinoldi, C., Ziai, Y., Zargarian, S. S., Nakielski, P., Zembrzycki, K., Haghghat Bayan, M. A., Zakrzewska, A. B., Fiorelli, R., Lanzi, M., Kostrzewska-Księżyk, A., Czajkowski, R., Kublik, E., Kaczmarek, L., & Pierini, F. (2022). In vivo chronic brain cortex signal recording based on a soft conductive hydrogel biointerface. *ACS Applied Materials & Interfaces*, *15*, 6283–6296. <https://doi.org/10.1021/acsami.2c17025>
- Rochford, A. E., Carnicer-Lombarte, A., Curto, V. F., Malliaras, G. G., & Barone, D. G. (2020). When bio meets technology: Biohybrid neural interfaces. *Advanced Materials*, *32*(15), 1903182. <https://doi.org/10.1002/ADMA.201903182>
- Rossetti, N., Hagler, J., Kateb, P., & Cicoira, F. (2021). Neural and electromyography PEDOT electrodes for invasive stimulation and recording. *Journal of Materials Chemistry C*, *9*(23), 7243–7263. <https://doi.org/10.1039/D1TC00625H>
- Sadeghi, A., Afshari, E., Hashemi, M., Kaplan, D., & Mozafari, M. (2023). Brainy biomaterials: Latest advances in smart biomaterials to develop the next generation of neural interfaces. *Current Opinion in Biomedical Engineering*, *25*, 100420. <https://doi.org/10.1016/J.COBME.2022.100420>
- Saleemi, M. A., Hosseini Fouladi, M., Yong, P. V. C., Chinna, K., Palanisamy, N. K., & Wong, E. H. (2021). Toxicity of carbon nanotubes: Molecular mechanisms, signaling cascades, and remedies in biomedical applications. *Chemical Research in Toxicology*, *34*(1), 24–46. <https://doi.org/10.1021/acs.chemrestox.0c00172>
- Sampson, S. L., Saraiva, L., Gustafsson, K., Jayasinghe, S. N., & Robertson, B. D. (2014). Cell electrospinning: An in vitro and in vivo study. *Small*, *10*(1), 78–82. <https://doi.org/10.1002/SMLL.201300804>

- Sandler, J. K. W., Kirk, J. E., Kinloch, I. A., Shaffer, M. S. P., & Windle, A. H. (2003). Ultra-low electrical percolation threshold in carbon-nanotube-epoxy composites. *Polymer*, *44*(19), 5893–5899. [https://doi.org/10.1016/S0032-3861\(03\)00539-1](https://doi.org/10.1016/S0032-3861(03)00539-1)
- Scaini, D., & Ballerini, L. (2018). Nanomaterials at the neural interface. *Current Opinion in Neurobiology*, *50*, 50–55. <https://doi.org/10.1016/j.conb.2017.12.009>
- Seker, E., Berdichevsky, Y., Begley, M. R., Reed, M. L., Staley, K. J., & Yarmush, M. L. (2010). The fabrication of low-impedance nanoporous gold multiple-electrode arrays for neural electrophysiology studies. *Nanotechnology*, *21*(12), 125504. <https://doi.org/10.1088/0957-4484/21/12/125504>
- Shah, K. G., Tolosa, V. M., Tooker, A. C., Felix, S. H., & Pannu, S. S. (2013). Improved chronic neural stimulation using high surface area platinum electrodes. *Annual International Conference of the IEEE Engineering in Medicine and Biology Society, 2013*, 1546–1549. <https://doi.org/10.1109/EMBC.2013.6609808>
- Shanmugam, M., Augustin, A., Mohan, S., Honnappa, B., Chuaicham, C., Rajendran, S., Hoang, T. K. A., Sasaki, K., & Sekar, K. (2022). Conducting polymeric nanocomposites: A review in solar fuel applications. *Fuel*, *325*, 124899. <https://doi.org/10.1016/J.FUEL.2022.124899>
- Shiddid, D., Leary, M., Choong, P., & Brandt, M. (2016). Just-in-time design and additive manufacture of patient-specific medical implants. *Physics Procedia*, *83*, 4–14. <https://doi.org/10.1016/J.PHPRO.2016.08.002>
- Shur, M., Fallegger, F., Pirondini, E., Roux, A., Bichat, A., Barraud, Q., Courtine, G., & Lacour, S. P. (2020). Soft printable electrode coating for neural interfaces. *ACS Applied Bio Materials*, *3*(7), 4388–4397. <https://doi.org/10.1021/acsabm.0c00401>
- Siddhanta, S. K., & Gangopadhyay, R. (2005). Conducting polymer gel: Formation of a novel semi-IPN from polyaniline and crosslinked poly(2-acrylamido-2-methyl propanesulphonic acid). *Polymer*, *46*(9), 2993–3000. <https://doi.org/10.1016/j.polymer.2005.01.084>
- Smith, A. T., LaChance, A. M., Zeng, S., Liu, B., & Sun, L. (2019). Synthesis, properties, and applications of graphene oxide/reduced graphene oxide and their nanocomposites. *Nano Materials Science*, *1*(1), 31–47. <https://doi.org/10.1016/j.nanoms.2019.02.004>
- Sola, A. (2022). Materials requirements in fused filament fabrication: A framework for the design of next-generation 3D printable thermoplastics and composites. *Macromolecular Materials and Engineering*, *307*(10), 2200197. <https://doi.org/10.1002/MAME.202200197>
- Soman, A., Mathew, F., Chacko, A., Alias, M., & Vionda, G. (2015). Interpenetrating polymer networks (IPNs): Hydrogels. *The Pharma Innovation*, *3*(8), 4086–4093. <https://doi.org/10.1081/e-ebpp-120042787>
- Song, E., Li, J., Won, S. M., Bai, W., & Rogers, J. A. (2020). Materials for flexible bioelectronic systems as chronic neural interfaces. *Nature Materials*, *19*(6), 590–603. <https://doi.org/10.1038/s41563-020-0679-7>
- Spencer, K. C., Sy, J. C., Ramadi, K. B., Graybiel, A. M., Langer, R., & Cima, M. J. (2017). Characterization of mechanically matched hydrogel coatings to improve the biocompatibility of neural implants. *Scientific Reports*, *7*(1), 1952. <https://doi.org/10.1038/s41598-017-02107-2>
- Spiers, M. E., Nielsen, D. J., Pavey, K. D., Truong, Y. B., Rutledge, G. C., Kingshott, P., & Eldridge, D. S. (2021). Conductive, acid-doped polyaniline electrospun nanofiber gas sensing substrates made using a facile dissolution method. *ACS Applied Materials and Interfaces*, *13*(44), 52950–52959. https://doi.org/10.1021/ACSAMI.1C08136/SUPPL_FILE/AM1C08136_SI_001.PDF
- Stachewicz, U., Qiao, T., Rawlinson, S. C. F., Almeida, F. V., Li, W. Q., Cattell, M., & Barber, A. H. (2015). 3D imaging of cell interactions with electrospun PLGA nanofiber membranes for bone regeneration. *Acta Biomaterialia*, *27*, 88–100. <https://doi.org/10.1016/J.ACTBIO.2015.09.003>
- Sung, C., Jeon, W., Nam, K. S., Kim, Y., Butt, H., & Park, S. (2020). Multimaterial and multifunctional neural interfaces: From surface-type and implantable electrodes to fiber-based devices. *Journal of Materials Chemistry B*, *8*(31), 6624–6666. <https://doi.org/10.1039/D0TB00872A>
- Sunwoo, S. H., Han, S. I., Joo, H., Cha, G. D., Kim, D., Choi, S. H., Hyeon, T., & Kim, D. H. (2020). Advances in soft bioelectronics for brain research and clinical neuroengineering. *Matter*, *3*(6), 1923–1947. <https://doi.org/10.1016/J.MATT.2020.10.020>
- Tondera, C., Akbar, T. F., Thomas, A. K., Lin, W., Werner, C., Busskamp, V., Zhang, Y., & Minev, I. R. (2019). Highly conductive, stretchable, and cell-adhesive hydrogel by nanoclay doping. *Small*, *15*(27), 1901406. <https://doi.org/10.1002/SMLL.201901406>
- Ura, D. P., & Stachewicz, U. (2022). The significance of electrical polarity in electrospinning: A nanoscale approach for the enhancement of the polymer fibers' properties. *Macromolecular Materials and Engineering*, *307*(5), 2100843. <https://doi.org/10.1002/MAME.202100843>
- Venkataraman, N., Rangarajan, S., Matthewson, M. J., Harper, B., Safari, A., Danforth, S. C., Wu, G., Langrana, N., Guceri, S., & Yardimci, A. (2000). Feedstock material property—Process relationships in fused deposition of ceramics (FDC). *Rapid Prototyping Journal*, *6*(4), 244–253. <https://doi.org/10.1108/13552540010373344>
- Vomero, M., Castagnola, E., Ciarpella, F., Maggolini, E., Goshi, N., Zucchini, E., Carli, S., Fadiga, L., Kassegne, S., & Ricci, D. (2017). Highly stable glassy carbon interfaces for long-term neural stimulation and low-noise recording of brain activity. *Scientific Reports*, *7*, 40332. <https://doi.org/10.1038/srep40332>
- Wang, K., Frewin, C. L., Esrafilzadeh, D., Yu, C., Wang, C., Pancrazio, J. J., Romero-Ortega, M., Jalili, R., & Wallace, G. (2019). High-performance graphene-fiber-based neural recording microelectrodes. *Advanced Materials*, *31*(15), e1805867. <https://doi.org/10.1002/adma.201805867>
- Wang, K., Tian, L., Wang, T., Zhang, Z., Gao, X., Wu, L., Fu, B., & Liu, X. (2018). Electrodeposition of alginate with PEDOT/PSS coated MWCNTs to make an interpenetrating conducting hydrogel for neural interface. *ACS Applied Materials and Interfaces*, *10*(1), 1465766. <https://doi.org/10.1080/09276440.2018.1465766>
- Wang, L. C., Wang, M. H., Ge, C. F., Ji, B. W., Guo, Z. J., Wang, X. L., Yang, B., Li, C. Y., & Liu, J. Q. (2019). The use of a double-layer platinum black-conducting polymer coating for improvement of neural recording and mitigation of photoelectric artifact. *Biosensors and Bioelectronics*, *145*, 111661. <https://doi.org/10.1016/J.BIOS.2019.111661>

- Wang, M., Mi, G., Shi, D., Bassous, N., Hickey, D., & Webster, T. J. (2017). Nanotechnology and nanomaterials for improving neural interfaces. *Advanced Functional Materials*, 28(12), 1700905. <https://doi.org/10.1002/adfm.201700905>
- Wang, P., Zhang, E., Toledo, D., Smith, I. T., Navarrete, B., Furman, N., Hernandez, A. F., Telusma, M., McDaniel, D., Liang, P., & Khizroev, S. (2020). Colossal Magnetoelectric effect in core-shell magnetoelectric nanoparticles. *Nano Letters*, 20(8), 5765–5772. <https://doi.org/10.1021/acs.nanolett.0c01588>
- Wang, X., Sun, X., Gan, D., Soubrier, M., Chiang, H. Y., Yan, L., Li, Y., Li, J., Yu, S., Xia, Y., Wang, K., Qin, Q., Jiang, X., Han, L., Pan, T., Xie, C., & Lu, X. (2022). Bioadhesive and conductive hydrogel-integrated brain-machine interfaces for conformal and immune-evasive contact with brain tissue. *Matter*, 5(4), 1204–1223. <https://doi.org/10.1016/J.MATT.2022.01.012>
- Wang, X. X., Yu, G. F., Zhang, J., Yu, M., Ramakrishna, S., & Long, Y. Z. (2021). Conductive polymer ultrafine fibers via electrospinning: Preparation, physical properties and applications. *Progress in Materials Science*, 115, 100704. <https://doi.org/10.1016/J.PMATSCI.2020.100704>
- Wang, Z., Zhang, F., Vijver, M. G., & Peijnenburg, W. J. G. M. (2021). Graphene nanoplatelets and reduced graphene oxide elevate the microalgal cytotoxicity of nano-zirconium oxide. *Chemosphere*, 276, 130015. <https://doi.org/10.1016/j.chemosphere.2021.130015>
- Wei, L., Wang, S., Shan, M., Li, Y., Wang, Y., Wang, F., Wang, L., & Mao, J. (2023). Conductive fibers for biomedical applications. *Bioactive Materials*, 22, 343–364. <https://doi.org/10.1016/J.BIOACTMAT.2022.10.014>
- Wellman, S. M., Eles, J. R., Ludwig, K. A., Seymour, J. P., Michelson, N. J., McFadden, W. E., Vazquez, A. L., & Kozai, T. D. Y. (2018). A materials roadmap to functional neural interface design. *Advanced Functional Materials*, 28(12), 1701269. <https://doi.org/10.1002/adfm.201701269>
- Wen, K.-P., Chen, Y.-C., Chuang, C.-H., Chang, H.-Y., Lee, C.-Y., & Tai, N.-H. (2015). Accumulation and toxicity of intravenously-injected functionalized graphene oxide in mice. *Journal of Applied Toxicology*, 35(10), 1211–1218. <https://doi.org/10.1002/jat.3187>
- WHO Report. (2007). *Neurological disorders affect millions globally*: WHO Report. Retrieved from <https://www.who.int/news/item/27-02-2007-neurological-disorders-affect-millions-globally-who-report>
- Widge, A. S., Jeffries-El, M., Cui, X., Lagenaur, C. F., & Matsuoka, Y. (2007). Self-assembled monolayers of polythiophene conductive polymers improve biocompatibility and electrical impedance of neural electrodes. *Biosensors and Bioelectronics*, 22(8), 1723–1732. <https://doi.org/10.1016/J.BIOS.2006.08.011>
- Won, C., Jeong, U.-J., Lee, S., Lee, M., Kwon, C., Cho, S., Yoon, K., Lee, S., Chun, D., Cho, I. J., & Lee, T. (2022). Mechanically tissue-like and highly conductive Au nanoparticles embedded elastomeric fiber electrodes of brain-machine interfaces for chronic in vivo brain neural recording. *Advanced Functional Materials*, 32(52), 2205145. <https://doi.org/10.1002/ADFM.202205145>
- Won, S. M., Song, E., Zhao, J., Li, J., Rivnay, J., & Rogers, J. A. (2018). Recent advances in materials, devices, and systems for neural interfaces. *Advanced Materials*, 30(30), e1800534. <https://doi.org/10.1002/adma.201800534>
- Woods, G. A., Rommelfanger, N. J., & Hong, G. (2020). Bioinspired materials for in vivo bioelectronic neural interfaces. *Matter*, 3(4), 1087–1113. <https://doi.org/10.1016/j.matt.2020.08.002>
- Wu, C., Liu, A., Chen, S., Zhang, X., Chen, L., Zhu, Y., Xiao, Z., Sun, J., Luo, H., & Fan, H. (2019). Cell-laden electroconductive hydrogel simulating nerve matrix to deliver electrical cues and promote neurogenesis. *ACS Applied Materials & Interfaces*, 11, 22152–22163. <https://doi.org/10.1021/acsami.9b05520>
- Wu, N., Wan, S., Su, S., Huang, H., Dou, G., & Sun, L. (2021). Electrode materials for brain-machine interface: A review. *InfoMat*, 3(11), 1174–1194. <https://doi.org/10.1002/INF2.12234>
- Wu, X., & Peng, H. (2019). Polymer-based flexible bioelectronics. *Science Bulletin*, 64(9), 634–640. <https://doi.org/10.1016/J.SCIB.2019.04.011>
- Wu, Y., Zhang, Q., Wang, H., & Wang, M. (2020). Multiscale engineering of functional organic polymer interfaces for neuronal stimulation and recording. *Materials Chemistry Frontiers*, 4(12), 3444–3471. <https://doi.org/10.1039/DOQM00279H>
- Xiao, H., Zhang, M., Xiao, Y., & Che, J. (2015). A feasible way for the fabrication of single walled carbon nanotube/polypyrrole composite film with controlled pore size for neural interface. *Colloids and Surfaces B: Biointerfaces*, 126, 138–145. <https://doi.org/10.1016/J.COLSURFB.2014.12.004>
- Xiao, M., Ulloa Severino, F. P., Iseppon, F., Cheng, G., Torre, V., & Tang, M. (2020). 3D free-standing ordered graphene network geometrically regulates neuronal growth and network formation. *Nano Letters*, 20(10), 7043–7051. <https://doi.org/10.1021/acs.nanolett.0c02107>
- Xiong, Z., Huang, W., Liang, Q., Cao, Y., Liu, S., He, Z., Zhang, R., Zhang, B., Green, R., Zhang, S., & Li, D. (2022). Harnessing the 2D structure-enabled viscoelasticity of graphene-based hydrogel membranes for chronic neural interfacing. *Small Methods*, 6(5), 2200022. <https://doi.org/10.1002/SMTD.202200022>
- Yan, H., Wang, Y., Li, L., Zhou, X., Shi, X., Wei, Y., & Zhang, P. (2020). A micropatterned conductive electrospun nanofiber mesh combined with electrical stimulation for synergistically enhancing differentiation of rat neural stem cells. *Journal of Materials Chemistry B*, 8(13), 2673–2688. <https://doi.org/10.1039/C9TB02864A>
- Yang, W., Ratnac, K. R., Ringer, S. P., Thordarson, P., Gooding, J. J., & Braet, F. (2010). Carbon nanomaterials in biosensors: Should you use nanotubes or graphene? *Angewandte Chemie International Edition*, 49(12), 2114–2138. <https://doi.org/10.1002/anie.200903463>
- Yao, G., Yin, C., Wang, Q., Zhang, T., Chen, S., Lu, C., Zhao, K., Xu, W., Pan, T., Gao, M., & Lin, Y. (2020). Flexible bioelectronics for physiological signals sensing and disease treatment. *Journal of Materiomics*, 6(2), 397–413. <https://doi.org/10.1016/J.JMAT.2019.12.005>
- Yin, P., Liu, Y., Xiao, L., & Zhang, C. (2021). Advanced metallic and polymeric coatings for neural interfacing: Structures, properties and tissue responses. *Polymers*, 13(16), 2834. <https://doi.org/10.3390/POLYM13162834>
- Yin, Y., Li, Z., Jin, J., Tussy, C., & Xia, J. (2013). Facile synthesis of poly(3,4-ethylenedioxythiophene) by acid-assisted polycondensation of 5-bromo-2,3-dihydro-thieno[3,4-b][1,4]dioxine. *Synthetic Metals*, 175, 97–102. <https://doi.org/10.1016/J.SYNTHMET.2013.05.001>

- Yoon, J., Yang, H. S., Lee, B. S., & Yu, W. R. (2018). Recent progress in coaxial electrospinning: New parameters, various structures, and wide applications. *Advanced Materials*, 30(42), 1704765. <https://doi.org/10.1002/ADMA.201704765>
- Young, R. J., & Lovell, P. A. (2011). *Introduction to polymers* (3rd ed., pp. 1–653). CRC Press. <https://doi.org/10.1201/9781439894156/INTRODUCTION-POLYMERS-ROBERT-YOUNG-PETER-LOVELL>
- Yu, H. J., Fridrikh, S. V., & Rutledge, G. C. (2004). Production of submicrometer diameter fibers by two-fluid electrospinning. *Advanced Materials*, 16(17), 1562–1566. <https://doi.org/10.1002/ADMA.200306644>
- Yuk, H., Lu, B., Lin, S., Qu, K., Xu, J., Luo, J., & Zhao, X. (2020). 3D printing of conducting polymers. *Nature Communications*, 11(1), 1–8. <https://doi.org/10.1038/s41467-020-15316-7>
- Yuk, H., Lu, B., & Zhao, X. (2019). Hydrogel bioelectronics. *Chemical Society Reviews*, 48(6), 1642–1667. <https://doi.org/10.1039/C8CS00595H>
- Yuk, H., Wu, J., & Zhao, X. (2022). Hydrogel interfaces for merging humans and machines. *Nature Reviews Materials*, 7(12), 935–952. <https://doi.org/10.1038/s41578-022-00483-4>
- Zare, E. N., Agarwal, T., Zarepour, A., Pinelli, F., Zarrabi, A., Rossi, F., Ashrafizadeh, M., Maleki, A., Shahbazi, M.-A., Maiti, T. K., Varma, R. S., Tay, F. R., Hamblin, M. R., Mattoli, V., & Makvandi, P. (2021). Electroconductive multi-functional polypyrrole composites for biomedical applications. *Applied Materials Today*, 24, 101117. <https://doi.org/10.1016/j.apmt.2021.101117>
- Zargarian, S. S., Haddadi-Asl, V., Kafraashian, Z., Azarnia, M., Mirhosseini, M. M., & Seyedjafari, E. (2019). Surfactant-assisted-water-exposed versus surfactant-aqueous-solution-exposed electrospinning of novel super hydrophilic polycaprolactone based fibers: Analysis of drug release behavior. *Journal of Biomedical Materials Research Part A*, 107(3), 597–609. <https://doi.org/10.1002/JBM.A.36575>
- Zhang, H., Shih, J., Zhu, J., & Kotov, N. A. (2012). Layered nanocomposites from gold nanoparticles for neural prosthetic devices. *Nano Letters*, 12(7), 3391–3398. <https://doi.org/10.1021/nl3015632>
- Zhang, M., Peng, X., Fan, P., Zhou, Y., & Xiao, P. (2022). Recent progress in preparation and application of fibers using microfluidic spinning technology. *Macromolecular Chemistry and Physics*, 223(5), 2100451. <https://doi.org/10.1002/MACP.202100451>
- Zhang, M., Tang, Z., Liu, X., & Van der Spiegel, J. (2020). Electronic neural interfaces. *Nature Electronics*, 3(4), 191–200. <https://doi.org/10.1038/s41928-020-0390-3>
- Zhang, Q., Huang, J.-Q., Qian, W.-Z., Zhang, Y.-Y., & Wei, F. (2013). The road for nanomaterials industry: A review of carbon nanotube production, post-treatment, and bulk applications for composites and energy storage. *Small*, 9(8), 1237–1265. <https://doi.org/10.1002/smll.201203252>
- Zhang, Y., & Rutledge, G. C. (2012). Electrical conductivity of electrospun polyaniline and polyaniline-blend fibers and mats. *Macromolecules*, 45(10), 4238–4246. <https://doi.org/10.1021/ma3005982>
- Zhang, Y., Zhang, T., Huang, Z., & Yang, J. (2022). A new class of electronic devices based on flexible porous substrates. *Advanced Science*, 9(7), 2105084. <https://doi.org/10.1002/adv.202105084>
- Zhao, Z., Spyropoulos, G. D., Cea, C., Gelinis, J. N., & Khodagholy, D. (2022). Ionic communication for implantable bioelectronics. *Science Advances*, 8(14), eabm7851. <https://doi.org/10.1126/SCIADV.ABM7851>
- Zhou, H.-B., Li, G., Sun, X.-N., Zhu, Z.-H., Jin, Q.-H., Zhao, J.-L., & Ren, Q.-S. (2009). Integration of Au nanorods with flexible thin-film microelectrode arrays for improved neural interfaces. *Journal of Microelectromechanical Systems*, 18(1), 88–96. <https://doi.org/10.1109/JMEMS.2008.2011122>
- Ziai, Y., Petronella, F., Rinoldi, C., Nakielski, P., Zakrzewska, A., Kowalewski, T. A., Augustyniak, W., Li, X., Calogero, A., Sabała, I., Ding, B., de Sio, L., & Pierini, F. (2022). Chameleon-inspired multifunctional plasmonic nanoplatfoms for biosensing applications. *NPG Asia Materials*, 14(1), 1–17. <https://doi.org/10.1038/s41427-022-00365-9>
- Zoratto, N., & Matricardi, P. (2018). Semi-IPNs and IPN-based hydrogels. In *Polymeric Gels* (pp. 91–124). <https://doi.org/10.1016/B978-0-08-102179-8.00004-1>
- Zou, Y., Wang, J., Guan, S., Zou, L., Gao, L., Li, H., Fang, Y., & Wang, C. (2021). Anti-fouling peptide functionalization of ultraflexible neural probes for long-term neural activity recordings in the brain. *Biosensors & Bioelectronics*, 192, 113477. <https://doi.org/10.1016/j.bios.2021.113477>
- Zummo, F., Esposito, P., Hou, H., Wetzl, C., Rius, G., Tkatchenko, R., Guimera, A., Godignon, P., Prato, M., Prats-Alfonso, E., Criado, A., & Scaini, D. (2021). Bidirectional modulation of neuronal cells electrical and mechanical properties through pristine and functionalized graphene substrates. *Frontiers in Neuroscience*, 15, 811348. <https://doi.org/10.3389/fnins.2021.811348>

How to cite this article: Ziai, Y., Zargarian, S. S., Rinoldi, C., Nakielski, P., Sola, A., Lanzi, M., Truong, Y. B., & Pierini, F. (2023). Conducting polymer-based nanostructured materials for brain–machine interfaces. *WIREs Nanomedicine and Nanobiotechnology*, 15(5), e1895. <https://doi.org/10.1002/wnan.1895>